OXFORD BROOKES UNIVERSITY,

A 1-D Theoretical Performance Analysis and Optimisation of a Bespoke Formula Student V-Twin Engine

Masters by Research Thesis

Ben Bradshaw

March 2019

Abstract

This paper examines the engine intended to power a SAE Formula Student car for the Oxford Brookes Racing Formula Student Team. The engine is an amalgamation of multiple students' research work over a number of years. Therefore, this projects main aim was validation of the engine setup and specifications resulting from previous work, and to find any potential theoretical optimisations that can be implemented before the engine is run for real on a Dynamometer.

The work analyses the engine's power performance and component design, as well as exploring the major parameters involved in race-engine design and development. The analysis was carried out via a 1-D simulation model constructed in GT-Suite. This was combined with combustion and dynamics models constructed in Excel, in addition to component and manifold analysis in SolidWorks and CATIA. The objectives of the work were –

- Construct a combustion and dynamics model in Excel to analyse the current engine setup.
- Identify areas of the engine design for improvement
- Validate the previous GT-Power model and construct a new GT-Power model based on the latest version of the GT-Suite software.
- Validate the findings in the Excel models using the GT-Power model.
- Analyse the current engine performance using all the models.
- Propose new hardware for the engine if needed.

The bespoke V-Twin engine development showed a 97-98 Brake Horse Power (BHP) theoretical Performance limit. However, the starting engine performance was 70 BHP and the power output was found to be unstable and unpredictable. The analyses of the internal components found that they were optimal for the power performance expected from the engine, with the exception that the current design of the intake and exhaust manifolds were found to limit performance, with the intake plenum found to be too small. The valve timing was also found to limit the power performance, with the timing requiring changing in order to optimise performance.

The validation, and the optimising recommended in this project, indicate that the engine's theoretical power performance could be improved from 70 BHP to 90 BHP. The engine with the improvements recommended in this project can now be mounted on a Dynamometer and the final stages of the engine's development can be completed in order to approve it for racing.

Acknowledgements

The Author would like to thank Dr. Changho Yang, for his continued support and mentoring through the project.

Thanks also go to Dr Fabrizio Bonatesta, for help and support on the project.

Thanks also go to Oxford Brookes University students, Luke Mortlock, Patrick Orchard and Tom Rogers.

Abbreviations

- AFR — Air Fuel Ratio
- BDC — Bottom Dead Centre
- BHP — Brake Horse Power
- CA — Crank Angle
- CAD — Computer Aided Design
- CFD — Computational Fluid Dynamics
- CR — Compression Ratio
- CoG — Centre of Gravity
- CAI — Compression Auto Ignition
- EGR — Exhaust Gas Recirculation
- EOC — End of Combustion
- EVO — Exhaust Valve Opening
- EVC — Exhaust Valve Closing
- FS — Formula Student
- FSAE — Formula Society of Automotive Engineers
- GDI — Gasoline Direct Injection
- HRR — Heat Release Rate
- MEP — Mean Effective Pressure
  - BMEP — Brake Mean Effective Pressure
  - IMEP — Indicated Mean Effective Pressure
- MPS — Mean Piston Speed (MPS)
- IVO — Inlet Valve Opening
- IVC — Inlet Valve Closing
- IPS — Instantaneous Piston Speed
- ID — Inlet Diameter
- LHV — Lower Heating Value
- MFB — Mass Faction Burned
- MAPO — Maximum Amplitude of Pressure Oscillations
- NA — Naturally Aspirated
- OBR — Oxford Brookes Racing
- PFI — Port Fuel Injection
- SFC — Specific Fuel Consumption
  - BSFC — Brake Specific Fuel consumption
- SAE — Society of Automotive Engineers
- SI — Spark Ignition
- SOC — Start of Combustion
- ST — Spark Timing
- TDC — Top Dead Centre
- VL — Valve Lift
- VO — Valve Overlap

Contents

Table of Figures

Chapter 1. Introduction

1. Introduction

A bespoke V-twin Spark Ignition (SI) engine has been developed by Students in the Mechanical Engineering and Mathematical Sciences department at Oxford Brookes University. The engine has been in development since 2006 for Oxford Brookes Racing (OBR) Formula Student (FS) team that competes in the Society of Automotive Engineers (SAE) internal Formula Student events alongside university teams from around the world. The engine is a 600CC Naturally Aspirated (NA) SI engine that is expected to be in the car by 2018/19.

The engine was started by Oxford Brookes University students as a theoretical project in 2005. The engine is based on 2 cylinders of a Cosworth DFV Formula 1 V8. Although the engine was designed and built from scratch, the first students used the DFV engine as a base for research into the area of small capacity engines that would be competitive in FS events. The engine is part of the first full engine and powertrain package designed and built entirely by students.

The project will explore the design of the engine's components and analyse the major parameters involved in race engine design and development. The aim and objectives of this project are –

- The aim of the project is to validate the current engine set up and components and to optimise the engine where possible

Objectives –

- Construct a combustion and dynamics model in Excel to analyse the current engine setup.
- Identify areas of the engine design for improvement
- Validate the previous GT-Power model and construct a new GT-Power model based on the latest version of the GT-Suite software.
- Validate the findings in the Excel models using the GT-Power model.
- Analyse the current engine performance using all the models.
- Propose new hardware for the engine if needed.

The project will look into the design and optimisation of inlet and exhaust systems and create Excel spread sheets to determine the key factors for cam design, and inlet and exhaust tuning.

This study seeks to optimise the engine where real-time data from testing the engine is not available. Therefore, the Heat Release Rate (HRR) and the Wiebe function were used to predict the engine’s combustion properties in conjunction with an Excel spreadsheet.

The project was subject to limitations, one of which was that not all parts of the engine and drivetrain had been built. For example, it was not possible to calibrate the engine as the gearbox had not been built. The project identified areas of the engine where changes would lead to improvement in engine performance. A cross section of the original engine can be seen in figure 1 and the specifications of the engine at the start of the project can be seen in Table 1.

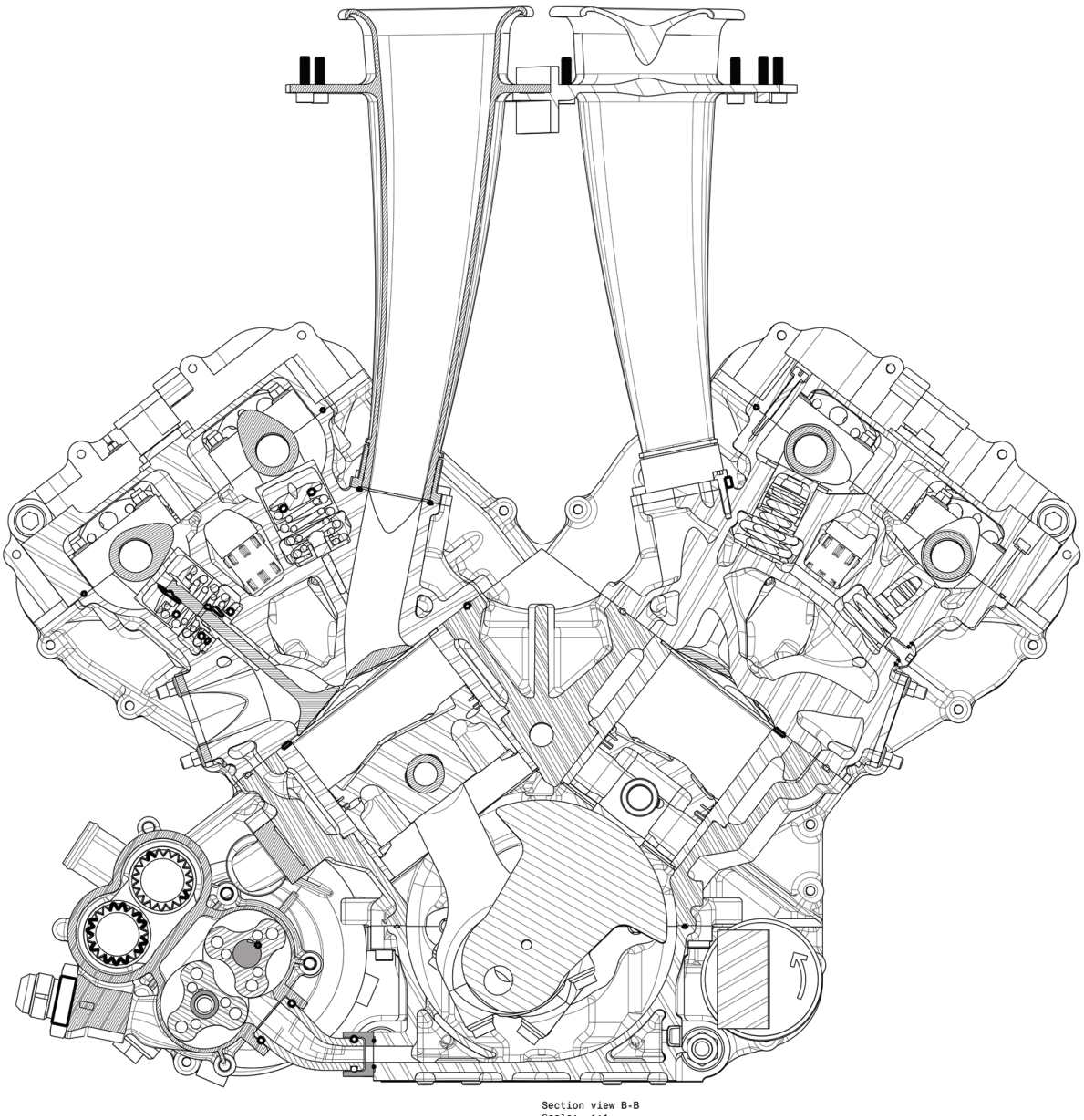

Figure 1: Cross section view of the V-Twin engine from the CATIA model.

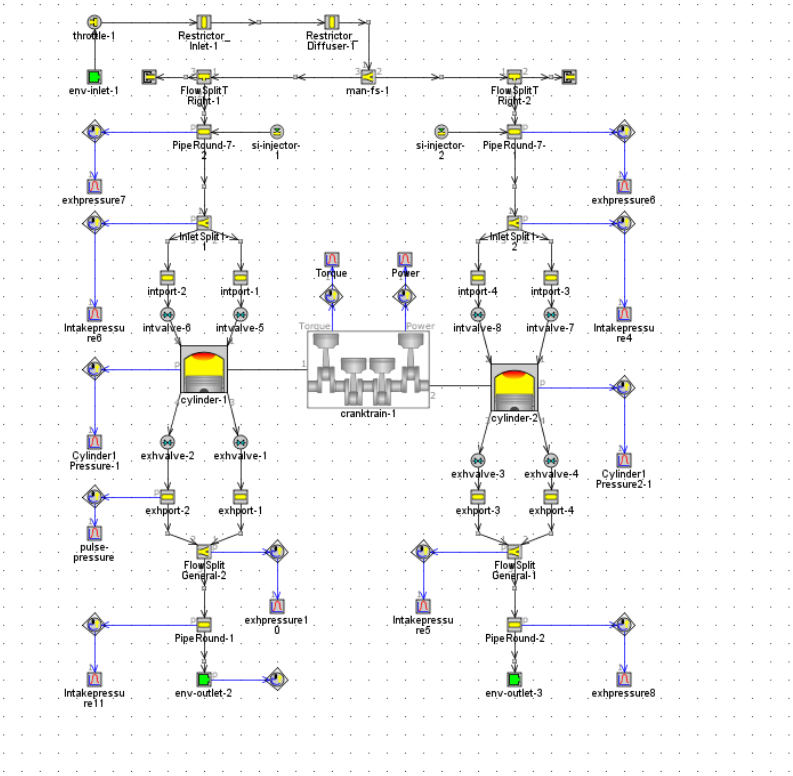

Figure 2: Original Engine Model Layout in GT-Power V6.1

The model seen in Figure 2: Original Engine Model Layout in GT-Power V6.1 is the reconstruction of the original model in the latest version of the GT-Power software, as the original software was out of date and was not cross compatible.

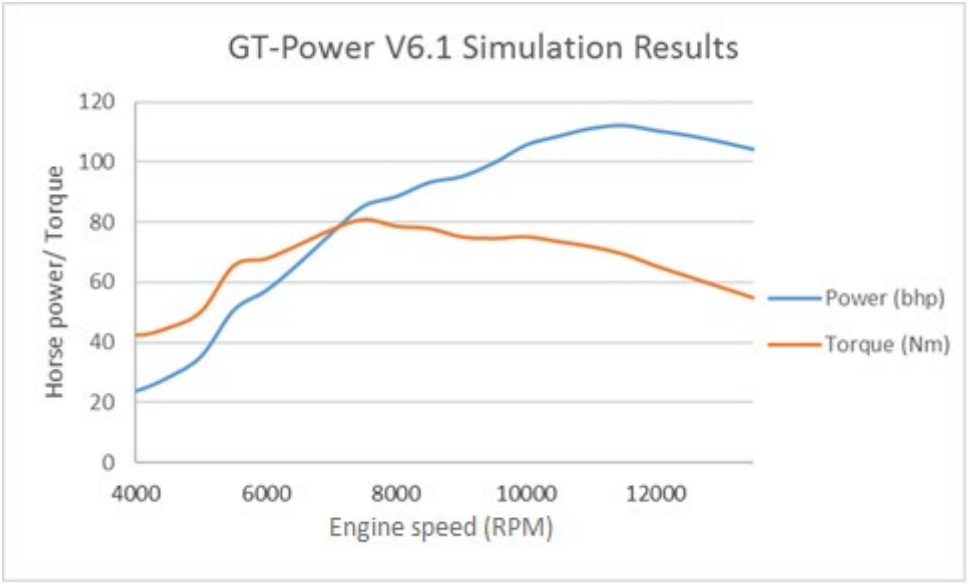

Figure 3: Power curve of the engine at the start of the project.

As can be seen in Figure 3: Power curve of the engine at the start of the project, the previous work on the engine had a smooth power curve with peak power performance of 112 Brake Horse Power (BHP) at 11,000 RPM. This engine performance and power curve was not achievable by the theoretical analysis and from the restrictor required by the FS regulations.

Base engine specifications		
Base Engine Parameters		
Compression Ratio (static)	RATIO	12.45
Compression ratio (Dynamic, 0.5mm rod stretch)	RATIO	14.30
Bore	MM	92.00
Swept Volume	CC	600.00
Stroke	MM	45.13
Idle rpm	RPM	4000
Peak Torque rpm	RPM	9000
Max rpm	RPM	12500
Angle of Cylinders (V-Angle)	DEG	75.00
Con-rod		
Con-rod Length	MM	103.00
Con-rod Big end Width	MM	20.00
Valve and Ports		
Inlet Valve Diameter	MM	38.12
Inlet Valve Stem Diameter	MM	7.00
Exhaust Valve Diameter	MM	31.85
Exhaust Valve Stem Diameter	MM	7.00
Inlet Port Diameter (at Venture Throat)	MM	27.50
Exhaust Port Diameter (Behind Seat Valve)	MM	26.00
Tappet Diameter	MM	33.764
Tappet Bore Diameter	MM	33.65
Inlet Port Length	MM	61.00
Exhaust Port Length	MM	55.00
Total Inlet Tract Length (Bellmouth to Valve Seat)	MM	326.80
Harmonic Order		3.5
Inlet Valve Lift	MM	10.978
Exhaust Valve Lift	MM	9.727
Camshaft		
Camshaft Bearing Surface Diameter	MM	25.00
Cam Bearing Internal Diameter	MM	25.050
Crankshaft		
Crankshaft Main Journal Bearing	MM	49.20
Crankshaft Small End Journal Diameter	MM	42.00
Cylinder Head/Block		
Cylinder Head Stud Angle	DEG	24.00
Cylinder Block Deck Height From Crank CR	MM	149.264
Other		
Main Oil Gallery Inside Dimeter	MM	12.00
Crank CR to Half Speed Stack CR	MM	82.32
Mean Inlet Tract Airspeed at 12,500rpm	M/S	105.00

Table 1: Original Engine Specifications

Chapter 2. Literature review

2. Literature Review

In this section the basics of an SI engine will be explored and broken down into their basic parameters. Although there are many different types of internal combustion engine, the V-Twin is a 4-stroke, spark ignited, petroleum fuelled (although other spark ignited fuels can be used) engine that converts heat addition and air expansion into rotary motion via the use of a sliding piston connected to a rotating crankshaft. The fundamentals of a 4-stroke engine are the Otto cycle, which can be simplified to the ignition stroke, exhaust stroke, induction stroke and compression stroke. Each stroke has a different characteristic in terms of pressure, temperature and air flow in and out of the cylinder. As there are multiple process going on within the engine that cannot be explained with one expression, each process/action must be broken down into smaller equations that can describe the different actions, parameters and characteristics.

2.1. Engine performance parameters

There are many ways of assessing engine performance. This section will explore the basics of some of them in order to further the understanding of engine design and development. The Indicated Work per cycle allows the engine's performance to be assessed using a simple pressure trace. Indicated Work per cycle is given by the equation, [1, 2] –

$$\boldsymbol{W_i = \int p\, x\, dV \approx -\sum_{-360}^{+360} p \times \Delta V}$$

Equation 1

The Indicated Power, which depends on engine speed, can then be found using the Indicated Work using the equation, [2] –

$$\boldsymbol{P_i = \frac{W_c \times N}{n_r}}$$

Equation 2

Mean Effective Pressure (MEP), is the work per unit volume and is an artificial parameter that cannot be measured, it is independent of engine displacement and therefore allows engines of varying displacements to be compared more easily, [2, 3] –

$$MEP = \frac{W}{\Delta V} = \frac{W}{V_d} = \frac{w}{\Delta v}$$

Equation 3

Or simply –

$$MEP = \frac{Work\ done\ per\ cycle}{Swept\ volume}$$

Equation 4

MEP can be broken down into different definitions, Indicated and BMEP are defined by, [2] –

$$IMEP = \frac{W_i}{\Delta v} \quad \text{and} \quad BMEP = \frac{W_b}{\Delta v} = \frac{W_{i \times \eta_m}}{\Delta v} = IMEP \times \eta_m$$

Equation 5

The Brake is the Indicated multiplied by the mechanical efficiency. To find the Mechanical Efficiency, the BMEP can be divided by the Mean Effective Pressure or the Brake Power can be divided by the Indicated Power, [2, 4] –

$$\eta_m = \frac{brake\ power}{indicated\ power} = \frac{BMEP}{IMEP}$$

Equation 6

To find the BMEP, the IMEP has to be multiplied by the Mechanical Efficiency

$$BMEP = IMEP \times \eta_m = \frac{p \times \eta_m}{\Delta v}$$

Equation 7

Air Fuel Ratio (AFR) is the ratio of fuel to air inside the combustion chamber. If oxidants other than air are used for combustion, the same equation applies. The AFR is given by the equation [1, 2, 5] –

$$AFR = \frac{m_a}{m_f}$$

Equation 8

The Equivalence Ratio, ϕ, is a variable that gives an indication on how similar the AFR is to the stoichiometric AFR. The stoichiometric AFR is the amount of air and fuel in the combustion chamber to required give complete combustion. The Equivalence Ratio is given by the equation [1, 2, 3, 6] –

$$\phi = \frac{AFR_{actual}}{AFR_{stoichimetric}}$$

Equation 9

The Equivalence Ratio can indicate how the engine is running, for example [2] –

$\phi = 1$ – Ideal fuelling (stoichiometric combustion)
$\phi > 1$ – Rich mixture (too much fuel for stoichiometric combustion)
$\phi < 1$ – Lean mixture to the engine (not enough fuel for stoichiometric combustion)

The engine will be run at equivalence ratio of 1 which is a stoichiometric air-fuel ratio of 14.7:1 for gasoline.

Specific Fuel Consumption (SFC) is the amount of fuel the engine is consuming for a given output, usually g/kWh, and can be found using the equation [1, 2] –

$$SFC = \frac{\dot{m}_f}{\dot{W}}$$

Equation 10

Volumetric Efficiency, η_v, shows how much air an engine can intake as a ratio of the total volume of the engine to the volume of air inducted during the intake stroke, at ambient conditions. Volumetric efficiency can show how much oxygen an engine has to burn and can give an indication of the correct amount of fuel needed for optimum performance. As the air

density is a factor in determining the η_v, if the density is taken from within the inlet system then only the flow losses around the valve and through the valve seat will be taken into account in the η_v. Typically, around 80 to 90% on road cars, it can be higher in race engines where expected lifespan is far shorter due to the much lower time the engine will be powering the car, often only a few races depending on the race series, [1, 7].

$$\eta_V = \frac{m_a}{\rho_{a,i} V_d} = \frac{\dot{m}_a n}{\rho_a V_d N}$$

Equation 11

Where η_v is the Volumetric Efficiency, m_a is the mass of air, V_d is the displacement volume and $\rho_{a,i}$ is the density of the air at the inlet, N is the speed of the engine and n is the number of crank shaft rotations per complete engine cycle. Inlet density may be taken as atmospheric but that will mean the losses within the inlet system will also be shown in the overall η_v.

Combustion Efficiency, η_c, indicates how much of the fuel has been burnt during the cycle. Lean AFRs normally have 95 to 98% η_C whereas rich mixtures have lower Combustion Efficiencies due to less oxygen available [1, 7].

$$\eta_C = \frac{h_R(T_A) - h_p(T_A)}{m_f Q_{LHV}}$$

Equation 12

Where h_R and h_p are the reference and pre-chamber enthalpy respectively and T_A is the ambient air temperature, Q_{LHV} is the calorific value of the fuel and m_f is the mass of fuel.

2.2. Combustion modelling

An in-cylinder pressure trace is a fundamental part of engine analysis and therefore a combustion model was deemed necessary to give an in-cylinder pressure trace. Another reason for constructing a combustion model is to help improve the understanding of how engine simulation software, such as GT-Power, work and identify any potential problems.

There are multiple types of combustion model, each with a different purpose. The different models have benefits and drawbacks.

Predictive vs Non-Predictive vs Semi-Predictive

A non-predictive combustion model imposes a burn rate based on pre-set combustion parameters and does not deviate from this known burn rate. Non-predictive models will give a pre-determined burn rate and aren't affected by the in-cylinder environment. A non-predictive combustion model allows quick analysis and predictions of known combustion profiles. However, a non-predictive model will not show if any changes of engines parameters will lead to a significant change in the combustion profile. Non-predictive models are not an appropriate choice of combustion model for simulating variables that directly affect the burn rate of the combustion event, [8, 9, 10, 11, 12]. It was found by Dr Hasse et al [13] that a non-predictive model in GT-Power could cut simulation times by more than 50% compared to a predictive model.

A predictive combustion model is based on the inputs important to the combustion process, such as temperature, pressure, spark timing, combustion chamber geometry, valve timing and fuel. Whilst the results are more accurate than from a none-predictive model, a predictive combustion model is complex and time consuming and relies on parameters that are hard to predict without real time in-cylinder data in order to calibrate them, [8, 9, 10, 11, 12].

A compromise between the two is a semi-predictive model. Semi-predictive models are affected by significant variables, and they react to changes in the variables but do not incorporate models to predict the outcomes, if these variables are unknown. Semi-predictive models incorporate non-predictive models, such as the Wiebe model, in order to calculate the combustion but rely on lookups or pre-set responses to calculate the outcomes of these significant parameters based on the Wiebe function. Semi-predictive models allow for a compromise between the accuracy and the calculation times but they require a far more combustion data on the particular area of interest in order to rely on the lookup directory, [8, 9, 10, 11, 12].

Chemical and empirical model

A chemical combustion model uses the atomic structure of the fuels and oxidants to predict the combustion event. Chemical combustion models tend to be theoretical and are predictive as they are based on events that are hard to measure accurately. Although a chemical combustion model can be an accurate predictive model, it cannot be used to analyse a real-time combustion event. The therefore data needs to be compared to a real-time combustion event of the same design in order to validate the results. A chemical kinetic combustion model calculates the concentration of species and global/elementary mechanism heat release. A chemical kinetic model combines parameters such as flame propagation, turbulent flow fields, diffusion fields, heat exchange fields, amongst others. The model can calculate concentrations of radicals and chemical species at any point within the model. A chemical kinetics system is a lot more complicated to produce than a chemical equilibrium or empirical model, [8, 9, 10, 11].

An empirical combustion model uses mathematical methods to analyse the combustion event. Empirical models can be used in post event analysis. Empirical methods must incorporate a lot of assumptions to be used as a predictive method but are useful to analyse the combustion event in real time or using post event data. A chemical equilibrium combustion model typically assumes harmonious combustion with a single zone and uniform parameters such as temperature and pressure, [8, 9, 10, 11].

Flame propagation and Combustion phasing

Flame propagation is the analysis of the combustion event by analysing the development of the flame from kernel, through to flame propagation, to extinguishment. Flame propagation analysis the physical flame and through the defined steps of the flames development in the cylinder [14, 15, 16].

Combustion phasing is the analysis of the combustion event by splitting the combustion profile into defined sections of in-cylinder charge burned and comparing them to the crank angle location of sections or anchor points. 50%MFB is commonly used as the combustion phase anchor and is defined as when half the in-cylinder charge is burned, depending on the CA location of the anchor can give different combustion characteristics and different engine performance [14, 15, 16].

Flame propagation is more analytical of the actual combustion event and therefore lends itself to theoretical analysis of the combustion event, while combustion phasing is the analysis of a combustion profile which lends itself to real-time and post real-time data combustion analysis. GT-Power has models for both types of combustion event although it was deemed that for this project it would be more appropriate to carry out combustion analysis, using combustion phasing, rather than flame propagation analysis. Combustion phasing was deemed appropriate for the project as it can be analysed using in-cylinder pressure data. Flame propagation requires the use of either a complex setup with specialist equipment such as see-through combustion chambers, or a theoretical chemical kinetic model both where deemed too resource heavy and time consuming. However, the principals of flame propagation were researched and investigated, so that it was applied to combustion model as well as the combustion phasing. Flame propagation theory for of combustion models can be seen in Flame Propagation section of the **Appendix** [14, 15, 16]**.**

2.2.1. Heat Release Rate

HRR is the rate at which energy, in terms of heat, is released by the fuel when it is burned. HRR is a critical parameter in terms of engine performance. The HRR inside a cylinder is typically larger than if the same air/fuel charge was combusted in a constant volume, closed system, due to the compression of the air inside the cylinder as the piston travels to Top Dead Centre (TDC). HRR can be calculated using different methods. The apparent HRR assumes that the change in pressure from compression and expansion for a given change in crank angle is proportional to the fuel burnt over the same interval and so the apparent HRR is calculated as the heat released per change in crank angle θ as a function of gamma, if a perfect gas is assumed. [2, 18] –

$$\delta Q_{hr} = [\, dU \,] + [\, \delta W \,] + [\, \delta Q_{Ht} \,]$$

Equation 13

this can be broken down into [2] –

$$\frac{dQ_{hr}}{d\theta} = \left[\frac{C_v}{R} \left(p \, \frac{dV}{d\theta} + V \, \frac{dP}{d\theta} \right) \right] + \left[p \, \frac{dV}{d\theta} \right] + \left[\frac{d\, Q_{ht}}{d\theta} \right]$$

Equation 14

and further [2, 7] –

$$\frac{dQ_{net}}{d\theta} = \left[\frac{C_v}{R} \left(p \, \frac{dV}{d\theta} + V \, \frac{dP}{d\theta} \right) \right] + \left[p \, \frac{dV}{d\theta} \right] = \left(\frac{C_v}{R} + 1 \right) p \, \frac{dV}{d\theta} + \frac{C_v}{R} V \, \frac{dP}{d\theta}$$

Equation 15

and finally [2, 7] –

$$\frac{dQ_{net}}{d\theta} = \left(\frac{\gamma}{\gamma - 1} \times p \frac{dV}{d\theta} \right) + \left(\frac{1}{\gamma - 1} \times V \, \frac{dP}{d\theta} \right)$$

Equation 16

where γ is the ratio of specific heats (typically 1.3 ~ 1.4).

One method is the single zone. The single zone equation is so-called as it uses an averaged value for gamma from the two zones, the two zones being unburnt and burnt. It is worked out using the equation [2, 7] –

$$\left(\frac{Q_{LHV} \times m_c}{\frac{A}{F} + 1} \right) \times dx_b - m_c \times Cv \times dT = p \times dV + A \times \bar{h} \times (T - T_w) + \frac{h \times V_{cr}}{\frac{\bar{R}}{\bar{M}} \times T_w} dp$$

Equation 17

where Cv is the specific heat at constant volume, x_b is the mass fraction burned, m_c is the mass of the charge, T is temperature, p is pressure, V is volume, $\bar{h}$ is the coefficient of average heat transfer, T_w is temperature of the wall, A/F is the air fuel ratio, Q_{HLV} is the lower heat value, A is the combustion chamber surface area.

A further equation can be used where the specific heats from the two zones are not averaged. This is a much more complicated equation [2, 18] –

$$\left(\frac{Q_{LHV\times}m_c}{\frac{A}{F}+1}+m_c\times Cv_u\times T_u-m_c\times Cv_b\times T_b\right)\times dx_b-m_c\times(1-x_b)\times Cv_u\times dT_u$$
$$-m_c\times x_b\times Cv_b\times dT_b-p\times dV_u-p\times dV_b$$
$$=A_u\times\bar{h}_u\times(T_u-T_w)+A_b\times\bar{h}_b\times(T_b-T_w)+\frac{h_u\times V_{cr}}{\frac{\bar{R}_u}{M_u}\times T_w}dp$$

Equation 18

where all the symbols mean the same as for the single zone, but the suffix u means unburnt and the suffix b means burnt. The integral of HRR can be represented as MFB. The MFB represents the amount of the fuel/air charge that has been burned per cycle. [18].

2.2.2. Mass Fraction Burned

Mass Fracture Burn (MFB) is a common combustion phasing indicator to determine the amount of fuel and air mixture that has been burned for a given crank angle, [19].

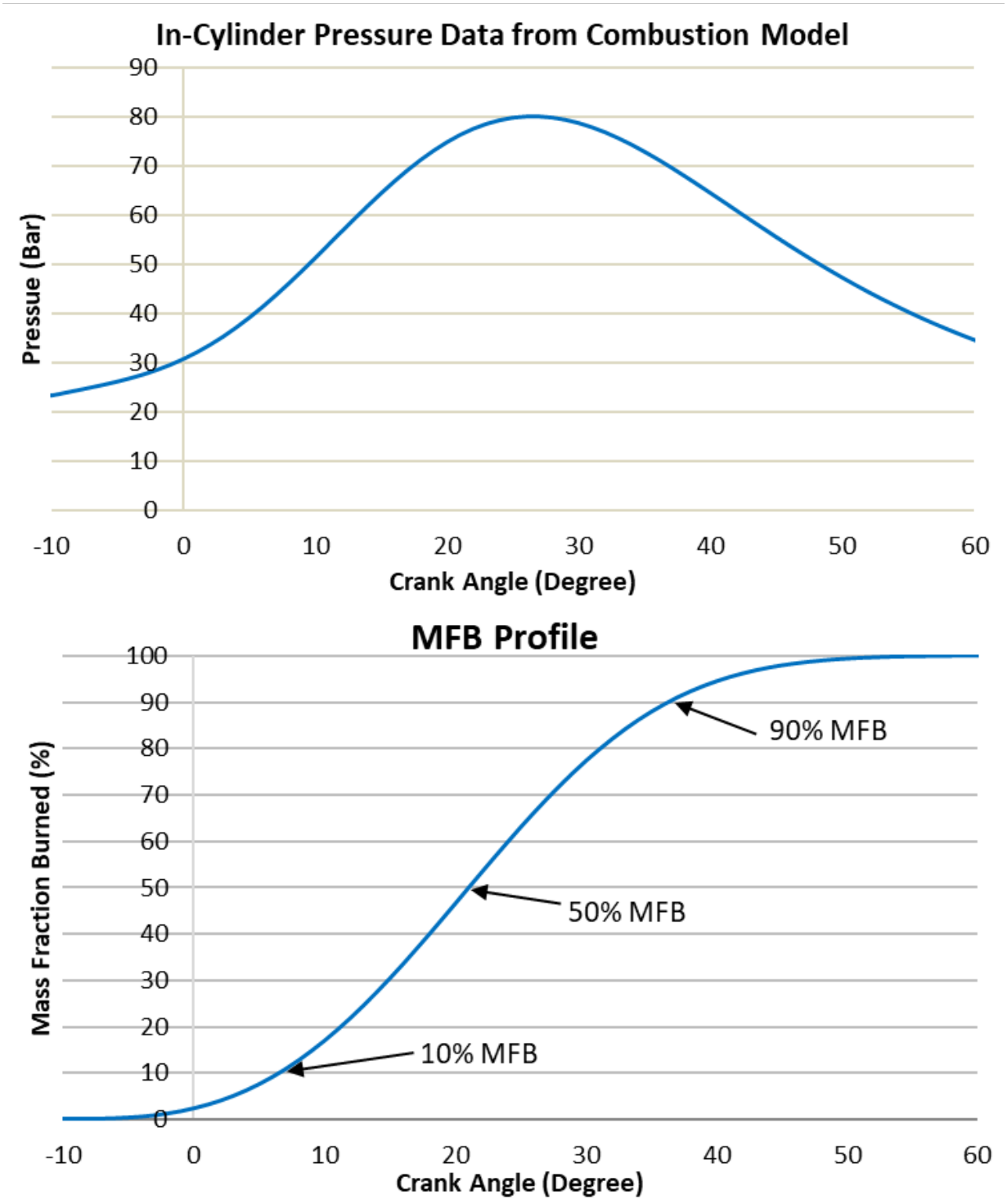

Figure 4: Mass Fraction Burned Vs In-cylinder pressure trace compared to crank angle.

Figure 4: Mass Fraction Burned Vs In-cylinder pressure trace compared to crank angle shows an in-cylinder pressure trace compared to a MFB profile, both are represented on a graph compared to crank angle and will be discussed later in the project.

MFB is the fraction of fuel burnt during combustion in relation to crank angle θ. One way of working out MFB is using the Wiebe Function, which is calculated using [19, 20]–

$$x_b = 1 - \exp[-a \times \left(\frac{\theta - \theta_0}{\Delta\theta}\right)^{m+1}]$$

Equation 19

where x_b is the MFB, θ_0 is the crank angle at the start of combustion, Δθ is the crank angle duration of combustion, m is the form factor, a is the efficiency parameter, and b is the amplitude correction factor, [18, 21]. Typically, a and m for an SI engine are a=5 and m=3, [1, 7, 41, 102].

$$x_b = \frac{\mu_b(i)}{\mu_b(total)} = \frac{\sum_{k=0}^{i} \Delta p_c(k)}{\sum_{k=0}^{n} \Delta p_c(k)}$$

Equation 20

Where n is the total number of crank angles. The MFB is the change in pressure within the cylinder in proportion to the mass of charge that is burnt. Another way of calculating MFB is to use pressure differentials form experimental data as seen in equation 20.

The MFB is commonly determined, in SI engines, by analysing the burn rate. This technique was developed by Rassweiler and Withrow [26], in 1938, and is considered accurate and computationally efficient, [2, 19] –

$$\Delta p = \Delta p_c + \Delta p_v = p_{1+1} - p_1$$

where Δp_c is the change in pressure due to combustion and Δp_v is the change of pressure due to the change in volume. As the crank moves through increments of θ_i through to θ_{i+1} so will the volume and the pressure move through increments of i thought to i + 1 [1, 2, 4, 19] –

$$\Delta p_c(i) = p_{i+1} - p_i \left(\frac{v_i}{v_{i+1}}\right)^{\gamma}$$

Equation 21

Hence the equation for change in pressure due to combustion (Δp_c) can be formed –

$$\Delta p_v = p_{i+1,v} - p_i = p_i \left[\left(\frac{v_i}{v_{i+1}}\right)^{\gamma} - 1\right]$$

Equation 22

Once HRR has been calculated, the data can be used to calculate the efficiency of the combustion. This is done by comparing the total heat released in combustion with the heat that was available from the fuel using the equation, [18] -

$$\eta_{combustion} = \frac{Q}{\left(\frac{m_c}{\frac{A}{F} + 1}\right) \times Q_{LHV}}$$

Equation 23

where A is the surface area of the combustion chamber, m_c is the mass of the charge, Q is heat and Q_{HLV} is the lower heat value.

The MFB curve can be split into three distinct points; 10%, 50% and 90% MFB, to highlight the combustion phasing [1, 17, 18]:

Start of combustion (10% of MFB) - There is a delay from spark ignition to the start of combustion that does not add much in terms of work done by the piston. MFB 0 – 10% is known as early flame development. The spark timing, and the subsequent ignition delay interval, have a significant effect on the shape and location of the MFB curve for a given Profile calibration. Therefore, MFB10 is a useful anchor point for comparison of combustion events and the first 10% is not used in the analysis. Ideally 0 – 100% MFB would be used for comparison but it is too difficult to experimentally define these locations on a MFB curve while MFB 10 allows for more accurate comparison of different MFB curves, [1, 17, 18, 22, 23, 24].

Midpoint (50% MFB) - The midpoint of combustion or 50% MFB is used to position the heat release curve and can give good indication of the efficiency of combustion by comparing it to TDC of the engine [1, 17, 18]. MFB50 is used as an anchor point to analyse the peak pressure during combustion as it allows for the combustion profile to be moved via a single reference point. MFB50 can be used as a good indicator of the point of maximum heat release, although it is not always accurate, [25, 22, 23, 24].

End of combustion (90% MFB) - The last 10% of combustion again adds little to no work to the piston as there is almost no heat given off from the charge as the majority of the fuel/air mixture has been burnt. It is hard to estimate when Flame extinguishment happens so again 90% allows more accurate comparison of MFB curves. Again, MFB90 is a useful anchor point in for comparison of combustion [1, 17, 18]. The coefficients; m, the form factor, a, the efficiency parameter, and b, the amplitude correction factor, of MFB are adjusted using the 10%, 50% and 90% combustion phasing points to get a more realistic combustion model, [18, 21, 22, 23, 24]. 90% MFB is used as there is often a ‘long burn out phase’ when analysing the real-time data, which is associated with the bad signal to noise ratio as found by [13].

Combustion duration (10-90% MFB) - The combustion duration MFB10-90 is an important parameter in engine development due to the amount of information that can be gathered from it, such as the speed of combustion and how that relates to the speed and movement of the piston, [22, 23, 24].

2.3. Dynamics model literature review

This section will look into the basic expressions and equations that describe component motion by displacement, velocity and acceleration.

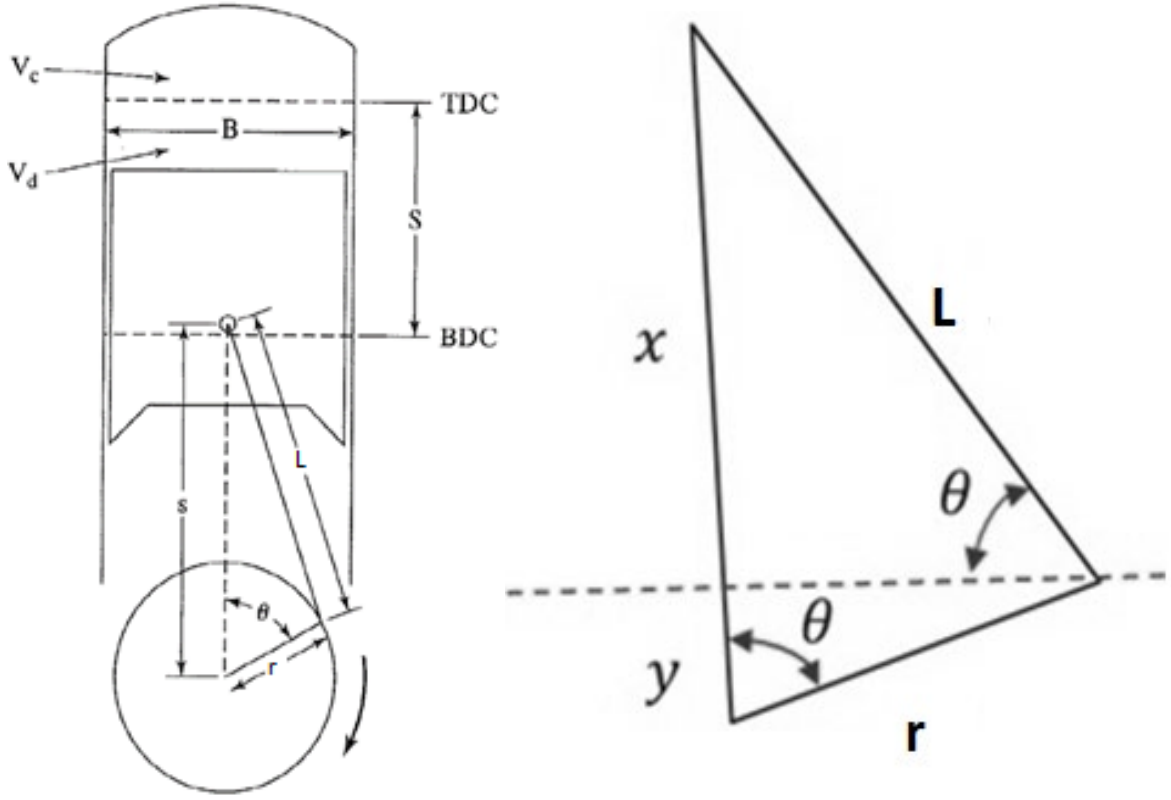

Figure 5: Engine cylinder schematic and breakdown representation of cylinder volume parameters [31, 110, 111]

The Compression Ratio is the ratio of the Total Volume to the Clearance Volume. The Clearance Volume is the volume at TDC and is sometimes referred to as the Combustion Chamber. The Swept Volume is the total volume the piston sweeps, and fluctuates from no volume at TDC to the max engine displacement at Bottom Dead Centre (BDC), [38, 39]. –

$$r_c = \frac{(V_d + V_c)}{V_c}$$

Equation 24

Due to the oscillations of the piston going up and down the stroke, a term can be formed by combining the total stroke length and the speed of the engine, this gives an indication of how many times, and how far, the piston has moved along the stroke per unit of time.

Piston displacement

The cylinder volume is the given by the equation –

$$V = \frac{\pi \times diameter^2}{4} \times length\ of\ cylinder$$

Equation 25

The Bore is the diameter and the Stoke is the length of the cylinder so therefore the Swept volume is given by [38, 39] –

$$V_{swept} = \frac{\pi}{4} \times B^2 \times S = V_{TDC} + V_{BDC}$$

Equation 26

The Cylinder Volume is the sum of the Clearance Volume V_c and the Displacement Volume V_d as a factor of θ, [1, 40]. The Clearance Volume, V_c, is defined by the area of the cylinder and the combustion chamber when the piston is at Top Dead Centre (TDC).

$$V = V_c + \frac{\pi \times B^2}{4} \times X$$

Equation 27

where X is the piston distance from TDC [1, 32]. To analyse the piston characteristics, the distance between the piston and the centre of axis of the crank shaft, X, has to be calculated to give the distance at any point in the stroke. Furthermore, the velocity and acceleration can be calculated by the derivative of the original distance calculation. [3, 5, 38, 39]. X can be found by the differential equation [1, 39, 41, 42] –

$$X = \frac{S}{2}\cos\theta + L\left[1 - \left(\frac{S}{2L}\sin\theta\right)^2\right]^{\frac{1}{2}}$$

Equation 28

where X is the piston position, s is the length of stroke and is equal to twice the crankshaft offset r, $\cos\theta + L$ is the primary force and $\left[1 - \left(\frac{S}{2L}\sin\theta\right)^2\right]^{\frac{1}{2}}$ is the secondary force term. L is the con-rod length

Piston velocity

The second differential of the piston distance equation gives Velocity [38, 39, 41, 42] –

$$\dot{X} = -\frac{S}{2}\omega\left(\sin\theta + \frac{\varepsilon}{2}\sin 2\theta\right)$$

Equation 29

where $\dot{X}$ is the approximation of the piston velocity, ω is the angular velocity and equates to the change in crank angle over change in time, dθ/dt, and ε is the con-rod-to-crankshaft offset ratio, and is equal to s/2L. The piston velocity will give an indication of flow velocity in and out of the engine, and the applied forces on the components, such as the con-rod and the journal bearings. It is an important factor in the analysis and development of the manifolds and the valve seats.

The equation is a function of time t and as θ=ωt. It will be preferable to present the equations as a function of crank angle θ, [1, 7] –

$$\dot{X} = S_p = \frac{dX}{dt} = \frac{dX}{d\theta}\frac{d\theta}{dt} = \frac{dX}{d\theta}2\pi N$$

Equation 30

therefore [38, 39] –

$$\frac{dX}{d\theta} = -a\sin\theta + \frac{1}{2}(L^2 - a^2\sin^2\theta)^{\frac{1}{2}}(-2a^2\sin\theta\cos\theta) = -a\sin\theta - \frac{a\sin\theta\cos\theta}{\sqrt{L^2 - \sin^2\theta}}$$

Equation 31

therefore [38, 39] –

$$|S_p| = \frac{dX}{dt} = 2\pi N\frac{dX}{d\theta} = 2\pi N\left(a\sin\theta - \frac{a\sin\theta\cos\theta}{\sqrt{L^2 - \sin^2\theta}}\right) = 2\pi N a\sin\theta\left(1 + \frac{\cos\theta}{\sqrt{L^2 - \sin^2\theta}}\right)$$

Equation 32

which leads to the piston speed as a function of crank angle θ [38, 39] –

$$|S_p| = (\pi \times S \times N) \times sin\theta \left[1 + \frac{cos\theta}{\sqrt{R^2 - sin^2\theta}}\right]$$

Equation 33

To find Instantaneous Piston Speed, the ratio must be used [38, 39] –

$$\frac{S_p}{\bar{S}_p} = \frac{\pi}{2}sin\theta \left[1 + \frac{cos\theta}{\sqrt{R^2 - sin^2\theta}}\right]$$

Equation 34

The Instantaneous Piston Speed (IPS) allows the speed of the piston to be analysed through the cycle and also allows for the maximum speed of the piston to be found, which gives the air flow velocity for the plenum analysis.

Piston acceleration

The third differential gives Acceleration [1, 39, 41, 42] –

$$\ddot{X} = -\frac{s}{2}\omega^2(\cos\theta + \varepsilon\cos 2\theta)$$

Equation 35

Where $\ddot{X}$ is the approximation of the piston acceleration.

Engine balancing

Engine balancing is a critical part of engine development because the internal components of the engine are subjected to large stress loads from the high inertia and gas loads applied to them. If rotating masses are not balanced then undue stress will be exerted on the engine, with the potential to cause fatigue and drastically reduce the life of the engine components. A balanced engine will not only run more smoothly, but potentially will be more efficient as there will be less force opposing the power stroke. In a piston-driven internal combustion engine the force from the pressure within the cylinder, created by the fuel combusting, is converted into a rotational motion by the crank slider mechanism [1, 7, 43]. To understand the engine dynamics and investigate the engine balancing the dynamics can be split into different sections [38, 39],

- Kinematics
- Pressure forces
- Momentum from both torque and inertia
- Balancing multiple cylinders

Analysis of engine dynamics and balancing can be split into 2 different sections; rotating and reciprocating masses. The motions of these masses cause inertia forces and vibrations within the engine [38, 39].

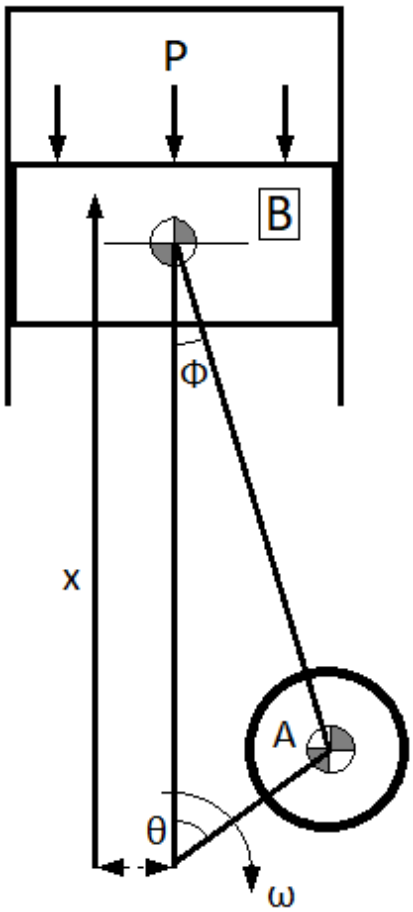

Figure 6: Diagram of both the reciprocating and rotating masses and the gas force pressure showing the forces acting on the engine components.

P, as seen in Figure 6: Diagram of both the reciprocating and rotating masses and the gas force pressure showing the forces acting on the engine components., is the pressure force acting on

the piston and it is internal so there should be minimal vibrations associated with it. Mass A is the rotating mass. Mass B is the reciprocating mass and must have the piston mass added to it.

2.3.1. Analysis of reciprocating and rotating masses

At the start of the development of the engine a lot of critical parameters are not known, such as the mass of the components, the Centre of Gravity (CoG) and the inertia forces. Due to the complexity of its motion and because within a piston there is a reciprocating mass and a rotating mass connected by the connecting rod, the con-rod has to be split into two components for anaylsis, one mass connected to the gudgeon pin and the other to the big end/crank pin [1, 7, 38, 39, 43].

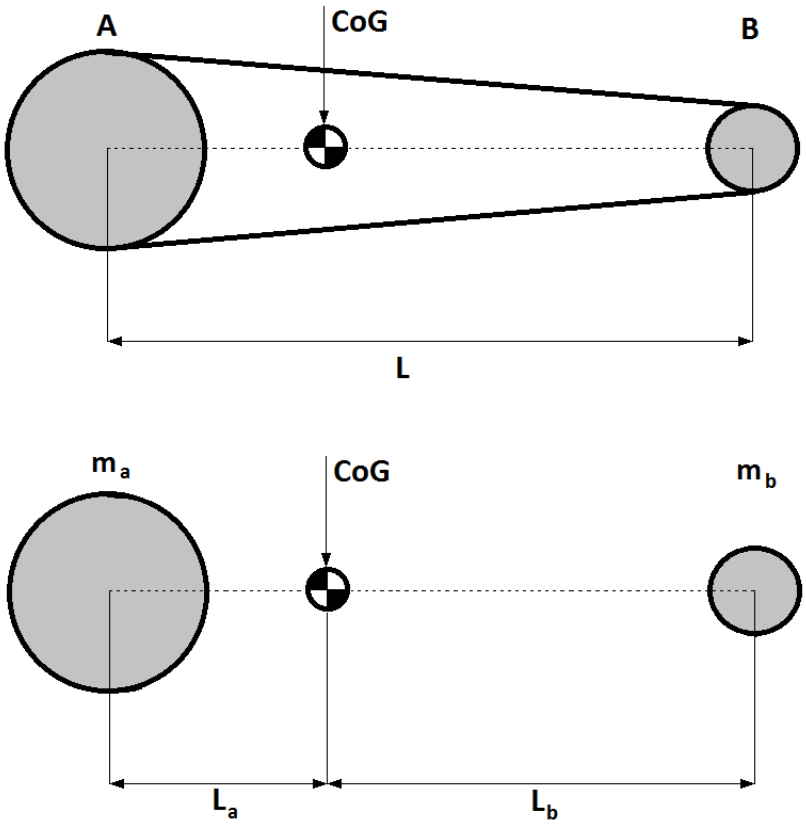

Figure 7: Diagram indicating the centre of gravity of the con-rod.

The total mass of the con-rod has been split into two masses, Mass A and Mass B, shown in Figure 7: Diagram indicating the centre of gravity of the con-rod.. This figure shows the CoG of the con-rod. Mass A incorporates the mass of the con-rod acting on the crank pin while Mass B is the mass of the con-rod acting on the gudgeon pin and the mass of the piston assembly [1, 7, 38, 39, 42, 44, 45].

$$m_A = m_c \frac{L_b}{L_a + L_b} \quad \textbf{and} \quad m_B = m_c \frac{L_a}{L_a + L_b} + m_p$$

Equation 36

The inertia forces-

$$a_B = \ddot{x} \cong -\frac{s}{2}\omega^2(\cos\theta + \varepsilon \cos 2\theta)$$

Equation 37

In order to balance the forces of the internal components, the equation above is used with both a positive and negative component. As shown below –

$$m_A\left[-\frac{s}{2}\omega^2(\cos\theta+\varepsilon\cos 2\theta)\right]=-m_B\left[\frac{s}{2}\omega^2(\cos\theta+\varepsilon\cos 2\theta)\right]$$

Equation 38

Acceleration of Mass A –

$$\frac{s}{2}\omega^2$$

Equation 39

Inertia force resulting from Mass A –

$$m_A\frac{s}{2}\omega^2$$

Equation 40

This will have components in both the X and Y direction

$$m_A\frac{s}{2}\omega^2\sin\theta\ \ \boldsymbol{and}\ m_A\frac{s}{2}\omega^2\cos\theta$$

Equation 41

Therefore F_i, the total inertia force, can be either expressed in terms of its X component or its Y component [38, 39,41]–

$$F_{i_x}=m_A\left(\frac{s}{2}\omega^2\sin\theta\right),$$

Equation 42

$$F_{i_y}=m_A\left(\frac{s}{2}\omega^2\sin\theta\right)+m_B\left[\frac{s}{2}\omega^2(\cos\theta+\varepsilon\cos\theta)\right]$$

Equation 43

The X and the Y components of F_i also act on the block and can cause the block of the engine to vibrate. The forces that can cause these vibrations are in equations [38, 39, 41] –

$$F_{s_x}=m_A\left(\frac{s}{2}\omega^2\sin\theta\right).$$

Equation 44

$$F_{s_y}=m_A\left(\frac{s}{2}\omega^2\sin\theta\right)+m_B\left[\frac{s}{2}\omega^2(\cos\theta+\varepsilon\cos\theta)\right]$$

Equation 45

The V-Twin, examined in this project, had the majority of its parts modelled and therefore, using the equations discussed in this section, allowed the con-rod to be split-up and analysed in the methodology section.

2.3.2. Forces within the engine

When the acceleration has been calculated then the forces due to the reciprocating masses can also be calculated. The Inertia forces are given by the equation [1, 39, 42] –

$$F_r=m_r\frac{s}{2}\omega^2(\cos\theta+\varepsilon\cos 2\theta)$$

Equation 46

Once the speed and acceleration of the reciprocating masses has been assessed then the forces due to these masses can be calculated using the equation [1, 7, 38, 39, 42, 44, 45] –

$$F_r = m_r \frac{s}{2}\omega^2(\cos\theta + \varepsilon\cos 2\theta)$$

Equation 46

Rotational mass counter weight calculation

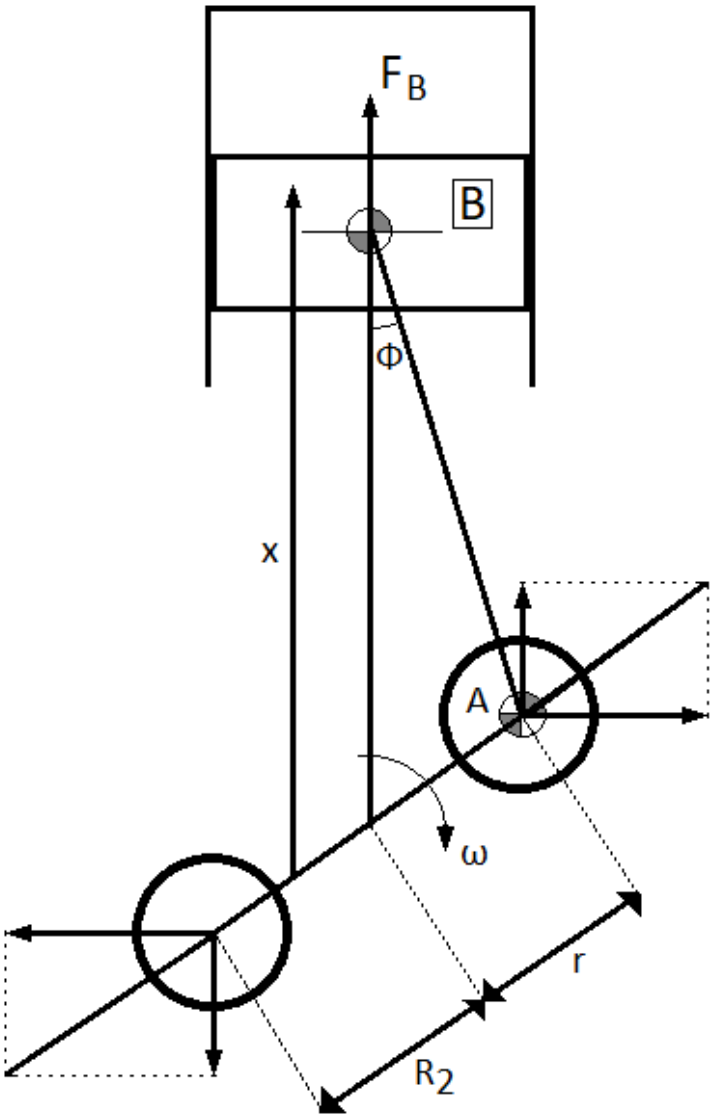

Figure 8: Diagram of the rotating mass and balancing mass.

The equation used to calculate the counter weight is given by, [1, 2, 39, 41] –

$$F_B = m_A(r\omega^2)$$

Equation 47

where F_{Bal} is the balancing force, m_a is the mass to be balanced, r is the distance to the rotating mass and ω is the rotational velocity

Once the Force to be balanced has been worked out then it must be balanced using the equation, [1, 2, 39, 41] –

$$F_{Bal} = m_{cw-B}(R\omega^2)$$

Equation 48

where F_{Bal} is the force needed to be countered, m_{cw-b} is the mass needed to counter the rotating mass, R is the distance of the balancing weight form the rotational axis, ω is the rotational velocity.

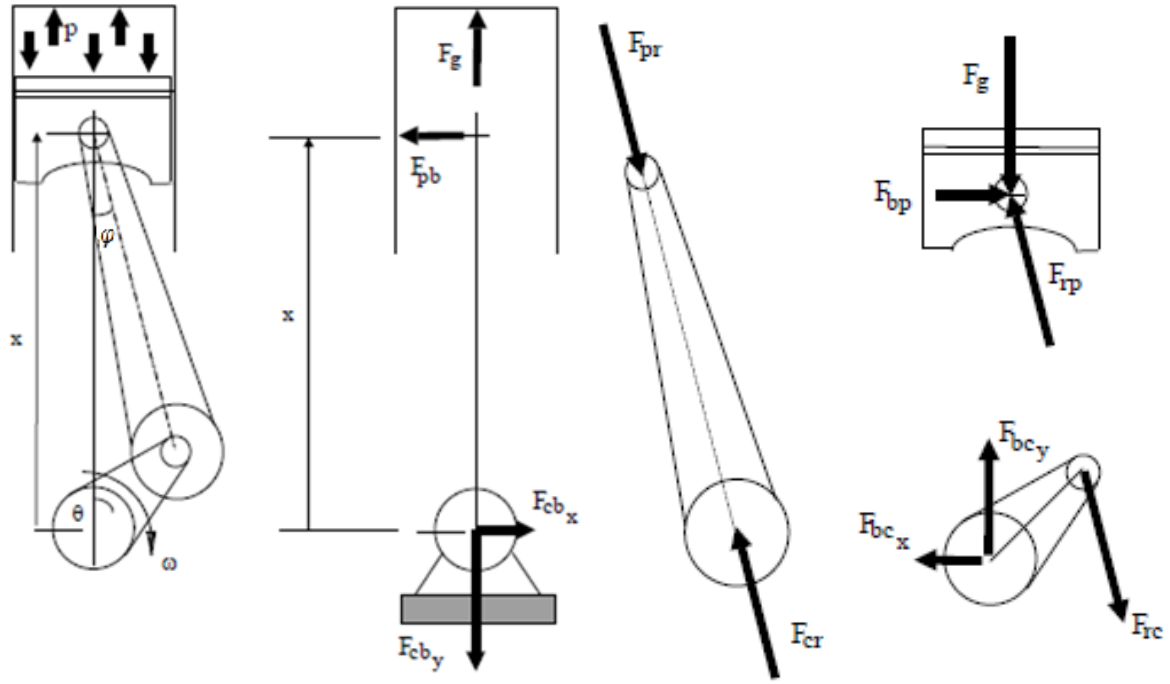

Figure 9: Representation of forces acting on the individual engine internal components [33, 110, 111]

Gas force on the piston is required to start the calculations for the crank slider mechanism. The equation used to find the gas force is [1, 39, 41] –

$$F_g = \frac{\pi}{4} d^2 p$$

Equation 49

Once the gas force has been calculated then the forces acting on the internal components of the engine can be determined. The force component F_{bp} can be calculated using trigonometry and the angle ϕ. The equation calculating F_{bp} is [1, 39, 41] –

$$F_{bp} = F_g \tan\varphi$$

Equation 50

Once the component F_{bp} has been calculated then the driving torque acting on the engine can be found by calculating the force component F_{rc} acting on the big end bearing. F_{rc} can be found using the negative of force component F_{pb} acting at a distance X from the crankshaft rotational axis. Thus the reaction torque due to F_{pb} can be calculated using the equation [1, 39, 41] –

$$T_g = -F_{pb}x = F_{bp}x = F_g \tan\varphi\, X$$

Equation 51

When the expression for X given above is substituted into the equation the driving torque calculation is given by [1, 39, 41] –

$$T_g = F_g \tan\varphi \left(a \times \cos\theta + (r^2 - a^2 \times cos^2\theta)^{\frac{1}{2}} \right)$$

Equation 52

To simplify the equation, ϕ can be taken out using the three expressions [1, 39, 41] –

$$\tan\varphi = \frac{\frac{S}{2}\sin\theta}{L\cos\varphi} \; \boldsymbol{and} \; \cos\varphi = \left[1 - \left(\frac{S}{2L}\sin\theta\right)\right]^{\frac{1}{2}} \; \boldsymbol{Therefore} \; \tan\varphi = \frac{\frac{S}{2}\sin\theta}{L\left[1 - \left(\frac{S}{2L}\sin\theta\right)\right]^{\frac{1}{2}}}$$

Equation 53

Using binomial theorem to expand the three expressions results in [1, 39, 41] –

$$[1 - (\varepsilon\sin\theta)^2]^{-\frac{1}{2}} = 1 + \frac{1}{2}(\varepsilon\cos\theta)^2$$

Equation 54

Rewriting the equation in terms of the square root in the denominator the higher order terms can be neglected, this gives [1, 39, 41] –

$$\tan\varphi \cong \frac{S}{2l}\sin\theta\left(1 + \frac{\varepsilon^2}{2}\sin^2\theta\right)$$

Equation 55

When the expression for gas torque is substituted into the equation the driving torque is given by the equation [1, 39, 41] –

$$T_g \cong F_g \frac{S}{2l}\sin\theta\left(1 + \frac{\varepsilon^2}{2}\sin^2\theta\right)\left[L - L\frac{\varepsilon^2}{4} + \frac{S}{2}\left(\cos\theta + \frac{\varepsilon}{4}\cos 2\theta\right)\right]$$

Equation 56

To simplify the equation it can be expanded, with all the terms of ε to a power greater than 1 neglected, the equation can be given by [1, 39, 41] –

$$T_g = F_g \frac{S}{2}\sin\theta\,(1 + \varepsilon\cos\theta)$$

Equation 57

2.3.3. Analysis of gas forces

The total torque forces acting on the crankshaft from the reciprocating masses are the sum of the torque forces, T_{tot}, which is the sum of both pressure T_g and inertia T_i. The Torque gas T_g from the pressure within the cylinder can be assessed by the equation [38, 39] –

$$T_g = F_g \frac{s}{2} \sin\theta \, (1 + \varepsilon \cos\theta)$$

Equation 57

This is an approximation of the Fourier expansion from the equation [38, 39] –

$$T_g = F_{bp} X = F_g \tan\varphi \, X$$

Equation 58

where [38, 39] –

$$F_g = \frac{\pi}{4} d^2 p$$

Equation 59

The equation for torque inertia is given by [38, 39] –

$$T_i = -m_B \times \left(\frac{S}{2}\right)^2 \times (\omega)^2 \times \sin\theta \times \left(\frac{\varepsilon}{2} + \cos\theta + \frac{3}{2} \times \varepsilon \times \cos 2\theta\right)$$

Equation 60

The torque inertia allows the amount of force required to start the internals rotating to be calculated, and shows how the internals will react after a force has been applied to them. The results of the torque inertia were input into the GT-power models to improve the accuracy. It's also important that the engine is properly balanced as an unbalanced engine will have a reduced the life span, because the unbalanced forces will cause excessive wear on the internal components. The extra loads caused by an unbalanced crankshaft will cause the engine to not run as smoothly and to consume more fuel for a given engine load. It is possible also for internal components to fail, with significant consequences for the engine.

2.4. Manifold design and optimisation

Design change and tuning of intake and exhaust manifolds can improve engine performance, using acoustics analysis, Helmholtz resonance theory and Ram effect [46]. This tuning process needs to be associated with valve timing control strategies. Optimised valve timings with tuned manifolds can offer 'natural supercharging effect' by using compressed inlet pressure. This optimisation was be evaluated using a developed GT-power 1D-simulation model in order to propose the future development of hardware.

It is well-established that a naturally aspirated engine can be tuned to have volumetric efficiencies of over 100% using the ram-air effect.

The rules governing the whole intake within the RS rule book are [47] –

IC1.4- Air Intake System

IC1.4.1- Air Intake System Location

All parts of the engine air and fuel control systems (including the throttle or carburettor, and the complete air intake system, including the air cleaner and any air boxes) must lie within the surface defined by the top of the roll bar and the outside edge of the four tyres. (See below).

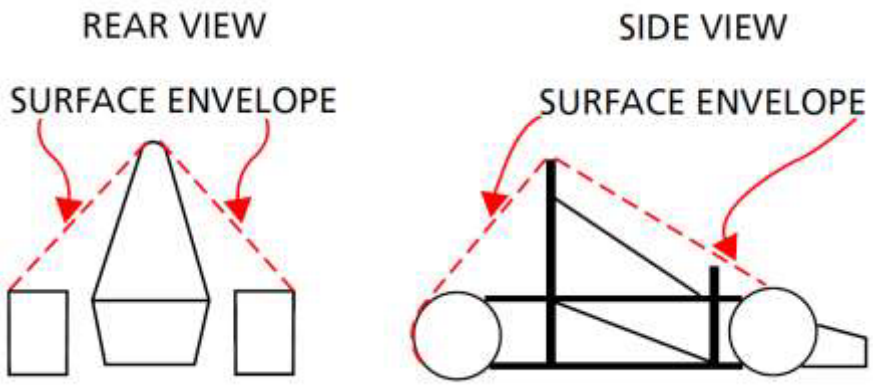

Figure 10: The space where an intake is permitted to be located according to the SAE FS rules [47]

2.4.1. Intake system

Optimisation of engine performance using intake and exhaust systems to increase power has been done almost as long as internal combustion engines have been around. There are multiple methods to calculate the optimal geometry required for a specific application. Most methods have positives and negatives. Acoustic analysis, via Helmholtz resonance theory and the Ram effect, can be used to improve the design of the intake and exhaust manifold. This tuning process needs to be associated with valve timing control strategies. Optimised valve timings with tuned manifolds can offer 'natural supercharging effect' by using compressed inlet pressure, [46, 48, 49].

The simplest way of describing the acoustic waves is to apply organ tuning theory to them using the equation below [48, 49] –

$$f_p = \frac{c}{4L}$$

Equation 61

where L is the effective pipe length, c is the speed of sound and f_p is the frequency of the pipe. One of the original pieces of work in the area was done by Helmholtz [50]. The theory was first introduced in Herman von Helmholtz's' book in 1862 [50]. The Helmholtz resonator theory is an effective way of tuning intake and exhaust manifolds. The origins of the theory come from Newton's 2nd law, shown in Figure 11: Comparison of the similarities between a Helmholtz resonator and a vibration absorber [49, 50].

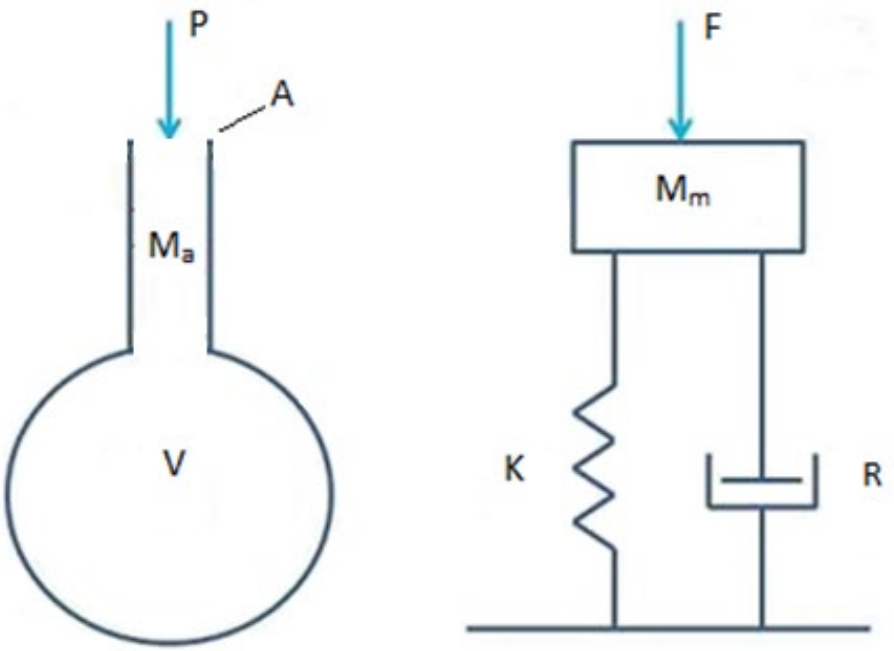

Figure 11: Comparison of the similarities between a Helmholtz resonator and a vibration absorber

$$m\frac{d^2x}{dt^2} = (p_i - p_v)A$$

Equation 62

where m is the total mass in the runner, A is the runner cross sectional area, pi is the pressure at the inlet, pv is pressure at the valve and x is the displacement of the air. Rearranging gives the equation [49, 50] –

$$m\frac{d^2x}{dt^2} + p_v A = A \times p_i$$

Equation 63

The assumption can then be made that the gas is acting as an ideal gas. Therefore, the adiabatic compression can be represented as [49, 50] –

$$dp = -\gamma p\frac{dv}{v} = -\gamma p\frac{dV}{V}$$

Equation 64

The instantaneous pressure can be described by [49, 50] –

$$p_v = \frac{\rho c^2 A}{V}x$$

Equation 65

The equation can then be substituted into the original expression to give [49, 50] –

$$m\frac{d^2x}{dt^2} + \frac{\rho c^2 A}{V}x = Ap_i$$

Equation 66

The resonator acts like a spring damper. Therefore, the equation of motion for a vibrating system can be used, which is [49, 50] –

$$F = m\frac{d^2x}{dt^2} + kx$$

Equation 67

And thus [49, 50] –

$$k = \frac{\rho c^2 A}{V},$$

Equation 68

$$F = Ap_i,$$

Equation 69

$$and\ m = \rho AL$$

Equation 70

When the equations are combined, the expression below is formed [49, 50] –

$$f = \frac{\omega}{2\pi} = \frac{c}{2\pi}\sqrt{\frac{k}{m}} = \frac{c}{2\pi}\sqrt{\frac{A}{L \times V}}$$

Equation 71

Where f is the frequency of the air, ω is the angular velocity of the engine, c is the speed of sound, k is the harmonic order, A is the area of the throat, L is the length and V is the volume for a given crank angle.

2.4.2. Restrictor design

The rules require the use of a restrictor to limit the amount of air that can enter the engine, and therefore the amount of power the engine can produce. The rules also limit the total displacement. The rules that govern the restrictor are, [47] –

IC1.1.3- If more than one engine is used, the total displacement cannot exceed 610 cc and the air for all engines must pass through a single air intake restrictor (see IC1.6 "Intake System Restrictor.")

IC1.6.1- In order to limit the power capability from the engine, a single circular restrictor must be placed in the intake system and all engine airflow must pass through the restrictor. The only allowed sequences of components are the following:
a. For naturally aspirated engines, the sequence must be (see Fig 1): throttle body, restrictor, and engine.

IC1.6.2- The maximum restrictor diameters which must be respected at all times during the competition are:
a. Gasoline fuelled cars - 20.0 mm (0.7874 inch)
b. E-85 fuelled cars – 19.0 mm (0.7480 inch)

IC1.6.3- The restrictor must be located to facilitate measurement during the inspection process.

IC1.6.4- The circular restricting cross section may NOT be movable or flexible in any way, e.g. the restrictor may not be part of the movable portion of a barrel throttle body.

IC1.6.5- If more than one engine is used, the intake air for all engines must pass through the one restrictor.

The restrictor is a critical part of the inlet system as it governs the amount of air that can enter the engine. It is critical in engine design to maximise the mass flowrate and minimise any losses through the restrictor. To start assessing the inlet system a mass flowrate must be calculated through the restrictor, as this is the start of the system and sets the upper limit of the amount of air than can enter the inlet. [68]

$$\dot{m}_{air} = \frac{A_{throat} \times P}{\sqrt{T}} \times \sqrt{\frac{\gamma}{R}} M \left(1 + \frac{\gamma - 1}{2} \times M^2\right)^{-\frac{\gamma+1}{2(\gamma-1)}}$$

Equation 72

M_{air} is the mass flow rate of air, T_{hroat} is the cross-sectional area of throat, P is the pressure, T is the temperature, R is the ideal gas constant, ϒ specific heat ratio and M is the Mach number.

2.4.3. Runner design

The rules governing the inlet runners are [47] –

IC1.7.5 The maximum allowable Inlet Diameter (ID) of the intake runner system between the restrictor and throttle body is 60 mm diameter, or the equivalent area (i.e. 2827 mm^2) if non-circular.

To model the pressure waves within the intake system the runners can be analysed using organ pipe tuning theory with the pressure waves within the runner described by the equation below [48, 49] –

$$f_p = \frac{c}{4L}$$

Equation 73

where L is the effective pipe length, c is the speed of sound and f_p is the frequency of the pipe. The organ pipe tuning theory takes into account how quickly sound can travel down a pipe of a set length but organ tuning theory does not take into account the diameter of the pipe, which can have a significant effect on the frequency of the waves. When the pipe diameters and volumes are taken into account the cylinder and intake can be thought of as a Helmholtz resonator, which can be described by the equation [48, 49] –

$$f_H = \frac{c}{2\pi}\sqrt{\frac{A}{L \times V}}$$

Equation 74

where A is the cross-section of the pipe area, L is the effective pipe length, V is the volume of the resonator, c is the speed of sound and f_H is the frequency. To minimise the assumptions in the Helmholtz resonator equation, the parameters are broken down further in the rest of this section [49, 68] –

The effective volume of the engine is half the displacement volume as this is when the piston is at its maximum velocity. The equation for describing the effective volume is [69] –

$$V_e = \frac{V_d}{2} + V_c$$

Equation 75

where V_d is the displacement volume and V_c is the clearance volume.

The length of the runner is ascertained from the equation, and as it is not the full length calculated as the length of runner needs to be separated from the port length. The length calculated is the full length on which the frequency acts, so it needs to be halved for the runner as the wave travels to the end and back. The equation to describe the runner length is [69] –

$$L = \frac{l + l_p}{2}$$

Equation 76

where l is the pipe/runner length and l_p is the port length.

The velocity of the wave does not always travel at the speed of sound. It travels at the wave propagation velocity, which can be described by [49, 69] –

$$C_w = a_0 + C_s$$

Equation 77

where C_s is the practical velocity and a_0 is the local speed of sound, and can be described by the equation [49, 69] –

$$a_0 = \sqrt{\gamma \times R \times T}$$

Equation 78

where R is the ideal gas constant, γ is the specific heat ratio and T is the temperature.
The practical velocity C_s can be described by the equation [70, 71] –

$$C_s = 2 \times \frac{2}{\gamma - 1} \times a_0 \times \left(\frac{P_i}{P_0}^{\frac{\gamma-1}{2\times\gamma}} \right)$$

Equation 79

where γ is the specific heat ratio, P_i is the incident pressure and P_0 is the reference pressure.
Once all these equations are brought together they can be rearranged to give length –

$$L = \frac{A}{V_e \times \left(\frac{f_H}{\frac{C_W}{2 \times \pi}} \right)^2}$$

Equation 80

The length required for the runners reduces as engine speed increases which is described by the final equation settled on to determine the length of the inlet runners was [70, 71] –

$$L = \left(\frac{955 \times c}{K \times N} \right)^2 \times \left(\frac{A}{V_{eff}} \right)$$

Equation 81

where L is the length in mm, c is the speed of sound in m/s, K is the number of revolutions per power cycle (2 for a four-stroke engine), N is the engine speed in RPM, A is the runner area, and V_{eff} is the effective volume defined by half the swept volume added to the clearance volume. This equation is also utilised to ascertain the exhaust length.

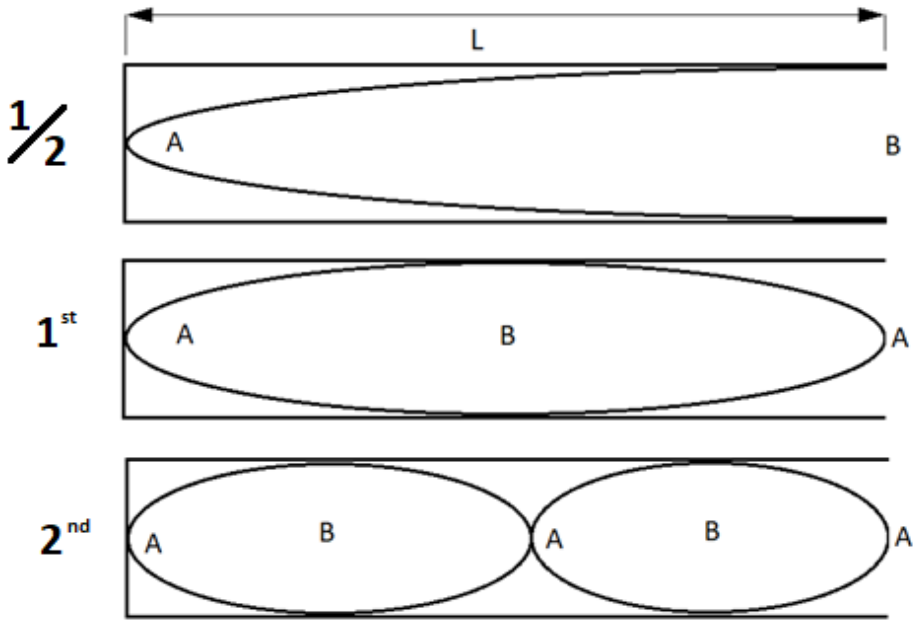

Figure 12: Comparison of wave forms of harmonic orders in a set pipe length

The harmonic orders are related to the peaks and troughs associated with the pressure waves within a pipe. As can be seen in Figure 12: Comparison of wave forms of harmonic orders, the waves within a pipe has have peaks, shown by B, and troughs, shown by A, which match up to either give a pressure increase or decrease for a particular frequency at with peak or trough. The wave length defines where these peaks and troughs are along the length of pipe and can mean two pipes of different lengths can still give the same benefits in terms of tuning. To ascertain which harmonic order will be most suited to the V-twin application, the equation below was utilised, [70, 71] –

$$L_n = \frac{L}{n}$$

Equation 82

where L_n harmonic length, L is the original length and n is the harmonic order.

2.4.4. Plenum design

The 2018 SAE Formula Student rules that govern the plenum are [47] –

IC1.7.4- Plenums anywhere upstream of the throttle body are prohibited. For the purpose of definition, a "plenum" is any tank or volume that is a significant enlargement of the normal intake runner system. Teams are encouraged to submit their designs to the Rules Committee for review prior to competition if the legality of their proposed system is in doubt.

In an ideal plenum the pressure will be close to atmospheric (or as low as possible) to create a pneumatic damper which will stop the pressure waves from the runner and restrictor from interfering with each other. Minimising pressure wave interference can maximise the RAM air effect, allowing an engine theoretically to have volumetric efficiencies of over 100%.

To assess the flow within the system the choked flow limit of the inlet port had to be assessed using the equation [68] –

$$\dot{m}_{air} = \frac{A_{throat} \times P}{\sqrt{T}} \times \sqrt{\frac{\gamma}{R}} \times \left(\frac{\gamma + 1}{2}\right)^{-\frac{\gamma+1}{2(\gamma-1)}}$$

Equation 72

2.5. Engine simulation literature review

1D engine simulation is an essential step in engine design and development. 1D simulations are essentially simplified 3D models and only deal in a single plane or direction. 1D simulation is commonly used to evaluate parameters such as valve dimensions and lift, as well as manifold design, [73]. If there is no access to experimental combustion data [81] has stated that a 1-D non-predictive model is the most accurate way to simulate the combustion event. [81] goes on to say that GT-Power was the chosen software for its versatility and extensive library of internal combustion engine components.

1D engine simulation commonly requires the building of a models composed of sub-models, each running a specific task/calculation. During this 'Block' building assumptions or simplifications must be made for each sub-model before the simulation can be run. 1D engine simulation is not a 'one stop shop' but the first step in the design process. Whilst 3D simulation might give more accurate results, the significant advantages in using 1D are that it is faster and less demanding of computing power, and therefore also less expensive. 1D engine simulation software allows for the quick identification of potential design problems and can highlight areas that need improving without the time and cost involved in developing a full 3D model, [73].

It was found by [75] that a non-predictive model in GT-Power could cut simulation times by more than 50% compared to a predictive model. One drawback of 1D simulation is the limited solvers unless implemented by external software such as Matlab or Simulink. However, engine development is an iterative process for which 1D analysis has been found to be an excellent starting point, [72, 73]. One limitation found by [76] was that the MFB profile calculated by the single Wiebe model cannot account for a combustion that has different rates of combustion before and after 50% MFB. This limitation can be calibrated by a double Wiebe function model within GT-Power, although real-time data is needed to calibrate the double Wiebe model while the single Wiebe model does not need the real-time data. [77] went onto say that although using the double Wiebe model increased the accuracy of the model is also increased computational complexity. When calculating a predictive model, engine modelling software was found by [76] to do a poor job of capturing transients and discontinuities, which is more evident when calculating stochastic engine operation. Whereas the effects of parameters such as BSFC, CR, fuel composition, BMEP, Knock and volumetric efficiency can be shown effectively by the simulations. [77] states that, due to the Wiebe model computing parameters as a function of engine geometries and operating conditions through physically based parameters, the user can have confidence in the simulations results for GT-Power, while using any of the heat release method of combustion simulation within GT-Power requires accurate in-cylinder temperature data for comparison and calibration.

There are multiple 1D engine simulation software products available on the market. Well known examples include GT-Power, Ricardo Wave and Virtual Engines. The software chosen for this project is GT-Power, which is a part of the GT-Suite simulation family of software, made up of multiple software packages which analyse different parts of the engine and powertrain. Each of the packages within GT-Suite is based upon a common library of equations, leading to the benefit that the multiple stages of engine development simulation can be integrated together into a coherent package. Simulations run on GT-Suite can also be integrated with simulations run on other software products, such as STAR-CD, Simulink, Matlab and EXCEL, [74].

GT-Power is, when calibrated correctly, known to be reliable based on evidence from a large user population who have tested and validated its real-time accuracy, [92, 93, 94]. Meyer, J, [79], states that engine simulation software should be used alongside engine test cell calibration, as a well calibrated model can allow more in-depth analysis of the engine than engine calibration in a test cell alone. This is due to GT-Power being able to calculate the residual gas fractions which would otherwise be very hard to measure accurately. Although GT-Power recommends between 25-200 points of data to calibrate the engine models while Kumar, M, et al, [80], only used 25 points due to time constraint. The project had an accuracy limit for the models of within ±5% efficiency accuracy and managed average IMEP inaccuracy of ±2.2% when compared to measured in-cylinder data. Hatlevold, E, S, [78], found that, with calibration from in-cylinder data, ±2% accuracy could be achieved with a GT-Power simulation model. Although Hatlevold goes onto say that it was common to find a discrepancy of ±4% when comparing peak pressure with real-time data.

In order to start the development of a GT-Power model, there are parameters that need to be known in order to start the process. The parameters that were needed to start the construction of the model can be seen in Table 2: Initial Engine Specs for Model Development, [82] –

section	parameter	value	unite	reference
engine characteristics	compression ratio	12.45	ratio	measured from engine
	firing order	1 then 2	-	measured from engine
	engine configuration	V-Twin	-	measured from engine
	angle of cylinders	75	deg	measured from engine
	2 or 4 stroke	4 stroke	-	measured from engine
cylinder geometry	bore	92	mm	measured from engine
	stroke	45.13	mm	measured from engine
	con-rod length	103	mm	measured from engine
	pin offset	0	mm	measured from engine
	piston bowl geometry	-	-	input from CAD models
	piston area	-	-	input from CAD models
	head area	-	-	input from CAD models
intake and exhaust system	geometry of manifolds	-	-	input from CAD models
	runners	311	mm	measured from engine
	exhaust	614	mm	measured from engine
	ports	-	-	input from CAD models
throttles	location	start of intake	-	input from CAD models
fuel injectors	number	2	-	measured from engine
	location	Port injection	-	measured from engine
	discharge coefficient	-	-	given by manufacturer
	air - fuel ratio	14.7	ratio	stoichiometric
	fuel type	pump gasoline	-	limited by SAE FS rules
intake and exhaust valves	Intake valve lift	10.978	mm	input from CAD models
	exhaust valve lift	9.727	mm	input from CAD models
	lift profile	-	-	input from CAD models
	discharge coefficients	-	-	calculated parameter
ambient state	pressure	1	bar	Ambient conditions
	temperature	300	K	Ambient conditions

Table 2: Initial Engine Specs for Model Development

Some of the critical outputs that can be extracted from an engine simulation are Power, torque, IMEP, BSFC and Volumetric Efficiency.

2.6. V-twin engine performance and calibration

2.6.1. Knock

Knocking or detonation is one of the main factors limiting modern SI engine performance. Knock is where the air/fuel charge within the cylinder self-combusts, causing higher temperatures and pressures in the cylinder. This can have a degrading effect on engine performance and can cause extreme pressure on components, and their wear and even failure. Knock detection is a critical part of engine development and engine performance optimisation. The leaner an engine runs the more likely that knock will occur due to the increased likelihood that pre-ignition or Compression Auto Ignition (CAI) would happen within the cylinder. Pre-ignition or CAI causes a sharp increase in pressure in the cylinder before the piston is at TDC. The increase in pressure can cause excessive pressure in the cylinder and can result in severe engine component damage. In effect, maximum fuel efficiency is achieved in conditions in which an engine is more likely to knock, as both are a function of less fuel being injected per cycle.

Ideally combustion starts at the sparkplug and propagates outwards towards the cylinder wall until the fuel/air charge is fully burnt, giving smooth and controlled combustion. The rate at which the charge burns gives the engine one of its performance characteristics. The optimal crank angle, after TDC, for peak pressure, and the time taken for the charge to burn, give an indication of which crank angle, before TDC, the fuel should be ignited. If the charge ignites before that given crank angle, or the fuel combusts quicker than its calculated time, the fuel can ignite as the piston is still compressing the air/charge inside the cylinder. This is knocking and can cause a peak in pressure and temperature far higher than it would otherwise have been. In some cases, the pressure inside the combustion chamber can be high enough to damage the internal components.

The higher the performance of the engine, the more likely there will be the conditions for knocking to occur. To reduce the risk of knock, parameters such as spark timing, injection timing, injection duration, CAM timing and AFR can be adjusted. Alternately these parameters can be kept at levels more consistent with optimum performance and knocking controlled with an anti-knock strategy.

Knock detection

There are two main ways to detect knock. The first is analysis of the in-cylinder pressure trace and the other is vibration or noise analysis of the engine. Within a non-knocking engine cycle, the heat released from the fuel follows a predictable profile. Within a knocking engine cycle the heat release rate has a measurably different profile. If knock is detected then anti-knock strategies can be put in place to limit it.

Vibrational or noise knock detection

Vibrational knock detection is usually done using a vibration sensor attached on the outside of the block. Vibrational analysis is a cheaper way of detecting knock, but it is not as accurate as the analysis of an in-cylinder pressure trace.

In-cylinder pressure knock detection

In-cylinder pressure knock detection is done using an in-cylinder pressure trace, which is an expensive but more accurate way of detecting knock.

Knock detection

One method of detecting auto ignition and knocking conditions is comparing the oscillations of the in-cylinder pressure trace, and is done using the equation [30, 31, 32] –

$$MAPO = \max[|\hat{p}|]_{TDC}^{TDC+N^0}$$

Equation 83

where MAPO is the Maximum Amplitude of Pressure Oscillations, $\hat{p}$ is the filtered in-cylinder pressure/pressure osculation signal and N is the number of crank angles chosen to compare.

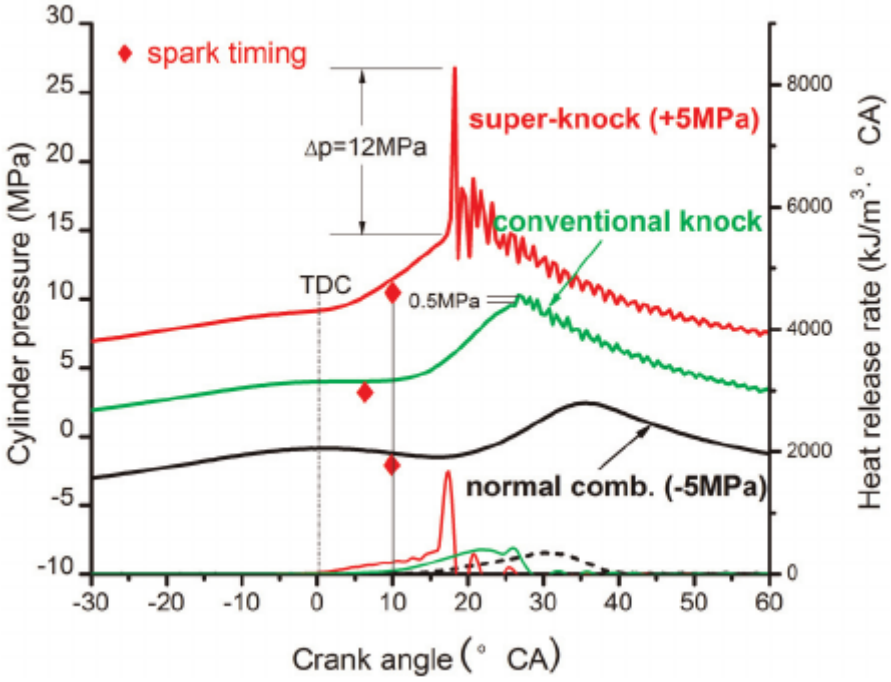

Figure 13: A comparison of Maximum amplitude of pressure oscillations over knocking cycles, [12].

Another method is using the HRR and comparing it to MFB50. When the auto ignition happens before MFB50 then the fuel/air mixture combusting in front of the flame front causes rapid increases in pressure and temperature, which can be detected using an in-cylinder pressure trace. Auto-ignition will also shorten the combustion duration and change the crank angle at which MFB50 takes place. The equation used for the HRR is [30, 31, 32] –

$$\frac{dQ}{d\theta} = \frac{1}{\gamma - 1} V \frac{dp}{d\theta} + \frac{\gamma}{\gamma - 1} p \frac{dV}{d\theta} + \frac{dQ_{ht}}{d\theta}$$

Equation 14

Q is the combustion heat energy release, Q_{ht} is the heat energy transfer to the chamber wall, V is the volume, θ is the crank angle and γ is the specific heat ratio. The time of auto-ignition is estimated by the solution of t_{aA} is given by the solution of [30, 31, 32] -

$$1 = \int_{t_{SOC}}^{t_{aA}} \frac{dt}{\tau_{ch}}$$

Equation 84

where $t_{aA} < t_{EOC}$ and t_{SOC} is the start of combustion time and t_{EOC} is the end of combustion time. For Hydrocarbons τ_{ch} is expressed by [30, 31, 32] –

$$\tau_{ch} = C_{a1} \times p^{-Ca2} \times exp\left(\frac{C_{a3}}{T_e}\right)$$

Equation 835

where T_e is the end-gas temperature. Ca1, Ca2 and Ca3 are fuel Octane Number which are given as $C_{a1} = 17.68 \times 10^{-3}$, $C_{a2} = 1.7$ and C_{a3} is 3800 according to [32] showing the higher the octane of the fuel used the more resistant it is to knock in the first place.

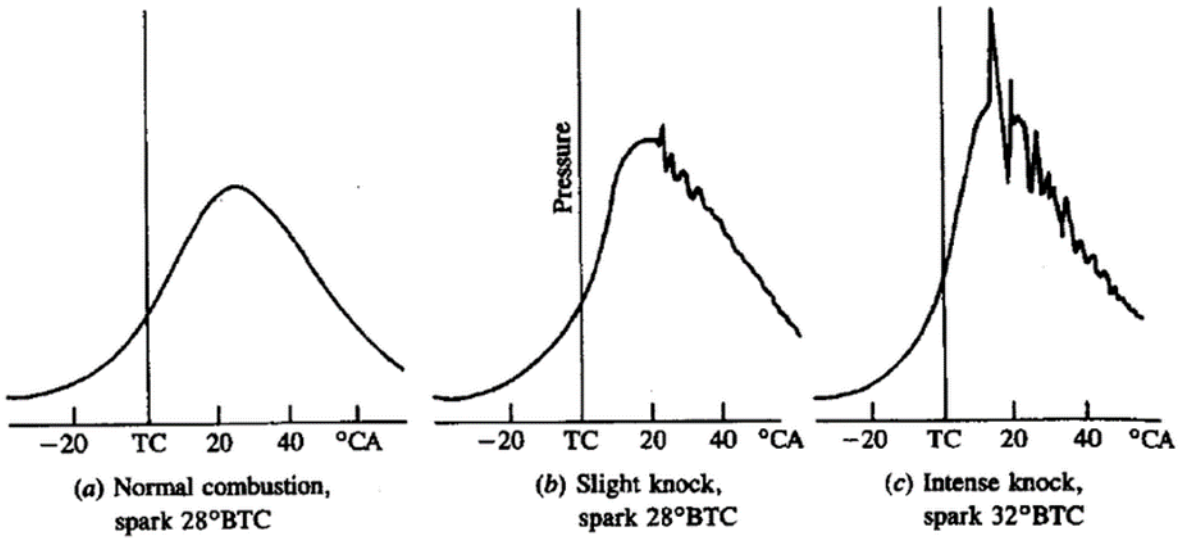

Figure 14: A comparison of knocking and non-knocking pressure traces, used to identify knocking engine cycles [1].

Another method of analysing knock is to detect the resonance, caused by auto-ignition. This resonance, which can occur after TDC and towards the end of combustion, can be detected within the cylinder, and can be calculated from in-cylinder pressure using the equation, [30, 31, 32] –

$$\frac{\partial^2 p}{\partial t^2} = C^2 \nabla^2 p$$

Equation 846

where t is time, C is the speed of sound and $\nabla^2 p$ is the Laplacian equation regarding change in pressure p, [30, 31, 32].

Anti-knock strategy

One of the easiest and quickest ways to reduce knock, is to retard the spark timing. This method can be applied individually to each cylinder, allowing performance to be optimised for each cylinder. This anti-knock strategy doesn't have to limit performance in all the cylinders to the same degree, therefore allowing a better overall performance.

Another method of countering knock is to delay the fuel injection timing as this will have a similar effect to the retarding the spark timing, but it can only be done on an engine with Direct Injection. Port Injection is reliant on the valve timing.

Another method is to use a higher Octane of fuel as higher Octane fuels have improved anti knock properties. Pump fuel ranges from 95 Octane to 101 Octane, and in this study the highest-Octane pump fuel of 101 Octane was be used as it helps reduce knock as well as improve performance.

Water injection can also allow in-cylinder temperatures to be reduced and therefore is another method to prevent engine knock.

Integration into the GT-Power model
All of the combustion profiles that can be selected, when constructing a GT-Power model, can utilise a predictive knock model by selecting a knock reference object within the selected combustion profile. The knock model reference objects allow phenomenological predictions of knock and/or pre-ignition tendencies based on multiple empirical correlations for induction time, based on work done by Worrent, Franzke and Eyzart et al [106, 107, 108]. However, the quantitative predictions of knock must be calibrated with experimental engine measurements, [10].

2.6.2. Valve Train

The valve train can be split into 6 main areas –

Valve Lift (VL) – The VL directly affects the performance of the engine, with a larger VL giving higher performance. This has been linked in some literature to the viscous effect of the attached jet having proportionately more impact with a smaller VL [7].

Inlet valve opening (IVO) – IVO has a large impact on engine performance as it directly affects the amount of air that can enter the engine [2]. Retarding the IVO past the piston TDC can help the inertia of the fluid to be overcome in the intake manifold, which should lead to an increase in volumetric efficiency [84, 85, 86]. In Reference [84] it was found that there was an increase in torque with IVO before Top Dead Centre (bTDC), with 20 degrees CA bTDC giving the best results. Retarding the IVO further caused the power to fall off again, the drop in power being assessed to be due to an increase in Exhaust Gas Recirculation (EGR), with lower performance due to some of the charge in the cylinder being made up of exhaust gas thus giving less oxygen to burn.

Inlet valve closing (IVC) – IVC has a large impact on engine performance and should take account of the application for which the engine is being designed [1, 86]. The ideal point of IVC is when there is the maximum volume of air in the cylinder. Following the ideal engine cycle, optimum IVC is at Bottom Dead Centre (BDC), although at this point there is still air coming into the engine from the natural supercharging effect caused by pressure differences in the engine. Taking into account the reduced time for air to enter the cylinder at higher engine speeds, IVC should be retarded to maximize the performance of the engine [45]. At lower engine speeds and when the engine isn't at wide-open throttle/fully loaded, the inlet IVC ideally should be advanced to reduce the pumping losses within the engine [88].

Exhaust valve opening (EVO) – EVO is a trade-off between extracting the maximum amount of exhaust gas from the cylinder and being able to extract the maximum amount of work from the engine delivered by expansion of the burnt charge [89]. The knock-on effect of an increase in exhaust gas in the cylinder at IVO is that there is a higher pressure in the cylinder and a reduction in the natural supercharging effect and therefore lower volumetric efficiencies [86, 89]. Another factor that has to be taken into account is that at higher engine speeds there is less time for the exhaust gas to be extracted and therefore the EVO should ideally be retarded. Reference [85] found that taking into account the exhausting of the burnt charge, the optimal EVO for race engines is about 90 degrees CA bBDC, and for road engines around 50-60 degrees CA bBDC. The EVO CA varies with engine speed as well as load, as both of these factors affect the in-cylinder pressure. A reduced in-cylinder pressure benefits from a retarded EVO, [86].

Exhaust valve closing (EVC) – EVC affects the amount of Exhaust Gas Recirculation (EGR) that is present in the engine. Advancing the EVC can increase the amount of exhaust gases in the cylinder at lower engine speeds, as indicated in [90]. This is done to improve the emissions of the engine. The negative effect of advancing the EVC, however, is that it reduces the performance and can cause instability in the combustion event, leading to knock from the increased combustion temperatures. At higher engine speeds an advanced EVC leads to higher volumetric efficiencies due to the natural supercharging effect, as the air is drawn in by the lower pressures in the exhaust and EGR is not allowed to happen as the valve closes at the optimal time [84, 85, 86].

Valve overlap (VO) – VO has to be controlled carefully as, depending on the engine speed, the VO can either be beneficial or detrimental to engine performance. At high engine speeds the overlap draws more air into the cylinder as, if the inlet frequencies are tuned right, there is lower pressure in the cylinder and even lower pressure in the exhaust manifold. A larger intake overlap benefits higher engine speeds while a smaller overlap benefits lower engine speeds. At lower engine speeds if there is too much overlap, there is a negative effect on the pressure differential. However, at higher engine speed, more time is needed for the effects to be seen, so a larger overlap is needed, which can increase volumetric efficiencies. However, at low engine speeds this effect can draw the air out into the exhaust causing lower volumetric efficiency [2, 5, 90].

Further work will look into the potential of variable valve timing, as this can offset some of the problems associated with having fixed valve timing. Variations in timing can potentially deliver benefits across the rev range and allow valve timing to be optimised at multiple engine speeds [101, 102].

2.7. Computational Fluid Dynamics (CFD)

Introduction

CFD is the solving of fluid dynamic problems via numerical analysis and algorithms which allow complicated fluid flows to be accurately predicted by computers. Computers are needed because of the complexity of the problems. Modern CFD software can not only calculate the fluid flow behaviour but also parameters such as heat transfer, mass and mechanical movements.

Navier-Stokes

The majority of Computational Fluid Dynamics (CFD) packages on the market utilise the Reynold-Averaged Navier-Stokes (RANS) equations which are the core of CFD. CFD packages have grown in complexity since the 1980s, especially with the physical modelling but with less emphasis on geometric complexity. On the other hand Computer Aided Design (CAD) have become commonplace, if not crucial, to the design process within industry with modern CAD packages allowing the development of complex shapes to be constructed with ease. In 1990 the first Mechanical Computer Aided Design (MCAD) system had a CFD package, SolidWorks FloWorks, incorporated into it. This allowed the CFD package to use the native CAD geometry without any required modification at the start of the process, [92]. SolidWorks FlowSim solves the Navier-Stokes Equations in the fluid region, which are formulations of Momentum, Mass and energy conservation Laws [91, 92, 93, 94].

The Continuity equation. A three-dimensional continuity equation for a compressible fluid can be used to describe the conservation of mass, [98]. –

$$\frac{\partial \rho}{\partial t} + \frac{\partial (\rho u_1)}{\partial x_i} = 0$$

Equation 857

where ρ is the fluid density, t is the temperature and u is the fluid velocity. The first term is the rate of change of density over the change in time. The net mass flow of the elements across the boundaries is described by the second term, [93, 99].

The Momentum equation. The rate of change of momentum can be described, according to Newton's second law, by the momentum equation known as the Navier-stokes equation, [98] –

$$\frac{\partial u_i}{\partial t} + u_j \frac{\partial u_i}{\partial x_j} = -\frac{1}{\rho}\frac{\partial p}{\partial x_i} + \frac{1}{p}\frac{\partial \tau_{ji}}{\partial x_j} + g_i$$

Equation 868

where g is the gravitational accelerator, ρ is the fluid density, τ is the Viscous stress Tensor, t is the fluid temperature and u is the fluid velocity, [92, 98].

The Energy equation. Internal energy, U, in an incompressible fluid for a constant c_p can be describe by, [98] –

$$\rho \frac{dU}{dt} = -p\frac{\partial u_i}{\partial x_i} + \Phi + \frac{\partial}{\partial x_i}\left(k_m \frac{\partial T}{\partial x_i}\right)$$

Equation 879

where g is the gravitational accelerator, ρ is the fluid density, τ is the Viscous stress Tensor, t is the fluid temperature and U is the fluid velocity [92, 98]. Where –

$$\Phi = 2\mu S_{ij}S_{ij} - \frac{2}{3}\mu S_{ii}S_{kk}$$

Equation 90

where μ is the dynamic viscosity and S_{ij} is the strain-rate tensor, given by, [92, 98] –

$$S_{ij} = \frac{1}{2}\left(\frac{\partial u_i}{\partial x_j} + \frac{\partial u_j}{\partial x_i}\right)$$

Equation 881

where g is the gravitational accelerator, ρ is the fluid density, τ is the Viscous stress Tensor, t is the fluid temperature and u is the fluid velocity [92, 98].

Meshing

CAD software is used to define solid models, whereas CFD software is used to describe the flow space. More commonly in CFD the Fluid space is created by Boolean subtraction of a solid model within CAD. This is then passed onto the CFD in order to mesh the model, [92]. Meshing can be done via irregularly distributed nodes for complex shapes, often referred to as unstructured mesh, or by structured mesh for less complex shapes. A combination of the two can be used, with unstructured meshes used around complex shapes and near boundaries, and the structured mesh used everywhere else. This is often referred to as partially structured mesh. This process is done via a mesh generator built into most CFD software [92, 98].

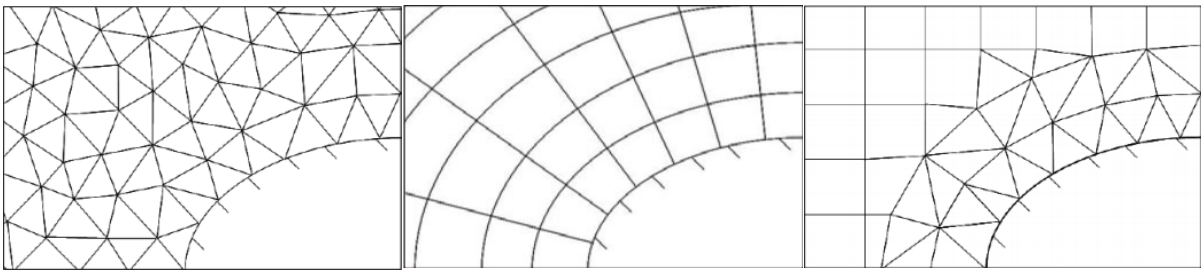

Figure 15: a shows of irregularly distributed mesh, b shows structured distributed mesh and c shows partially structured mesh, [92].

The start of the meshing process usually happens at the surfaces, by means of Delaunay triangulation [96], then the space is meshed via the surface triangulation. The mesh is often generated with tetrahedral elements [97] that meet the Delaunay criterion [96]. It is often the case that, once the mesh has been generated, the user will have to solve any ambiguities and/or defects within the mesh or sort out any over-defined areas [92, 93, 94].

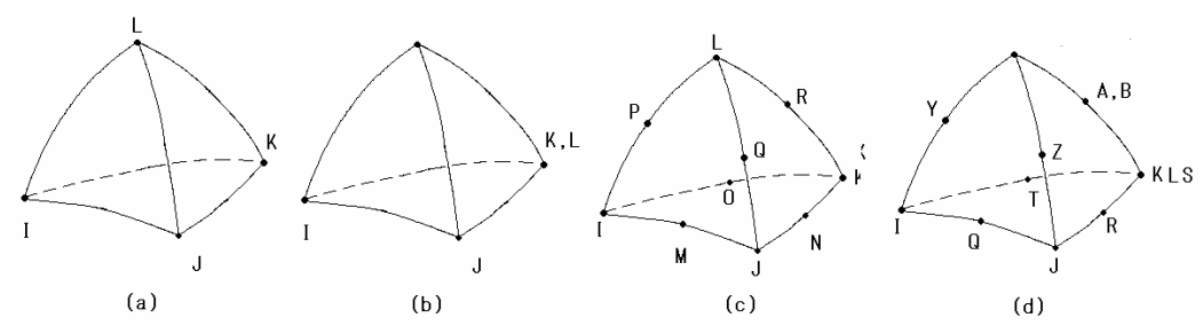

Figure 16: a is a first order tetrahedral element with 4 nodes, b is a degenerate first order tetrahedral element with 8 nodes, c is a second order tetrahedral element with 10 nodes, d is a degenerate second order tetrahedral with 20 nodes, [6].

The nodes lie on the intersection of the boundaries of the cells and are normally the starting points for the construction of the elements [97, 100].

Boundary conditions
The boundary conditions of the CFD simulation are an important part of setting up a simulation and are critical to the accuracy of the results. They can be split into different sections

Inlet and outlet boundaries
The inlet and outlet boundaries describe parameters such as Mass Flow Rate and velocities that are either entering or being drawn out of the fluid body. They normally describe the start of the simulation, but they can also be the parameter that is being measured if there is an event happening within the fluid body, [92, 93, 96, 98, 99].

Wall boundaries
The wall boundary is the edge of the fluid body that is not an inlet or outlet. The wall conditions describe how the fluid interacts with the wall in terms of parameters such as friction and shear force, allowing the turbulence and boundary layers of the fluid to be calculated within the fluid body. The heat transfer to and from the walls is also a critical parameter for accurate CFD simulations, [92, 93, 97, 98, 99].

Symmetry and axis boundary conditions
The common way of reducing simulation time and computing power required within industry is to halve a symmetrical model. Although this is may reduce the accuracy of a simulation, due to time constraints of processing power of a computer, this may be a preferable way of simulation. However as a lot of fluid flow simulations, especially turbulent or non-symmetrical inlet conditions, can give a number of possible simulation results, this may reduce the accuracy further, [92, 93, 95, 98, 99].

Initial conditions
The initial conditions boundaries relate to how the fluid in the fluid body is acting before the simulation starts, as this can have an effect on the results. More accurate initial conditions can improve the accuracy as well as the time taken for the simulation to run. Initial conditions also relate to the ambient conditions of the fluid entering the fluid body, [92, 93, 98, 99].

Chapter 3.Methodology

3. Methodology

3.1. Combustion

The combustion process will be analysed using combustion phasing, as this allows the combustion process to be broken down and analysed without going into a chemical kinetic combustion model, which would be too complex and time consuming. Representing the in-cylinder combustion through combustion phasing will highlight key areas of the combustion and allow for further analysis. Combustion phasing will be represented by the use of Heat Release Rate (HRR) and Mass Fraction Burn (MFB). Analysing combustion phasing through HRR and MFB will allow different areas of combustion to be analysed, such as the efficiency of the combustion and where optimal peak pressure should ideally be within the cycle.

The combustion model theory was combined into an Excel template to analyse the combustion process and allow for further tests of the different Wiebe model parameters to be incorporated into the GT-power model. Figure 18**: A representation of the combustion model constructed in Excel.** shows a representation of the Excel model, the figures from the model have been shown in detail throughout the project so a detailed view was not deemed necessary.

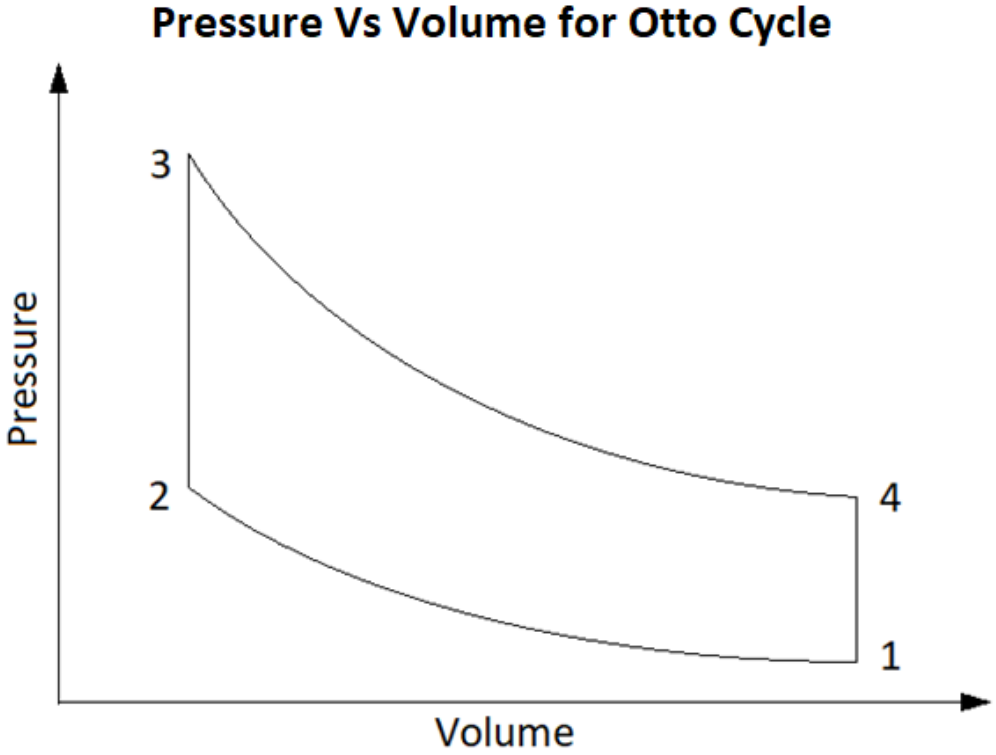

Figure 17: Otto cycle Pressure Volume profile

The PV diagram shown in Figure 17: represents the combustion stroke of the Otto cycle. The start of the cycle is at 1, the reduction in volume and increase in pressure comes from the piston compressing the air inside the cylinder and finishes at 2. From 2 to 3 is the heat/pressure addition at constant volume from combustion. 3 to 4 is the reduction of pressure and increase in volume as the piston moves back down the cylinder. 4 to 1 is back to the start of the cycle but doesn't include the exhaust and the intake stroke which accounts for the change in pressure due to the intake of ambient air. When the value for energy release is calculated then the Otto cycle trace can be calculated and the results put into an Excel Spreadsheet in order to allow analysis of the engine and the combustion model. The Otto cycle, for the compression and

expansion stroke, uses the ideal gas equation expression pV^{γ}=constant and is calculated using the following equations [1, 7, 41, 45] –

$$P(\theta) = p_0\left(\frac{V_c + V_d}{V(\theta)}\right)^{\gamma} \; and \; T(\theta) = T_0\left(\frac{V_c + V_d}{V(\theta)}\right)^{\gamma-1} \; for \; compression$$

Equation 892

$$P(\theta) = p_3\left(\frac{V_c}{V(\theta)}\right)^{\gamma} \; and \; T(\theta) = T_3\left(\frac{V_c}{V(\theta)}\right)^{\gamma-1} \; for \; expansion$$

Equation 903

The Otto cycle assumes that there is ideal heat addition which means that all the heat that can be released by the fuel/air charge is released at the optimal point. Due to the compression at TDC, this is assumed to be the ideal point for the energy to be released, although it is a little after TDC as this is when the piston starts to move back down the cylinder and therefore comes under least resistance from the forces of inertia. Energy release must be worked out using the equations [1, 7, 41, 45] –

$$T_3 = T_2\frac{m_{fuel}h_{LHV}}{m_{air}c_{va}} \; \boldsymbol{and} \; p_3 = p_2\frac{T_3}{T_2}$$

Equation 914

After TDC the Otto cycle follows isentropic expansion with the equations [1, 7, 41, 45] –

$$T_3 = T_2 + \frac{m_{fuel}h_{LHV}}{m_{air}c_{va}} \; \boldsymbol{and} \; p_3 = p_2\frac{T_3}{T_2}$$

Equation 925

The Mass Fraction Burn by McCuiston, Lavoie and Kauffman (MLK) model, [109], can be used to create a experimental combustion model or a theoretical combustion model can be constructed using the Wiebe method. An experimental version matches known data, such as a pressure trace, in order to construct the model. Whereas a theoretical model uses the fundamental equations in order to construct the model. Once the Q_{cycle} has been worked out, then the heat release can be calculated using the Wiebe function over the combustion phase [1, 7, 41, 45] –

$$Q_{Cycle} = m_{fuel}h_{LHV} = \frac{mass_{air}}{AFR}h_{LHV}$$

Equation 936

Once the Q_{cycle} has been worked out, then the heat release can be calculated, using the Wiebe function, over the combustion phase [1, 7, 41, 45] –

$$x_b = \frac{Q_{actual}}{Q_{cycle}} = \; 1 - \exp[\,-a \; \times \left(\frac{\theta - \; \theta_0}{\Delta\theta}\right)^{m+1}\,]$$

Equation 19

Where x_b is the mass fraction burn, θ_0 is the crank angle at the start of combustion, and $\Delta\theta$ is the crank angle duration of combustion. The typically for a and m for an SI engine are a=5 and m=3. In order to show the $dQ/d\theta$ in terms of J/Rad [1, 7, 41, 45] –

$$\frac{dQ}{\mathrm{d}\theta} = \frac{Q_n - Q_{n+1}}{\theta_n - \theta_{n+1}}$$

Equation 947

The parameters m, a and b were investigated and compared to those for similar engines to create a more accurate combustion model and improve the simulations run in GT-power, [19, 20].

For the shaft work of the engine, [1, 7, 41, 45] –

$$\dot{W}_{shaft} = \frac{dW_{shaft}}{dt} = \frac{(p - p_0)dV}{dt} = \tau\omega$$

Equation 958

Where τ is the toque and ω is the angular velocity, [1, 7, 41, 45].

In order to get the torque independent of velocity then divide through by angular velocity ω, and because ω=θ/t, to get [1, 7, 41, 45]-

$$\tau = \frac{dW_{shaft}}{d\theta} = \frac{(p - p_0)dV}{d\theta}$$

Equation 969

N	12000	rpm	200	rps	72000
bore	0.092	m			1256.6371
stroke	0.04513	m			
crank offset	0.022565	a	m		
con rod length	0.103	m	r (L)	0.022518	m
ε	0.21907767	AFR	14.7		
rpm	12000		R=2l/S	4.564591	
t/CA	1256.637061	72000	ω		
rads/360deg	6.283185307				
Vd	300	CC	0.000300007	mC	
Vc	26.20	CC	2.62015E-05	mC	
Cr	12.45				
pressure	1	100000	Pa		
temperature	20	293	K		
R air	287	j/kg K			
V	326.21	cc to mc	0.000326208		
mass air	0.00038792	Kg			
mass fuel	2.63893E-05				
AFR	14.7				
hLHV	46000000	j/kg			
Qcycle	1213.907834	Jules	1213.907834		
θ0 (s)	-10	deg	-0.174532925	-0.174533	
Δθ	60	deg	1.047197551	1.047198	0.8726646
hLHV	46	Mj/kg	a	5	
Y	1.4		m	3	
Y	1.3	ustry standard			
Cv	718				
R air	287	0.287	R/Cv	0.399721	
Cv air	718	0.718			
T1	293	T2	624.3360692	T3	4982.6253
P1	1	P2	26.52895584	P3	211.71906
V1	326.21	V2	26.20	V3	26.20
				T4	2338.3388
P1	100000	Pa		P4	
	4358.289277			V4	326.21
max p Weibe	80.0213	bar			
p/Area	53195.03	N			
force/area	5422.53	Kg	force/area	5.42	ton

	A	B	C	D	E	F	G	H	I	J	K	L
1								wrong	OTTO compression		Otto expansion	
2	θ (deg)	θ (rad)	t	Vd	Vθ	Vθ CC	dv/dθ	dv/dθ	P(θ) Otto	T(θ) Otto	P(θ) Otto	T(θ) Otto
3	-360	-6.28319	-0.005	0	2.62015E-05	26.20145343		4.4808E-20	26.5289558	624.336069	211.719063	4982.62535
4	-359	-6.26573	-0.00499	2.79E-08	2.62293E-05	26.2293044	2.7851E-08	3.1914E-06	26.4923418	624.137114	211.426858	4981.03755
5	-358	-6.24828	-0.00497	1.11E-07	2.63128E-05	26.31284447	8.35401E-08	6.3813E-06	26.383051	623.541985	210.554643	4976.28801
6	-357	-6.23083	-0.00496	2.51E-07	2.6452E-05	26.45203513	1.39191E-07	9.5682E-06	26.2027176	622.555843	209.115461	4968.41793
7	-356	-6.21337	-0.00494	4.45E-07	2.66468E-05	26.64681225	1.94777E-07	1.2751E-05	25.9540008	621.187148	207.130532	4957.49482
8	-355	-6.19592	-0.00493	6.96E-07	2.68971E-05	26.89708607	2.50274E-07	1.5927E-05	25.6404919	619.447452	204.628518	4943.61086
9	-354	-6.17847	-0.00492	1E-06	2.72027E-05	27.20274131	3.05655E-07	1.9097E-05	25.2665928	617.351118	201.64455	4926.8807
10	-353	-6.16101	-0.0049	1.36E-06	2.75636E-05	27.56363721	3.60896E-07	2.2257E-05	24.8373737	614.914994	198.21909	4907.43878
11	-352	-6.14356	-0.00489	1.78E-06	2.79796E-05	27.97960764	4.1597E-07	2.5408E-05	24.3584163	612.158036	194.396685	4885.43638
12	-351	-6.12611	-0.00488	2.25E-06	2.84505E-05	28.45046118	4.70854E-07	2.8546E-05	23.8356528	609.100909	190.224678	4861.03843
13	-350	-6.10865	-0.00486	2.77E-06	2.8976E-05	28.97598129	5.2552E-07	3.1672E-05	23.2752072	605.765583	185.751942	4834.42027
14	-349	-6.0912	-0.00485	3.35E-06	2.95559E-05	29.55592642	5.79945E-07	3.4783E-05	22.6832461	602.174926	181.027691	4805.76439
15	-348	-6.07375	-0.00483	3.99E-06	3.019E-05	30.19003014	6.34104E-07	3.7878E-05	22.065844	598.352316	176.100404	4775.25737
16	-347	-6.05629	-0.00482	4.68E-06	3.0878E-05	30.87800136	6.87971E-07	4.0955E-05	21.4288674	594.321287	171.016898	4743.08703
17	-346	-6.03884	-0.00481	5.42E-06	3.16195E-05	31.61952451	7.41523E-07	4.4014E-05	20.7778793	590.105198	165.821571	4709.43977
18	-345	-6.02139	-0.00479	6.21E-06	3.24143E-05	32.41425971	7.94735E-07	4.7053E-05	20.1180654	585.726952	160.555809	4674.4984
19	-344	-6.00393	-0.00478	7.06E-06	3.32618E-05	33.26184303	8.47583E-07	5.007E-05	19.454181	581.208755	155.257561	4638.44012
20	-343	-5.98648	-0.00476	7.96E-06	3.41619E-05	34.1618867	9.00044E-07	5.3064E-05	18.790518	576.571918	149.96108	4601.43502
21	-342	-5.96903	-0.00475	8.91E-06	3.5114E-05	35.11397936	9.52093E-07	5.6034E-05	18.1308886	571.836702	144.69679	4563.64478
22	-341	-5.95157	-0.00474	9.92E-06	3.61177E-05	36.11768635	1.00371E-06	5.8978E-05	17.4786246	567.022202	139.491281	4525.2218
23	-340	-5.93412	-0.00472	1.1E-05	3.71725E-05	37.17254999	1.05486E-06	6.1896E-05	16.8365884	562.146271	134.367396	4486.30857
24	-339	-5.91667	-0.00471	1.21E-05	3.82781E-05	38.27808983	1.10554E-06	6.4785E-05	16.2071936	557.225475	129.344399	4447.03728
25	-338	-5.89921	-0.00469	1.32E-05	3.94338E-05	39.43380304	1.15571E-06	6.7645E-05	15.5924332	552.275073	124.438194	4407.52971
26	-337	-5.88176	-0.00468	1.44E-05	4.06392E-05	40.63916467	1.20536E-06	7.0474E-05	14.9939117	547.309024	119.661587	4367.89727
27	-336	-5.86431	-0.00467	1.57E-05	4.18936E-05	41.89362802	1.25446E-06	7.3271E-05	14.4128807	542.340015	115.024565	4328.24121
28	-335	-5.84685	-0.00465	1.7E-05	4.31966E-05	43.19662501	1.303E-06	7.6035E-05	13.8502749	537.379501	110.534589	4288.65295
29	-334	-5.8294	-0.00464	1.83E-05	4.45476E-05	44.54756652	1.35094E-06	7.8765E-05	13.3067493	532.437757	106.196886	4249.21448
30	-333	-5.81195	-0.00463	1.97E-05	4.59458E-05	45.9458428	1.39828E-06	8.1459E-05	12.7827138	527.523941	102.014727	4209.99889
31	-332	-5.79449	-0.00461	2.12E-05	4.73908E-05	47.39082386	1.44498E-06	8.4117E-05	12.2783672	522.646159	97.9896994	4171.07088
32	-331	-5.77704	-0.0046	2.27E-05	4.88819E-05	48.88185987	1.49104E-06	8.6737E-05	11.7937282	517.811539	94.1219516	4132.48733
33	-330	-5.75959	-0.00458	2.42E-05	5.04183E-05	50.41828163	1.53642E-06	8.9318E-05	11.3286642	513.026299	90.4104248	4094.29787
34	-329	-5.74213	-0.00457	2.58E-05	5.19994E-05	51.99940094	1.58112E-06	9.1859E-05	10.8829169	508.29582	86.853059	4056.54544
35	-328	-5.72468	-0.00456	2.74E-05	5.36245E-05	53.62451111	1.62511E-06	9.4358E-05	10.4561259	503.624718	83.4469778	4019.26688
36	-327	-5.70723	-0.00454	2.91E-05	5.52929E-05	55.2928874	1.66838E-06	9.6816E-05	10.0478491	499.016907	80.1886517	3982.49342
37	-326	-5.68977	-0.00453	3.08E-05	5.70038E-05	57.00378751	1.7109E-06	9.9231E-05	9.65758031	494.475669	77.074042	3946.25126
38	-325	-5.67232	-0.00451	3.26E-05	5.87565E-05	58.75645203	1.75266E-06	0.0001016	9.28476513	490.003714	74.098724	3910.56203
39	-324	-5.65487	-0.0045	3.43E-05	6.05501E-05	60.55010499	1.79365E-06	0.00010393	8.92881416	485.603234	71.2579938	3875.44321
40	-323	-5.63741	-0.00449	3.62E-05	6.2384E-05	62.38395436	1.83385E-06	0.00010621	8.58911435	481.275962	68.5469588	3840.90865
41	-322	-5.61996	-0.00447	3.81E-05	6.42572E-05	64.25719251	1.87324E-06	0.00010844	8.26503856	477.023217	65.9606142	3806.96885
42	-321	-5.60251	-0.00446	4E-05	6.6169E-05	66.16899686	1.9118E-06	0.00011063	7.95595355	472.845952	63.4939062	3773.63145
43	-320	-5.58505	-0.00444	4.19E-05	6.81185E-05	68.11853029	1.94953E-06	0.00011276	7.66122654	468.744797	61.1417848	3740.90145

Figure 18: A representation of the combustion model constructed in Excel.

The combustion model allowed critical factors of the combustion event to be analysed post simulation and allowed for a greater understanding of the combustion event, the outcomes of the model development were –

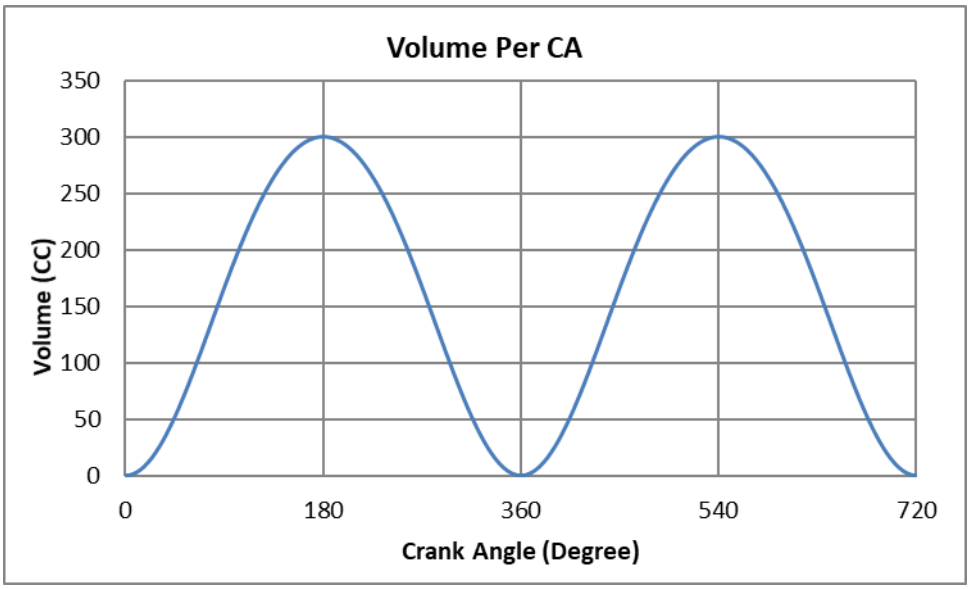

Figure 19: Volume displacement profile from Excel combustion model.

The starting point of the of the combustion model was to get a volume displacement profile, as this allowed the pressure change inside the cylinder, due to compression, to be calculated.

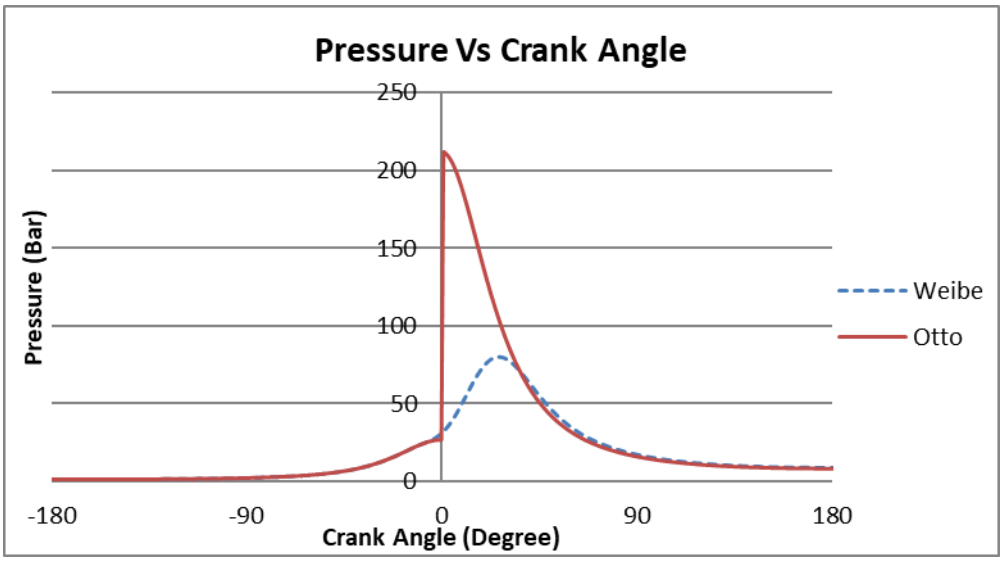

Figure 20: Pressure comparison of the Otto cycle and Wiebe function.

The next step in the combustion model development was to calculate the pressure change due to both the compression of the air from the piston and the combustion of the fuel.

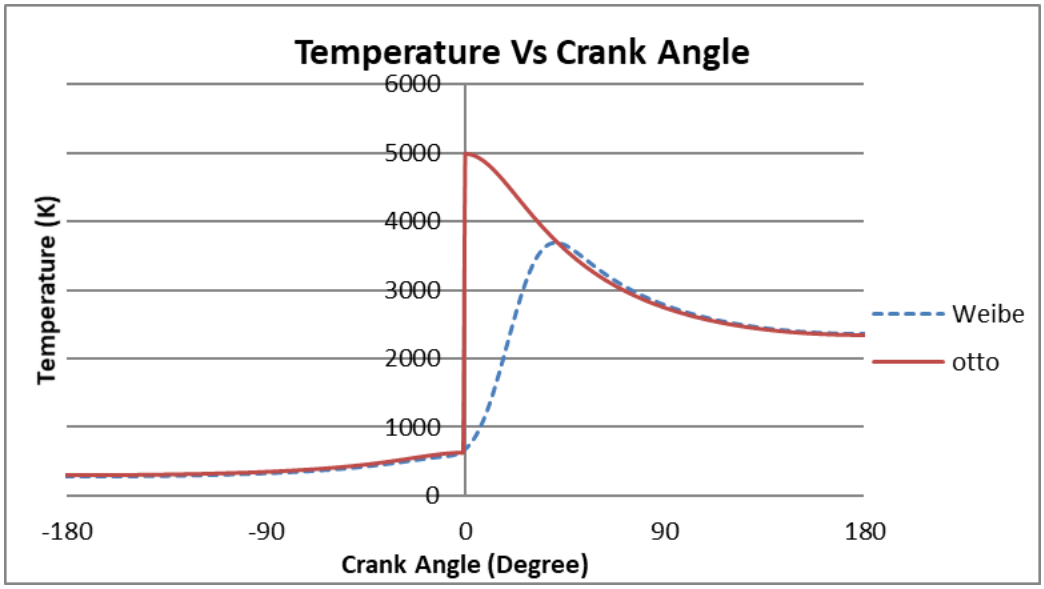

Figure 21: Temperature comparison of Otto cycle and Wiebe functions.

From the pressure change, the temperature change could be calculated

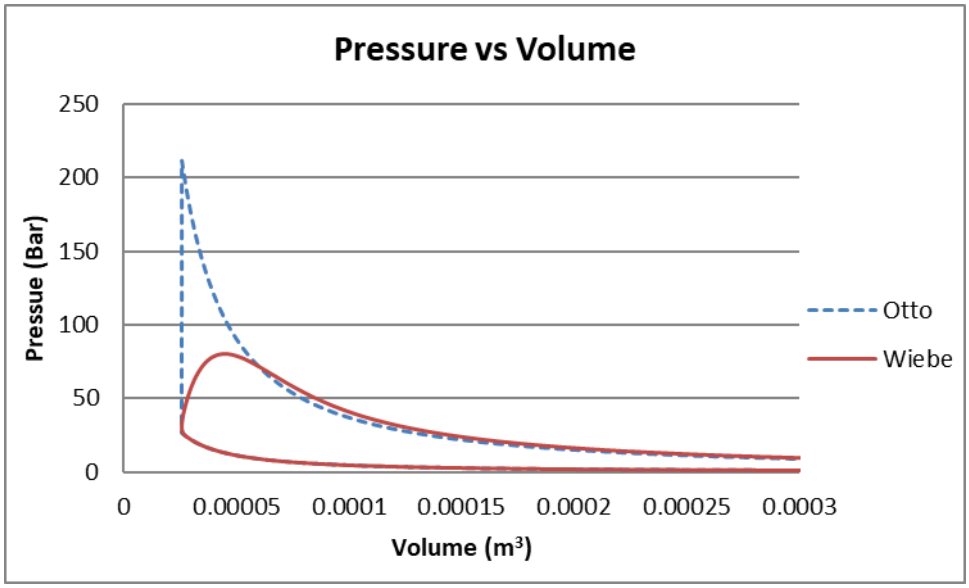

Figure 22: Pressure Vs Volume graphs for Wiebe function and Otto Cycle.

Once the temperature and pressure change had been calculated, then the pressure vs volume diagram could be constructed. This is a very useful tool in analysing the combustion event.

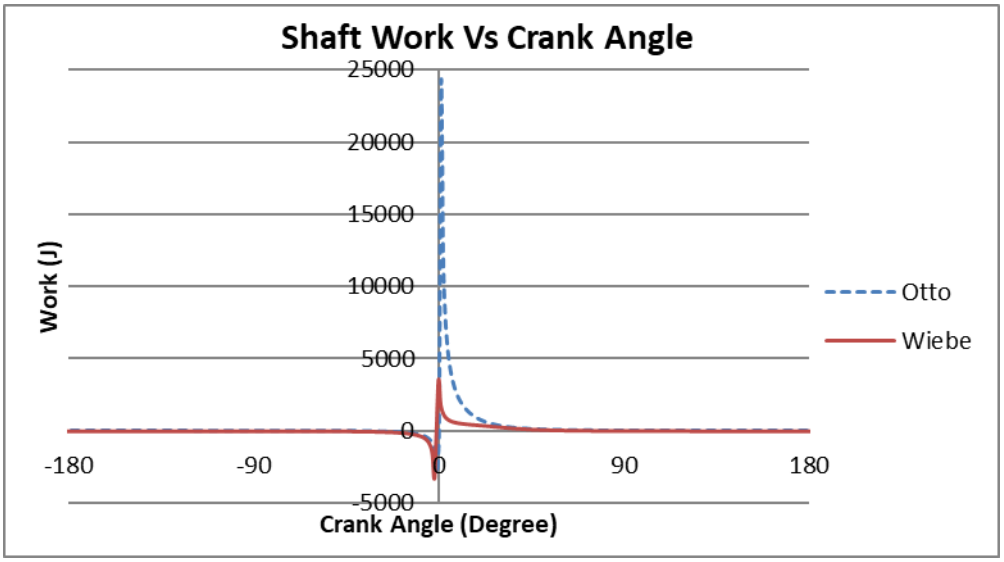

Figure 23: Shaft work for both Otto cycle and Wiebe function.

The shaft work gives an indication of how much positive and negative work is being done by the combustion event onto the piston and can give power performance indications.

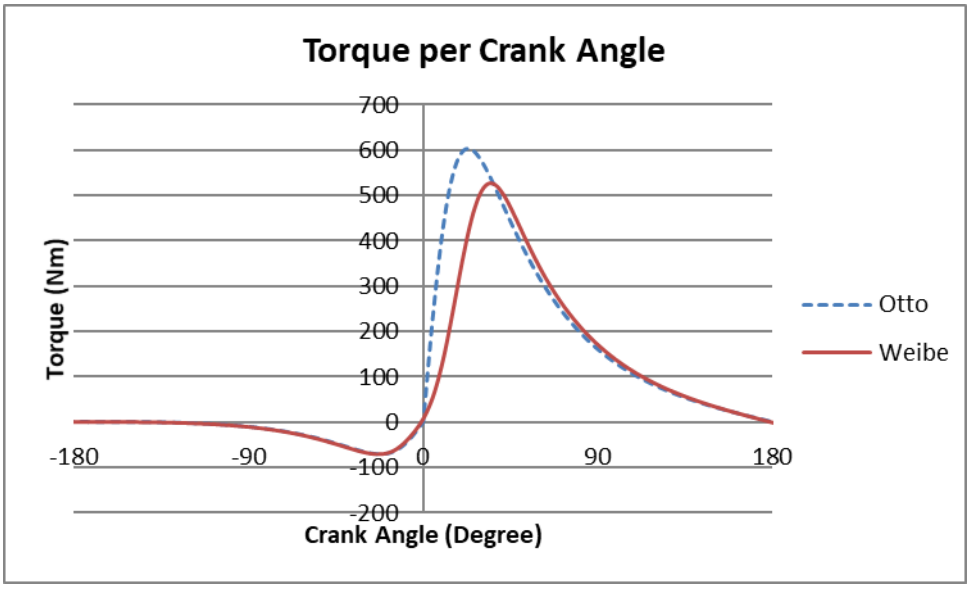

Figure 24: Torque per crank angle for the Otto cycle and Wiebe function.

The Torque per CA graph is directly related to the shaft work graph and is related and shows the instantaneous torque applied to the piston per crank angle.

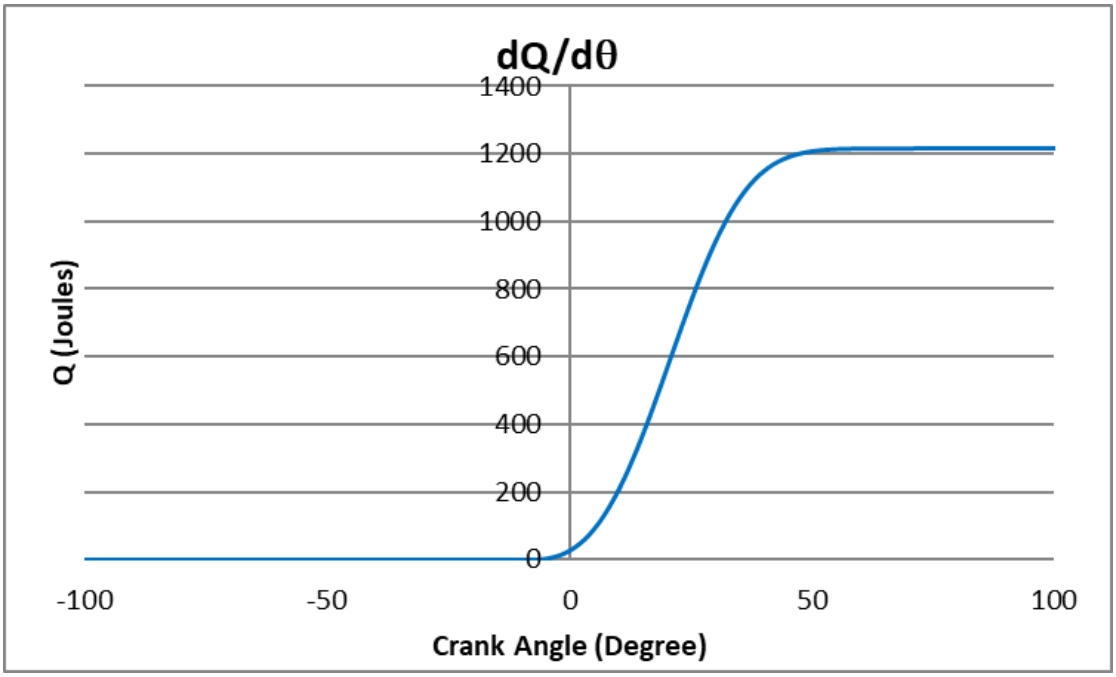

Figure 25: dQ/dθ profile.

The dQ/dθ profile shows how much energy is realised for the fuel per crank angle and is directly linked to the MFB curve. Although most simulations calculate the dQ/dθ from the MFB curve it is still a critical factor in understanding the combustion event.

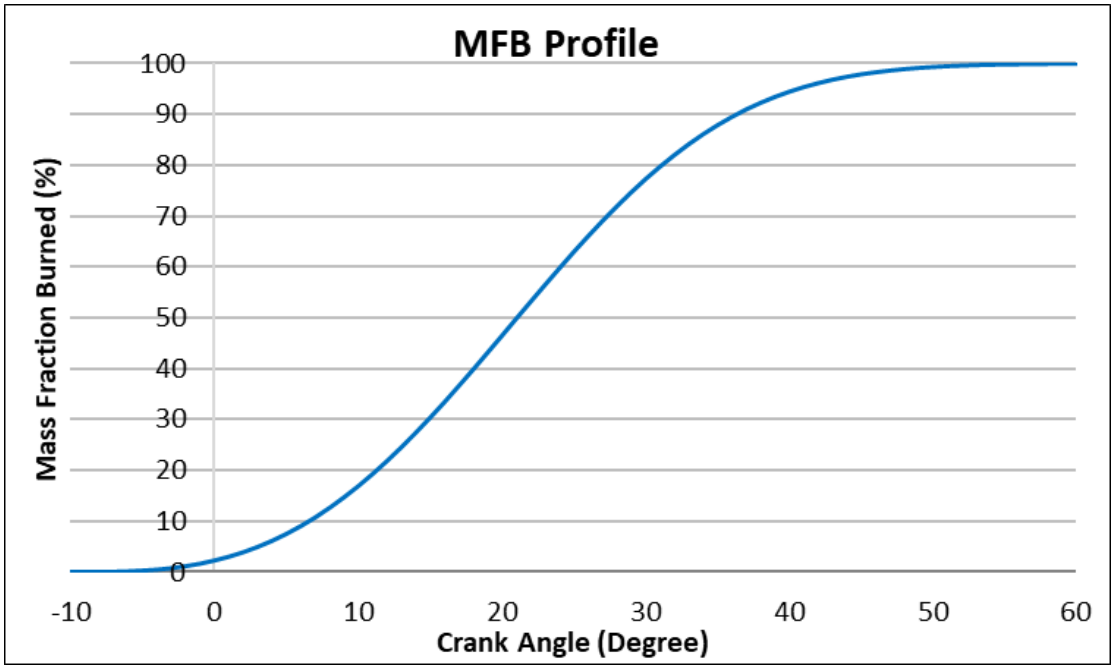

Figure 26: MFB profile for the Wiebe function.

The mass faction burn profile is the critical outcome of the combustion model. It allows the combustion event to be compared and contrasted over different combustion events and shows the potential power performance of an engine.

3.2. Dynamics

The engine studied in this project is based on 2 cylinders of a Cosworth DFV Formula 1 V8. The engine dynamics had to be checked in order to be sure that parameters such as the con-rod length, crankshaft counterweight and crank offset where validated for the engine. The CAD software CATIA R5V24 was used to location the Centres of Mass for the current components among other parameters.

One of the key parameters examined was Mean Piston Speed (MPS), which is a key area in engine development as the higher the MPS, the quicker the flame propagation happens within the cylinder. This can be seen in the flame propagation research section of the Appendix. However, the higher the MPS the larger the internal frictions and therefore the larger the mechanical efficiency losses and fatigue and wear of components. However, MPS also affects volumetric flow rate of air into the cylinder, as at lower speeds more air can be transferred into the cylinder per cycle. However, this is countered by a lower pressure differential between outside and inside the cylinder which acts to reduce airflow into the cylinder.

Piston acceleration is also an important factor in analysing the forces acting on the internal components such as the piston or journal bearings. A dynamics model constructed in an Excel spreadsheet was used to ascertain the forces acting on the crank slider mechanism using the equations below. Reducing the peak acceleration of the piston will result in reduced forces acting on the engine internals. This is because F=ma and, as the mass remains constant, reducing the acceleration will also reduce the forces, thus reducing wear and fatigue. Reduced acceleration of the piston will also result in more time for gas exchange.

Taking all of these factors into account the selected MPS will be a compromise between the benefits and disadvantages of high and low piston speeds. For this project an MPS of 30m/s was chosen which is consistent with the previous research and development of this engine, [1, 26, 27, 39, 41, 42].

The data collected from the CAD models was input into the Excel spreadsheets using the equations from the literature review. Figure 27**: A representation of the dynamics model constructed in Excel.** shows a representation of the Excel model. The figures from the model have been shown in detail throughout the project so a detailed view is not deemed necessary. The following equations where used to construct the Excel model -

Piston displacement –

$$X = \frac{s}{2}\cos\theta + L\left[1 - \left(\frac{s}{2L}\sin\theta\right)^2\right]^{\frac{1}{2}}$$

Equation 28

Piston velocity [1, 39, 41, 42] –

$$\dot{X} = -\frac{s}{2}\omega\left(\sin\theta + \frac{\varepsilon}{2}\sin 2\theta\right)$$

Equation 29

Piston acceleration [1, 39, 41, 42] –

$$\ddot{X} = -\frac{s}{2}\omega^2(\cos\theta + \varepsilon\cos 2\theta)$$

Equation 35

where X¨is the approximation of the piston acceleration,

Gas Torque [38, 39] –

$$T_g = F_g \frac{s}{2} \sin\theta \, (1 + \varepsilon \cos\theta)$$

Equation 57

Torque inertia [38, 39] –

$$T_i = -m_B \times \left(\frac{S}{2}\right)^2 \times (\omega)^2 \times \sin\theta \times \left(\frac{\varepsilon}{2} + \cos\theta + \frac{3}{2} \times \varepsilon \times \cos 2\theta\right)$$

Equation 60

The project will cover analysis of the forces over 4k,9k,and 12k RPM in order to analyse the forces but particular attention will be paid to 9k RPM as this is used to located peak torque.

	deg	rad	X	X.	X. +75deg	X..	X../g	primary	secondary	F	Pressure			CA	Pressure
1	deg	rad	X	X.	X. +75deg	X..	X../g	primary	secondary	F	Pressure			CA	Pressure
2	1	0.017453	0.125561	-0.60328	-28.9719	-43429.48	-4427.062	-20200.96	-4423.557	-24624.5	657.848	1.62354	2	2	657.848
3	2	0.034907	0.125551	-1.20628	-28.9909	-43398.94	-4423.949	-20191.73	-4415.471	-24607.2	657.8997	2.40527	2		
4	3	0.05236	0.125533	-1.80871	-28.9997	-43348.06	-4418.763	-20176.35	-4402.006	-24578.4	657.9658	3.18713	3	3	657.9658
5	4	0.069813	0.125509	-2.4103	-28.9986	-43276.89	-4411.508	-20154.82	-4383.177	-24538	658.0899	3.9691	4	4	658.0899
6	5	0.087266	0.125478	-3.01076	-28.9876	-43185.47	-4402.189	-20127.15	-4359.008	-24486.2	658.1967	4.75107	5	5	658.1967
7	6	0.10472	0.125441	-3.6098	-28.9667	-43073.87	-4390.812	-20093.36	-4329.529	-24422.9	658.2433	5.53302	6	6	658.2433
8	7	0.122173	0.125396	-4.20716	-28.9362	-42942.17	-4377.388	-20053.44	-4294.774	-24348.2	658.2485	6.3149	6		
9	8	0.139626	0.125345	-4.80255	-28.8961	-42790.47	-4361.924	-20007.41	-4254.788	-24262.2	658.2758	7.09662	7	7	658.2758
10	9	0.15708	0.125286	-5.39569	-28.8465	-42618.88	-4344.433	-19955.29	-4209.617	-24164.9	658.3642	7.87814	8	8	658.3642
11	10	0.174533	0.125221	-5.98631	-28.7875	-42427.53	-4324.926	-19897.09	-4159.317	-24056.4	658.4662	8.65942	9	9	658.4662
12	11	0.191986	0.12515	-6.57414	-28.7192	-42216.54	-4303.419	-19832.83	-4103.95	-23936.8	658.4703	9.4405	9		
13	12	0.20944	0.125071	-7.15891	-28.6418	-41986.09	-4279.927	-19762.53	-4043.583	-23806.1	658.2784	10.2213	10	10	658.2784
14	13	0.226893	0.124986	-7.74033	-28.5554	-41736.33	-4254.468	-19686.21	-3978.29	-23664.5	657.8716	11.00183	11	11	657.8716
15	14	0.244346	0.124894	-8.31816	-28.4601	-41467.44	-4227.058	-19603.89	-3908.149	-23512	657.3162	11.7821	12	12	657.3162
16	15	0.261799	0.124795	-8.89212	-28.356	-41179.62	-4197.719	-19515.6	-3833.248	-23348.8	656.7112	12.56204	13	13	656.7112
17	16	0.279253	0.12469	-9.46195	-28.2433	-40873.09	-4166.472	-19421.37	-3753.675	-23175	656.128	13.34167	13		
18	17	0.296706	0.124578	-10.0274	-28.1221	-40548.05	-4133.339	-19321.22	-3669.53	-22990.7	655.5723	14.12103	14	14	655.5723
19	18	0.314159	0.12446	-10.5882	-27.9925	-40204.75	-4098.344	-19215.18	-3580.914	-22796.1	654.998	14.9001	15	15	654.998

Figure 27: A representation of the dynamics model constructed in Excel.

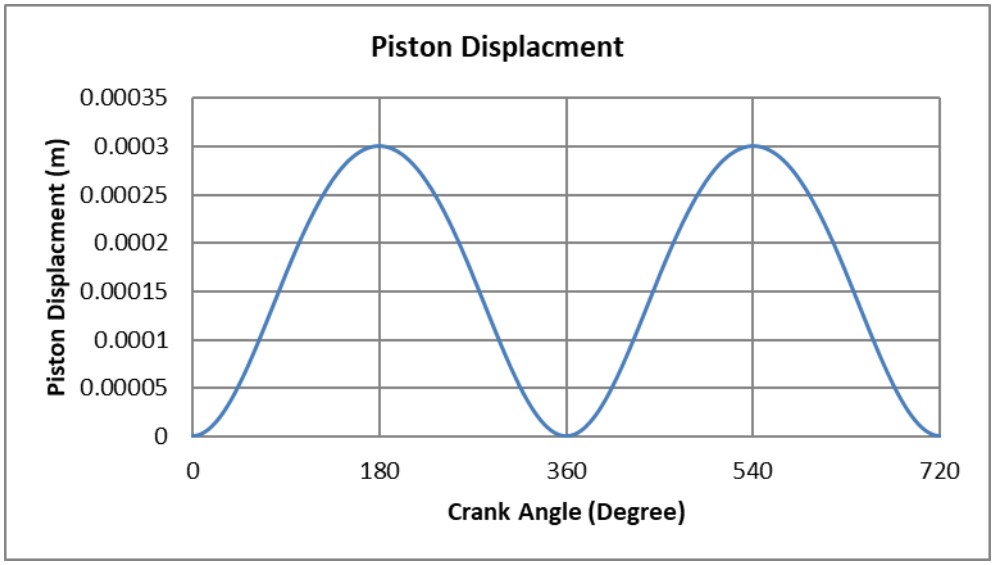

Figure 28: Piston displacement.

The start of the dynamics model is to calculate the distance the piston is down the stroke. This will allow other parameters to be calculated.

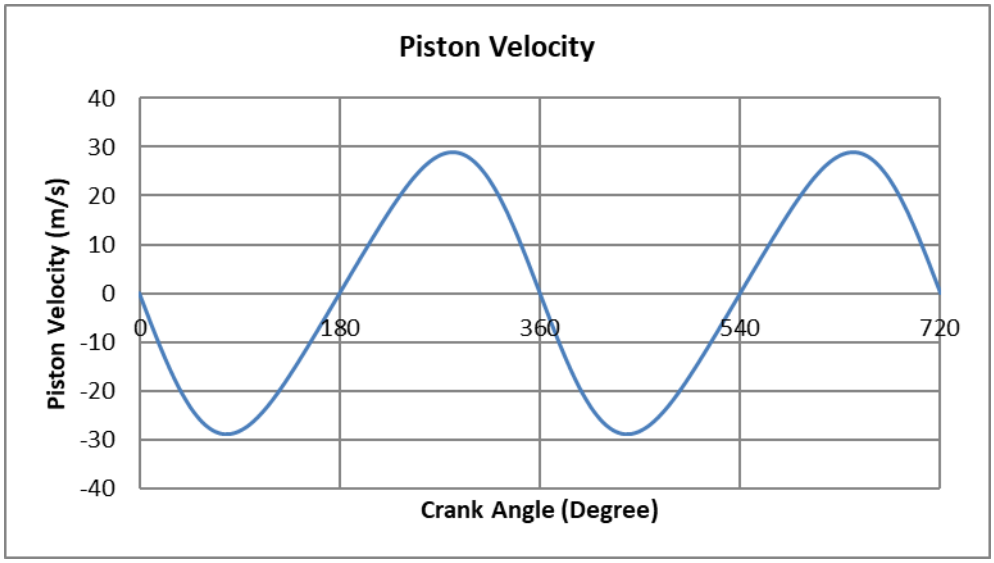

Figure 29: Piston velocity.

Once the displacement has been calculated, the velocity can be calculated when combined with engine speed.

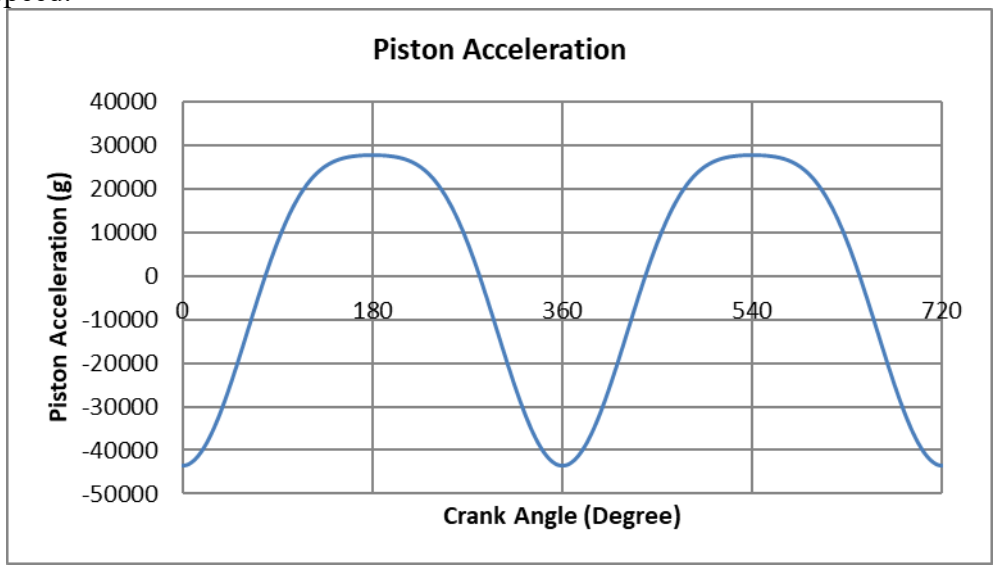

Figure 30: Piston acceleration.

The final stage in the series of differential equations is the piston acceleration which is an important parameter as it allows the forces exerted on the piston, by the other engine dynamics, to be calculated.

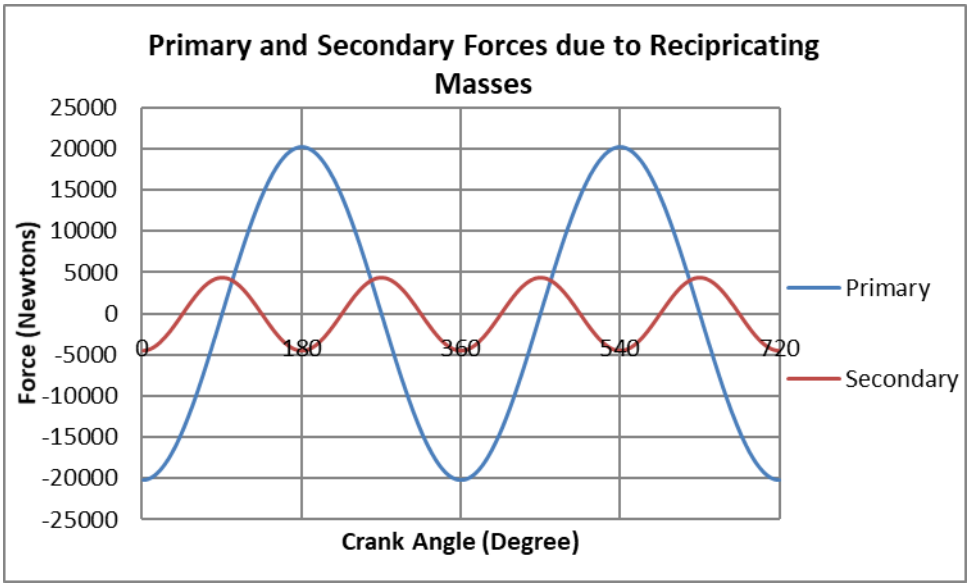

Figure 31: Comparison of the primary and secondary forces.

The forces expected on the piston are made up of a primary force, from the reciprocating movement of the piston, and a secondary force, from the rotating movement of the crank shaft. Both these forces can be thought of as independent forces although they both act on the piston.

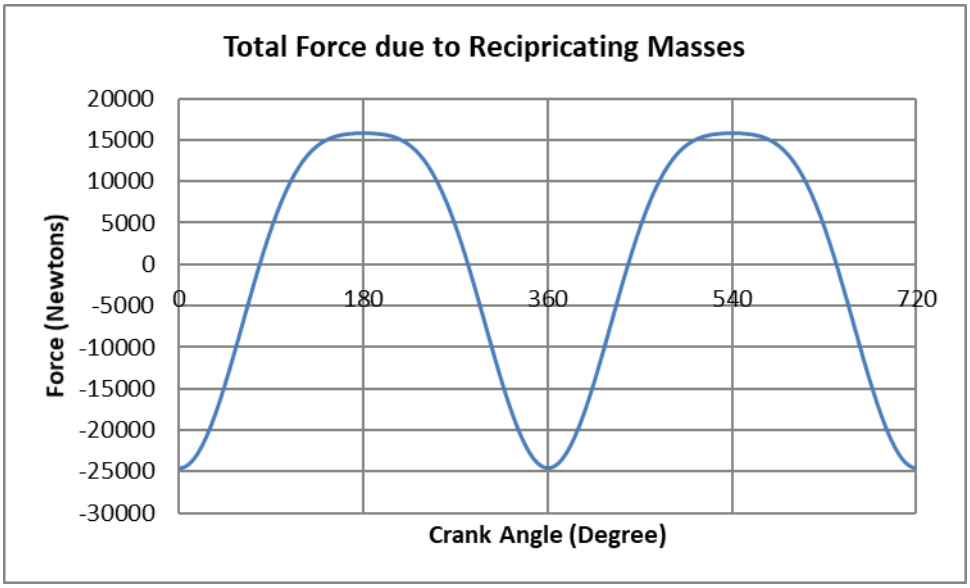

Figure 32: Combination of the primary and secondary forces due to the masses.

The combination of the primary and secondary forces give a non-uniform profile due to the secondary force occurring at twice the frequency of the primary.

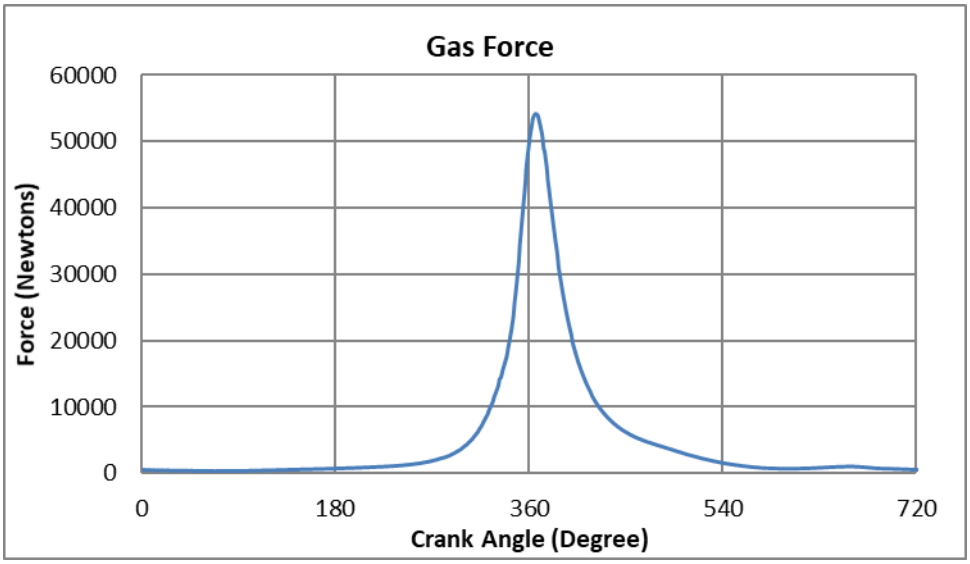

Figure 33: Gas force applied onto the piston.

The gas force is a critical factor in the forces exerted onto the engine internals and is calculated by the combustion model, although data can be acquired from the GT-Power model.

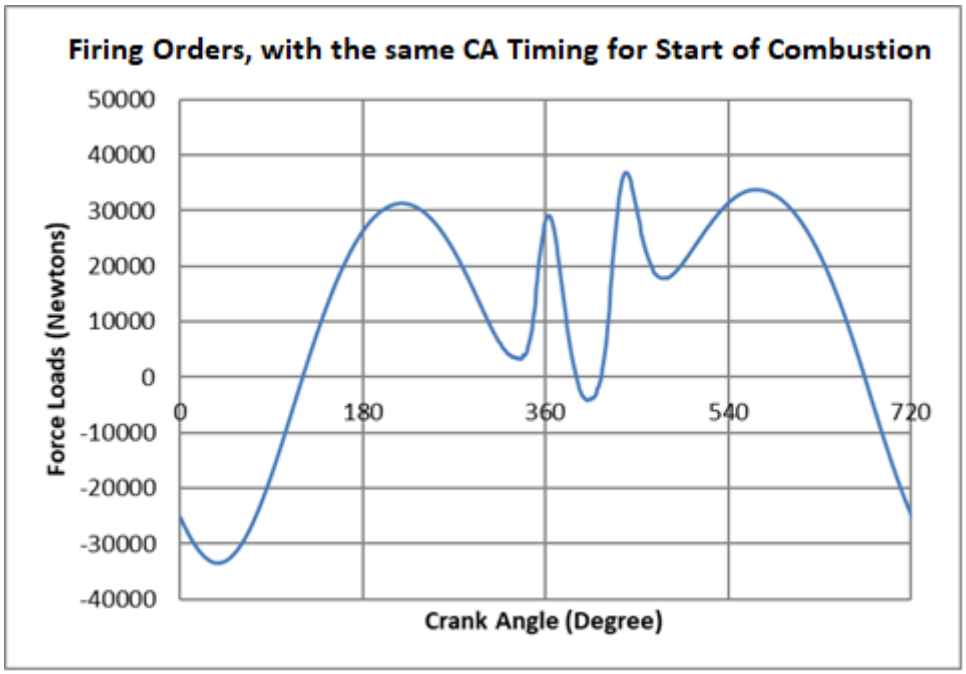

Figure 34: Analysis of the effects of force on same phase firing orders.

In order to analysis the total force acting on the internals, the gas force and the force to the internal masses are combined. As the two pistons are out of line and can fire either in the same phase or out of phase, it was deemed a worthwhile test to calculate the overall force that can be exerted on the internals if the firing orders wherein phase and out of phase.

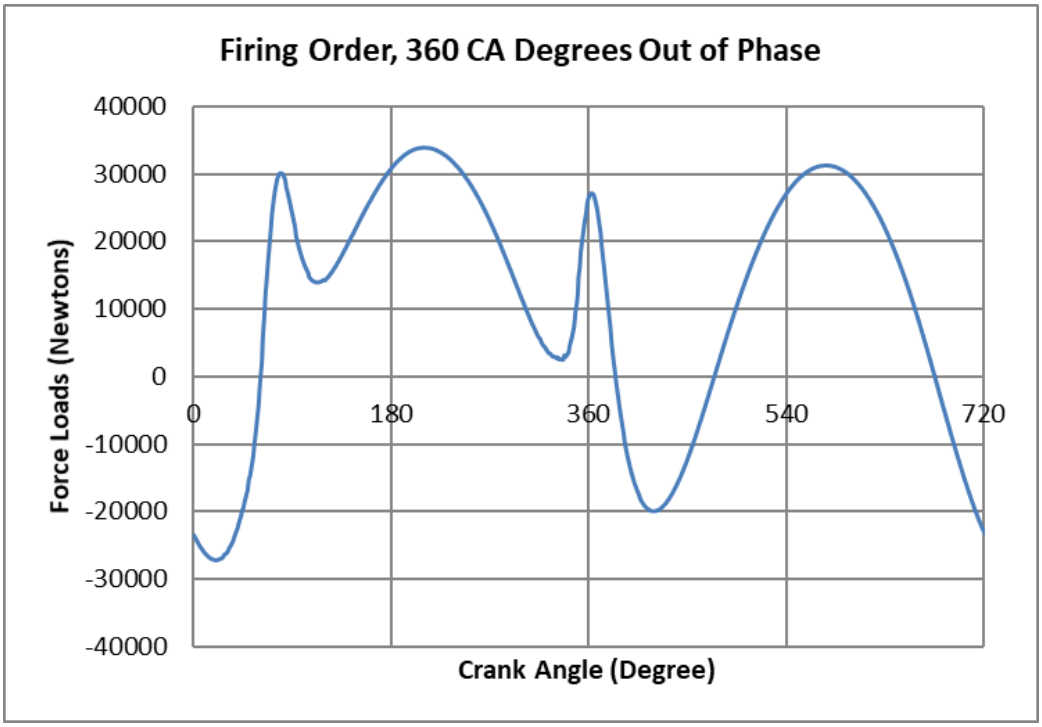

Figure 35: Analysis of the effects of force on out of phase firing orders.

The analysis of the both the in phase and the out of phase firing orders showed that a firing order 360 degrees out of phase reduced the overall force by a significant amount.

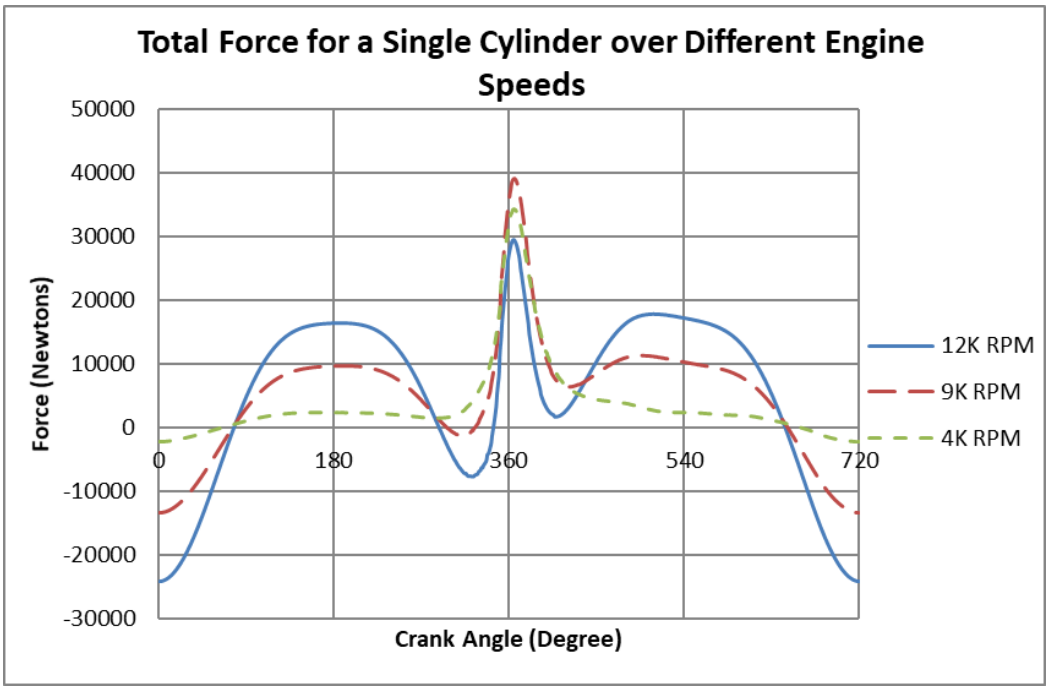

Figure 36: Analysis of the total force over the RPM range.

Once the forces and been calculated and the fire orders decided then the total forces could be calculated over the RPM range. The 3 RPMs chosen to analyse the total forces were 4,000 RPM as this was ideal, 9,000 RPM as this was deemed optimal for peak torque, and 12,000 RPM as this was near the top of the RPM range.

3.3. GT–Power model

The GT-Power model has been developed alongside a combustion model and analysis of the engine dynamics, which has furthered the understanding of the engine. The model developed using GT-Power was used to analyse the engine and continue its development.

The combustion object selected for the GT-Power model was the 'EngCylSIWiebe' model. The object imposes a burn rate using the Wiebe function in order to approximate the shape, for a typical combustion profile, of the SI burn rate. The model allows for implementing a 'reasonable' burn rate if in-cylinder pressure data is not available, which it was not for this project, [12].

The parameters that were utilised in order to calculate the burn rate of the GT-Power Wiebe model were, [12]; -

-Anchor Angle (AA), which is the anchoring angle of the Wiebe curve. The AA is the number of crank angles between the TDC and 50% MFB.
-Duration (D), is the number of crank angles the combustion curve takes to get from 1 0% MFB to 90% MFB.
-Wiebe exponent (E), which is typically a default value of 2.
-Fraction of Fuel Burned (CE), which is the percentage of the total fuel burned in the combustion event.
-Burned Fuel Percentage Anchor Angle (BM), which is 50% MFB and used as an anchor point.
-Burned Fuel Percentage at Duration Start (BS), which is 10% MFB and is used to define the start of combustion.
-Burned Fuel Percentage at Duration End (BE), which is 90% MFB and is used to define the end of combustion.

The Wiebe model in the Combustion object calculates the constants; –

- BMC = - ln (1-BM), which is the burned midpoint constant. **Equation 100**

- BSC = - ln (1-BS), which is the burned start constant. **Equation 971**

- BEC = - ln (1-BE), which is the burned end constant. **Equation 982**

$$- WC = \left[\frac{D}{\frac{1}{BEC^{(E+1)}} - \frac{1}{BSC^{(E+1)}}}\right]^{-(E+1)}$$, which is the Wiebe constant. **Equation 993**

$$- SOC = AA - \frac{(D)(BMC)^{\frac{1}{(E+1)}}}{\frac{1}{BEC^{(E+1)}} - \frac{1}{BSC^{(E+1)}}}$$, which is the start of combustion **Equation 1004**

Once these constants have been calculated, then the cumulative burn rate is calculated normalised to 1.0, with the combustion starting at 0.0 and is finished when the 'fraction of fuel burned attribute' is calculated to be 1.0. The combustion objects calculates the Wiebe function using the equation, [12] –

$$- Combsution(\theta) = (CE)\left[1 - e^{-(WC)(\theta - SOC)^{(E+1)}}\right]$$

Equation 1015

With the architecture of the Wiebe function described in the combustion literature review clearly visible, in the equation above.

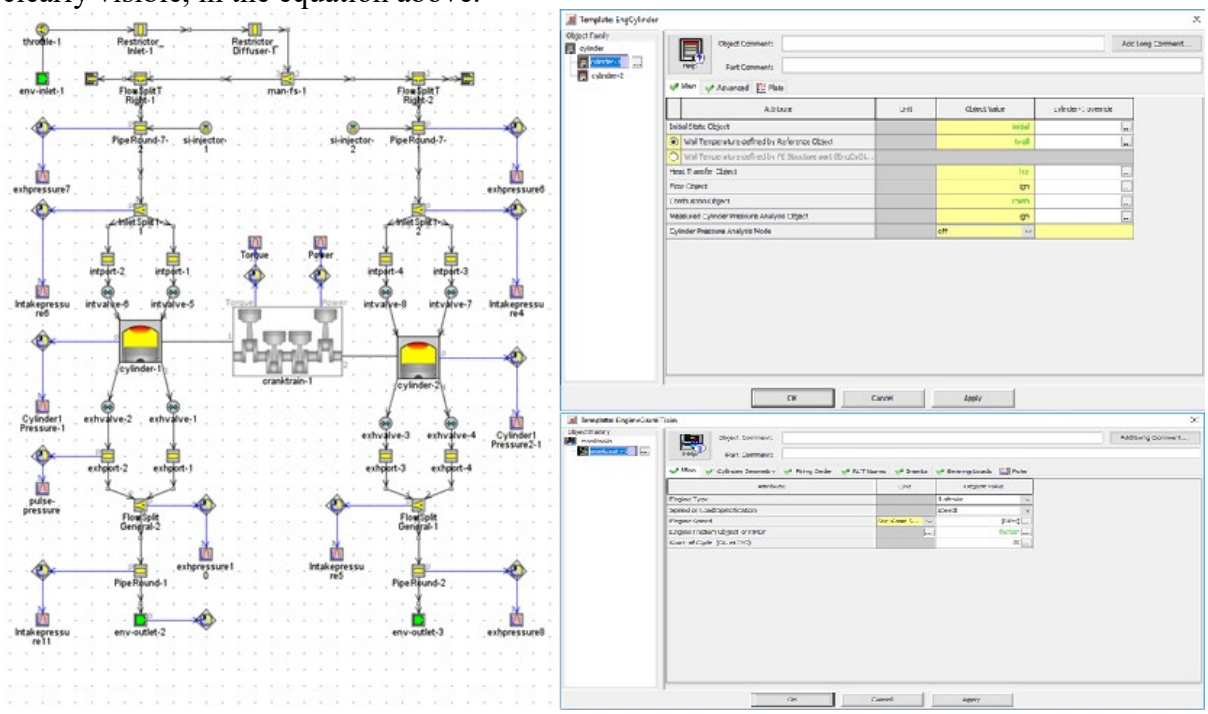

Figure 37: The original engine model setup used in version GT-Power 6.1. The work was done carried out at Oxford Brookes Universities by the students there.

This is a simplified model with a lot of assumptions that was re-created in GT-Power V7.1. A lot of the features had changed but the parameters were given in spreadsheets and where input into the model.

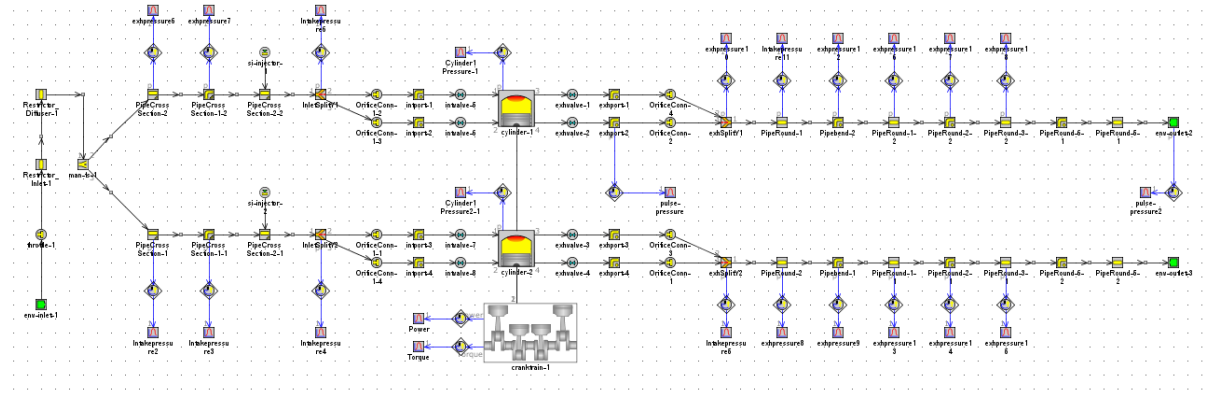

Figure 38: Original model of the engine used to analyse the changes proposed for the engine. In GT-Power V 7.1. This was the original starting point of the project.

This was the first model constructed by the Formula Student V-Twin powertrain team in version GT-Power V7.1.

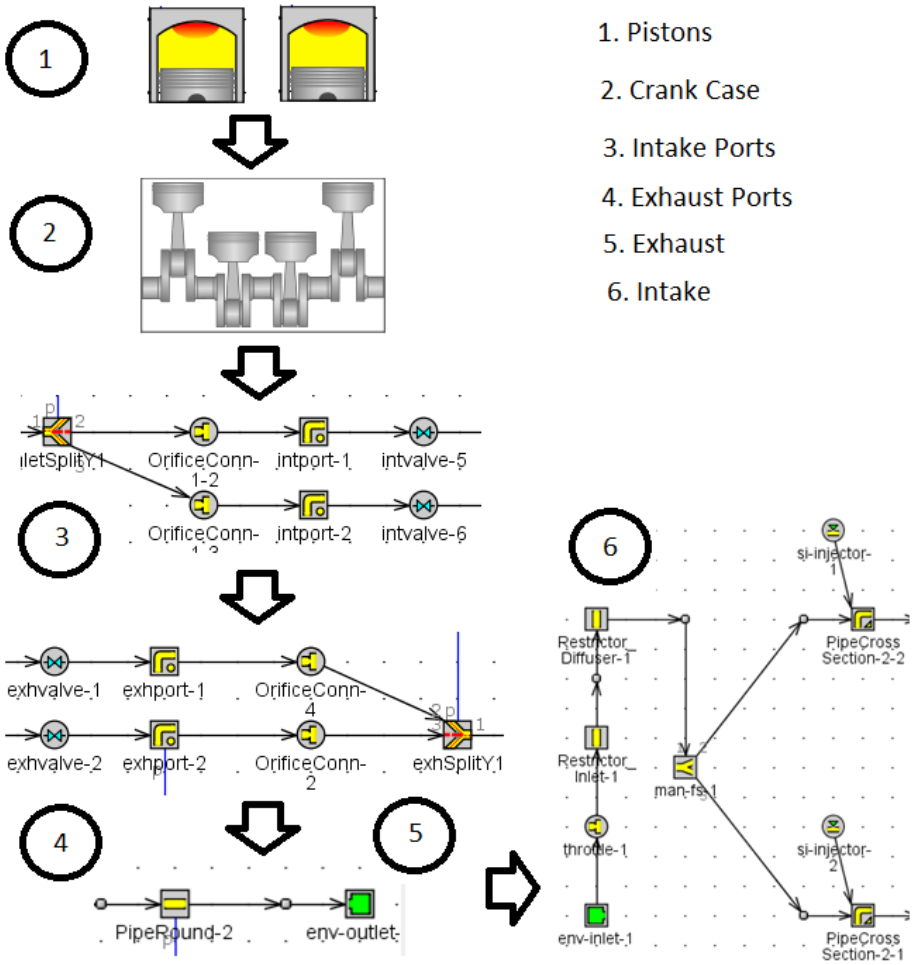

Figure 39: GT-Power model development flow chart

As seen above, the GT-Power model was started with the combustion model, shown by the pistons. The crank case was then added with the engine dynamics. After the ports where added. The ports had the valve train built into them. After the exhaust was added which discharges to the atmosphere. Finally the inlet manifold was added, which has the injectors and as an inlet to the open air. The final model can be seen below.

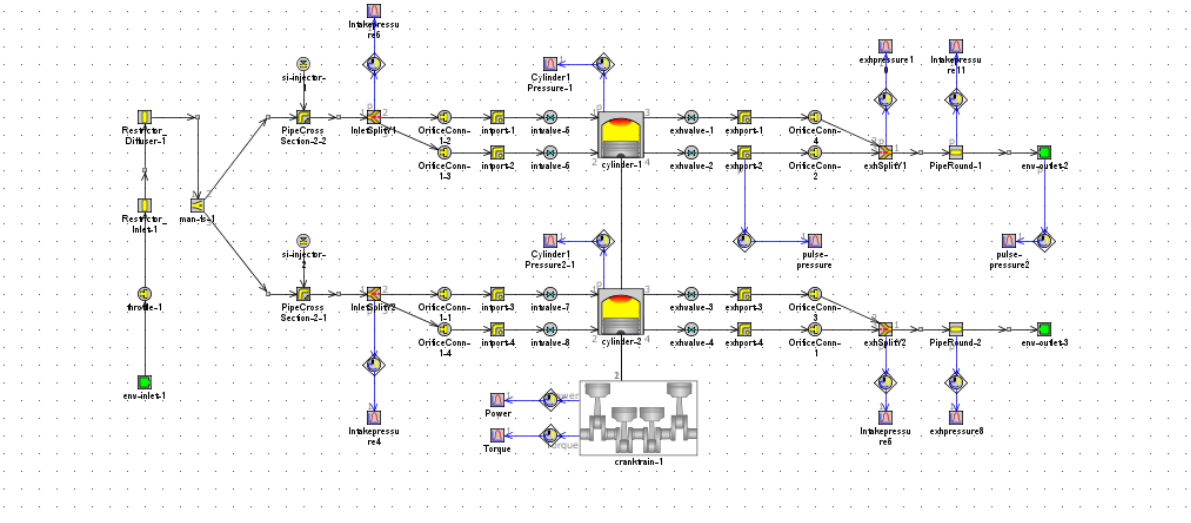

Figure 40: The final setup for the engine model in version GT-Power V2016.

The majority of parameters within a GT-Power model are set to a default setting ‘def’ in order to give a generic engine model. If a more accurate model is wanted, or a better combustion model is needed, then some of the parameters need changing. The more parameters changed from ‘def’ to the optimal value, the more accurate the model will be for that parameter, and the closer to the desired outcome. Most of the values acquired were a result a combination of the work done on the combustion and engine dynamic models and work done on the background of the engine.

The parameters of the GT-Power model can be found in GT-Power model development section of the **Appendix.**

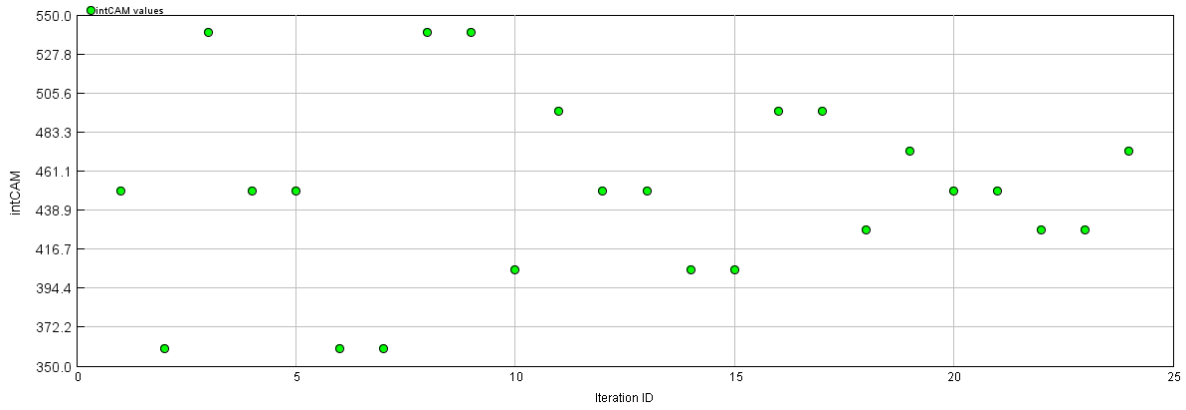

Figure 41: A representation the sweep function on GT-Power.

Figure 41: A representation the sweep function on GT-Power. Shows an example of the optimisation of Camshaft Anchor angle on the GT-Power Optimiser. The optimisation process used a sweep function that rans the model through different iterations of the same parameter within a range of values that the user set. When analysing the valve timing,

The valve sweep of the valve train was done using a simplified model to make the process quicker. The process was done with a sweep with steps across the full intake and exhaust strokes. Using a simplified model does not give 100% accurate results but allows the full extent of the area of max performance to be analysed more quickly, as the simplified model is far quicker to simulate. A full model was used to identify the best possible valve timing setup for the engine. Doing a full sweep of the strokes is also unrealistic as the valve would hit the piston during parts of the stroke. A further analysis of the engine model will be carried out to verify the crank angles at which either of the valve set will hit the pistons. Average torque analysis was done between the results over the range of RPMs of the valve sweep. This was done to show which had the smoothest torque curve.

3.4. Valvetrain methodology

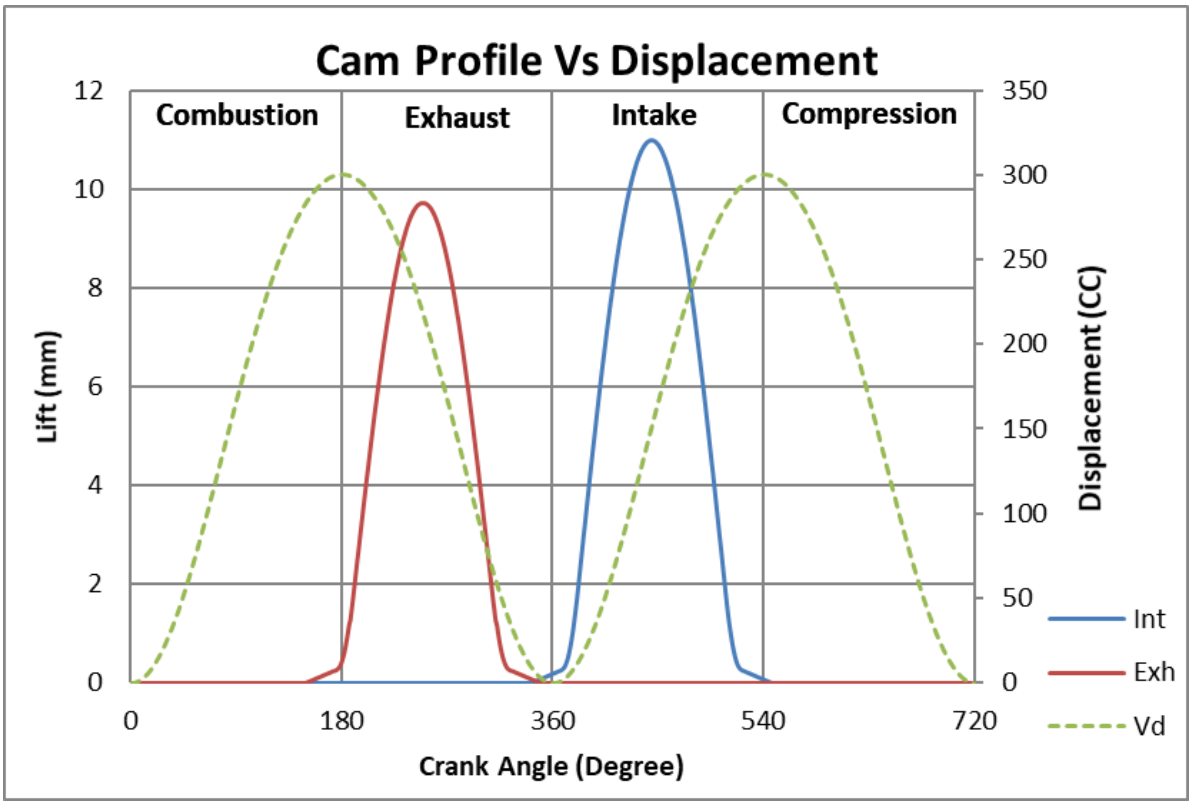

Figure 42: Comparison of Exhaust and Intake valve opening profiles Vs Displacement Volume, showing original valve timings and areas of importance such as valve overlap.

The start of this process was to analyse the current valve train, by looking at the cam lobe shape and design. The initial analysis of the cam lobe shape/cam profiles, shown in Figure 42: Comparison of Exhaust and Intake valve opening profiles Vs Displacement Volume2 indicates that it is set up for high engine revolutions. The valve overlap at 1mm of valve lift is over 50mm which is quite high. The EVO is almost at two thirds of the combustion stroke, happening at 489 degrees Crank Angle (CA), showing that some of the combustion is being compromised to get the maximum amount of exhaust gases out of the exhaust valve. The majority of the usable combustion will have happened by the point of EVO. Advancing the EVO has allowed for the IVO to be advanced, with the IVO at 1mm happening at 688 degrees CA, and the crossover of the valve overlap happening over 10 degrees into the exhaust stroke. This advancing of the IVO, and having the overlap occurring within the exhaust stroke, will allow the maximum amount of exhaust gases to be forced out of the cylinder. The intake valve is open for over 250 degrees CA, which is almost a third of the total CA degrees for the stroke. The large opening CA range of the intake valve shows that the engine is set up for high RPMs, as there is a compromise from air escaping back from either blow-back at the valve overlap or air escaping back into the intake on the compression stroke, but both will help maximise the amount of time available for air to get into the engine. Although there will be a slight loss in performance, it will be compensated for by the number of power strokes happening within a given time for the higher RPM of the engine.

3.5. Manifold methodology

The CFD was done in SolidWorks FLowSim which is an integrated CFD package within SolidWorks software. It uses the models constructed within the software in order to create the flow body [1, 2, 7, 8].

3.5.1. Intake CFD

In order to calculate the mass flow rate for any CFD simulations, the maximum mass flow rate into the system was deemed to be a critical factor. This is because the restrictor has an effect on the amount of air the system can intake and causes a significant restriction on the system, hence it is implemented by FASE via the rules to restrict engine power. The current restrictor is an aluminium tube with the throttle inside the assembly. The current diameter is 19mm to ensure that it is within the 20mm restrictor limit from the FASE formula student rules. The 1mm margin allows for tolerances in machining and in the official's measuring equipment.

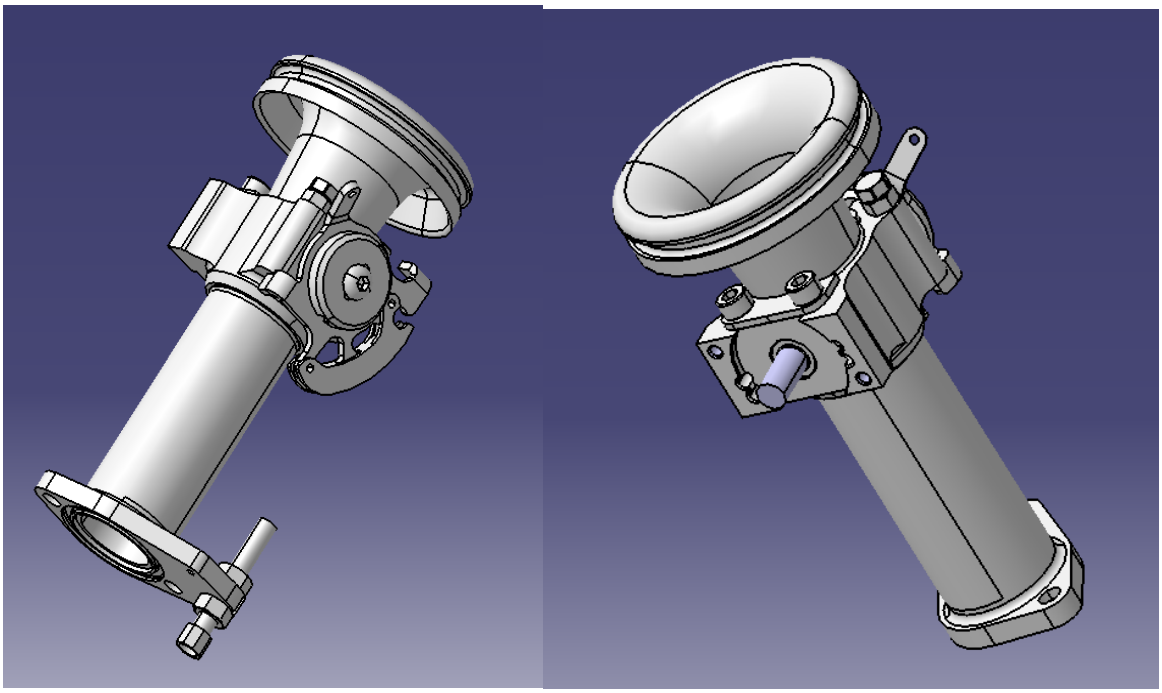

Figure 43: CAD of the AT-Power FSAE Throttle Part number from the FS servers FS08-02-520 (FS CAD) [103]

To assess the restrictor, the mass flow rate of air through the system needs to be calculated. This also helped in the construction of the combustion model in excel, and was done using the equation –

$$\dot{m}_{air} = \frac{A_{throat} \times P}{\sqrt{T}} \times \sqrt{\frac{\gamma}{R}} \times \left(\frac{\gamma + 1}{2}\right)^{-\frac{\gamma+1}{2(\gamma-1)}}$$

Equation 72

Which gave –

$$\dot{m}_{air} = \frac{4.57 \times 10^{-3} \times 101325}{\sqrt{300}} \times \sqrt{\frac{1.4}{287}} \times \left(\frac{1.4+1}{2}\right)^{-\frac{1.4+1}{2(1.4-1)}} = 2.0379\ kg/s$$

Equation 72

For this calculation the air entering the restrictor was deemed to be at ambient conditions of 300K temperature and 1 bar pressure. The value of 2.0379 kg/s is the theoretical upper limit and will be hard to achieve in reality due to the boundary layer between the restrictor surface and the 19mm diameter throat [60].

Once the intake mass flow rate had been calculated then the intake runner lengths were calculated in Excel and verified in GT-Power, the equation used was –

$$L = \left(\frac{955 \times c}{K \times N}\right)^2 \times \left(\frac{A}{V_{eff}}\right)$$

Equation 81

The results can be seen in the manifold results section.

3.5.2. Exhaust CFD

The initial conditions for the exhaust CFD were estimated values that were taken from the initial GT-Power model. The values used were 1 bar pressure and 1000K temperature, which give a speed of sound of 633.88 m/s. The maximum theoretical flow through the port was also calculated in order to give the CFD an initial mass flow rate into the system. The choked flow limit of the exhaust port had to be assessed using the equation [68] –

$$\dot{m}_{air} = \frac{A_{throat} \times P}{\sqrt{T}} \times \sqrt{\frac{\gamma}{R}} \times \left(\frac{\gamma + 1}{2}\right)^{-\frac{\gamma+1}{2(\gamma-1)}}$$

Equation 72

which gave –

$$\dot{m}_{air} = \frac{3.19 \times 10^{-3} \times 101325}{\sqrt{1000}} \times \sqrt{\frac{1.4}{287}} \times \left(\frac{1.4 + 1}{2}\right)^{-\frac{1.4+1}{2(1.4-1)}} = 0.7792\ kg/s$$

Once the mass flow rate and initial gas conditions were input into the CAD and the simulations run, it was an iterative process of comparing the results with the exhaust pressure traces from GT-Power in order to calculate the optimal exhaust length. The initial exhaust and inlet runner lengths were calculated with the equation –

$$L = \left(\frac{955 \times c}{K \times N}\right)^2 \times \left(\frac{A}{V_{eff}}\right)$$

Equation 81

The results can be seen in the manifold results section.

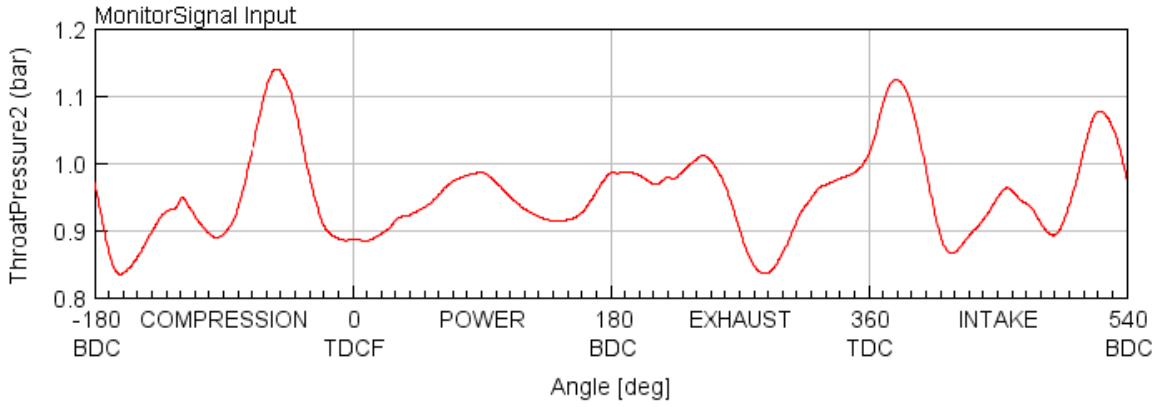

Figure 44: Pressure trace from the inlet runner simulated in GT-Power.

The GT-Power simulations and CFD were done alongside an Excel spreadsheet in order to calculate the exhaust length that were then verified in the GT-Power model. Figure 44**: Pressure trace from the inlet runner simulated in GT-Power.** shows the pressure trace from the inlet runner simulated in GT-Power. The pressure trace shows the reciprocating pressure waves used in intake design to maximise the RAM air effect that is used in manifold design.

Chapter 4. Results and Discussion

4. Results

4.1. Combustion model

Mass Fraction Burn (MFB) and Heat Release Rates (HRR) are two important parameters to consider in engine development and in understanding engine behaviour. Both parameters relate to how much of the charge is burned within the cylinder at any given time. One way of measuring the HRR and the MFB is using the Wiebe function. This is the base model used within the combustion model of GT-power. HRR data normally allows for a MFB profile to be calculated for further analysis of the combustion event, [21].

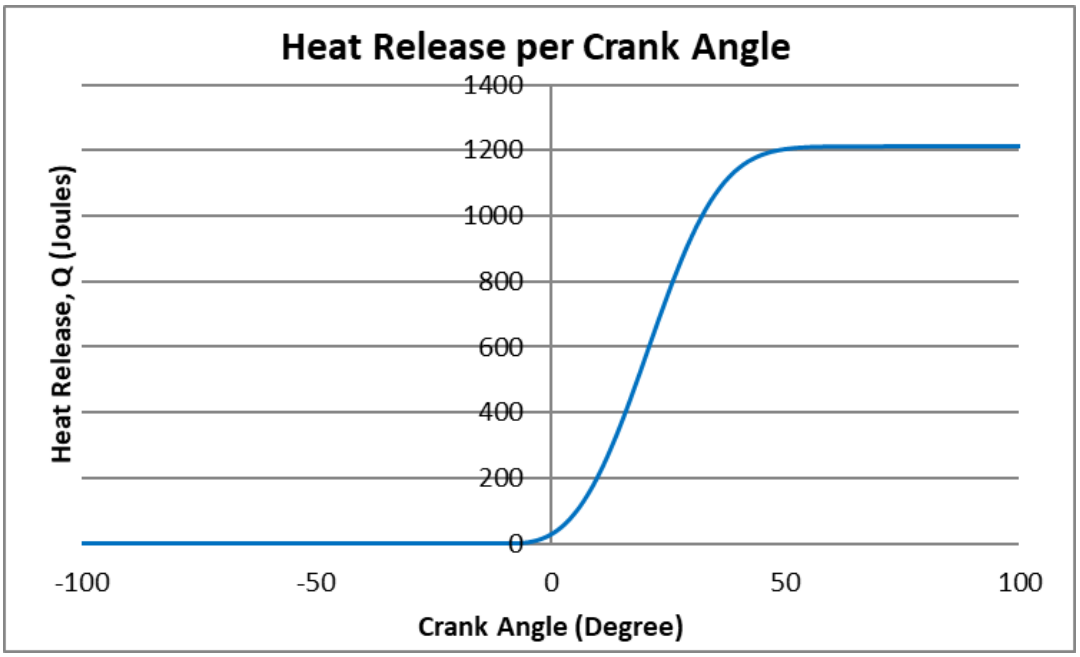

Figure 45: Heat release per crank angle

The heat release rate per crank angle profile, seen in Figure 45: Heat release per crank angle5, is similar to a MFB profile and the two are related as seen in Figure 46: Mass Fraction Burned Vs Crank angle6.

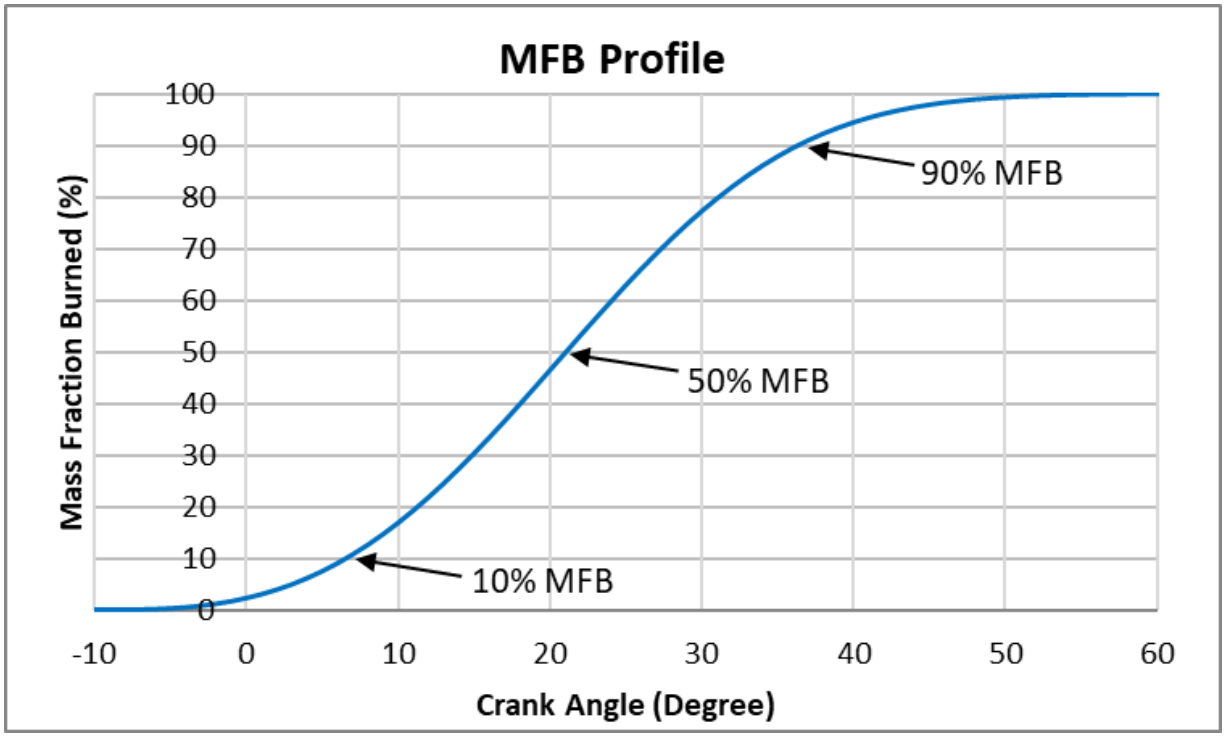

Figure 46: Mass Fraction Burned Vs Crank angle.

The start of the process was to find the volume of each cylinder using the column equation and the graph from the Excel spreadsheet, seen in Figure 47: Displacement per cylinder of the V-Twin including clearance volume.

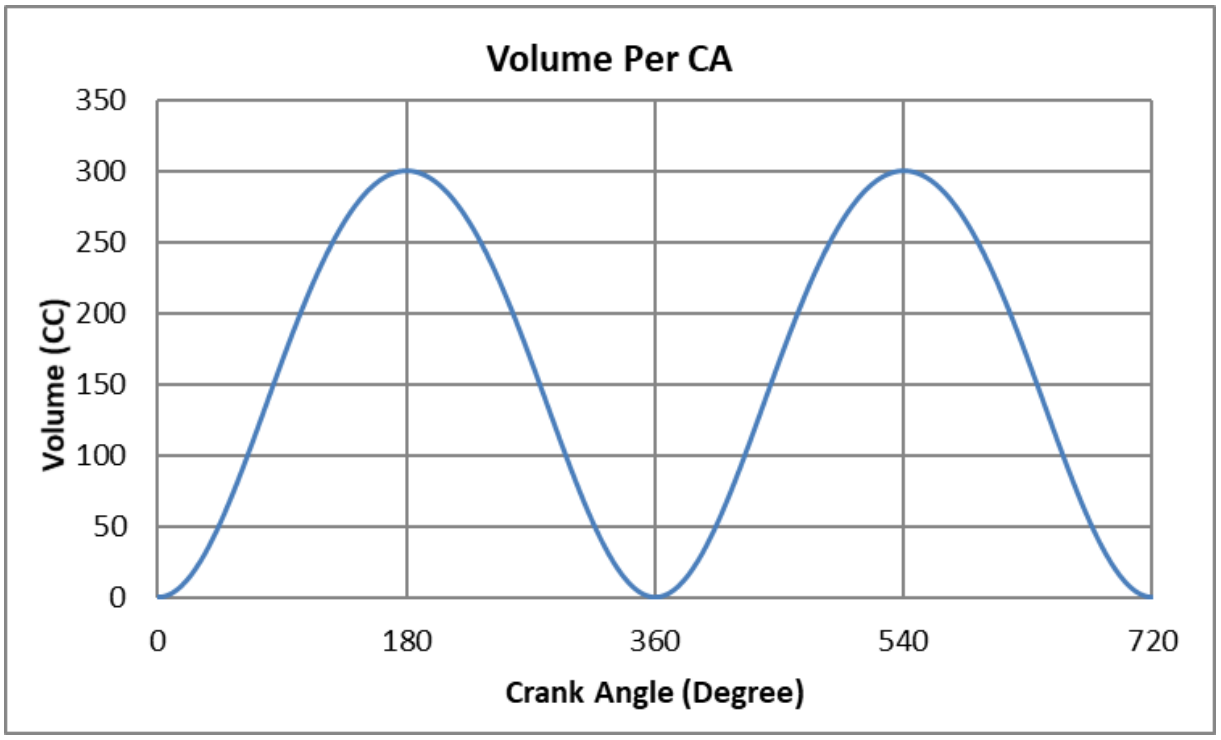

Figure 47: Displacement per cylinder of the V-Twin including clearance volume

The equation employed in this calculation uses the individual gas constant R for air, which is 287J/Kg K. P_0 and T_0 are both reference parameters taken at ambient conditions so room temperature and atmospheric pressure were used, and the volume V is $V_c + V_d$. Thus, the equation is [1, 7, 41, 102]:

$$m = \frac{p_0(V_c + V_d)}{RT_0} = \frac{1 \times 10^5 \times ((26.2009 + 300) \times 10^{-6})}{287 \times 300} = 0.3789 \times 10^{-3} Kg$$

Equation 72

Once the mass of air has been found, the mass of fuel can be worked out. For a gasoline engine the stoichiometric air-fuel ratio is 14:7 so the mass of fuel can be worked out using the equation [1, 7, 41, 102]:

$$\lambda = \phi^{-1} = \frac{\alpha}{\alpha_{stoichiometric}} \implies \alpha = \frac{mass_{air}}{mass_{fuel}} = 14.7$$

Equation 102

The equation can be rearranged for mass of fuel, which can be calculated thus [1, 7, 41, 102]:

$$mass_{fuel} = \frac{mass_{air}}{14.7} = \frac{0.3789 \times 10^{-3} Kg}{14.7} = 0.0264 \times 10^{-3} Kg$$

Equation 8

Once the mass of fuel has been calculated then then the heat release can be calculated using the equation [1, 7, 41, 102]:

$$Q_{Cycle} = m_{fuel} h_{LHV} = \frac{mass_{air}}{AFR} h_{LHV} = \frac{0.3789 \times 10^{-3}}{14.7} \times 46 \times 10^6 = 1185.6735 J$$

Equation 103

where h_{LHV} for gasoline equals 46 MJ/kg [1, 7, 41, 102]. The assumptions that were made in order to calculate this number were that the air was at ambient conditions of 1 bar pressure and 300 degrees kelvin, the AFR was assumed to be Stoichiometric at 14.7:1, and the Lower heating value was assumed to be 46 MJ/kg.

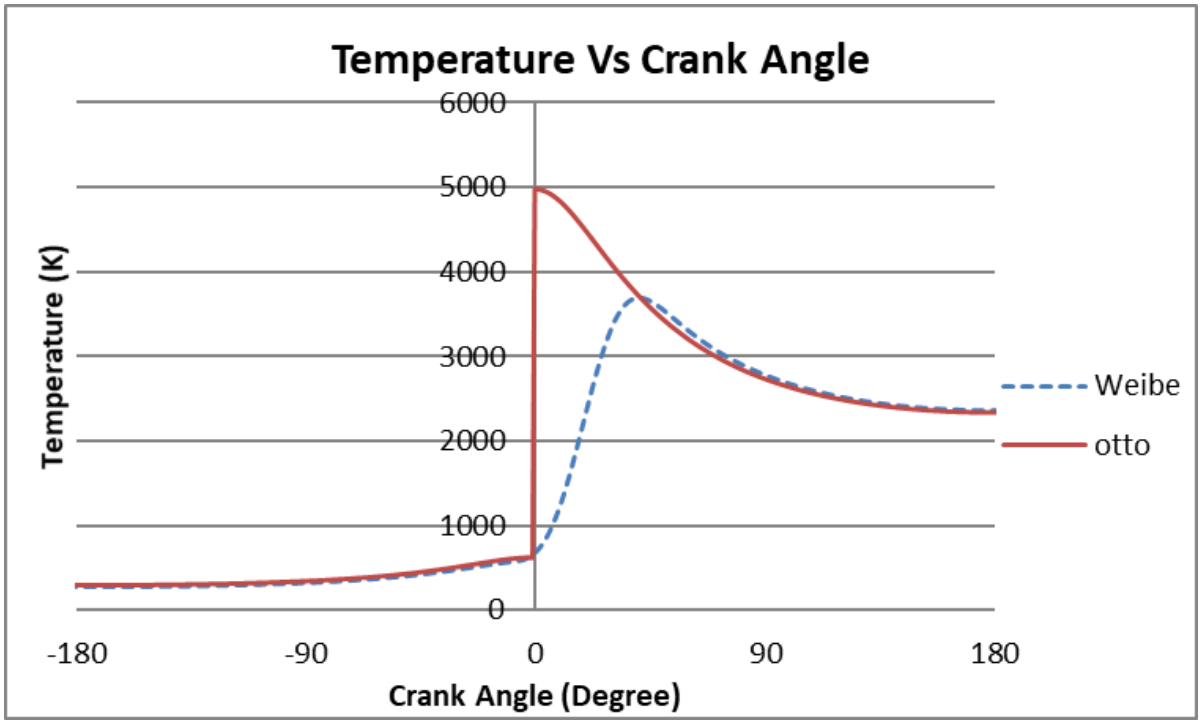

Figure 48: Temperature comparison of the Wiebe and Otto cycles calculated using the Excel template.

The analysis of the combustion profiles of the two different methods clearly shows the difference between them. Figure 48: Temperature comparison of the Wiebe and Otto cycles8 shows the heat increase of the Otto cycle is instantaneous and is over 1400 Kelvin greater than on the Wiebe method. The Otto cycle shows a 30% increase in temperature over the Wiebe method, which is unlikely. The Wiebe function shows a more realistic combustion profile and demonstrates the problems with the assumptions made when calculating the Otto cycle.

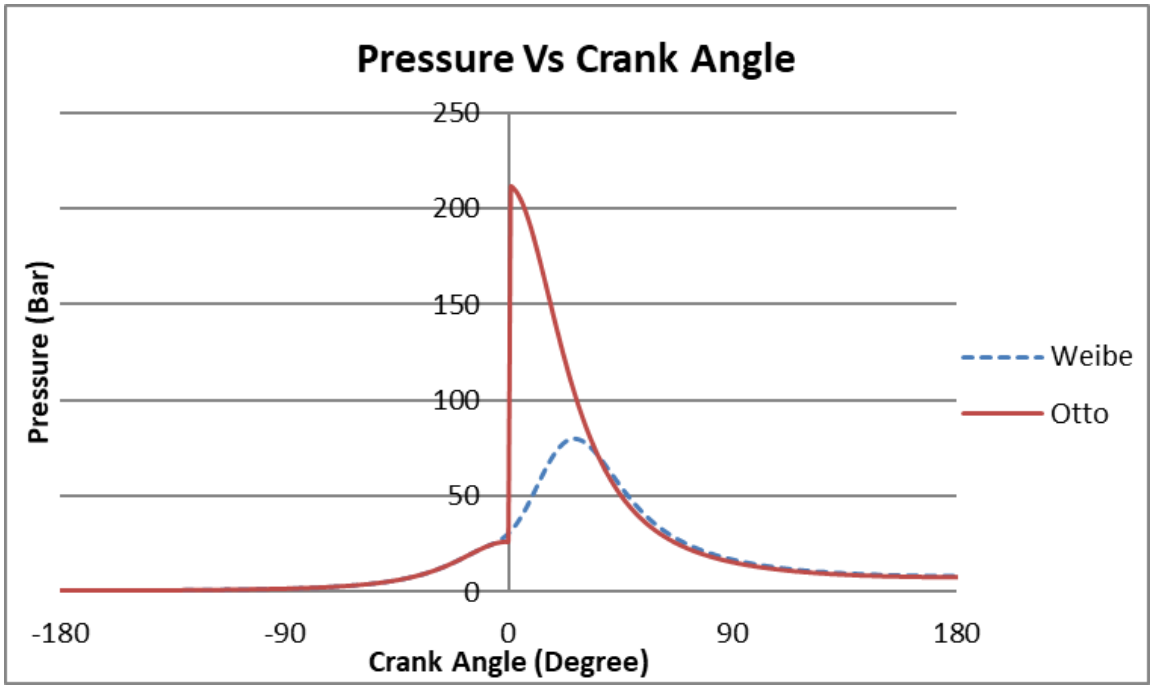

Figure 49: Pressure comparison of the Wiebe and Otto cycles, calculated using the Excel Template.

The Otto cycle in Figure 49: Pressure comparison of the Wiebe and Otto cycles9 shows a pressure increase of 140 Bar higher than the Wiebe cycle, which again is deemed unrealistic. The maximum pressure of the Wiebe function is 80 Bar, when combined with the 40% thermal and 97% mechanical efficiencies normally seen in internal combustion engines a realistic figure of 25-30 Bar is seen, which is to be expected from a high-performance race engine. The overall energy efficiency of the system for the heat work can be found using the equation [1, 7, 41, 102] –

$$\eta \equiv \frac{W_{net}}{Q_{positive}} = 1 - \frac{1}{r^{\Upsilon-1}} = 1 - \frac{1}{12.45^{1.4-1}} = 0.6353$$

Equation 12

This gives a total of 63.63% thermal efficiency which is an unrealistic value and far too high, and is attributed to not taking into account other losses in the system, such as thermal loss to the wall, unburnt fuel, pumping losses, loss of pressure round the piston ring and engine friction. Most modern car engines have a thermal efficiency of around 35%, with F1 cars having efficiencies of around 50% which are the highest seen in internal combustion engines designed for cars. Such efficiencies are achieved by very careful control of the combustion event, special lubricants and heat resistant coatings for the engine and using turbochargers and an energy recovery system connected to the exhaust and gear box, which are well out of the scope of this project in terms of time and budget. For this application of engine the overall efficiency will be around 35% [1, 7, 41, 102].

4.1.1. Conclusions

The analysis of the combustion model used in the GT-power model made assumptions regarding the parameters a and m, as they needed to be consistent with the Wiebe function data represented in the $\frac{dQ}{d\theta}$ graph. This can only be done with experimentation data and not theoretical data. Values of a=5 and m=3 were used in the first interpretations of the GT-power model. Any future experimental data will allow the model to be made more accurate, as the a and m values can be matched to the unique combustion profile of each individual engine [1, 7, 21, 41, 102]. The analysis of the final GT-Power model can be seen in section **4.4. GT-Power model results**.

4.2. Dynamics model data and discussion

The first step of the analysis of the internal components is to check the current designs. One parameter of the engine that needs to be assessed is piston speed as this has major implications for the rest of the engine, the ideal speed being 30 m/s. An Excel spreadsheet was constructed to run sweeps of the con-rod and crankshaft lengths and asses the effects they have on the internals. An Excel spreadsheet was deemed the best method as the calculations have already been assessed in the literature review. The analysis was done at 9,000rpm as this was where peak torque would be ideal located and thus was used as an anchor.

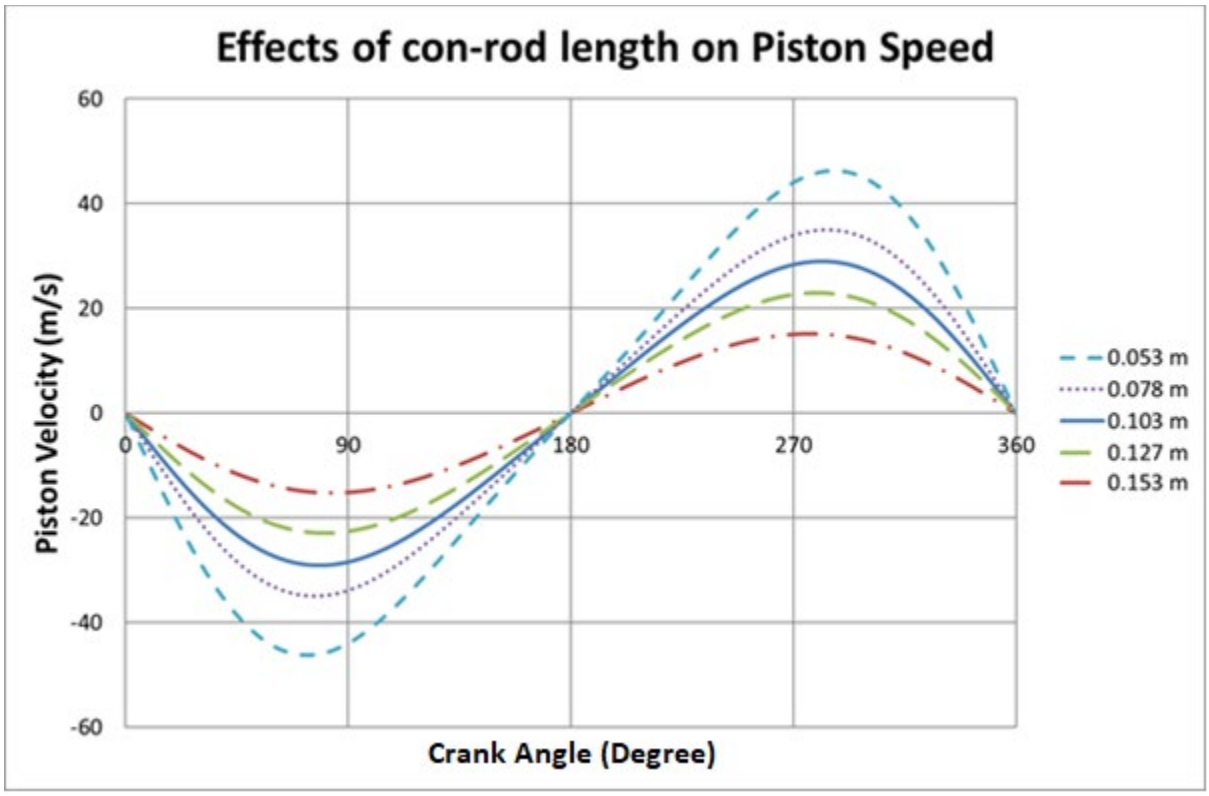

Figure 50: Piston velocities by different con rod lengths.

The con-rod length makes a difference to piston speed. Step changes, during the sweep, of around 25 mm, which gave differences of over 20 m/s.

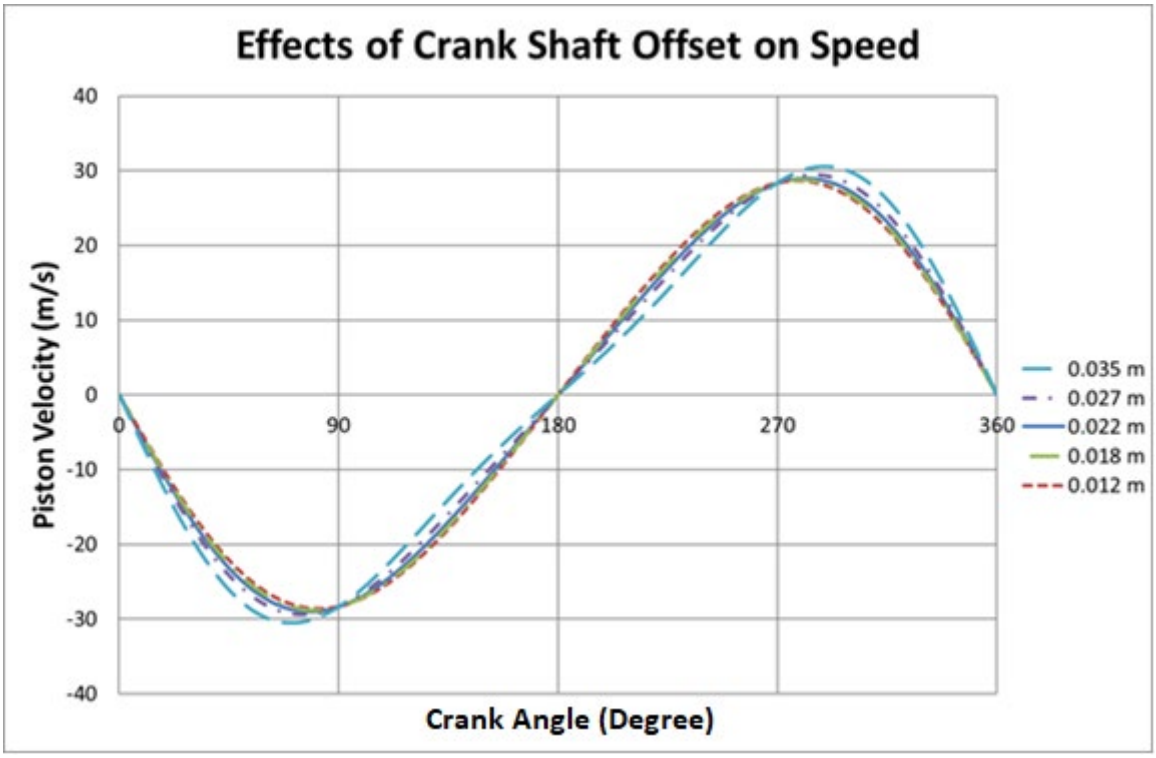

Figure 51: Piston velocities by different crank shaft offset lengths.

The crank offset had a limited impact upon piston speed. With sweeps of 5 mm the impact was only a few m/s between the longest and the shortest crank offset.

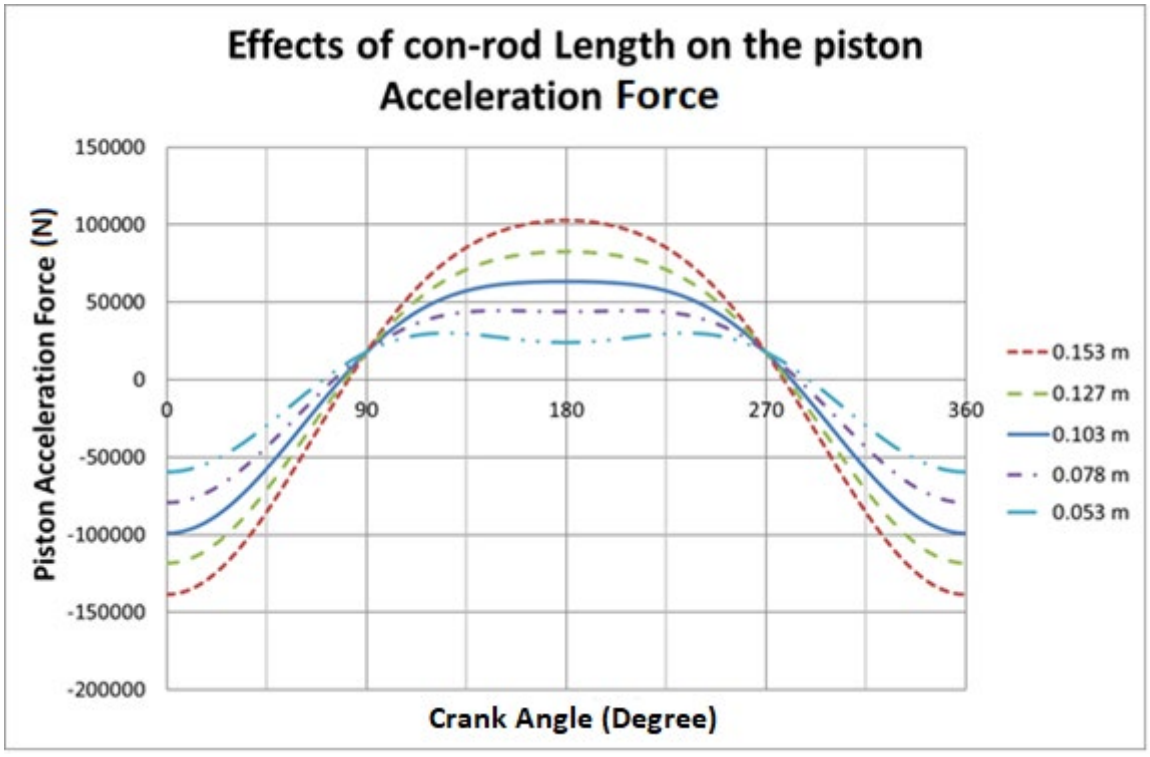

Figure 52: Piston acceleration by different con rod lengths.

The con-rod has a big impact on the acceleration in terms of the forces applied to internals with the same 20mm sweep. The noticeable difference with the sweep is the shape. A smoother shape is preferable as it will aid in flow in and out of the cylinder.

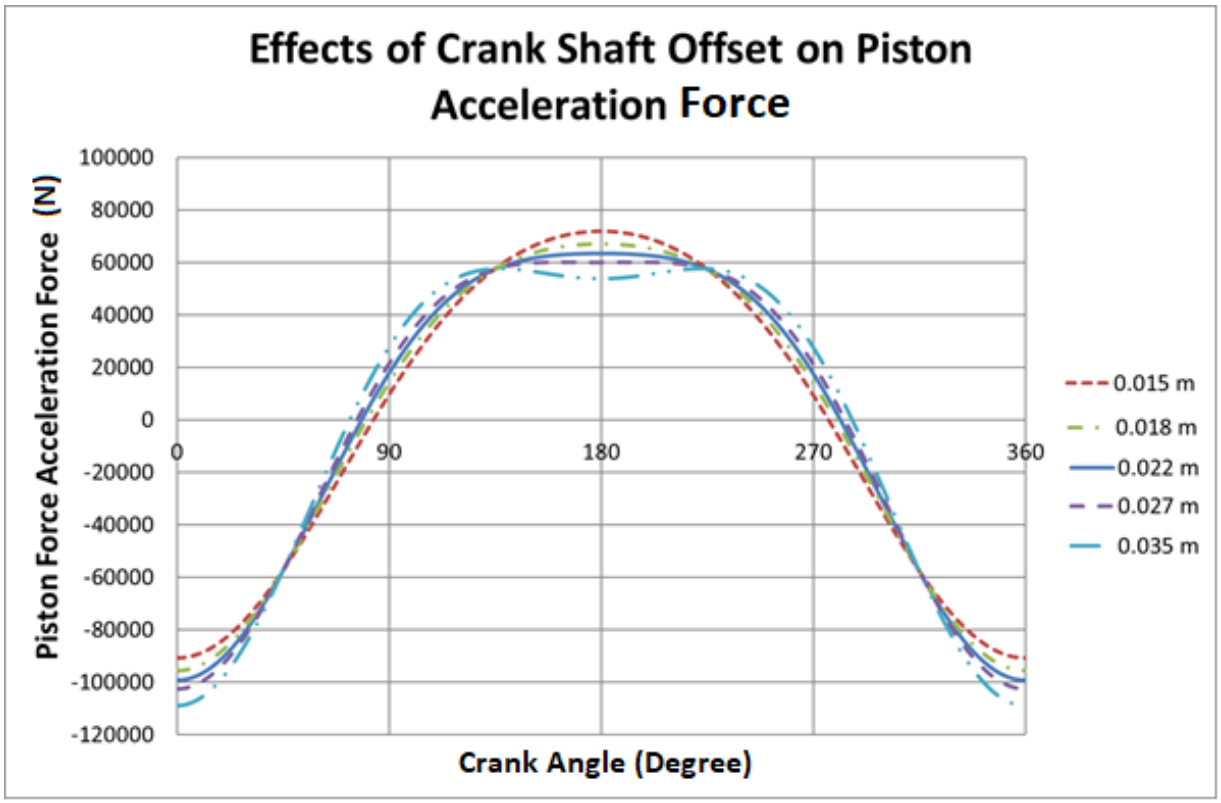

Figure 53: Piston acceleration by different crank shaft offset lengths.

The crankshaft off-set makes a small difference in terms of acceleration over the same 10mm sweep step, but has an impact on the shape of the acceleration profile. Again, the lowest peak with the smoothest profile is the optimal shape.

Section Summary

Reducing the peak acceleration of the piston will result in more time for gas exchange. It will also result in less force acting on the engine internals as F=ma, so reducing the acceleration will reduce the force, given that the mass is staying the same. The maximum piston speed has a lot of knock-on effects, and is ideally limited to around 30 m/s as this limits the forces exerted on the internal components. The internal dynamics are directly related to the instantaneous piston speed. When the lengths were analysed the original parameters of crank offset of 45.13mm and the con-rod length of 103mm were found to maintain a max piston speed of 30m/s, whist having the smoothest acceleration profile with the lowest peak.

Assessment of internal forces

The piston is an NME-Cosworth PA2622 with a bore of 92mm. The con-rod is an NME 103mm Con-rod sourced from the Nicholson McLaren pattern for the Cosworth XB part, made by Farndon Components. Both are made from steel. A table of the original engine specs can be found in **Table 1.**

material property	Con-rod	Piston
Volume (m^3)	$1.2e^{-005}$	$1.097e^{-004}$
Area (m^2)	0.026	0.038
Mass (Kg)	0.418	0.297
Density (Kg/m^3)	8410	2710

Table 3: Material Properties for the con-rod and piston

The starting point to analysing the engine internals starts with the piston characteristics

Piston displacement –

$$X = \frac{S}{2}\cos\theta + L\left[1 - \left(\frac{S}{2L}\sin\theta\right)^2\right]^{\frac{1}{2}}$$

Equation 28

Piston velocity –

$$\dot{X} = -\frac{S}{2}\omega\left(\sin\theta + \frac{\varepsilon}{2}\sin 2\theta\right)$$

Equation 29

Piston acceleration –

$$\ddot{X} = -\frac{S}{2}\omega^2(\cos\theta + \varepsilon\cos 2\theta)$$

Equation 35

Although to start the analysis of the engine internals, as per the literature review, the masses have to be split up into the reciprocating and the revolving masses. This was done within CATIA V5R20 as the material properties were added to the components, which showed where the centre of mass was for the con-rod seen in Figure 54: Analysis of the con-rods centre of mass using CATIA R5V24. and used the equation [1, 7, 38, 39, 42, 44, 45] –

$$m_A = m_c\frac{L_b}{L_a + L_b} \quad \textbf{and} \quad m_B = m_c\frac{L_a}{L_a + L_b} + m_p$$

Equation 35

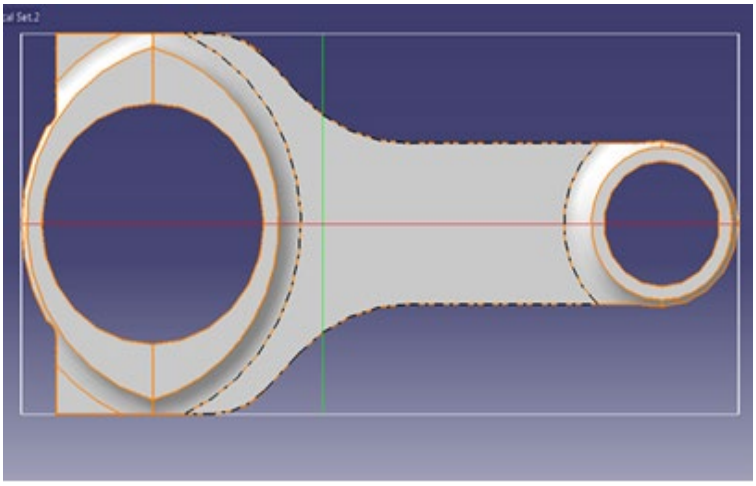

Figure 54: Analysis of the con-rods centre of mass using CATIA R5V24.

Once the Centre of Mass has been found the model of the con-rod can be split into two sections: the reciprocating and rotating masses.

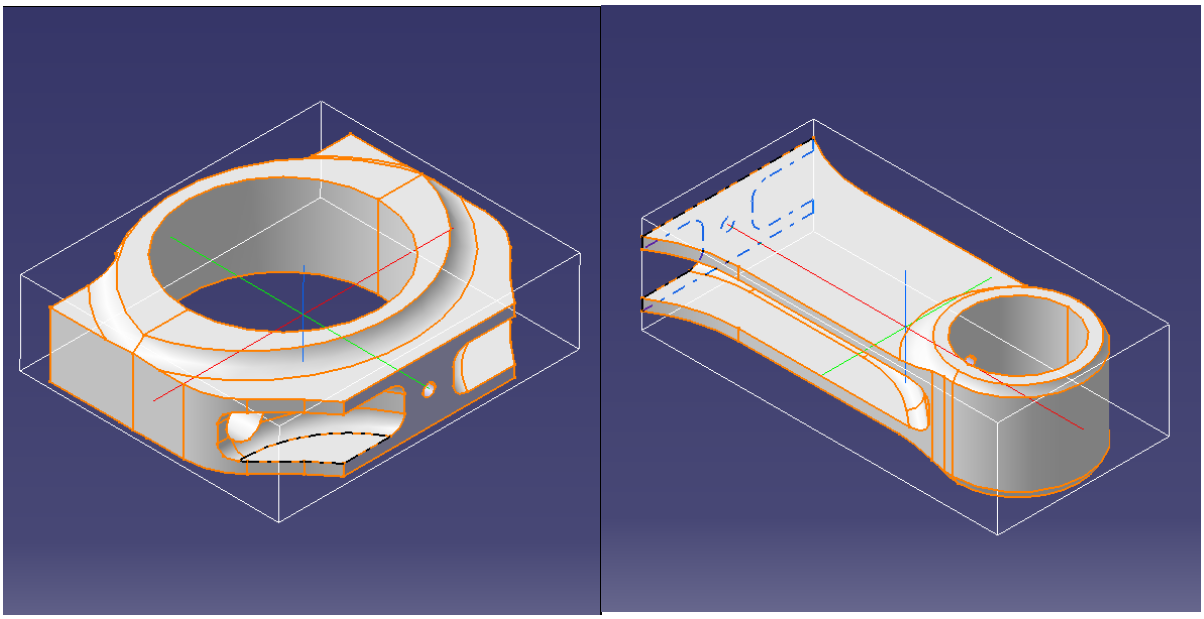

A) Showing the con-rod section added to the rotating mass.
B) Showing the con-rod section added to the reciprocating mass

Figure 55: The two sections of con-rod for each assembly of the reciprocating and the rotating masses.

The con-rod was split into the two sections to analyse each component of the mass, as part of the mass affects the rotating and part effects the reciprocating mass. Figure 55: The two sections of con-rod for each assembly of the reciprocating and the rotating masses.5 shows the split con-rod masses and was done in order to add the optimal masses to the rotating show by A, and reciprocating mass, shown by B, that are used to analyse the engine dynamics.

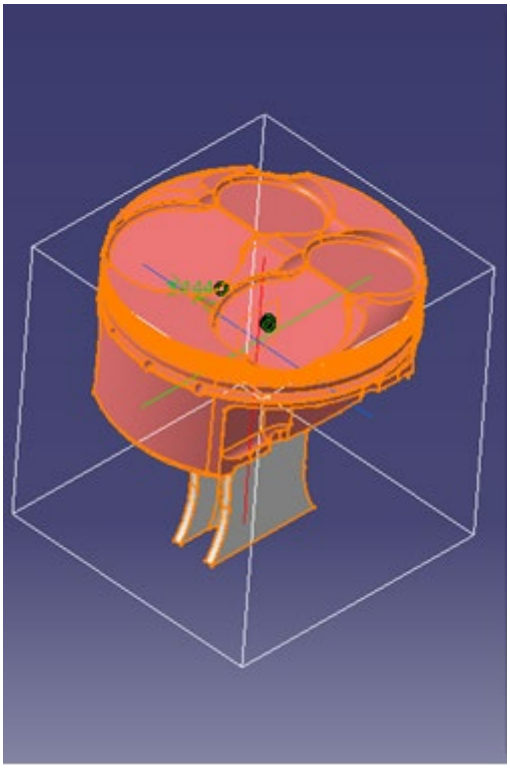

Figure 56: CATIA Piston Assembly to analyse the mass.

The small end of the con-rod together with the piston assembly makes up the reciprocating mass. The piston assembly is made up of the piston, small end of the con-rod, gudgeon pin, gudgeon pin spacer and the various piston rings and circlips to hold the assembly together. The reciprocating mass assembly has a weight of 0.567kg which, when factored into the analysis of the piston characteristics, allow the forces on the engine to be calculated.

The big end of the con-rod is added to the rotating mass, along with the big end bearings, con-rod bolts, and the crankshaft. The crankshaft was cut off at the axis to analyse the weight of all the components above the axis, so the amount of counterweight could be ascertained. The analysis found that the counter balance weight recommended by previous work effectively balanced the rotating mass and will be discussed further on in the project.

4.2.1. Forces within the engine

The first step in analysing the engine was to calculate the piston velocities. These were found to reach peaks of just less than 30 m/s at 12k RPM, the engines redline, which is the highest engine speed and therefore is the RPM where peak piston velocity should occur, seen in Figure 57: Piston velocity at 12.5k RPM acquired from Excel model.

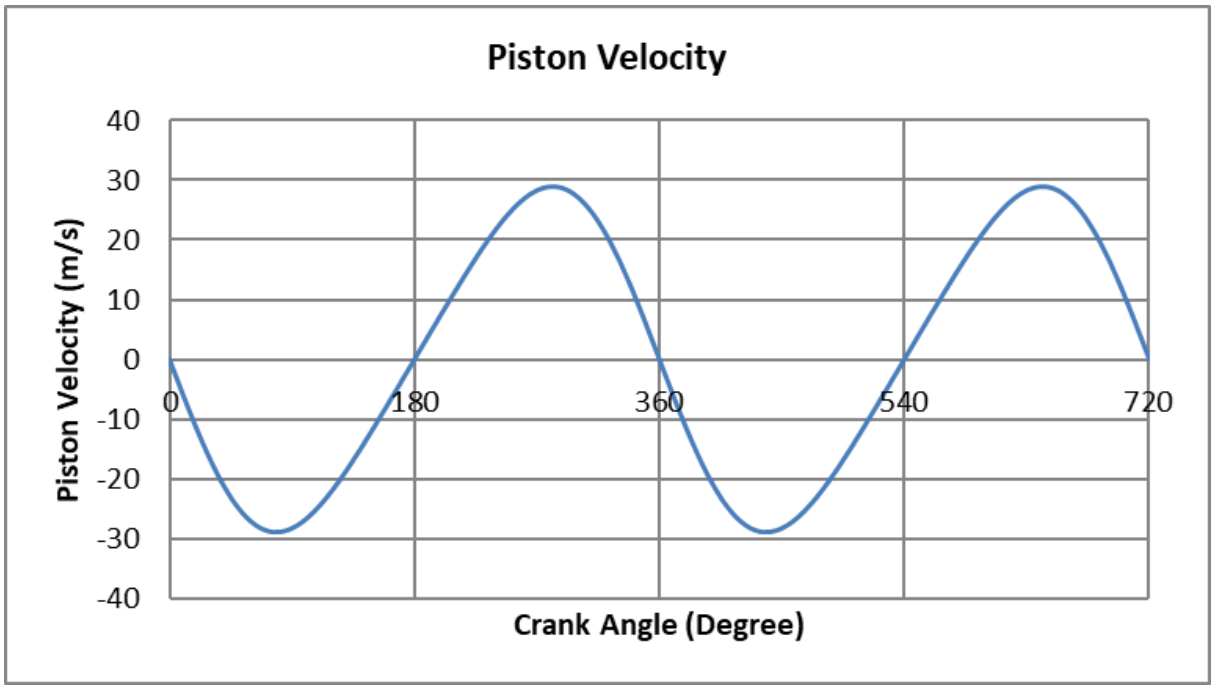

Figure 57: Piston velocity at 12.5k RPM acquired from Excel model.

There are two pistons in the engine, each of which have forces associated with them, and these forces are out of phase. The net effect of the combined forces has to be calculated with this in mind. The pistons are 70^0 CA difference between the two cylinders and therefore the firing orders are 70^0 CA out of phase.

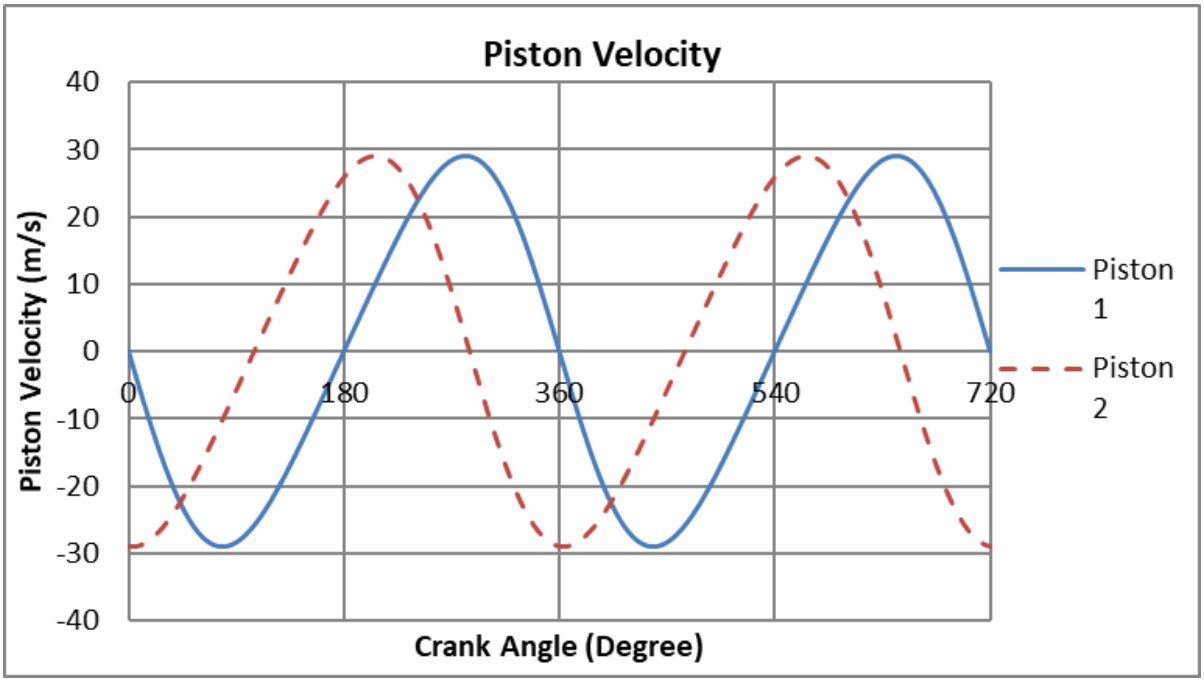

Figure 58: Analysis of both piston velocities.

The piston is subject to accelerations of up to 27,800 g in the positive direction and 43,400 g in the negative direction, seen in Figure 59: Analysis of piston acceleration at 12k RPM..

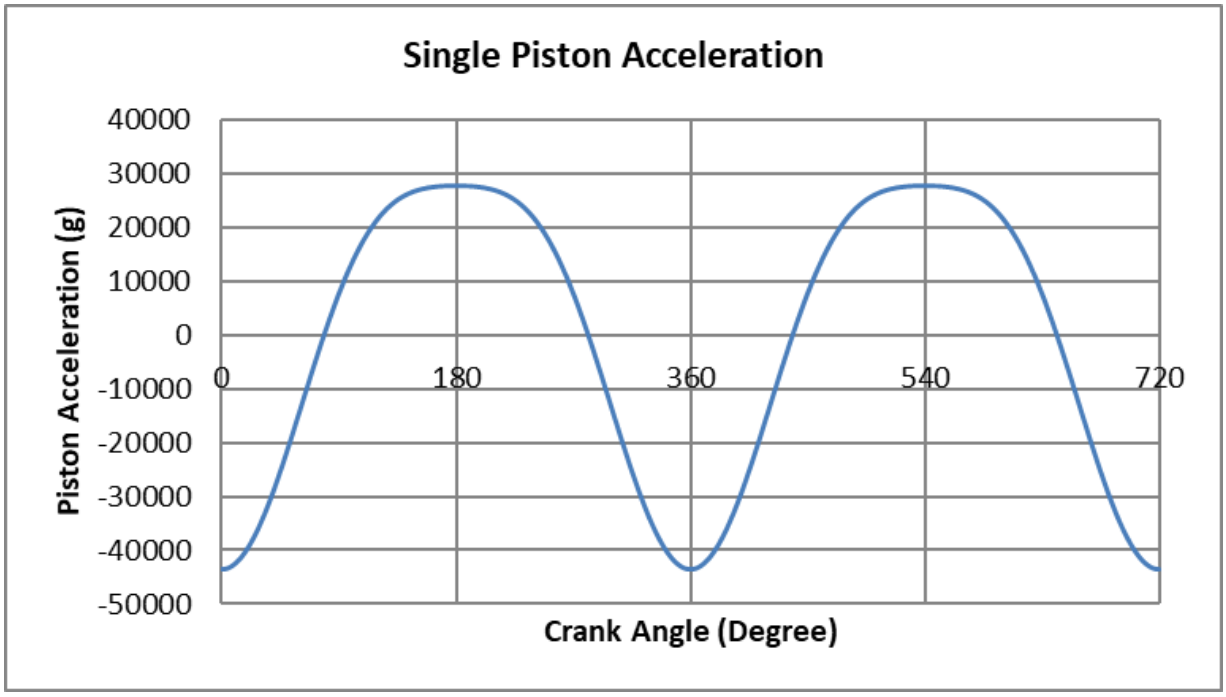

Figure 59: Analysis of piston acceleration at 12k RPM.

The rotation of the crank shaft and the swinging of the con-rod gives the piston acceleration profile seen in the piston acceleration graph and accounts for the sharp troughs. The primary force associated with the reciprocating mass has peaks at around 20,000 Newtons, while the secondary force peaks at around 4,500 Newtons. The primary forces are due to movement of the piston mass, and the secondary force is a product of changing acceleration vectors through the stroke. The primary and secondary forces will be felt as a vibrational force within the engine. Vibrations reduce the smoothness of the engine as well as increasing fuel consumption and reducing power due to the wasted energy. If the vibration are too excessive then the forces will start to wear the internal components and can even cause catastrophic failures within the engine.

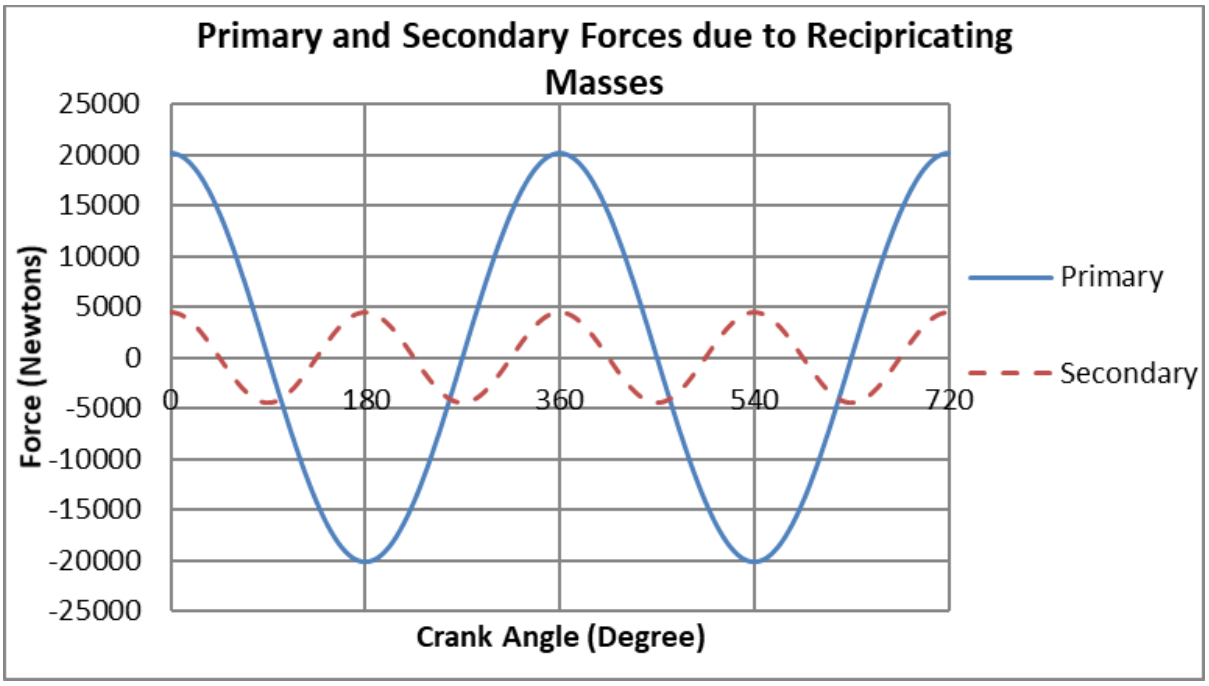

Figure 60: Primary and Secondary reciprocating forces

The secondary force is roughly 22% of the total force and so cannot be ignored. The combined force seen in Figure 60: Primary and Secondary reciprocating forces60, which peaks of 25,000 Newtons in the negative direction.

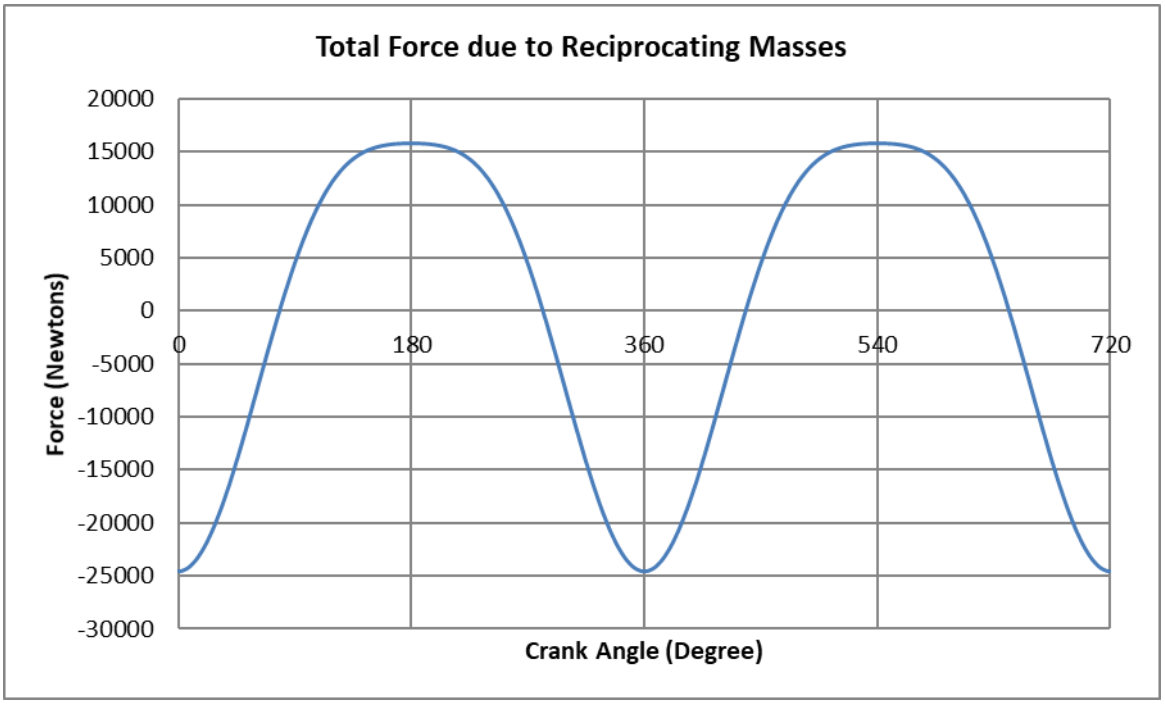

Figure 61: Total reciprocating forces over a full 4 Stroke cycle.

The primary and the secondary forces due to the reciprocating masses have been summed. The resultant force has reduced peaks in the positive direction of 1,600, but the peaks in the negative direction are around 25,000, as seen in Figure 61: Total reciprocating forces over a full 4 Stroke cycle.. This is due to the forces cancelling each other out in the positive direction whereas in the negative direction the forces combine resulting in a larger peak.

4.2.2. Balancing rotating masses

Mass A is the mass rotating around the crankshaft, which creates a force that acts radially away from the axis of rotation of the crankshaft. This force can cause wear and damage to the internal components of the engine such as the bearing and crankshaft. In order to counter this force another weight is positioned the opposite side of the rotational axis in order to counteract this force as much as possible, preferably negating it altogether. Using equation 47, discussed in the dynamics section of the literature review, to balance the rotating mass, it can be found the force needed to be balanced at 12000 RPM is, [1, 2, 31, 33] –

$$F_B = m_A(r\omega^2) \rightarrow (0.1224 \times 1256.637^2) \times 1.48 = 286063\,N$$

Equation 467

This give a force to be balance of 286063 N or 286kN.

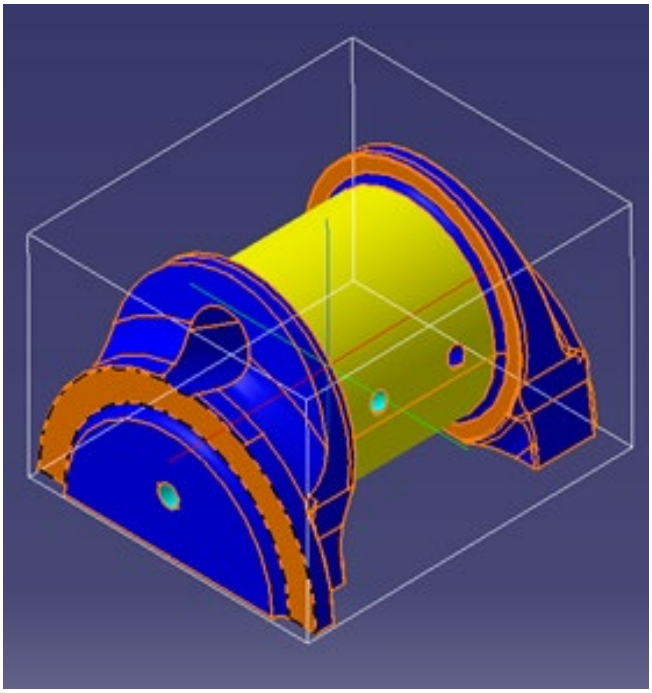

Figure 62: Crank offset above the crank shaft axis.

The crankshaft offset was modelled in CATIA which gave an initial weight and offset for the crankshaft seen in Figure 62: Crank offset above the crank shaft axis.. The next step was then to add all the other components that make up the bottom end of the con-rod, including the model of the cut off big end.

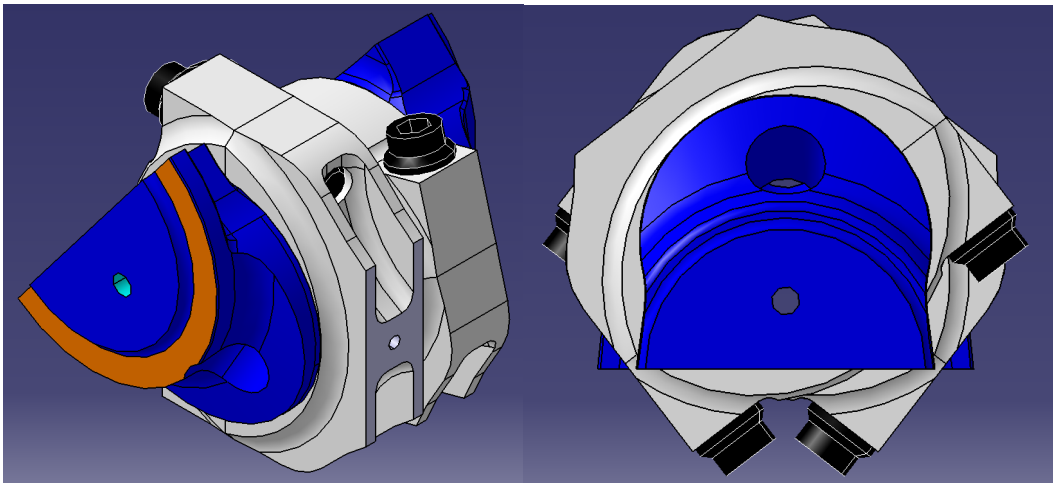

Figure 63: Rotating mass assembly above the axis of the crank shaft.

The model of the total mass that is connected to the crankshaft offset seen in Figure 63: Rotating mass assembly above the axis of the crank shaft.. This is the mass that needs to be balanced by a crankshaft counter-weight. The components that make up this assembly are the big end bearings, the big end and the bolts. These are all taken into account in the mass analysis with a total of 1.48 Kg.

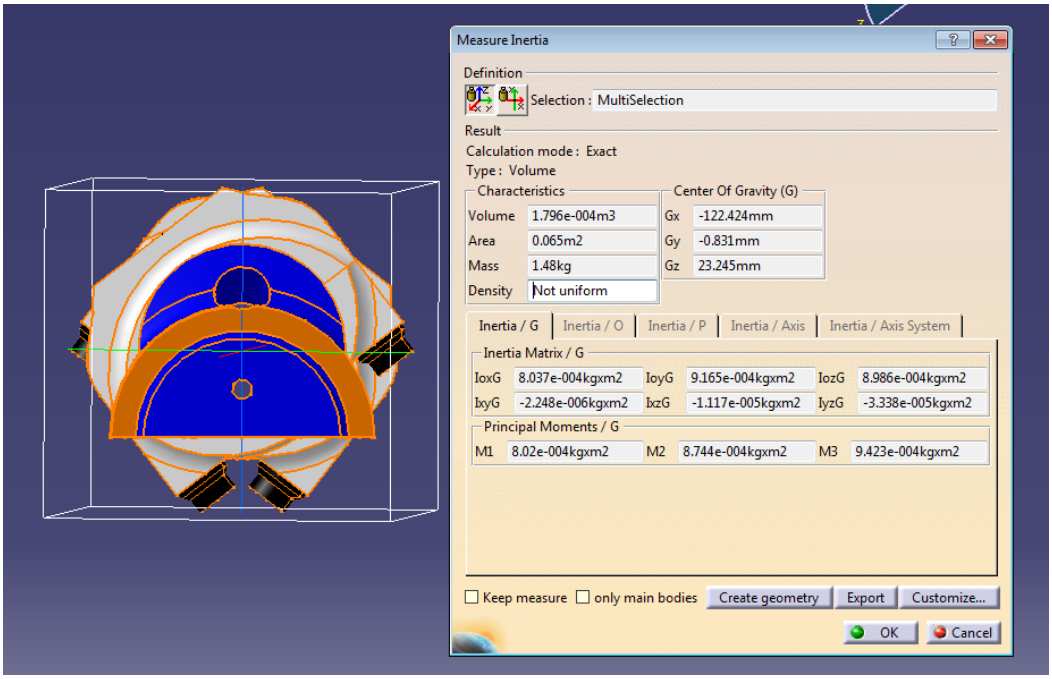

A) Showing the Properties of the unbalanced rotating mass

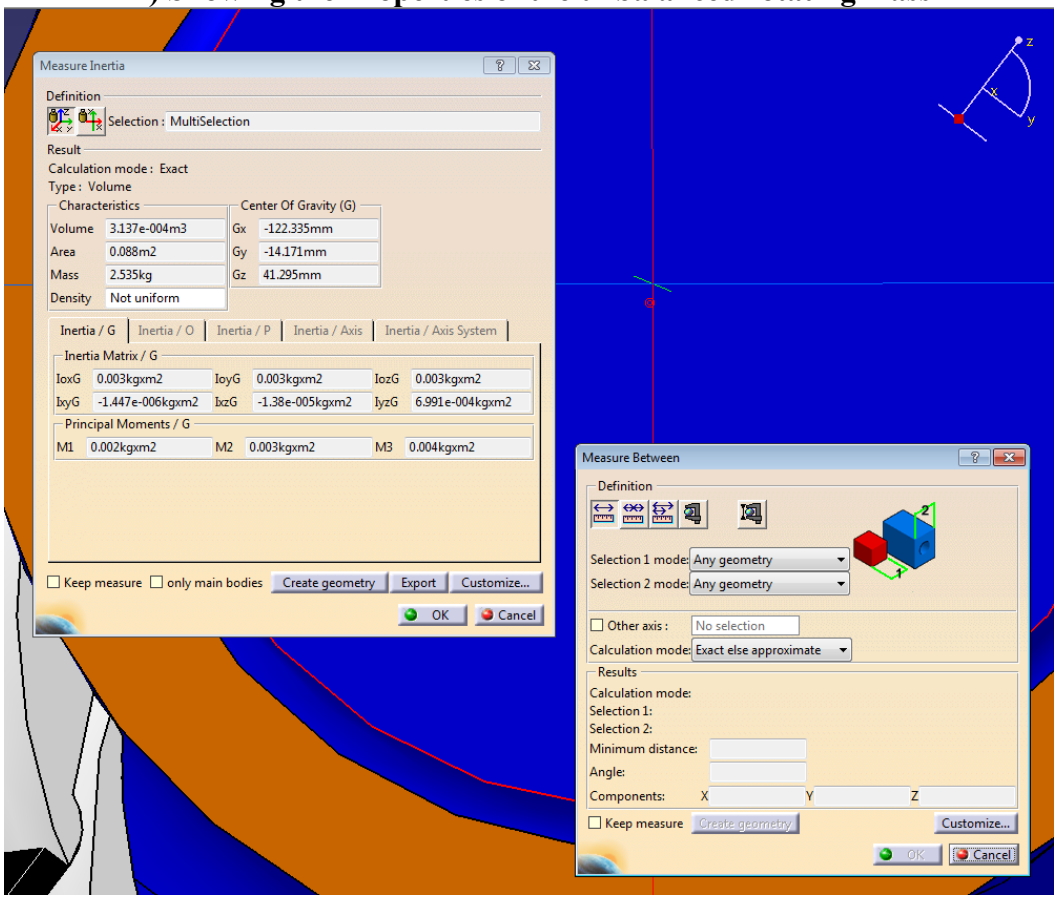

B) Showing the geometry and CoM of the unbalanced rotating mass

Figure 64: Total mass of rotating assembly with all the components.

CATIA can be used to assess the Centre of Mass in the model. Adding weight to the assembly below the revolution axis will move the Centre of Mass towards the axis shown in Figure 64: Total mass of rotating assembly with all the components.. Once the appropriate Gx, Gy or Gz

coordinate, depending on the model orientation, is roughly equal to 0 then the mass will be balanced around the central rotating point, as the model axis is set on the rotational axis of the crankshaft.

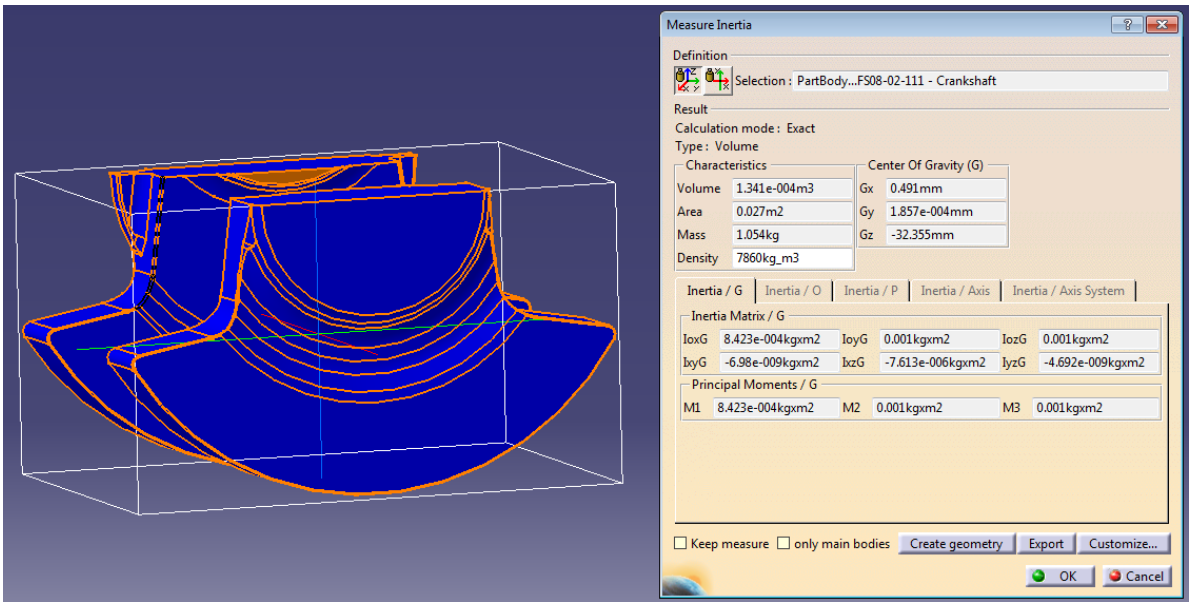

A) Counter weight for the rotating mass

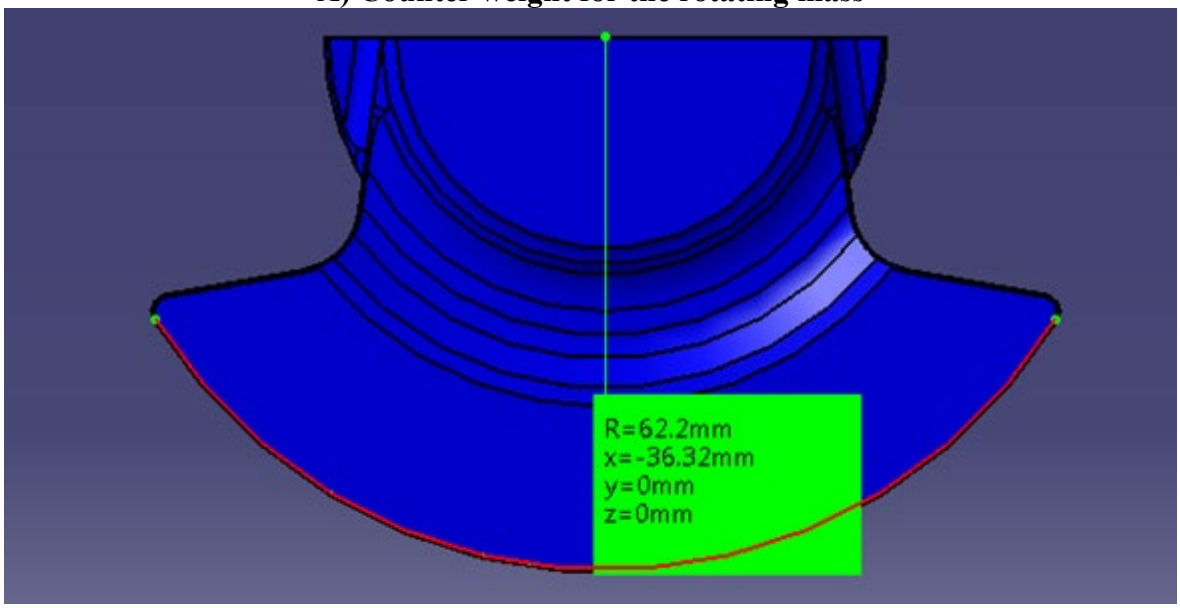

B Size of counter weight for rotating mass

Figure 65: Analysis of counterweight in CATIA V5R20.

CATIA gives a centre of mass of the component when the material properties are input, which allows the designs to be analysed quickly and accurately seen in Figure 65: Analysis of counterweight in CATIA V5R205. To minimise the mass required for the counter-weight, it is positioned away from the axis. This is because, for a given weight, the further from axis a given weight is, the larger the effect/counter force is on the other components. The counter-weight is positioned as far from the axis as possible, whilst retaining structural integrity of the whole assembly, to allow for the minimum counter-weight to be used, therefore minimising the weight of the whole assembly. This makes the engine lighter and minimises the forces acting on different components, which reduces fatigue and wear within the engine.

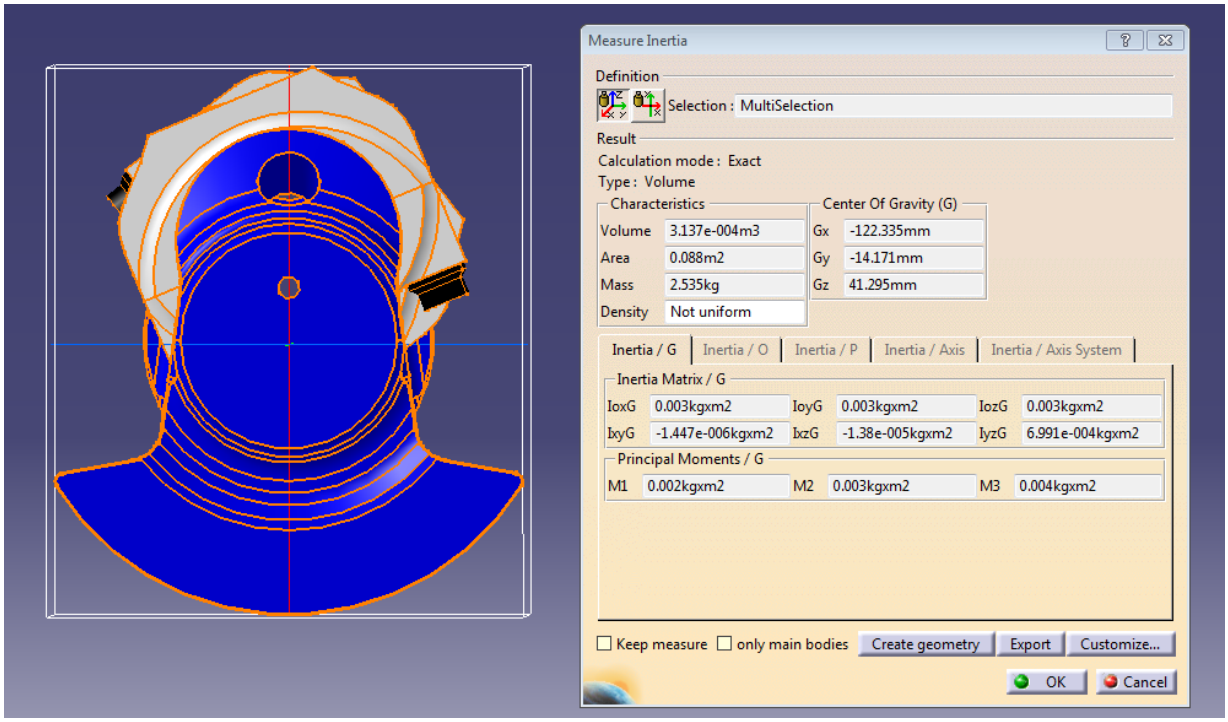

A) Rotating mass assembly with material properties.

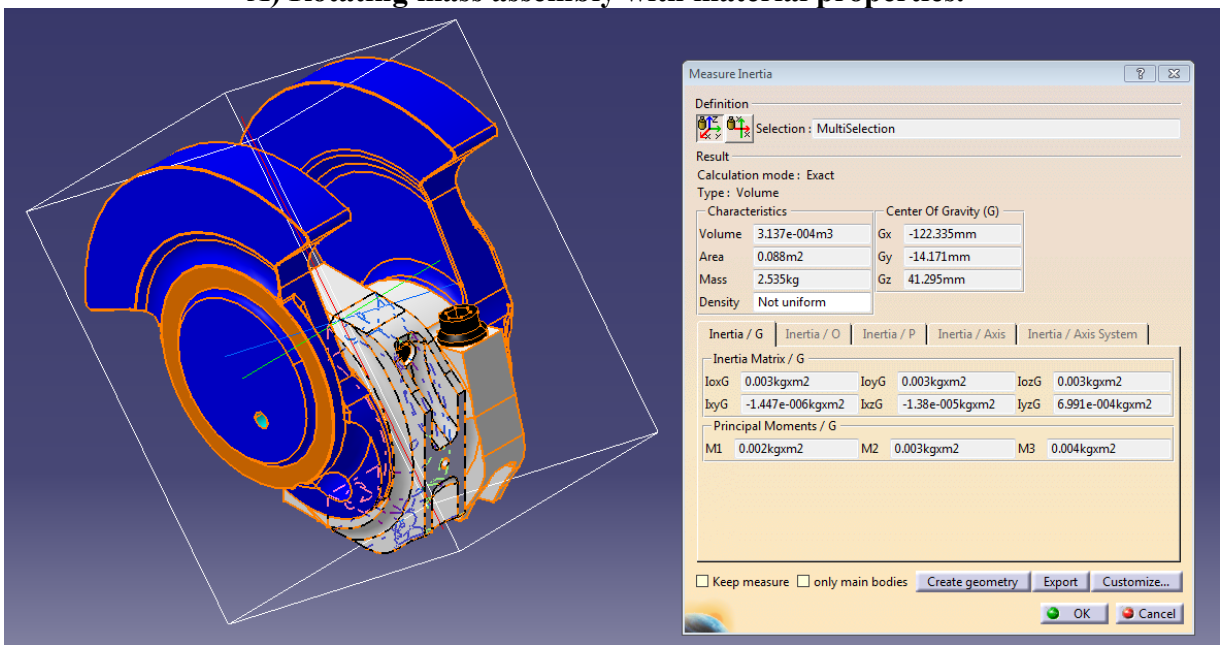

B) Isometric view of rotating mass assembly with the material properties.

Figure 66: Finished rotating assembly with counter weight added in.

It is common practice in the automotive industry to over-balance the crankshaft to compensate for the gas loads. However, the gas loads are not even, and the over-balancing will cause excessive force on the engine components for more than the short period of time the gas force is acting on the piston which is addressed in section later section.

The total rotation inertia for the rotational mass and the counter balance was shown to be in balance as the rotational mass had a centre of mass 0.1224 meters for the rotational axis while the counter balance mass had its centre of mass 0.1725 meters for the rotational mass and they had a total mass of 1.48 Kg and 1.05 Kg respectively as shown below –

For the rotating mass –

$$F_B = m_A(r\omega^2) \rightarrow (0.1224 \times 1256.637^2) \times 1.48 = 286063\,N$$

Equation 47

For the counter balance mass –

$$F_{Bal} = m_{cw-B}(R\omega^2) \rightarrow (0.1725 \times 1256.637^2) \times 1.05 = 286063\,N$$

Equation 48

One argument for over-balancing the crank to account for the gas force is to reduce the pressure on the top half of the bearing, but a well-designed oil system will create an oil pocket between the bearing and crankshaft which will dissipate this force. The gas loads are well in excess of the compensating force delivered by an excessive counter balance, which is therefore not desirable due to the extended strain exerted on the crankshaft from overbalancing.

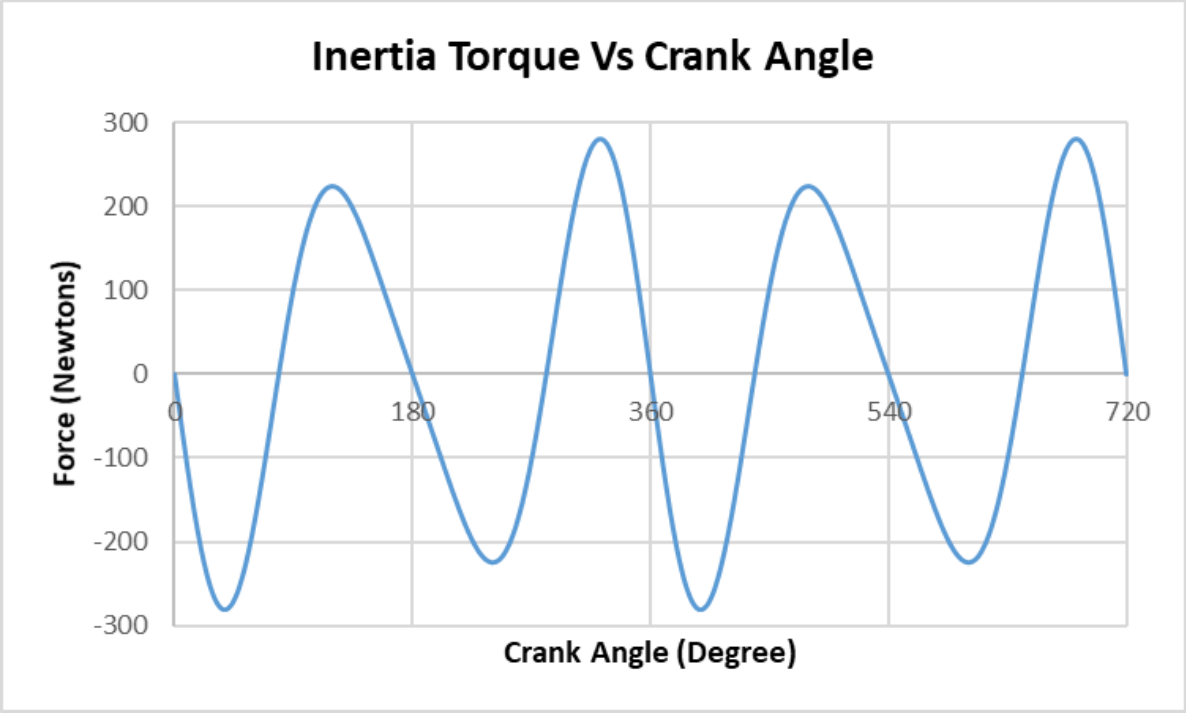

Figure 67: Torque inertia of the combined reciprocating masses at 12k RPM.

Using the same Excel template, the torque inertia was assessed and the results implemented into the GT-power model to improve the accuracy of the simulations.

Assessment of the combined forces

The Pressure trace was extracted from GT-Post and was input into the dynamics model, in Excel, for post simulation analysis. The results, seen in Figure 68: Pressure plot from GT-Post and plot of Gas force from Excel dynamics model, show the in-cylinder peak pressure rises to over 80 bar, which equates to around 55,000 Newtons of force exerted on the piston at 9,000 RPM.

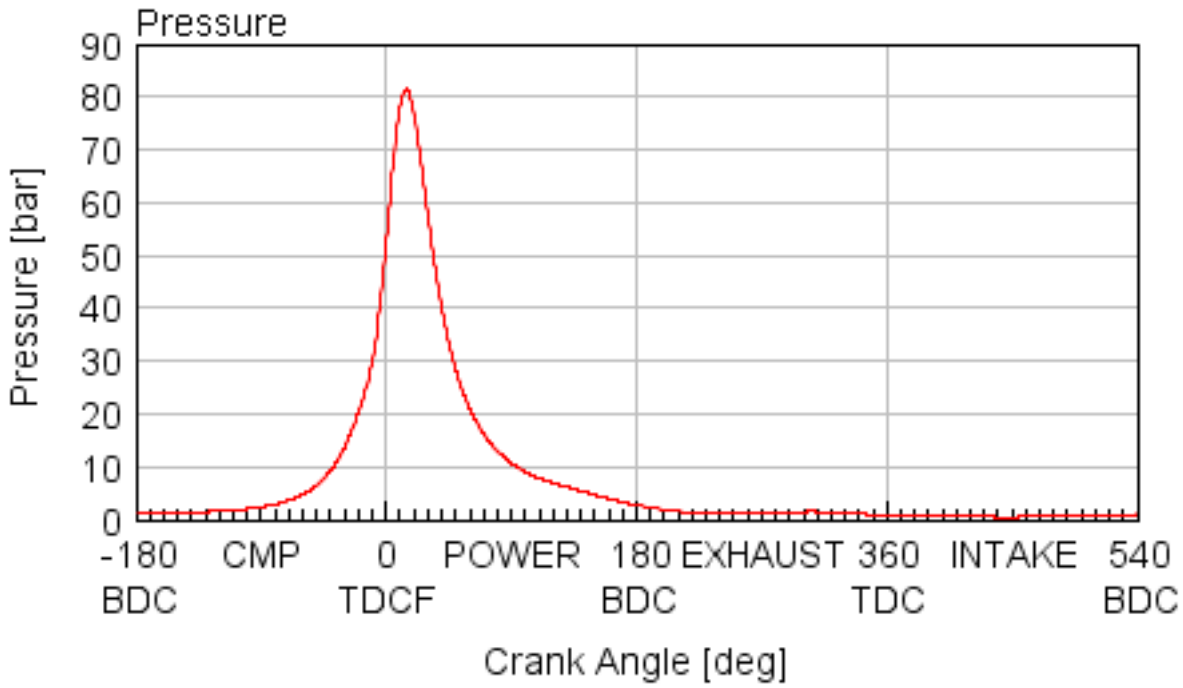

A) Pressure plot from GT-Post at 9000 RPM.

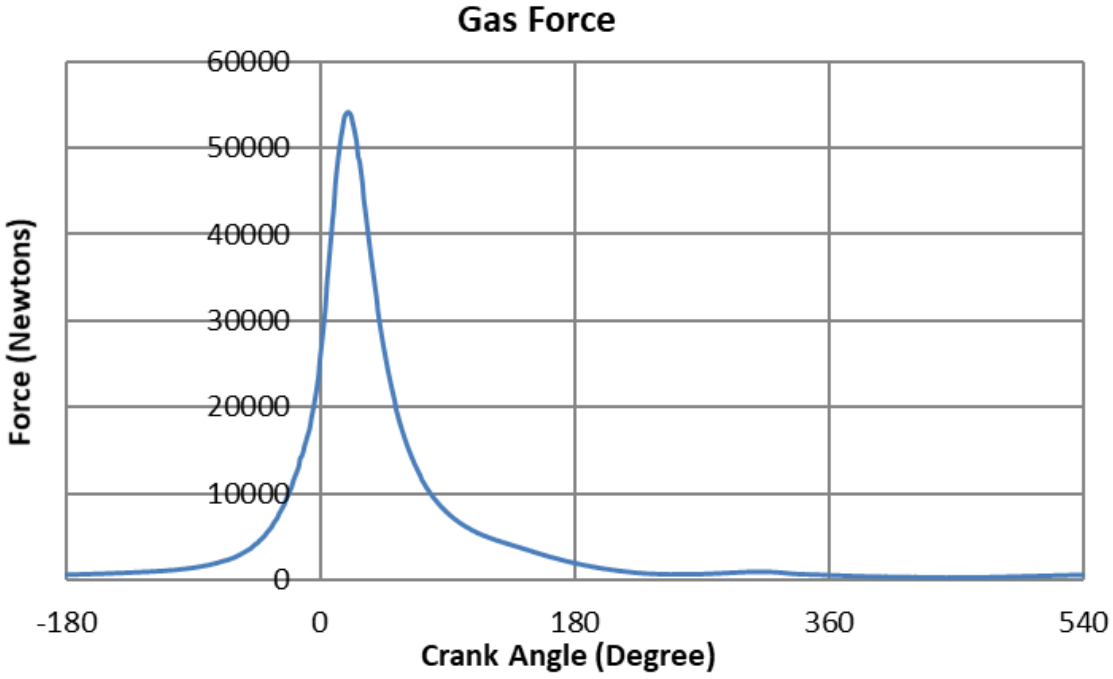

B) Excel dynamics model plot of the gas force at 9,000 RPM.

Figure 68: Pressure plot from GT-Post and plot of Gas force from Excel dynamics model.

Once the gas forces and inertia of the reciprocating masses are combined it is possible to analyse the overall force acting on the crankshaft, as shown in Figure 69: Combined Gas forces and inertia of reciprocating masses from the Dynamics model..

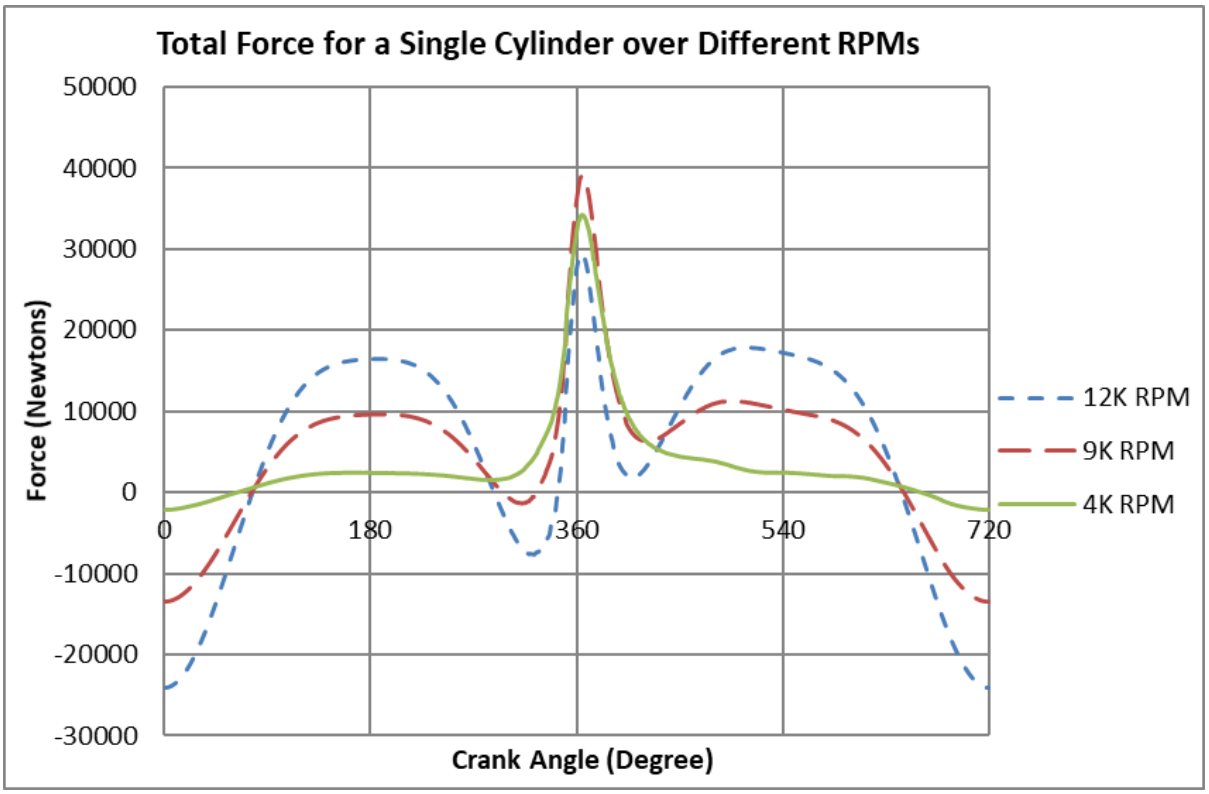

Figure 69: Combined Gas forces and inertia of reciprocating masses from the Dynamics model.

Figure 69: Combined Gas forces and inertia of reciprocating masses from the Dynamics model.9 shows the forces from the reciprocating mass increases with engine speed. However, when combined with the gas forces, the 9,000 RPM gas force has a proportionately larger impact on the overall force as it makes up a much larger load than the equivalent at 12,000 RPM.

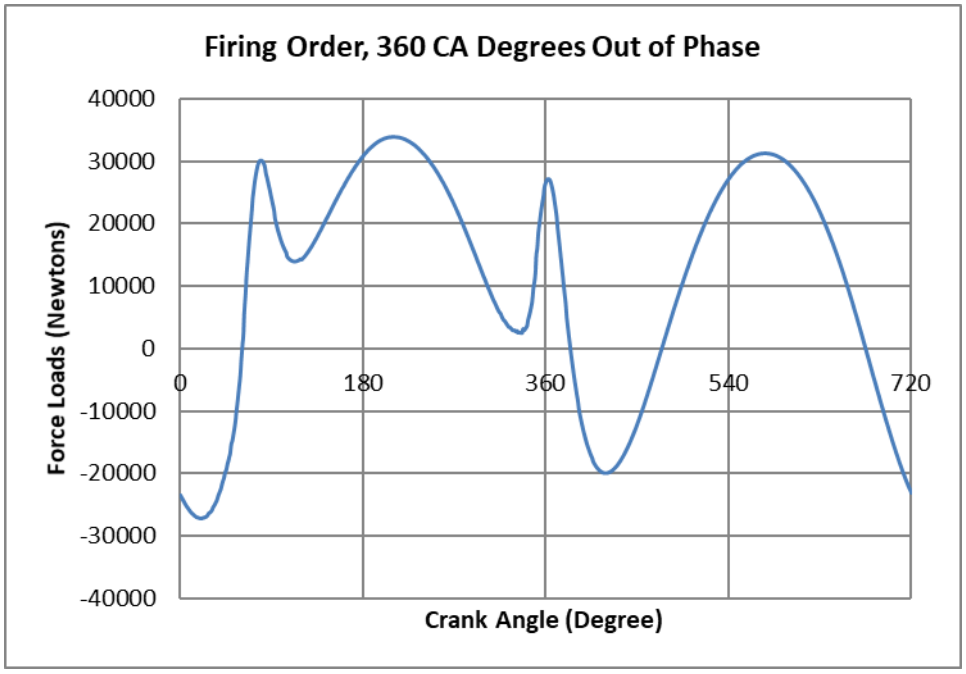

A) Out of phase firing order loads.

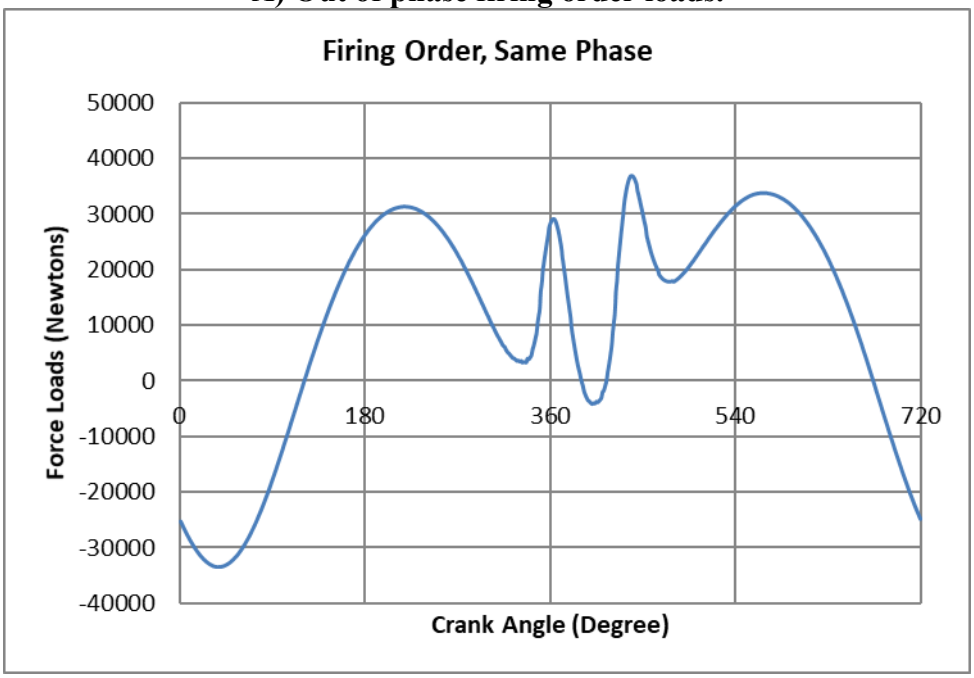

B) Same phase firing order loads

Figure 70: A shows out of phase firing order loads. B shows same phase firing loads. Both at 12k RPM.

The combustion phasing needs to be analysed as this will dictate the gas loads applied to the internal components at different crank angles. The firing orders are always 75 crank-angle degrees out of phase due to the 75 Degree V on the engine, but the phase difference is a factor of 180 degrees out, as that is the amount of rotation one of the 4 combustion phases requires. Figure 70: shows the same-phase firing order exhibits a maximum load of 37,000 Newtons and the out-of-phase has a maximum load of roughly 33,000 Newtons. Therefore to reduce the loads on the internal components the 360 degrees out-of-phase firing order will be used.

4.2.3. Section Summary

The work carried out in developing the dynamics model for the V-twin engine has not only allowed the current dynamics to be explored, and further understanding to be achieved. The work carried out in the dynamics section helped develop the GT-Power model by aiding detailed analysis of the components and their masses, and the data was input into the GT-Power model where relevant.

4.3. Manifold design and analysis

The inlet manifold was analysed within the GT-Power model to assess the current designs. Due to the iterative process of engine development, the GT-Power model was used to analyse the initial calculations and allowed further analysis of any potential improvements that can be demonstrated by the simulations.

4.3.1. Intake plenum size

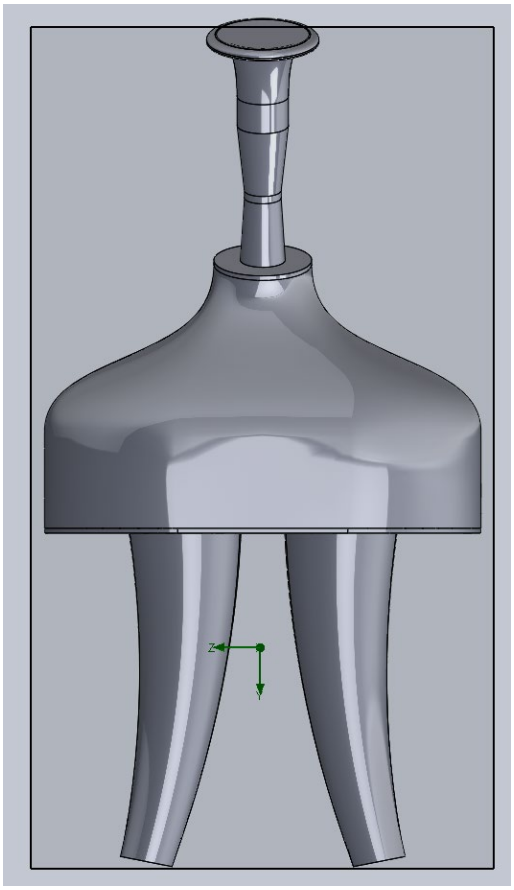

Figure 71: CAD model of the original intake manifold

One restriction found with the original design was the restrictor was too small, the original 2.67 litre plenum was found to need an increase in volume to 4.12 litres. Combined with the other modifications proposed, such as different runner lengths and exhaust length, this gave a 10BHP increase over the original model.

4.3.2. Intake manifold

There were some other areas of the intake that could potentially be improved such as the shape. The original had a flat bottom where as a rounded shape could give flow benefits as there are less sharp corners within the system.

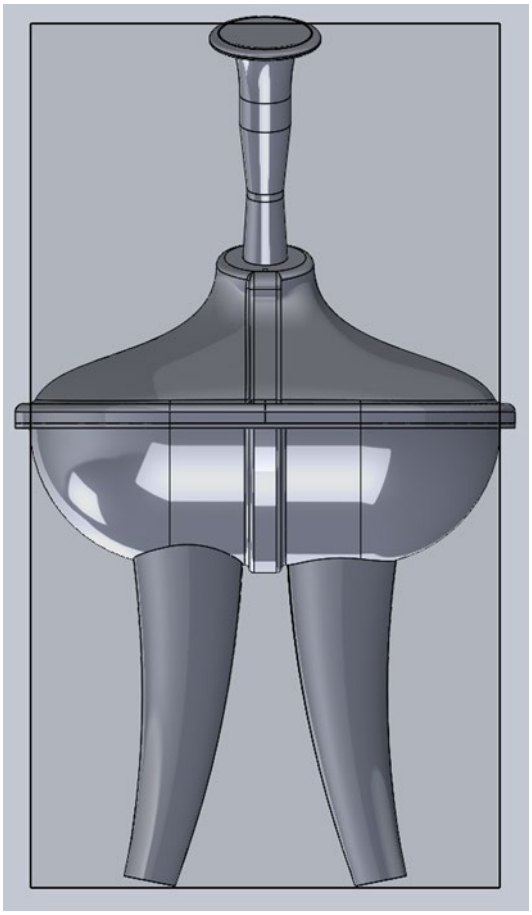

Figure 72: CAD representation of what a potential intake manifold could look like with the proposed modifications.

4.3.3. Runner analysis

The equations for the intake were calculated at ambient conditions of 1 bar atmospheric pressure and 300K room temperature, which gave a speed of sound of 344 m/s. The calculated lengths of the inlet runner were analysed in GT-Power, with their harmonic orders as well, to ascertain the optimal length for the runner. The results can be seen in Table 4.

Intake runner length in mm									
Intake		Harmonic Order							
		1	1.5	2	2.5	3	3.5	4	4.5
RPM	4000	3572.74820	2381.83214	1786.37410	1429.09928	1190.91607	1020.78520	893.18705	793.94405
	5000	2286.55885	1524.37257	1143.27942	914.62354	762.18628	653.30253	571.63971	508.12419
	6000	1587.88809	1058.59206	793.94405	635.15524	529.29603	453.68231	396.97202	352.86402
	7000	1166.61166	777.74111	583.30583	466.64466	388.87055	333.31762	291.65291	259.24704
	8000	893.18705	595.45803	446.59353	357.27482	297.72902	255.19630	223.29676	198.48601
	9000	705.72804	470.48536	352.86402	282.29122	235.24268	201.63658	176.43201	156.82845
	10000	571.63971	381.09314	285.81986	228.65588	190.54657	163.32563	142.90993	127.03105
	11000	472.42951	314.95301	236.21476	188.97181	157.47650	134.97986	118.10738	104.98434
	12000	396.97202	264.64802	198.48601	158.78881	132.32401	113.42058	99.24301	88.21601
	13000	338.24835	225.49890	169.12418	135.29934	112.74945	96.64239	84.56209	75.16630

Table 4: Intake runner length and harmonic order comparison.

Figure 73: Pressure trace from the inlet runner simulated in GT-Power. shows the pressure trace from the inlet runner simulated in GT-Power, showing the reciprocating pressure waves used in intake design to maximise the RAM air effect that is commonly used in manifold design.

The method of calculating the runners can be seen in the manifold methodology.

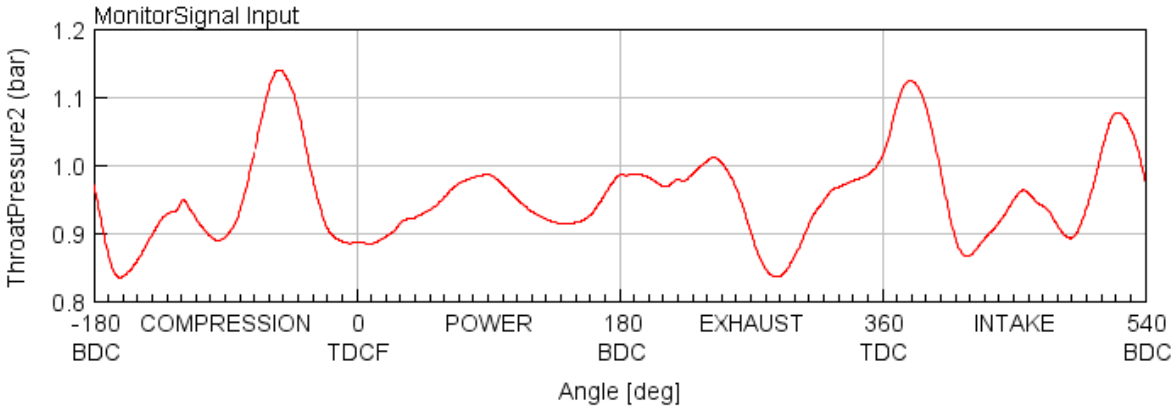

Figure 73: Pressure trace from the inlet runner simulated in GT-Power.

GT-power optimiser was used to find the ideal runner length, as well as using an iterative process of testing which looked at the pressure waves that were created for different runner lengths. The ideal length was found to be 380 mm, but this is far too long because the runners would have interfered with each other, as seen in Figure 74: Runner angle analysis and curvature. A way of shortening the runner length was to taper the runner, as the tapering effect gives the acoustic properties of a longer runner of constant diameter. This is because the increase in diameter slows down the speed of sound within the runner and therefore slows down the pressure waves. Thus, a shorter, tapered pipe will give a similar time for a pressure wave to travel down it, as would a longer straight pipe.

The mass flow rate of 0.3109 kg/s was used as the outlet mass flow rate of the port.

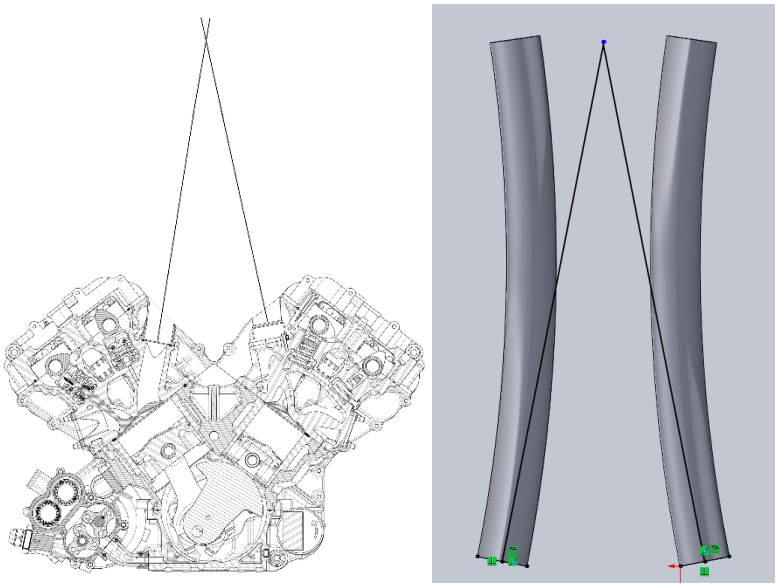

Figure 74: Runner angle analysis and curvature.

Figure 74: Runner angle analysis and curvature shows that if the runners were to follow a straight path from the inlet port they would intersect, which means they need to be curved to avoid flow intersection and allow them to fit. Another consideration for curving them was in order to fit the fuel injectors.

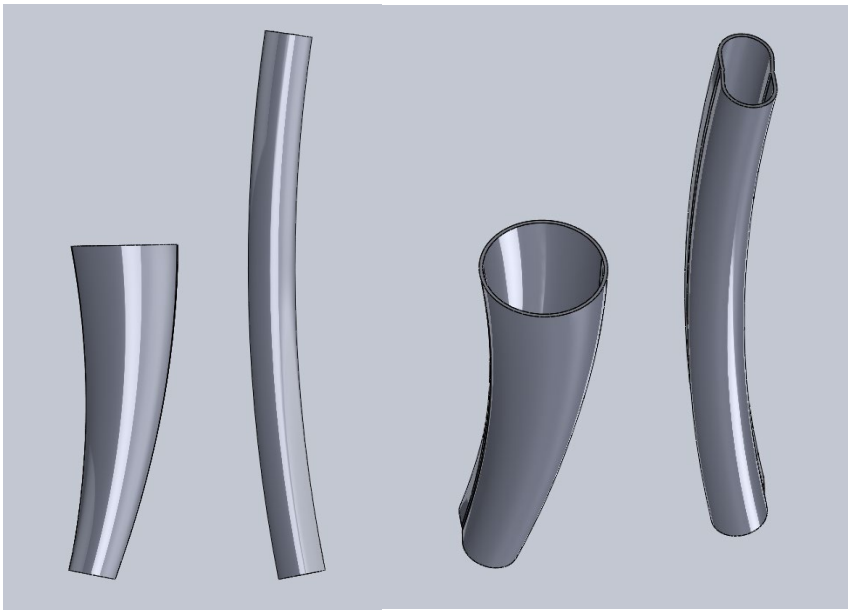

Figure 75: Length reducing expansion representation of the runner.

Figure 75: Length reducing expansion representation of the runner shows runners that have the same acoustic properties, but the runners that are flared have a significantly shorter length.

The GT-Power model indicated that the flared runner length should be 333mm, compared a straight runner length of 380mm.

4.3.6. Exhaust design

The equations for the exhaust were calculated using estimated values that were taken from the initial GT-Power model. The values used were 1 bar pressure and 1000K temperature, which give a speed of sound of 633.88 m/s. In table 5 the potential exhaust lengths depend on their harmonic orders.

Exhaust length in mm									
Exhaust		Harmonic Order							
		1	1.5	2	2.5	3	3.5	4	4.5
RPM	4000	4353.20326	2902.13550	2176.60163	1741.28130	1451.06775	1243.77236	1088.30081	967.37850
	5000	2786.05008	1857.36672	1393.02504	1114.42003	928.68336	796.01431	696.51252	619.12224
	6000	1934.75700	1289.83800	967.37850	773.90280	644.91900	552.78772	483.68925	429.94600
	7000	1421.45412	947.63608	710.72706	568.58165	473.81804	406.12975	355.36353	315.87869
	8000	1088.30081	725.53388	544.15041	435.32033	362.76694	310.94309	272.07520	241.84463
	9000	859.89200	573.26133	429.94600	343.95680	286.63067	245.68343	214.97300	191.08711
	10000	696.51252	464.34168	348.25626	278.60501	232.17084	199.00358	174.12813	154.78056
	11000	575.63018	383.75346	287.81509	230.25207	191.87673	164.46577	143.90755	127.91782
	12000	483.68925	322.45950	241.84463	193.47570	161.22975	138.19693	120.92231	107.48650
	13000	412.13759	274.75839	206.06879	164.85503	137.37920	117.75360	103.03440	91.58613

Table 5: Table of engine speed Vs harmonic order to give exhaust lengths in mm

The method for calculating the exhaust length can be seen in the manifold methodology section, previously. When comparing the results of the harmonic analysis of the exhaust length it is necessary to ensure that the overall exhaust is sufficient to allow clearance from the chassis and any critical components. This, however, this will affect the aerodynamics of the car and thus have to be examined further but the aerodynamics and chassis developers. From the point of view of this project, for engine performance, peak torque is delivered at 9000 RPM. Therefore, the exhaust length should be 859.89mm which matches the 1st harmonic order. This is long enough to exit the chassis and is a recommendation from this project that should be further examined by the aerodynamics and chassis developers.

Furthermore, analysis of the flow through a mock-up of the exhaust system shows that there could be some improvement to the original intended design of exhaust. The original exhaust system design shows flow problems, highlighted by the flow separation from the surface, shown in Figure 75.

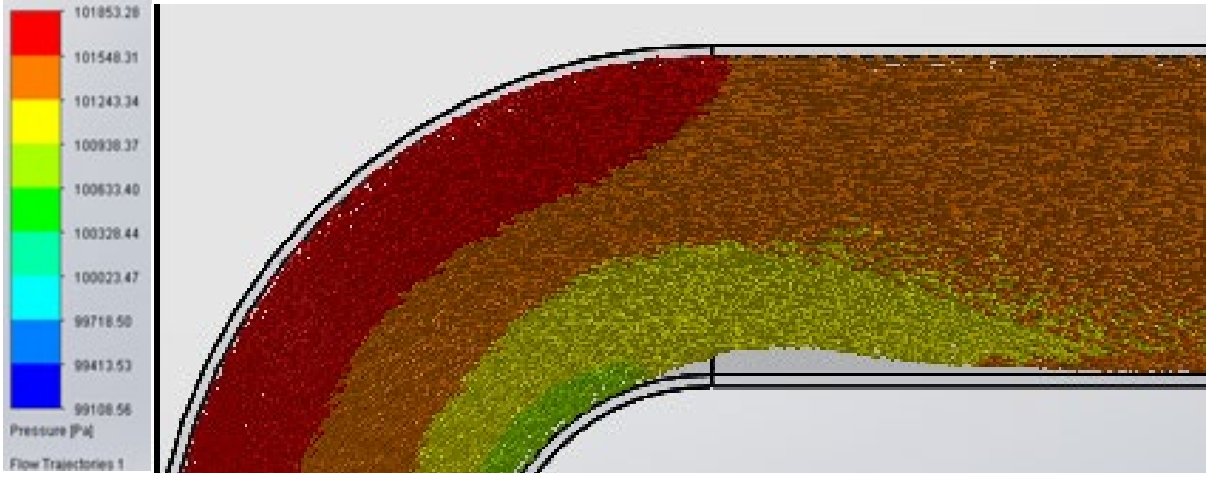

Figure 76: Flow analysis of exhaust pressure distribution using CFD.

Figure 77: analysis of flow within the current and proposed exhaust system. shows the flow in the original system has a lot of flow separation from the system wall, which causes pressure build ups.

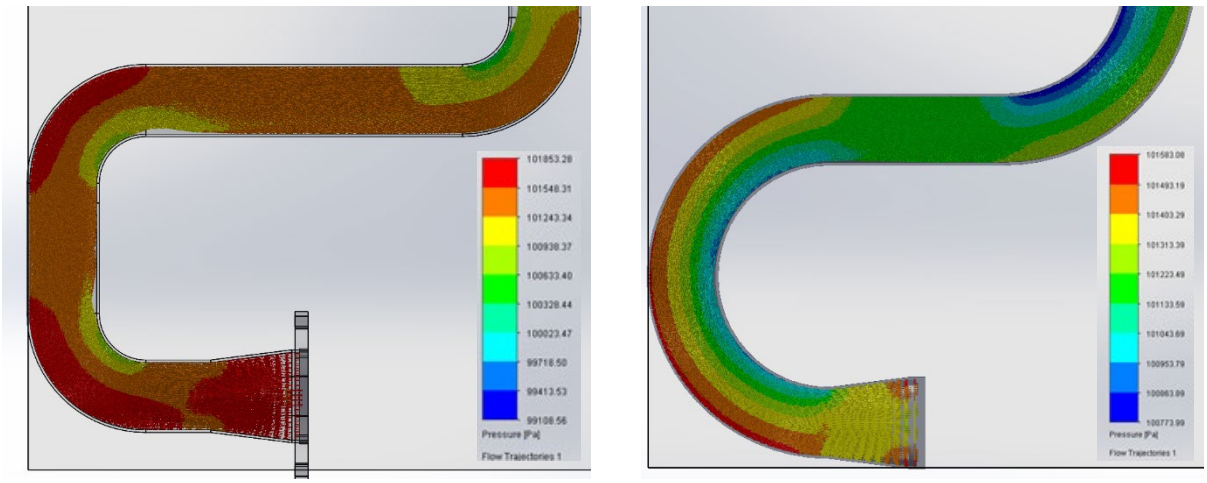

A) Current design pressure distribution. **B) Proposed design pressure distribution.**

Figure 77: analysis of flow within the current and proposed exhaust system.

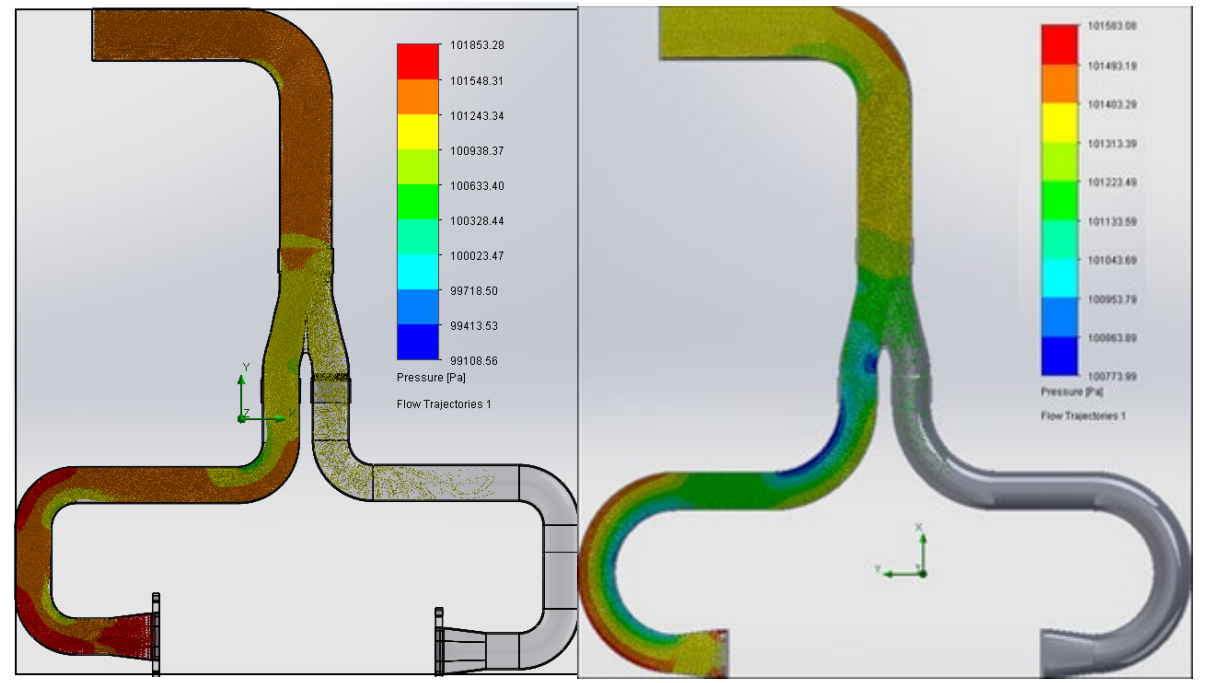

A) Current design pressure distribution. **B) Proposed design pressure distribution.**

Figure 78: Side by side comparison of the pressure within the current exhaust and the original.

Figure 78: Side by side comparison of the pressure within the current exhaust and the original. shows the smoother bends in the proposed design change allow a smoother run for the exhaust gas to flow through the system and reduces the flow separation, resulting in less turbulent flow.

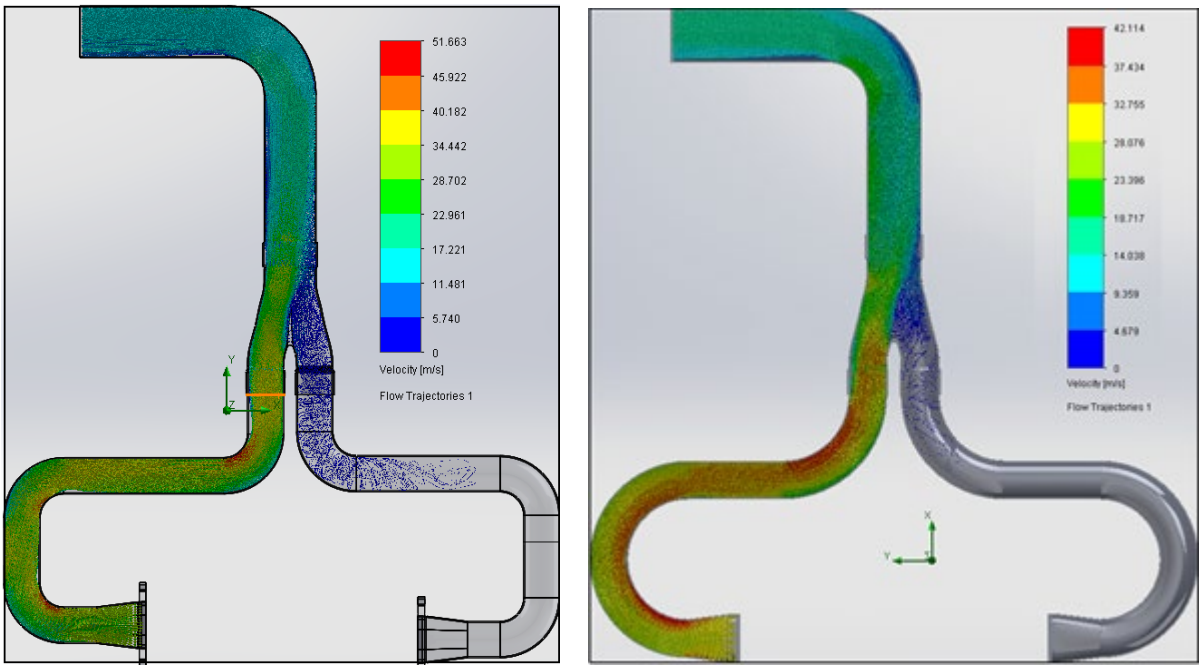

A) Current design velocity distribution. **B) Proposed design velocity distribution.**

Figure 79: Side by side comparison of the velocity within the current exhaust and the original.

Figure 79: Side by side comparison of the velocity within the current exhaust and the original. shows the smoother flow through the proposed system, meaning reduced flow resistance, resulting in higher velocities than in the original design. Higher flow velocity in the exhaust is important because it reduces the pressure. Reducing the pressure creates a higher pressure differential between the exhaust and the cylinder which improves the extraction of exhaust gas within the cylinder, which can improve the combustion due to reduced exhaust gas left over in the cylinder during the intake stroke.

Section Summary

The exhaust system needs to be of a length that would protrude into the air flow around the car and therefore would interfere with the aerodynamics. Therefore, the chassis designers and aerodynamicists will be given the optimal length but the final placement of the exhaust should be left to the aero department. The exhaust length indicated by the GT-Power model is 850mm long between flow splits, which is an increase from the 668mm in the original design.

Section summary

This project found that the inlet manifold design can be improved in a number of ways. An increase in size of the plenum from 2.67 to 4.12 litres would give a 10BHP increase in power performance over the original design. Giving the plenum a rounder shape could further increase performance. Analysis of the runner design shows that the use of curved, flared runners also improves performance by maximising the RAM air effect within the required dimensions. The project also found that the exhaust design can also be improved. First, having a smoother curve in the exhaust manifold reduces pressure in the system and improves gas flow. Secondly, by matching the exhaust length to the appropriate harmonic order for 9000 RPM, which is the RPM chosen for peak torque, performance is also improved. Taken together, these design

improvements could result in a giving a maximum of 6% increase in peak torque at 9000 rpm and a 19% increase in peak torque at 12000 rpm.

4.3. V-twin engine performance and calibration

Valve train and control strategies

The sweeps for the valves were analysed via GT-power simulation and the results were input into Excel spreadsheets.

Torque	Intake Valve Anchor Crank Angle					
Exhaust Valve Anchor Crank Angle		360	405	450	495	540
	180	-3.69	-3.59	-3.61	-3.94	-3.77
	225	8.09	12.73	13.08	8.69	2.17
	270	13.29	16.51	15.53	9.66	-2.32
	315	12.54	16.68	15.12	10.09	-2.24
	360	0.97	-1.45	14.04	8.65	-1.45

Table 6: Max Torque Valve Anchor Sweep Table of Results.

Power (HP)	Intake Valve Anchor Crank Angle					
Exhaust Valve Anchor Crank Angle		360	405	450	495	540
	180	-2.26	-2.36	-2.20	-2.21	-2.12
	225	11.36	18.41	22.21	14.64	-1.37
	270	12.13	23.17	24.81	16.28	-1.92
	315	7.30	19.26	22.25	13.87	-1.57
	360	0.95	-1.22	15.48	8.47	-1.22

Table 7: Max Horse Power Valve Anchor Sweep Table of Results.

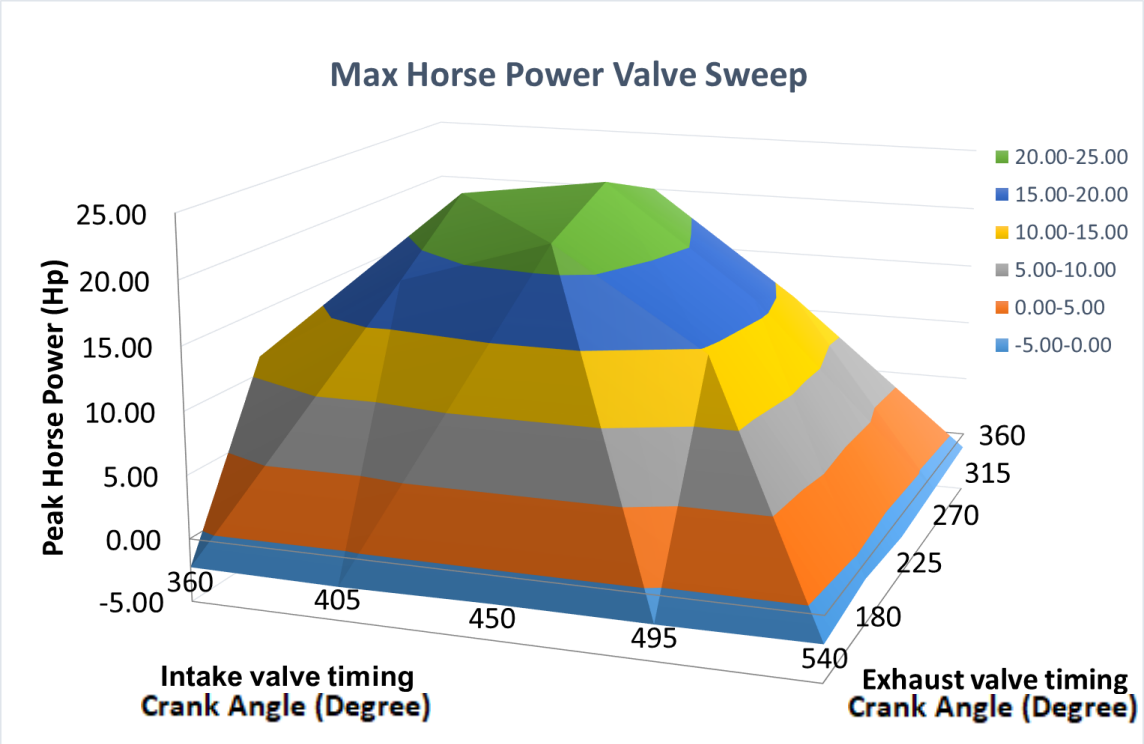

Figure 80: Max Power Valve sweep.

Figure 80: Max Power Valve sweep indicates the intake and exhaust valve timing that will give max Horse Power. This area is 450-495 CA for the intake and 180-225 CA for the exhaust.

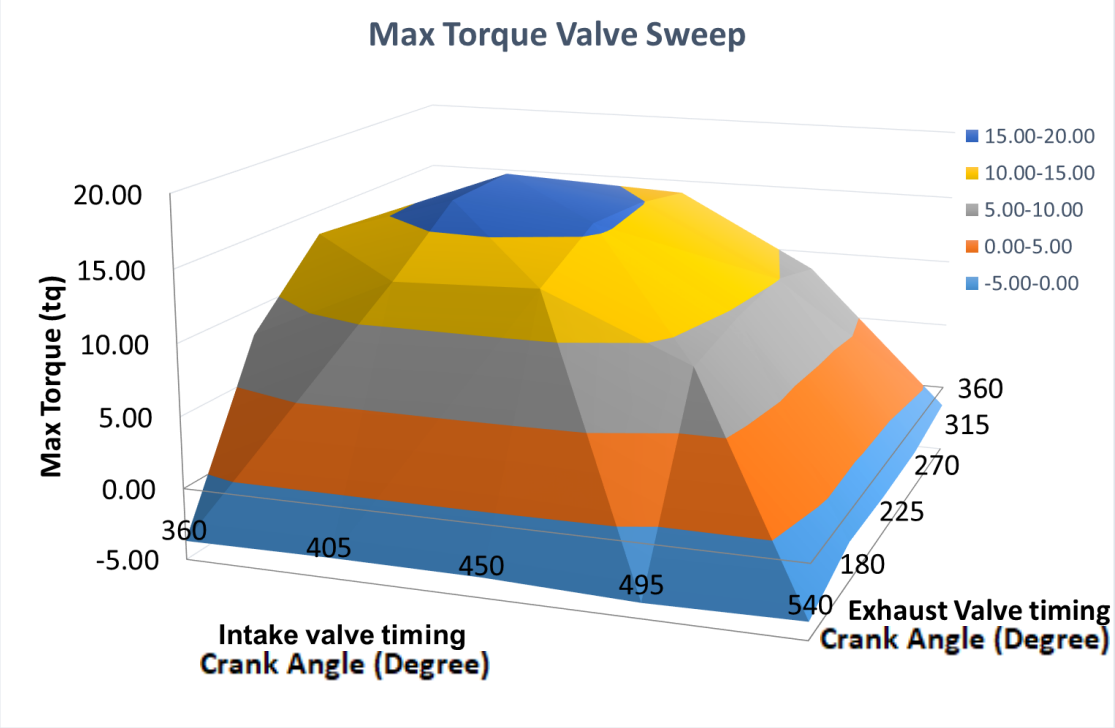

Figure 81: Max Torque Valve sweep.

The area of interest for the torque is 405-450 CA for the intake and 225-270 CA for the exhaust as seen in Figure 81.

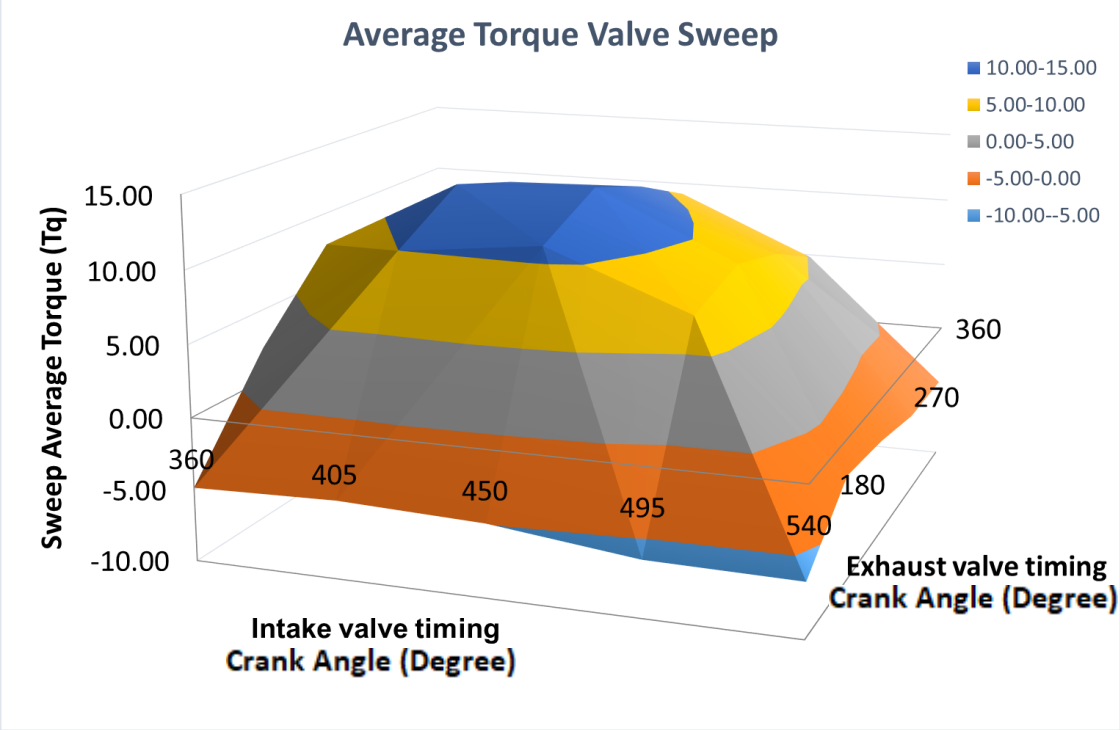

Figure 82: Average Horse Power Valve sweep

The average horse power valve sweep highlighted a specific area compared to the other sweeps. The area was around the 450 CA intake and the 270 CA exhaust, as seen in figure 82.

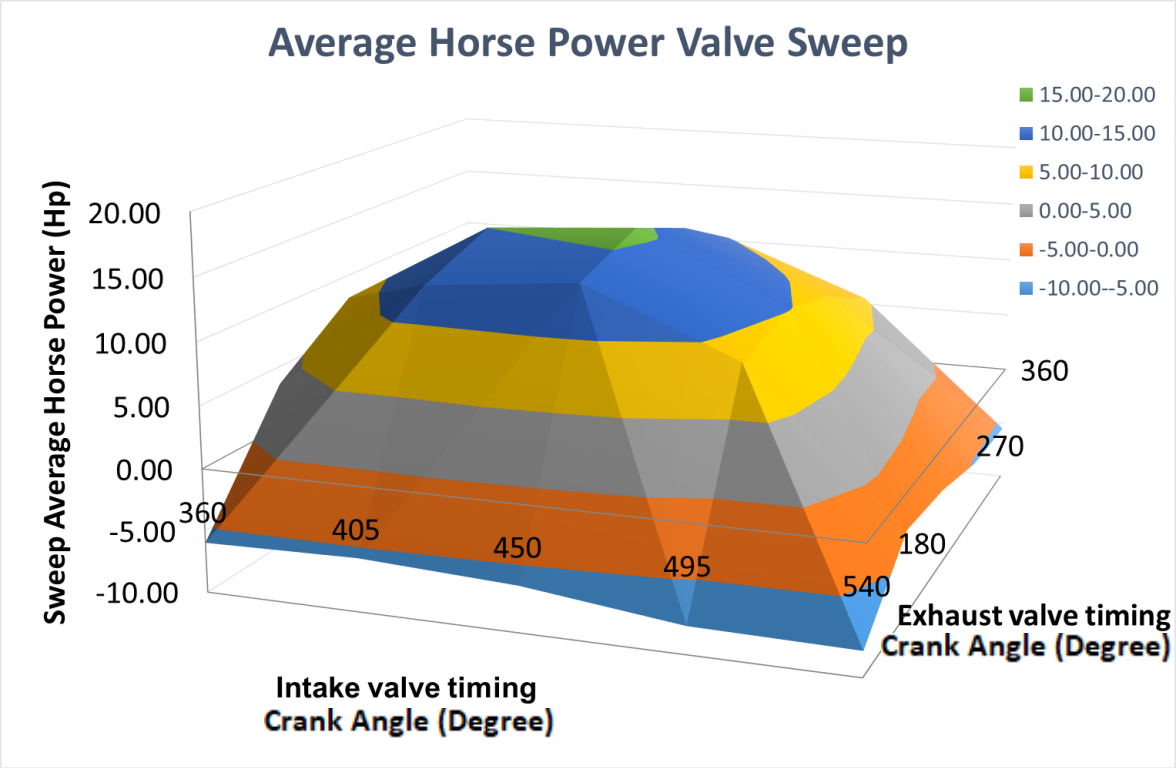

Figure 83: Average Torque Valve Sweep

The average torque sweeps showed an area that was 450-495 CA of the intake and 225-270 CA of the exhaust, as seen in Figure 83.

Once the broad sweeps had been analysed then a more focused valve sweep was done to narrow the search down to a specific crank angle. The final sweep was done over 405-495 CA intake and 225-315 CA exhaust. The analysis was done at 9,000 RPM, as the chosen anchor point for peak torque.

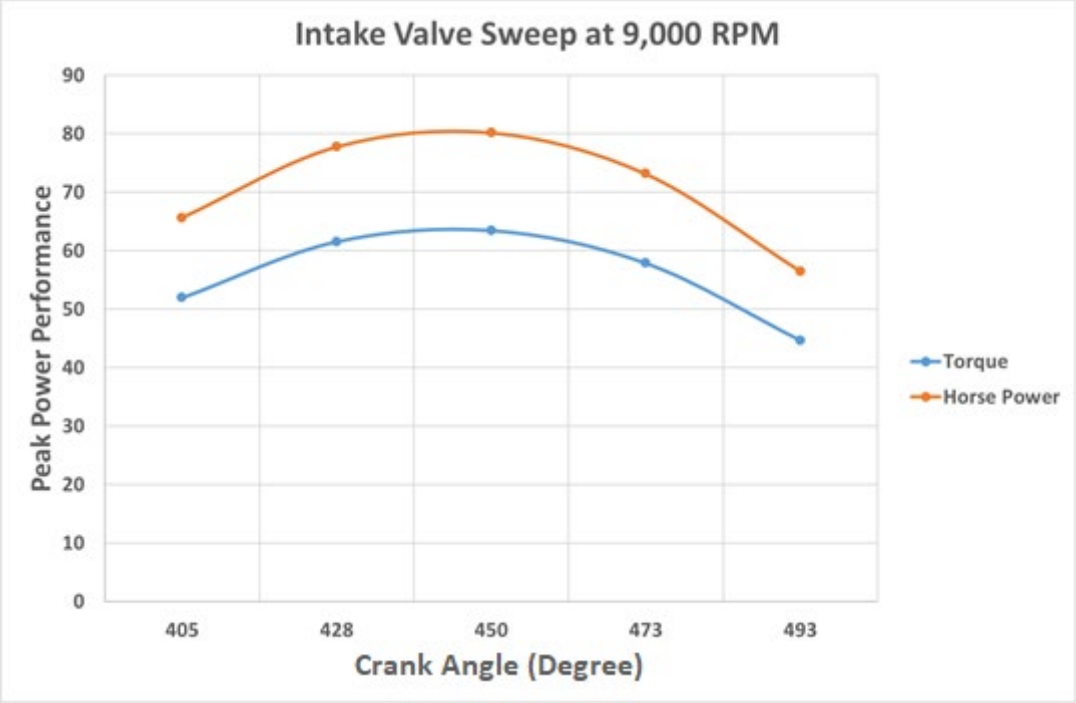

Figure 84: Detailed intake valve Sweep

The detailed intake sweep shows the peak HP and Torque was achieved at 445 CA°.

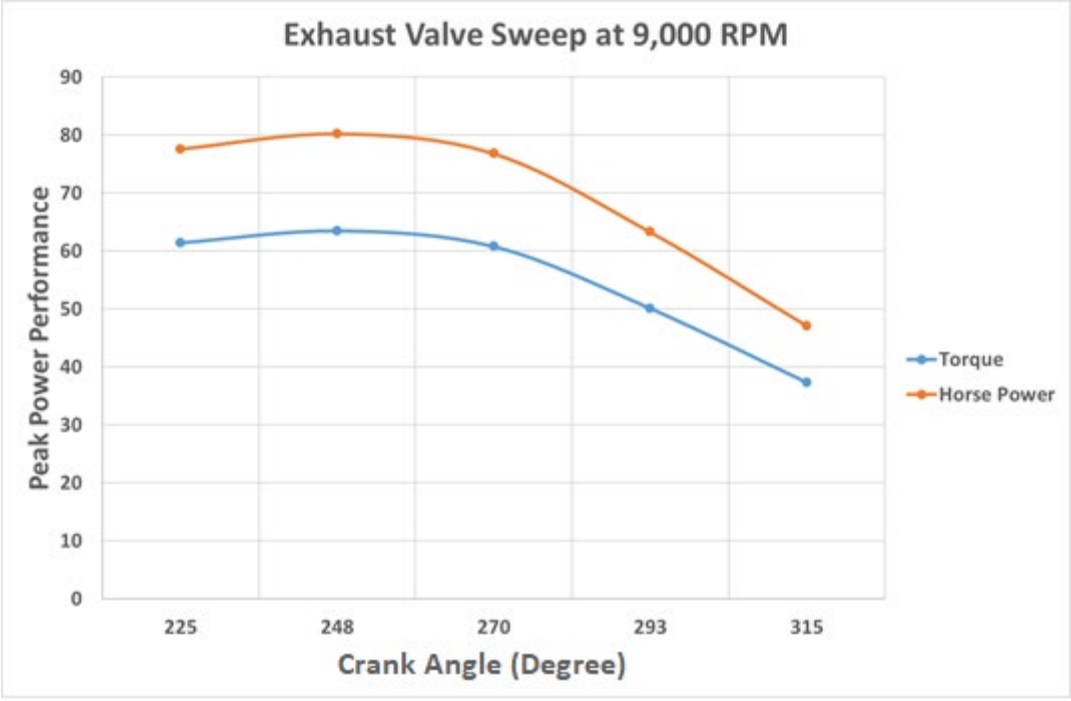

Figure 85: Detailed exhaust valve Sweep

The detailed exhaust sweep shows that the peak power and Torque was achieved at 250 CA°.

4.3.3. Valve train

The different sweeps brought up different areas of interest, depending on whether average or max torque or horse power was looked at. The valve timings of 250 CA and 445 CA were chosen as the optimal settings. The movement of the valve train anchor angle gave an increase of 2% in peak torque across the midrange, with less than 1% decrease in performance above 11000 RPM and below 5000 RPM. Combined with the improvements proposed for the intake and exhaust, this change in valve timings will further increase performance.

4.4. GT-Power model results.

This section discusses the engine performance and combustion characteristics expected following implementation of the new manifold design and geometry. The GT-Power model results show that the new manifold design significantly affects the engine performance and combustion. Particularly, the volumetric efficiency and combustion duration are significantly improved, which leads to the higher effective work output, indicate by IMEP.

Parameter	Unite	Original Model	Final Model
Torque	Nm	62.92	65.60
Engine Power	Kw	59.31	61.83
IMEP	Bar	14.79	15.35
Vol_{eff}	%	85.05	88.96
Air Flow Rate	Kg/hr	159.67	167.01
Peak Pressure	Bar	78.37	78.12
MFB10	^{0}CA	-2	-2.1
MFB50	^{0}CA	11.20	10.51
MFB90	^{0}CA	35.3	29.30
MFB10-90	^{0}CA	33.34	27.21

Table 8: Highlighted engine performance parameters

The figures in
Table 8: Highlighted engine performance parameters show the key engine performance parameters that were used to compare the performance of the GT-Power models. The GT-Power model development can be seen in the GT-Power section of the **Appendix**.

4.4.1. In-cylinder Pressure

The original and the final models were compared at 9000 RPM, this being the RPM chosen for peak torque, and allowing the two models to be easily compared and contrasted.

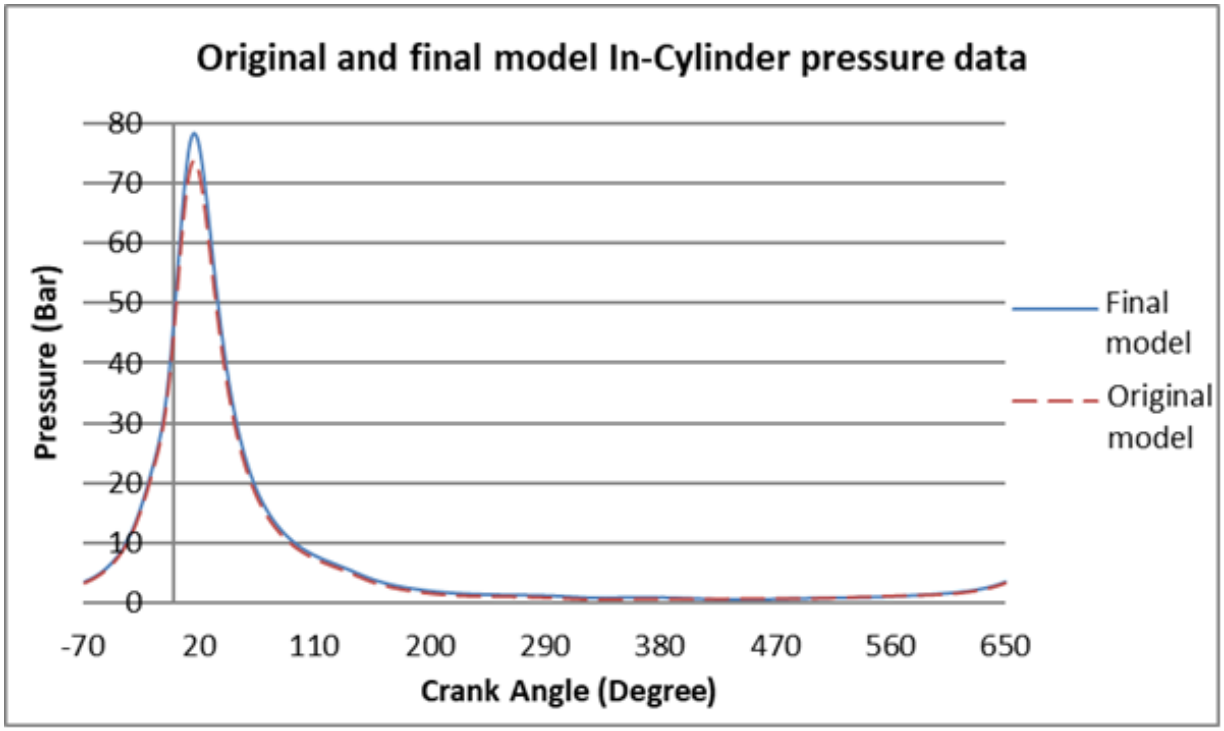

Figure 86: Original vs final GT-Power model in-cylinder pressure data.

The peak in-cylinder pressure of the final model is 78 Bar, which is an increase of 5 Bar over the peak of 73 Bar in the original model. The IMEP of the final model is 15.34 Bar which is higher than the original model's IMEP of 14.79 Bar, showing the average in-cylinder pressure in the final model is higher than that of the original. A reduced peak pressure should also marginally reduce the wear on the internal components. The peak pressure difference between the two was 7 Bar, this difference being in line with the power difference between the two models.

4.4.2. Pressure vs Volume diagram

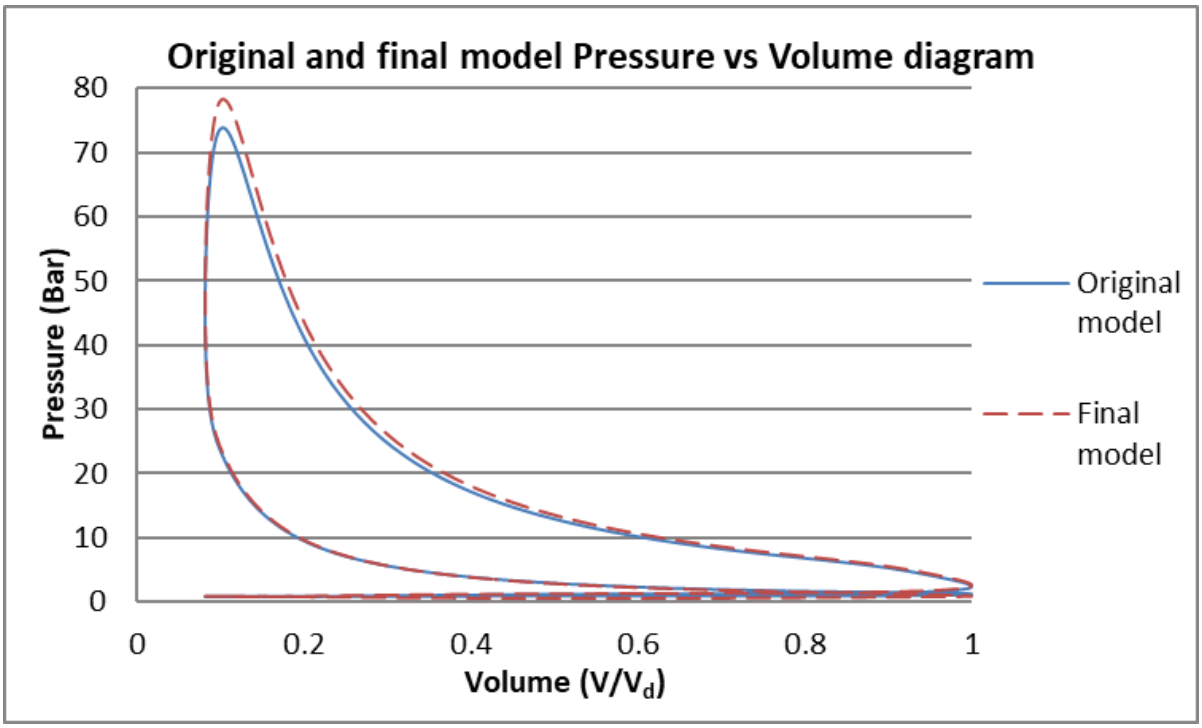

Figure 87: Original and Final GT-Power model Pressure vs Volume.

The pressure-volume diagrams show very similar traces. However, when analysed the final model shows a larger increase in pressure per change in volume when the piston is near TDC. The trace shows that there is a larger increase in pressure towards the peak before the volume starts to increase. After the peak pressure, the final model maintains its pressure per unit volume better than the original. The maintenance of pressure would explain why the IMEP is clearly higher in the final model, while having a smaller peak. The original model has an IMEP of 14.8 bar while the final model has an IMEP of 15.3 Bar.

4.4.3. Mass Fraction Burned

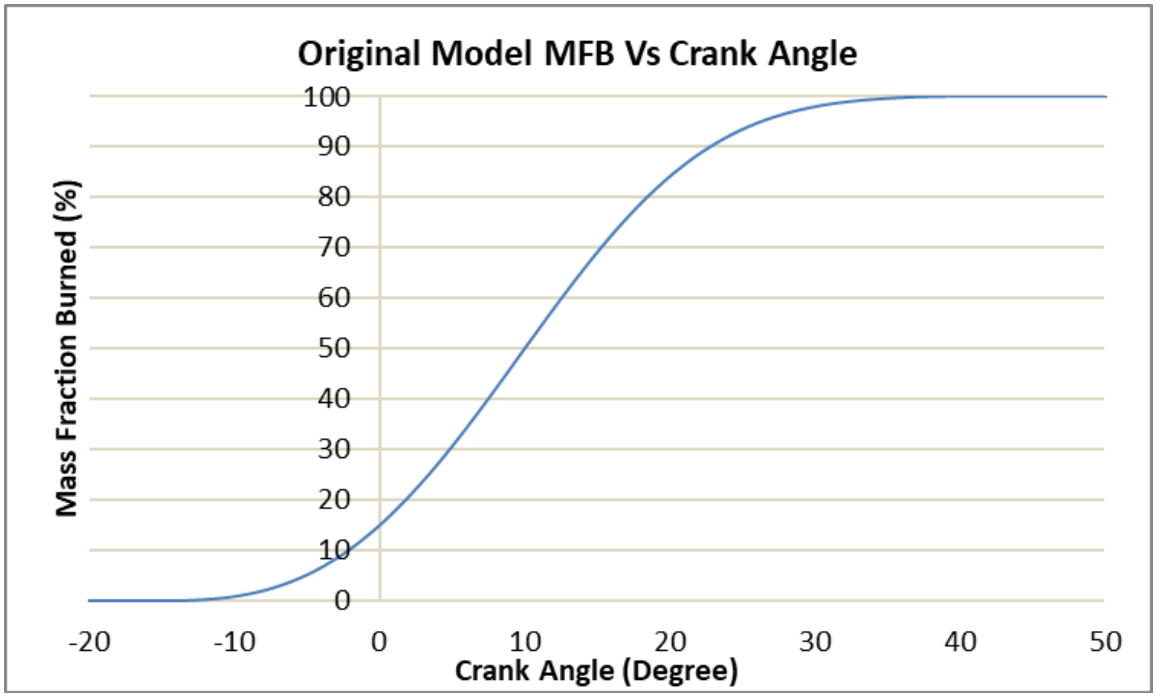

Figure 88: Original GT-Power Mass Fraction Burned trace.

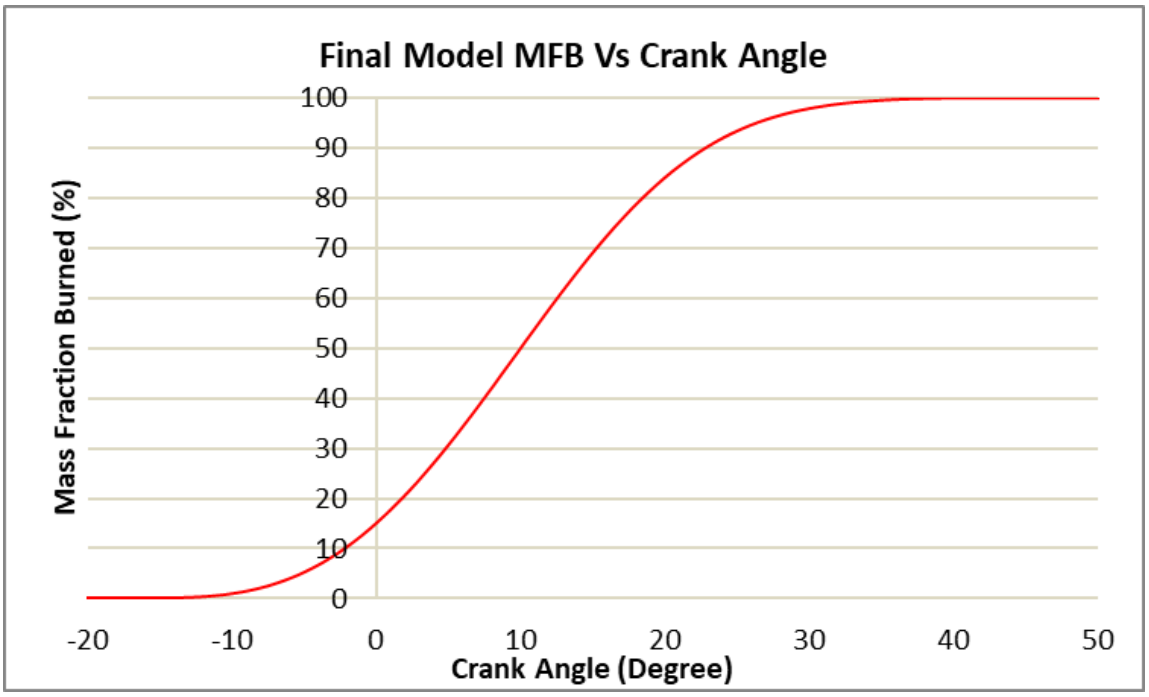

Figure 89: Final GT-Power model Mass Fraction Burned.

The final model's MFB10-90, which represents combustion duration, was over 5 CA^0 less than the original's 33.3 CA^o. The shorter combustion duration of the final model would result in the higher average in-cylinder pressures. Though the MFB10 and MFB50 were at similar CA in both the original and final models, the final model's MFB90 was over 6^0 sooner within the cycle, showing that the second phase of combustion happened in a shorter time period in the final model.

4.4.4. Power performance Curve

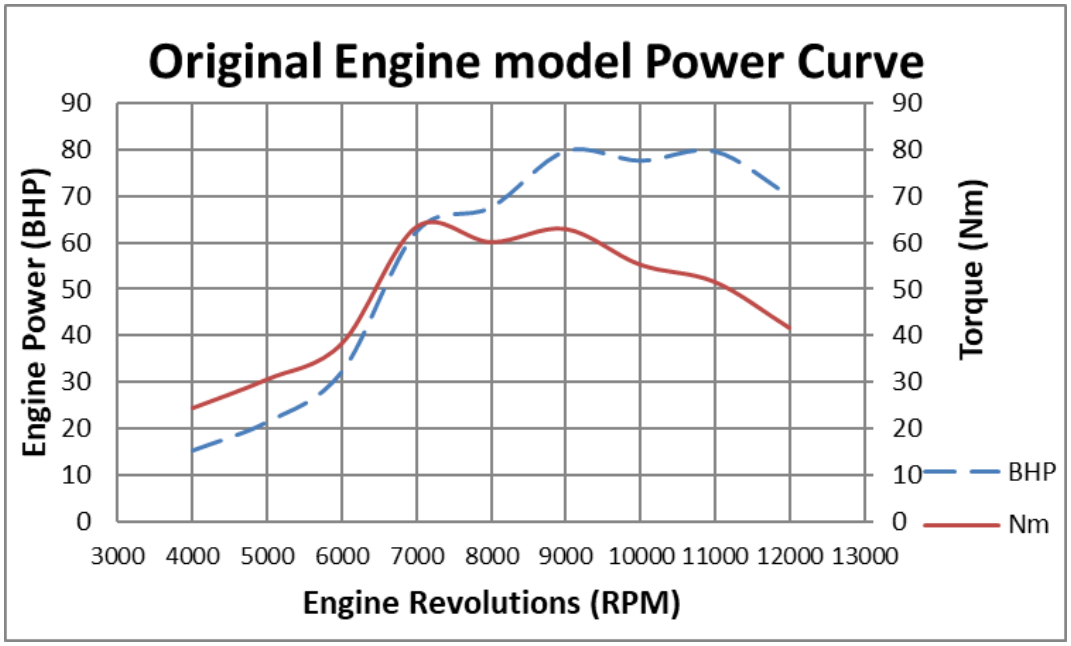

Figure 90: Original GT-Power models power performance curve.

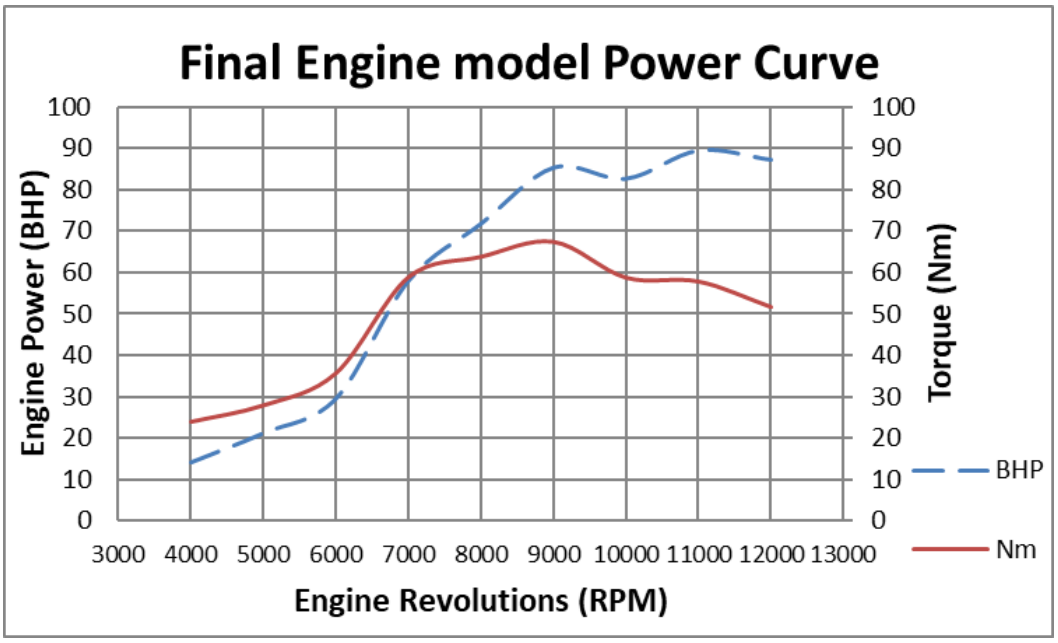

Figure 91: Final GT-Power models Power Performance curve.

The final model has a torque curve that shows a clear improvement at between 9,000 RPM to 10,000 RPM, although there was still a depression around 5,000 RPM. The idle of the engine is 4,000 RPM so the depression at 5,000 RPM was not considered too detrimental to the engine's performance. However, the increase in torque after 9,000 RPM results in a more stable and consistent power curve, as seen in Figure 91: Final GT-Power models Power Performance curve.1. The power curves show that the final model shows significant improvement in engine power performance. The drop off in power in the original model indicates a restriction caused by the plenum being too small.

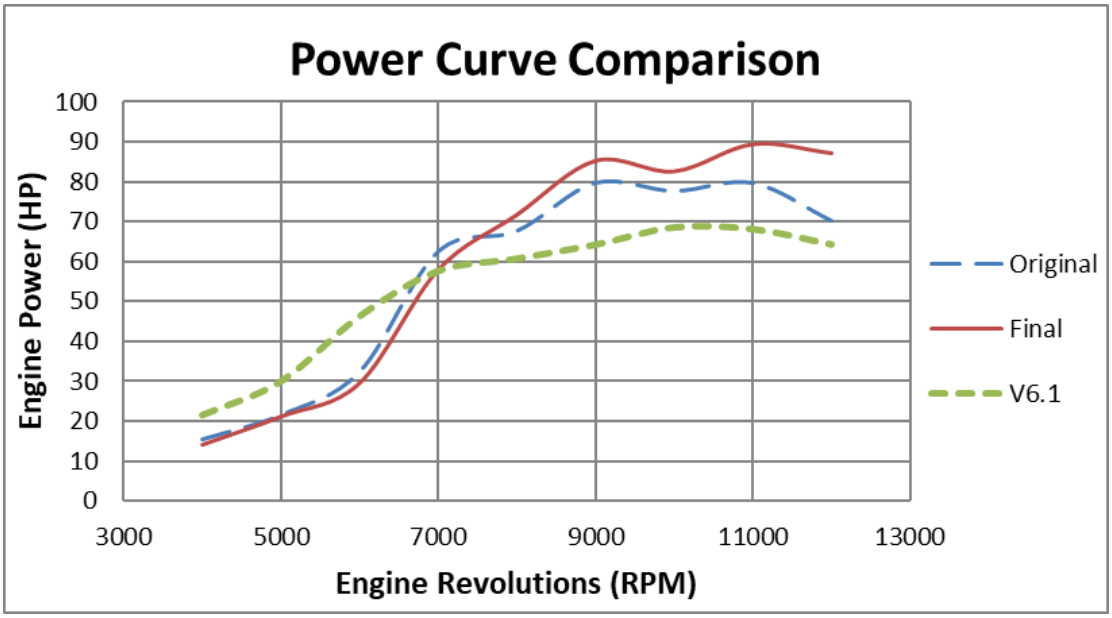

Figure 92: Power Curve Comparison

The proposed improvements reduced performance by about 5% up to 7000 RPM, but thereafter increased power performance, from a 6% increase in power performance up to a 19% increase in performance at the top-end of the rev range. The loss of low-end power is worth the significant improvement in the top-end power, as this engine is designed to be used on a racetrack where low-end performance is not important, but top-end power is vital. The new design shows particular improvement compared to the drop off in top-end power of the original model. As seen in Figure 92: Power Curve Comparison2, the final design shows a smoother power curve that doesn't drop away as the original model's power curve does. The smoother power curve is due to combined effects of the changes in the manifolds and valve timings with a more top-end of the engine's RPM range focused optimisation. Figure 92: Power Curve Comparison2 also shows the clear difference in the power curve from the simulations done in the previous version of GT-Power, version V6.1.

The difference between the two power curves is in part due to a combination of a change in plenum design, a change in intake design, improved exhaust manifold design and exhaust length. It is also due to the change in valve timing anchor, as the valve train overlap is 2 degrees more. The change in valve timing will allow more time for the scavenging effect and therefore allow more clean air into the piston. This benefit is seen at higher RPM. The scavenging effect would explain the increase in power performance at the top-end of the power curve when approaching the 12,500 RPM redline.

4.4.5. Section Summary

The performance increase from the improvements to the engine proposed in this project were clear. The area that showed a large improvement over the original model was the volumetric efficiency, which is due to improved combustion, demonstrated by the MFB figures. The overall power of the final model was higher across the rev range, apart from at 5,000 RPM, with a peak 90 BHP in the final model, compared with 70 BHP in the original. An interesting comparison between the work carried out in this project and the previous work on V6.1 is the drop in the power curve from 7,000 RPM for all three models and again a slight drop at 10,000 RPM. This drop at 7,000 RPM and again at 10,000 RPM is likely to be caused by the restrictor or the ports, as these were the only things which remain the same in each model.

Chapter 5. Conclusions

5. Conclusions

This project looked into the development and optimisation of a bespoke Formula Student V-twin engine based on 2 cylinders of a Cosworth DFV V8, to the point where it could be can be approved for testing on a Dynamometer. As the engine has not yet been prepared for dyno testing, there is no real time data available in order to validate the combustion and GT-Power models, therefore the work done in this project is purely theoretical and must be validated when the engine has been run and the results examined. However, the project has highlighted several areas of design improvement which should significantly improve performance.

This project has shown great potential to improve the V-Twin's performance for Formula Student (FS) competitions in the future. The original target figure set by the engine design team at the start of the project was a power output of 100 BHP. Upon analysing the basics of the engine, and taking into account the rules set out by the FSAE FS event rules, it was concluded that although 100 BHP could be achieved using turbochargers, in Naturally Aspirated form the engine will be limited to about 96-97 BHP by the air restrictor required by the regulations. This theoretical figure of 96-97 BHP is the upper limit and will be hard to achieve when the car is on the track. The difference between the original model and the model incorporation the improvements recommended in this project, in terms of peak pressure at 9000 RPM, was 4.6 Bar, which is expected from the power performance increase shown by the power curves.

In order to improve engine performance, this project investigated the deigns of both intake and exhaust systems. Individual sections were looked at, including the restrictor, the intake plenum, the runners and exhaust manifold. The project found that significant improvements in power output where achievable through changes in the design of the inlet manifold, including plenum size and shape, and length and shape of the runners, and the shape of the exhaust manifold and pipe lengths. The later will require further consideration by aerodynamicists and chassis designers as the final cars design is refined. Increasing the plenum size from 2.67 to 4.12 litres gave a maximum of 6% increase at 9000 rpm and a 19% increase in performance at 12000 rpm. The other changes indicated by the project are an increase in runner length from 333mm to 380mm, and an exhaust length increase from 668mm to 850mm.

The valve train was analysed using the GT-Power model that was developed alongside the combustion and dynamics models. The results for the valve train show that the design is near optimal. The cam anchor angle was the valve train parameter that was found to have the biggest impact on the engine performance. This would, however, also depend on the ambient conditions of the track and the engine map/spark timing chosen. The valve timing recommended is exhaust CA of 250 and intake CA of 455, which is only a minor change from the original exhaust CA of 255 and intake CA of 462. The movement of the valve train anchor angle gave an improvement of 2% increase across the midrange with less than 1% decrease in performance below 5000 RPM and above 11000 RPM. This is due to a combination of factors. The increase in performance in the midrange is due to the increase in valve overlap of 2 degrees and the resulting pressure differential. The decrease in performance is due to the reduced time for the combustion event at low and very high RPMs resulting from the increased valve overlap. The improvement delivered in the mid RPM range combined with the improvements to the inlet and exhaust systems will deliver a more significant improvement in power performance overall.

Incorporating all the design changes identified in this project delivers a theoretical peak power performance of the engine of 90 BHP, this is a significant improvement on the original model's of 79 BHP. Similarly, the average power performance rose from 62 to 66 bhp. Furthermore,

the final model's torque curve was smoother than the original model. The proposed improvements to the engine showed a loss in performance of about 5%, between 4000 RPM and 7000 RPM, which is a less important RPM range for a race car, but in the significant RPM range for racing power performance was improved from 6% up to 19% towards the top-end of the RPM range. This is significant improvement in engine design.

The original restrictor design is deemed satisfactory, as changes would result in only minor improvements in performance while the current design ensures compliance with the rules, and the current valve train and internal components were found to be satisfactory. However, new hardware is recommended as a result of this project including a larger and more rounded plenum, flared, curved runners and a more rounded exhaust manifold. Runner and exhaust pipe lengths are also modified. The hardware changes recommended will deliver significant improvements to power performance.

Overall the changes to hardware design and timings identified in this project should deliver significant power performance improvements to the engine that was the subject of this study. It is therefor recommended that they be incorporated into the design of the engine to be taken forward to the next stage of development.

Further work

The next stage for development of this engine is to get it running and to validate the simulation results from this project. This will allow final design improvements for the engine to be optimised, within the rules, and to the drivers' liking.

The exhaust must be designed in parallel with the chassis designers and aerodynamicists, and cannot be completed until the designs can be validated with a running engine.

This project successfully identified scope for optimisation of a Naturally Aspirated (NA) engine. However, a previous project found that Turbocharging the engine would deliver significant gains to engine performance. Turbocharging could therefore be considered as part of the future work for the engine.

6. References

[1] Heywood, J. B. Internal Combustion Engine Fundamentals. McGraw Hill, Automotive Technology Series, 1988.

[2] Nigus, H. Kinematics and Load Formulation of Engine Crank Mechanism. Federal TVET Institute, School of Mechanical Technology, Automotive Technology Department, Addis Ababa, Ethiopia. Mechanics, Materials Science & Engineering, ISSN 2412-5954. 2015.

[3] Dr Timmins, S. Power Train Theory. Department of Mechanical Engineering. University of Delaware. Available at http://www.me.udel.edu/meeg425/. 2013.

[4] Ranjbarkohan, M. Asadi, M, R. Rasekh, M. Hoseini, A, H. Kheiralipour, K. Kinematics and kinetic analysis of the slider-crank mechanism in otto linear four cylinder Z24 engine. Department of Mechanical Engineering, Islamic Azad University, Buinzahra branch, Qazwin, Iran. Department of Agricultural Machinery, University of Mohaghegh Ardabili, Ardabil, Iran. Mechanic Engineering in Megamotor Company, Tehran, Iran. Department of Mechanical Engineering of Agricultural Machinery, University of Tehran, Karaj, Iran. Journal of Mechanical Engineering Research Vol. 3(3), pp. 85-95. ISSN 2141 – 2383. 2011.

[5] Chatlatanagulchai, W. Rhienprayoon, S. Yaovaja, K. Wannatong, K. Air/Fuel Ratio Control in Diesel-Dual-Fuel Engine by Varying Throttle, EGR Valve, and Total Fuel. Kasetsart University, PTT, Thai-German Petroleum & Chemical, PTT. SAE Technical Paper 2010-01-2200. 2010.

[6] Turner, J, W, T. Pearson, R, J. Bell, A. de Goede, S. Woolard, C. Iso-Stoichiometric Ternary Blends of Gasoline, Ethanol and Methanol: Investigations into Exhaust Emissions, Blend Properties and Octane Numbers. Lotus Engineering, Sasol Technology (Pty) Ltd, University of Cape Town. SAE Technical Paper 2012-01-1586. 2012.

[7] Stone, R. Introduction to Internal Combustion Engines. Basingstoke: Macmillan, 1985.

[8] Wagner Roberto da Silva Trindade, Rogério Gonçalves dos, Combustion modelling applied to the engines using 1D simulation code, 25th SAE Brasil International, Congress and Display, Sao Paulo, Brasil, 2016.

[9] Liang, Y. Pope, S B. Pepiot, P. An adaptive methodology for the efficient implementation of detailed chemistry in simulations of turbulent non-premixed Combustion. Sibley School of Mechanical and Aerospace Engineering, Cornell University. Paper # 114TF-0378. 2015.

[10] Grill, M. Bargende, M. Rether, D. Schmid, A. Quasi-dimensional and Empirical Modeling of Compression-Ignition Engine Combustion and Emissions. FKFS, IVK Univ. of Stuttgar. SAE paper 2010-01-0151. 2010.

[11] Harish Kumar, R. Antony, A, J. Progressive Combustion in SI-Engines—Improved Empirical Models for Simulating and Optimizing Engine Performance. Sri Siddhartha Institute of Technology, Sahyadri Institute of Technology. SAE paper 2008-01-1630. 2008.

[12] Engine Performance Application Manual. GT-Suite. Version 7.5. Gamma Technologies. PDF. www.gtisoft.com. 2014.

[13] Dr Hasse, C, F. Dr Wensing, M, E. Combustion modeling for virtual SI engine calibration with the help of 0D/3D methods. Faculty of Mechanical Engineering, Process Engineering and Energy Engineering. Technical University Bergakademie Freiberg. Von der Fakultät für Maschinenbau,Verfahrens- und Energietechnik der Technischen Universität Bergakademie Freiberg genehmigte. zur Erlangung des akademischen Grades Doktor-Ingenieur (Dr.-Ing.) vorgelegt. Von Diplom-Ingenieur Sebastian Grasreiner aus Erfurt. 2012.

[14] Wang, S. Prucka, R. Zhu, Q. Clemson University. Prucka, M. Dourra, H. FCA US LLCA. Real-Time Model for Spark Ignition Engine Combustion Phasing Prediction. SAE Technical Paper 2016-01-0819. 2016.

[15] Siokos, K. He, Z. Prucka, R. Clemson University. Assessment of Model-Based Knock Prediction Methods for Spark-Ignition Engines. SAE Technical Paper. 2017-01-0791. 2017.

[16] Klimstra, J. The Optimum Combustion Phasing Angle - A Convenient Engine Tuning Criterion. Research Department N. V. Nederlandse Gasunie Groningen, The Netherlands. SAE Technical Paper 852090. 1985.

[17] Salazar, F. internal combustion engine. Department of aerospace and mechanical engineering. University of Notre Dame. 1998.

[18] The Calculation of Mass Fraction Burn of Ethanol-Gasoline Blended Fuels Using Single and Two-Zone Models, Michigan Technological University, Yeliana. C, Cooney. J, Worm. J, Naber. SAE 2008-01-0320, 2008

[19] Brown, B, R. Combustion Data Acquisition and Analysis. Final Year Project. Available at https://www.catool.org/files/FinalProjectReport.pdf. Department of Aeronautical and Automotive Engineering, Loughborough University. 2014.

[20] Yeliana, C. Cooney, J. Worm, D. Michalek, J. Naber. Wiebe Function Parameter Determination For Mass Fraction Burn Calculation in a Ethanol-Gasoline Fuelled Engine, Michigan Technological University, Journal of KONES Powertrain and Transport. 2008.

[21] Yeliana, C. Cooney, J. Worm, D. Michalek, J. Naber. Wiebe Function Parameter Determination for Mass Fraction Burn Calculation in an Ethanol-Gasoline fuelled SI Engine. Michigan Technological University Journal of KONES Powertrain and Transport, Vol. 15, No. 3. 2008.

[22] Hires, S, D. Tabaczynski, R, J. Noval, J, M. The Prediction of Ignition Delay and Combustion Intervals for a Homogeneous Charge, Spark Ignition Engine. Ford Motor Company. SAE Technical Paper 780232. 1978.

[23] Tabaczynski, R, J. Ferguson, C, R. Radhakrishnan, K. A Turbulent Entrainment Model for Spark-Ignition Engine Combustion. Reciprocating Engines Research Department

Engineering and Research Staff, Ford Motor Company. Sloan Automotive Laboratory, Massachusetts Institute of Technology. SAE Technical Paper 770647. 1977.

[24] Yeliana. Parametric combustion modeling for ethanol-gasoline fuelled spark ignition engines. Dissertations, Master's Theses and Master's Report, Michigan Technology University. 2010.

[25] Pipitone, E. A Comparison between Combustion Phase Indicators for Optimal Spark Timing. Journal of Engineering for Gas Turbines and Power SEPTEMBER 2008, Vol. 130. 052808-1. 2008

[26] Ghanaati, A. Darus, M. Said, M. andwari, A. A mean value model for estimation of laminar and turbulent flame speed in spark-ignition engine. University of Malaysia Pahang. International journal of automotive and mechanical engineering, volume 11, UMP publisher. 2015.

[27] Sodré, J. A Parametric Model for Spark Ignition Engine Turbulent Flame Speed. SAE Technical Paper 982920. 1998.

[28] Mantilla, J. Garzón, D. Galeano, C. Combustion model for spark ignition engines operating on gasoline-ethanol blends. Engenharia Térmica Vol. 9, Universidad Nacional de Colombia. 2010.

[29] Lipatnikov, A, N. Chomiak, J. Modeling of Pressure and Non-Stationary Effects in Spark Ignition Engine Combustion: A Comparison of Different Approaches. Chalmers University of Technology - Goteborg, Sweden. SAE Technical Paper 2000-01-2034. 2000.

[30] Borg, J, M. Alkidas, A, C. Characterization of Auto-ignition in a Knocking SI Engine Using Heat Release Analysis. Automotive Products Research Laboratory, Hitachi America Ltd. Dept. of Mechanical Engineering, Oakland University, Michigan. SAE Technical Paper Series. 2006-01-3341. 2006.

[31] Amiel, R. Tartakovsky, L. Effect of Flight Altitude on the Knock Tendency of SI Reciprocating Turbocharged Engines. Technion Israel Inst. of Technology. SAE Technical Paper 2016-32-0006. 2016.

[32] Douaud, A, M. Eyzat, P. Four-octane-number method for predicting anti-knock behaviour of fuels and engines. SAE Technical Paper No. 780080. 1978.

[33] Blizard, N. Keck, J. Experimental and theoretical investigation of turbulent burning

[34] model for internal combustion engines. SAE Technical Paper No. 740191; 1974.

[35] Ferguson, C. Tabaczynski, J. Radhakrishnan, K. A turbulent entrainment model for spark-ignition engine combustion. SAE Technical Paper No. 770647; 1977.

[36] Tabaczynski, R. Trinker, F. Shannon, B. Further refinement and validation of a turbulent flame propagation model for spark-ignition engines. Combustion and Flame. 1980;39:111-21.

[37] Kaprielian, L. Demoulin, M., Cinnella, P. Daru, V. Multi-zone quasi-dimensional combustion models for spark-ignition engines. SAE Technical Paper No. 2013-24-0025; 2013.

[38] Van-Zwol, F. Formula student V-twin Race Engine Lubrication system. Dissertation for MSc in Racing Engine Design. Oxford Brookes University. Student number: 06069218. 2007.

[39] Liu, C, Q. Orzechowski, J. Theoretical and Practical Aspects of Balancing a V-8 Engine Crankshaft. DaimlerChrysler Corporation. SAE Technical Paper 2005-01-2454. 2005.

[40] Tunestål, P. Estimation of the In-Cylinder Air/Fuel Ratio of an Internal Combustion Engine by the Use of Pressure Sensors. Doctoral thesis. Department of Heat and Power Engineering. Lund Institute of Technology. 2001.

[41] Malaysia, N, Z. Carden, P. Bell, D. Design and Analysis of a Lightweight Crankshaft for a Racing Motorcycle Engine, Ricardo UK. SAE Technical Paper 2007-01-0265. 2007.

[42] Jaques, P. Heat Transfer, Tribology and design of piston assembly for V-Twin Engine. MSc Dissertation. Oxford Brookes university school of technology September. 2007.

[43] Tabaczynski, R. Trinker, F. Shannon, B. Further refinement and validation of a turbulent flame propagation model for spark-ignition engines. Combustion and Flame. 1980;39:111-21.

[44] Nigus, H. Kinematics and Load Formulation of Engine Crank Mechanism. Mechanics, Materials Science & Engineering, October 2015 – ISSN 2412-5954. 2015.

[45] Borg, J, M. Alkida, A, C. Investigation of the Effects of Autoignition on the Heat Release Histories of a Knocking SI Engine Using Wiebe Functions. Hitachi Europe GmbH. Oakland University. SAE Technical Paper series 2008-01-1088. 2018.

[46] Potul, S. Nachnolkar, R. Bhave, S. Analysis Of Change In Intake Manifold Length And Development Of Variable Intake System. ISSN 2277-8616 international journal of scientific and technology research volume 3, issue 5, 2014.

[47] 2016 Formula SAE® Rules, SAE International. Available at http://fsaeonline.com/page.aspx?pageid=e179e647-cb8c-4ab0-860c-ec69aae080a3. 2016.

[48] Stone, C, R. Etminan, Y. Review of Induction System Design and a Comparison between Prediction and Results from a Single Cylinder Diesel Engine. Brunel University. SAE Technical Paper Series 921727. 1992.

[49] Cox, R, J, N. Formula Student Engine Design and Development – The Design and development of a varying geometry inlet manifold. Oxford Brookes University Dissertation, module number U04599. Student number 04091584. 2009.

[50] Helmholtz, H, A, J, E. On The Sensations Of Tone As A Physiological Basis For The Theory Of Music. New York: Dover Publications. Print. 1954.

[51] Matins, L, R. Guimarães, G, P. Fragassa, C. Acoustical Performance of Helmholtz Resonators Used as Vehicular Silencers. Federal University of Ouro Preto. Mechanical Engineering Department. Brazil. 498 ▪ VOL. 46, No 4. Available at

https://www.mas.bg.ac.rs/_media/istrazivanje/fme/vol46/4/8_lr_martins_et_al.pdf. PDF. 2018.

[52] Mathews, R. Gardiner, A. Increasing the compression pressure in an engine by using a long intake pipe. National Advisory Committee for Aeronautics, No.180. 1924.

[53] Capetti, A. Effect of intake pipe in the volumetric efficiency of an internal combustion engine. National Advisory Committee for Aeronautics, No.501. 1927.

[54] Dennison, E, S. Inertia supercharging of engine cylinders, Transactions of the American Society of Mechanical Engineers Oil Gas and Power 55 (1933) 53–64. 1933.

[55] Mariucci, V, E. An Experimental and Computational investigation of the Effect of Primary Intake Runner Geometry on the Performance of a Single Cylinder Engine. Thesis for a master of science degree from Ohio state University. 2006.

[56] Prosser, T, G. Induction Ramming a Motored High-Speed Four-Stroke Reciprocating Engine—Influence of Inlet Port Pressure Waves on Volumetric Efficiency. IMechE Volume 188 pp. 577-584. 1974.

[57] Engelman, H, W. The Tuned Manifold: supercharging without a blower, ASME paper 53-DGP-4, 1953.

[58] Winterbone, D, E. Pearson, R, J. Design Techniques for engine manifolds. Wave Action Methods for IC Engines. Published professional Engineering Publishing Limited, London. Printed by J W Arrowsmith Limited. UK. 1999.

[59] Winterbone, D, E. and Yoshitomi, M. The Accuracy of Calculating Wave Action in Engine Intake Manifolds. International Congress and Exposition Detroit, Michigan February 26 - March 2,1990. Depart of Mechanical Engineering UMIST, Manchester, England and Komatsu Limited Oyarna-shi, Japan. SAE paper series 900677. 1990.

[60] Yoshitomi, M. Investigation of wave action inside intake manifold of a reciprocating internal combustion engine. MSc thesis. Depart of Mechanical Engineering UMIST, Manchester, England. 1989.

[61] Pearson, R, J. A linear model for synthesis of intake manifolds. MSc thesis. Depart of Mechanical Engineering UMIST, Manchester, England. 1988.

[62] Winterbone, D, E. Pearson, R, J. Theory of engine manifold design. Wave Action Methods for IC Engines. Published professional Engineering Publishing Limited, London. Printed by J W Arrowsmith Limited. UK. 2000.

[63] Broome, D. Induction Ram. Part I, II, II. Automobile Engineer. April, pp. 130-133, May, pp. 180-184; June, pp. 262-267. 1969.

[64] Bujak, J, Z. Contribution to discussion of Kastner. Proceedings of the Institution of Mechanical Engineers 153 June 1945. Pp 215 – 217. 1945.

[65] Kastner, L, J. Induction Ramming Effects in Single-Cylinder Four-Stroke Engines. Proceedings of the Institution of Mechanical Engineers June 1945 153: 206-220, 1945.

[66] Benajes, J. and Reyes, E. Galindo, J. Peidro, J. Predesign Model for Intake Manifolds in Internal Combustion Engines. Universidad de La Coruña and Universidad Politécnica de Valencia. SAE Technical Paper Series 970055. 1997.

[67] Peidro, J, L. Predesign of intake manifolds in internal combustion engines. PhD thesis. Universidad Politecnica de Valencia. 1990.

[68] Shami, C, J. Air Induction Design for Restricted Race Engines. Master of Science Thesis. Department of Mechanical Engineering and Materials Science. Duke University. 2014.

[69] Singhal, A. Parveen, M. Air Flow Optimization via a Venturi Type Air Restrictor. Proceedings of the World Congress on Engineering 2013 Vol III. London. 2013.

[70] Rickwood, R. Conversion of a Chevrolet LS7 engine for LMP1 use: Inlet, exhaust and noise attenuation. Oxford Brookes University. Racing Engine Design MSc Dissertation. Student Number 07076108. 2008.

[71] Vaughan, V. Delagrammatikas, G, J. Varibale runner length intake manifould design: an interim progress report. Cooper union. SAE Technical Paper Series 2010–10–1112, 2010.

[72] Mackey, D, O. Crandall, J, G. Chatfield, G, F. Ashe, M, C. Optimization of Exhaust-Pipe Tuning on a 4-Stroke Engine Using Simulation. SAE 2002 World Congress. Detroit, Michigan. SAE Technical Paper 2002-01-002. 2002.

[73] Westin, F. and Ångström, H-E. Simulation of a Turbocharged SI-Engine with Two Software and Comparison with Measured Data. The Royal Institute of Technology (KTH), Stockholm. Reprinted From: Spark Ignition and Compression Ignition Engines Modelling 2003. SAE Technical Paper 2003-01-3124. 2003.

[74] Tartakovsky, L. Baibikov, V. Gutman, M. Veinblat, M. Simulation of Wankel Engine Performance Using Commercial Software for Piston Engines. Technion Israel Inst. of Technology. Reif, J. Elbit Systems Ltd. SAE Technical Paper 2012-32-0098. 2012.

[75] Dr Hasse, C, F. Dr Wensing, M, E. Combustion modeling for virtual SI engine calibration with the help of 0D/3D methods. Faculty of Mechanical Engineering, Process Engineering and Energy Engineering. Technical University Bergakademie Freiberg. Von der Fakultät für Maschinenbau,Verfahrens- und Energietechnik der Technischen Universität Bergakademie Freiberg genehmigte. zur Erlangung des akademischen Grades Doktor-Ingenieur (Dr.-Ing.) vorgelegt. Von Diplom-Ingenieur Sebastian Grasreiner aus Erfurt. 2012.

[76] Ukidave, S, S. Development of a technique for achieving an optimum BSFC for LAF engine. Michigan Technological University. Dissertations, Master's Theses and Master's Reports. 2011.

[77] Yeliana. Parametric combustion modeling for ethanol-gasoline fuelled spark ignition engines. Dissertations, Master's Theses and Master's Reports. Michigan Technological University. 2010.

[78] Hatlevold, E, S. Assessment of engine performance and exhaust emission at changing operating conditions and under fault conditions. Department of Marine Technology, Norwegian University of Science and Technology. MSc Thesis. 2010-02-24. 2010.

[79] Meyer, J. INNOVATIONS IN REPRESENTATION AND CALIBRATION OF RESIDUAL GAS FRACTION AND VOLUMETRIC EFFICIENCY IN A SPARK IGNITED, INTERNAL COMBUSTION ENGINE. Presented in Partial Fulfillment of the Requirements for the Degree Master of Science. Ohio State University. 2008.

[80] Kumar, M. VENKATESHMOHAN, V. Predictive Diesel Combustion Using DI-Pulse in GT-Power. Department of Applied Mechanics, Division of Combustion, CHALMERS UNIVERSITY OF TECHNOLOGY, Göteborg, Sweden. 2015

[81] Kakaee, A, H. Mafi, sh. Improving Simulation Accuracy of a Downsized Turbocharged SI Engine by Developing a Predictive Combustion Model in 1D Simulation Software. Automotive Engineering Faculty, Iran University of Science and Technology. International Journal of Automotive Engineering. 2017

[82] Cylinder pressure traces and heat release rates of typical super-knock, conventional knock, and normal combustion. Jpeg. Available at https://www.researchgate.net/figure/Cylinder-pressure-traces-and-heat-release-rates-of-typical-super-knock-conventional_fig5_273919738. 2018

[83] Ukidave, S, S. Development of a technique for achieving an optimum BSFC for LAF engine. Michigan Technological University. Dissertations, Master's Theses and Master's Reports. 2011.

[84] Kutaeba, J, M. Yousef, S, H. Osama, H. Effect of valve lift at different IVO ,IVC and OVERLAP angles on SI Engine performance. The 7th Jordanian International Mechanical Engineering Conference. 2010

[85] Lumley, J. Engines, an introduction. Cambridge UK, Cambridge universities print. 1999.

[86] Badhum, T. The development of a VVT solution for the Ricardo E6 and a study of VVT Strategy. Oxford brooks university final year project interim report. Oxford brooks university. Student Number 11064990. 2016.

[87] Dr Samuel, S. Combustion in SI engines, U04584 Automotive Engines module, Oxford Brookes University, 2015.

[88] Kim, J.Bae, C. An investigation on the effects of late intake valve closing and exhaust gas recirculation in a single-cylinder research diesel engine in the low-load condition. Proc IMechE Part D: J Automobile Engineering 2016, Vol. 230(6) 771–787_ IMechE 2015.

[89] The Impact of valve events upon engine performance and emissions. VALVE EVENT.doc. Mechadyne International. 2006. Available at http://www.mechadyne-int.com/vva-reference/papers/the-impact-of-variable-valve-actuation-on-engine-performance-and-emissions.pdf

[90] Longfei Chen1, Richard Stone2 and Dave Richardson3 Effect of the valve timing and the coolant temperature on particulate emissions from a gasoline directinjection engine fuelled with gasoline and with a gasoline–ethanol blend. Proc IMechE Part D: J Automobile Engineering 226(10) 1419–1430_ IMechE 2012.

[91] Arsie, I. Di Leo, R. Pianese, C. De Cesare, P. Air-Fuel Ratio and Trapped Mass Estimation in Diesel Engines Using In-Cylinder Pressure. Università di Salerno. Magneti Marelli Powertrain. SAE Technical Paper 2017-01-0593. 2017.

[92] Dr Sobachkin, A. Dr Dumnov, G. Numerical Basis of CAD-Enabled CFD. White Pape. SolidWorks. Dassault Systems, France. Mentor Graphics Corporation Analysis Division, Russia. PDF. 2014.

[93] Keskinen, J-P. Vuorinen, V. Kaario, O. Larmi, M. Large Eddy Simulation of the Intake Flow in a Realistic Single Cylinder Configuration. Aalto University. SAE Technical Paper 2012-10-0137. 2012.

[94] Basara, B. Poredos, A. Gorensek, P. Scale-Resolving Simulations of the Flow in Intake Port Geometries. AVL List GmbH. SAE Technical Paper 2016-01-0589. 2016.

[95] Chit, O, J. Omar, A, A. Asrar, A. Reynolds Averaged Navier-Stokes Flow Computation of RAE2822 Airfoil Using Gas-kinetic BGK Scheme. Proceedings of the International MultiConference of Engineers and Computer Scientists 2009 Vol II IMECS 2009, March 18 - 20, 2009, Hong Kong. ISBN: 978-988-17012-7-5. PDF. 2009.

[96] Cheng, S-W. Dey, T, K. Shewchuk, J, R. Delaunay Mesh Generation. International Standard Book Number: 978-1-58488-730-0 Hardback. C7303. 2012.

[97] Fan, Q, Y. Kuba, M. Nakanishi, J. Coupled Analysis of Thermal Flow and Thermal Stress of an Engine Exhaust Manifold. Software CRADLE Co., Ltd. SAE Technical Paper 2004-01-1345. 2004.

[98] Hellsvik, R. Transient Simulation of Ventilation Rate and Moisture load for Cold Attic Constructions - A CFD Analysis. Master's Thesis in Applied Mechanics. Department of Civil and Environmental Engineering. CHALMERS UNIVERSITY OF TECHNOLOGY, Gothenburg, Sweden. REPORT NO. 2015:57. 2015.

[99] Andersson,B. Anderson, R. Håkansson, L. Mortensen, M. Sudiyo, R. van Wachem, B. Computational Fluid Dynamics for Engineers. Cambridge University Press. ISBN 978-1-107-01895-2 Hardback. 2012.

[100] Swant,N. Yamakawa, S. Singh, S. Shimada, K. Automatic Hex-Dominant Mesh Generation for Complex Flow Configurations. SAE Technical Paper 2018-01-0477. 2018.

[101] Valentini, P, P.Pennestri, E. Design and simulation of a variable-timing variable-lift cam mechanism, Department of Mechanical Engineering, University of Rome 'Tor Vergata', Rome, Italy. 2009.

[102] Martienz, Isidoro. Combustion Modelling of a Gasoline Engine by the Wiebe Function. Microsoft Word Document. Available at http://webserver.dmt.upm.es/~isidoro/bk3/c15/Combustion.pdf. 2017.

[103] Oxford Brookes Racing private team server. Edited and used by Bradshaw, B, W, P. 15105795. Current and past CAD models designed in CATIA V5R20 and Solidworks 2016. All Intellectual Property owned by OBR and Oxford Brookes University and all rights reserved. 2017

[104] Bradshaw, B, W, P. 15105795. CAD models designed in CATIA V5R20 and Solidworks 2016. All Intellectual Property owned by OBR and Oxford Brookes University and all rights reserved. 2017.

[105] Mortlock, L, T, O. Investigation of a Turbocharging system on the Brookes V-Twin Engine by 1-D Simulation with GT-Power and Its Evaluation of Performance. Student Number: 13085589. Dissertation Module Number: U04599. 2017.

[106] Franzke, D, E. Beitrag zur Ermittlung eines Klopfkriteriums der ottomotorischen Verbrennung und zur Vorausberechnung der Klopfgrenze. Ph.D. Thesis. Technical University of Munich. 1981.

[107] Worret, R. Bernhardt, S. Schwarz, F. Spicher, U. Application of Different Cylinder Pressure Based Knock Detection Methods in Spark Ignition Engines. Institut für Kolbenmaschinen, University of Karlsruhe. Germany. SAE Technical Paper 2002-01-1668. 2002.

[108] Douaud, A, M. Eyzat, P. Four-Octane-Number Method for Predicting the Anti-Knock Behavior of Fuels and Engines. Institut Français du Pétrole. France. SAE Technical Paper 780080. 1979.

[109] McCuiston, F, D, Jr. Lavoie, G, A. Kauffman, C, W. Validation of a Turbulent Flame Propagation Model for a Spark Ignition Engine. Department of Aerospace Engineering, University of Cincinnati. Fuels and Lubricants Department, Ford Motor Co. SAE Technical Paper 770045. 1977.

Picture credits

[110] Dr Yang, C. Performance and Efficiency Analysis of Engines. U04584 Automotive Engines lecture series, Oxford Brookes University, 2015.

[111] Dr Wang, W. J. In-Cylinder Pressure Measurement and Analysis. PowerPoint presentation, University of Essex, 2015.

7. Bibliography

[1] Mindworks. Engine performance parameters, University of Idaho, 2015

[2] thecartech. Engine formulas, http://www.thecartech.com/subjects/engine/engineformulas.htm, 2015

[3] Yeliana, C. Cooney, J. Worm, D. Michalek, J. Naber. Wiebe Function Parameter Determination For Mass Fraction Burn Calculation in a Ethanol-Gasoline Fuelled Engine, Michigan Technological University, Journal of KONES Powertrain and Transport. 2008.

[4] Alden, C. investigation in to downsizing engine trends, limitations encountered in the attempt to raise efficiency. Oxford Brookes University Final year project BSc motorsport technology, department of mechanical engineering and mathematical sciences. 2015

[5] Pulkrabek, W. Engineering Fundamentals of the internal combustion engine. University of Wisconsin. 1997

[6] Deng, B. Fu, J. Zhang, D. Yang, J. Feng, R. Liu, J. Li, K. Liu X. The heat release analysis of bio-butanol/gasoline blends on a high speed SI (spark ignition) engine. Written by the State Key Laboratory of Advanced Design and Manufacturing for Vehicle Body, Hunan University, 410082 Changsha, China, Department of Industrial Technology and California State University, Fresno, Fresno, CA 93740-8002, USA, Chongqing Longxin Engine Co., Ltd, 400060 Chongqing, China. 2013.

[7] Rassweiler, G. Withrow, L. Motion Pictures of Engine Flames Correlated with Pressure Cards. SAE Proceedings. 1938

[8] Lackner, K. Chapter 3, the concept of viscosity. Columbia University. 2002. Available at http:/ /www.columbia.edu/itc/ldeo/lackner/E4900/Themelis3.pdf

[9] Prof Inamdar, S. Laminar & Turbulent Flows. Watershed sciences research group. University of Delaware. 2010

[10] Ghanaati, A. Darus, M. Said, M. andwari, A. A mean value model for estimation of laminar and turbulent flame speed in spark-ignition engine. University of Malaysia Pahang. International journal of automotive and mechanical engineering, volume 11, UMP publisher. 2015.

[11] Sodré, J. A Parametric Model for Spark Ignition Engine Turbulent Flame Speed. SAE Technical Paper 982920. 1998.

[13] Mantilla, J. Garzón, D. Galeano, C. Combustion model for spark ignition engines op2erating on gasoline-ethanol blends. Engenharia Térmica Vol. 9, Universidad Nacional de Colombia. 2010.

[13] Lower, S. Collison and activation, the Arrhenius Law, WEB available at http://www.chem1.com/acad/webtext/dynamics/dynamics-3.html, 2009. Modified 2015

[14] Dogahe, M. Estimation of mass fraction of residual gases from cylinder pressure data and its application to modeling for SI engine. Journal of Applied Mathematics, Islamic Azad University of Lahijan, Vol.8. 2012.

[15] Blizard, N. Keck, J. Experimental and theoretical investigation of turbulent burning model for internal combustion engines. SAE Technical Paper No. 740191; 1974.

[16] Ferguson, C. Tabaczynski, J. Radhakrishnan, K. A turbulent entrainment model for spark-ignition engine combustion. SAE Technical Paper No. 770647; 1977.

[17] Kaprielian, L. Demoulin, M., Cinnella, P. Daru, V. Multi-zone quasi-dimensional combustion models for spark-ignition engines. SAE Technical Paper No. 2013-24-0025; 2013.

[18] Heywood, J. B. Internal Combustion Engine Fundamentals. McGraw Hill, Automotive Technology Series, 1988.

[19] Dr Yang, C. Performance and Efficiency Analysis of Engines. U04584 Automotive Engines lecture series, Oxford Brookes University, 2015.

[20] Kutaeba, J, M. Yousef, S, H. Osama, H. Effect of valve lift at different IVO ,IVC and OVERLAP angles on SI Engine performance. The 7th Jordanian International Mechanical Engineering Conference. 2010

[21] Lumley, J. Engines, an introduction. Cambridge UK, Cambridge universities print. 1999.

[22] Kim, J.Bae, C. An investigation on the effects of late intake valve closing and exhaust gas recirculation in a single-cylinder research diesel engine in the low-load condition. Proc IMechE Part D: J Automobile Engineering 2016, Vol. 230(6) 771–787_ IMechE 2015.

[23] Ferguson, R. C. and Kirkpatrick, A. T.; "Internal combustion engines Applied thermodynamics", 2nd Edition, John Wiley and sons inc., New York, 2001.

[24] Valentini, P, P.Pennestri, E. Design and simulation of a variable-timing variable-lift cam mechanism, Department of Mechanical Engineering, University of Rome 'Tor Vergata', Rome, Italy. 2009

[25] Longfei Chen1, Richard Stone2 and Dave Richardson3 Effect of the valve timing and the coolant temperature on particulate emissions from a gasoline directinjection engine fuelled with gasoline and with a gasoline–ethanol blend. Proc IMechE Part D: J Automobile Engineering 226(10) 1419–1430_ IMechE 2012

[26] Nigus, H. Kinematics and Load Formulation of Engine Crank Mechanism. Mechanics, Materials Science & Engineering, October 2015 – ISSN 2412-5954. 2015.

[27] Jaques, P. Heat Transfer, Tribology and design of piston assembly for V-Twin Engine. MSc Dissertation. Oxford Brookes university school of technology September. 2007.

[28] Ling, J. Tun, L, T, Y. CFD Analysis of Non-Symmetrical Intake Manifold for Formula SAE Car. School of Aerospace, Mechanical and Mechatronic Engineering. SAE Technical Paper Series 2006-01-1976. 2006.

[29] Garner, C, P. Hargrave, G K. Versteeg, H, K. and Viv J. Page. Development of a Validated CFD Process for the Analysis of Inlet Manifold Flows with EGR. Loughborough University and Perkins Engines Company Ltd. SAE Technical Paper Series 2002-01-0071. 2002.

[30] Cui, Y. Pan, W.Leylek, J, H. and Sommer, R, G. Jain, S, K. Cylinder-to-Cylinder Variation of Losses inIntake Regions of ICEnginesin Intake Regions of IC Engines. Clemson University and Caterpillar, Inc. SAE Technical Paper Series 981025. 1998.

[31] Shaw, C, T. Lee, D, J. and Richardson, S, H. Pierson, S. Modelling the Effect of Plenum-Runner Interface Geometry on the Flow Through an Inlet System. University of Warwick and Jaguar Engineering Centre. SAE Technical Paper Series 2000-01-0569. 2000.

[32] Shinde, P, A. Research and optimization of intake restrictor for Formula SAE car engine. Mechanical Engineering, Smt. Kashibai Navale College of Engg, Pune. International Journal of Scientific and Research Publications, Volume 4, Issue 4, April 2014 1 ISSN 2250-3153. 2014.

[33] Davies, P. Piston Engine Intake And Exhaust System Design. Institute of Sound and Vibration Research, University of Southampton, England. Journal of Sound and Vibration (1996) 190(4), 677-712. 1995.

[34] Ceviz, M, A. Intake plenum volume and its influence on the engine performance, cyclic variability and emissions. Department of Mechanical Engineering, Faculty of Engineering, University of Ataturk, Turkey. 2006.

[35] Hwang, I, G. Myung, C-L. Park, S. and In C-B. Yeo, G, Y. Theoretical and Experimental Flow Analysis of Exhaust Manifolds for PZEV. Korea University and Hyundai Motor Company. SAE Technical Paper Series 2007-01-3444. 2007.

[36] Lakshmikantha, M. Kec, M. Optimization of Exhaust Systems. Eberspaecher North America, Inc. SAE Technical Paper Series 2002-01-0059. 2002.

[37] Gonzalez, I, L. FS08 V-twin Cylinder Head Design. Oxford Brookes University. MSC dissertation. Student Number 06072985. 2007.

[38] Bush, P. Telford, C. and Boam, D. Bingham, J. A Design Strategy for Four Cylinder SI Automotive Engine Exhaust Systems. Arvin Exhaust, Ltd. And National Engineering Laboratory. SAE Technical Paper Series 2000-01-0913. 2000.

[39] Martensson, J. Flardh, O. Modeling the Effect of Variable Cam Phasing on Volumetric Efficiency, Scavenging and Torque Generation. SAE Technical Paper Series 2010-01-1190. 2010.

[40] Shaw, C, T. Lee, D, J. Tichardson, S, H. Pierson, S. Modelling the effect of plenum-runner interface Geometry on the flow through an inlet system. University of Warwick. Jaguar Engineering Centre. SAE Technical Paper Series. 2000-02-0569. 2000.

[41] Bradshaw, B, W, P. CAD work carried out by Bradshaw on Solidworks 2016/17. 15105795. 2016/17.Ferguson, R. C. and Kirkpatrick, A. T.; "Internal combustion engines applied thermodynamics", 2nd Edition, John Wiley and sons inc., New York, 2001.

[42] Brown, B. Combustion Data Acquisition and Analysis, Department of Aeronautical and Automotive Engineering, Loughborough University. 2014.

[43] Alden, C. investigation in to downsizing engine trends, limitations encountered in the attempt to raise efficiency. Oxford Brookes University Final year project BSc motorsport technology, department of mechanical engineering and mathematical sciences. 2015

[44] Salazar, F. internal combustion engine. Department of aerospace and mechanical engineering. University of Notre Dame. 1998.

[45] Rassweiler, G. Withrow, L. Motion Pictures of Engine Flames Correlated with Pressure Cards. SAE Proceedings. 1938

[46] Taylor, J. MCKee, R. McCullough, G. Cunningham, G. McCartan C. Computor Simulation and Optimisation of an Intake Camshaft for a Restricketed 600 CC Four-Stroke Engine. Queen's University Belfast. SAE Technical Paper Series 2006-32-0071. 2006.

[47] McClintock, S. Walkingshaw, J. McCartan, C. McCullough, G. Cunningham, G. Camshaft Design For an Inlet-Restricted FSAE Engine. Queen's University Belfast. SAE Techinical Paper deries 2008-32-0073. 2008

[48] McKee, R, H. McCullough, G. Cunningham, G. Taylor, J, O. McDowell, N. Taylor, J, T. McCullough, R. Experimental Optimisation Of Manifould and Comashaft Geometries for a Restricted 600 CC Four Clinder Four-Stroke Engine. Queen's University Belfast. SAE Techincal Paper 2006-32-0070. 2006

[49] Brown, B. Combustion Data Acquisition and Analysis, Department of Aeronautical and Automotive Engineering, Loughborough University. 2014.

[50] Rassweiler, G. Withrow, L. Motion Pictures of Engine Flames Correlated with Pressure Cards. SAE Proceedings. 1938

[51] Alden, C. investigation in to downsizing engine trends, limitations encountered in the attempt to raise efficiency. Oxford Brookes University Final year project BSc motorsport technology, department of mechanical engineering and mathematical sciences. 2015

[52] Mittal, M . Zhu, G .Schock , H. Fast mass-fraction-burned calculation using the net pressure method for real-time applications. Department of Mechanical Engineering, Michigan State University, East Lansing, MI, USA. 2008

[53] Brown, N M. Characterisation of emissions and combustion stability of a port fuelled spark ignition engine. PhD thesis, University of Nottingham. 2009

[54] Potul, S. Nachnolkar, R. Bhave, S. Analysis Of Change In Intake Manifold Length And Development Of Variable Intake System. ISSN 2277-8616 international journal of scientific and technology research volume 3, issue 5, 2014

[55] Winterbone, D, E. Pearson, R, J. Design Techniques for engine manifolds. Wave Action Methods for IC Engines. Published professional Engineering Publishing Limited, London. Printed by J W Arrowsmith Limited. UK. 1999.

[56] Cox, R, J, N. Formula Student Engine Design and Development – The Design and development of a varying geometry inlet manifold. Oxford Brookes University Dissertation, module number U04599. Student number 04091584. 2009.

[57] Winterbone, D, E. Pearson, R, J. Theory of engine manifold design. Wave Action Methods for IC Engines. Published professional Engineering Publishing Limited, London. Printed by J W Arrowsmith Limited. UK. 2000.

[58] The Impact of valve events upon engine performance and emissions. VALVE EVENT.doc. Mechadyne International. 2006. Available at http://www.mechadyne-int.com/vva-reference/papers/the-impact-of-variable-valve-actuation-on-engine-performance-and-emissions.pdf

[59] Badhum, T. The development of a VVT solution for the Ricardo E6 and a study of VVT Strategy. Oxford brooks university final year project interim report. Oxford brooks university. Student Number 11064990. 2016.

[60] Ojapah, M M. Experimental Studies of Performance and Emissions in a 2/4-Stroke Engine with Gasoline and Ethanol. A thesis submitted for the degree of Doctor of Philosophy. School of Engineering and Design, Brunel University London. 2014

[61] Kutaeba, J, M. Yousef, S, H. Osama, H. Effect of valve lift at different IVO ,IVC and OVERLAP angles on SI Engine performance. The 7th Jordanian International Mechanical Engineering Conference. 2010

[62] Nouhov, D. Investigation of the Effect of Inlet Valve Timing on the Gas Exchange Process in High-Speed Engines, A Doctoral Thesis, Loughborough University, Institute Repository. 2004.

[63] Yang, C. Investigation of combustion and performance characteristics of CAI combustion engine with positive and negative valve overlap. A thesis submitted for the degree of Doctor of Philosophy. School of Engineering and Design, Brunel University. 2008

[64] Huber, R. Dynamics of Variable Valve Trains and Extrapolation Methods for Time-Stepping Schemes. Lehrstuhl für Angewandte Mechanik, Technischen Universität München. 2012

[65] Valentini, P, P.Pennestri, E. Design and simulation of a variable-timing variable-lift cam mechanism, Department of Mechanical Engineering, University of Rome 'Tor Vergata', Rome, Italy. 2009

[66] Lumley, J. Engines, an introduction. Cambridge UK, Cambridge universities print. 1999.

[67] Kim, J.Bae, C. An investigation on the effects of late intake valve closing and exhaust gas recirculation in a single-cylinder research diesel engine in the low-load condition. Proc IMechE Part D: J Automobile Engineering 2016, Vol. 230(6) 771–787_ IMechE 2015.

[68] Ferguson, R. C. and Kirkpatrick, A. T.; "Internal combustion engines Applied thermodynamics", 2nd Edition, John Wiley and sons inc., New York, 2001.

[69] Longfei Chen1, Richard Stone2 and Dave Richardson3 Effect of the valve timing and the coolant temperature on particulate emissions from a gasoline directinjection engine fuelled with gasoline and with a gasoline–ethanol blend. Proc IMechE Part D: J Automobile Engineering 226(10) 1419–1430_ IMechE 2012

[70] Pulkrabek, W W. Engineering Fundamentals of the Internal Combustion Engine. Second edition. Pearson education limited. 2014

[71] Gatowski, J, A. Balles, E, N. Chun, K, M. Nelson, F, E. Ekchian, J, A. Heywood, J,B. Heat Release Analysis of Engine Pressure Data.Sloan Automotive Laboratory, Massachusetts Institue of Technology. Fules and Lubricants Meeting & exposition Baltimore, Maryland. SAE Technical Paper Series 841359. 1984.

Appendix
Model development

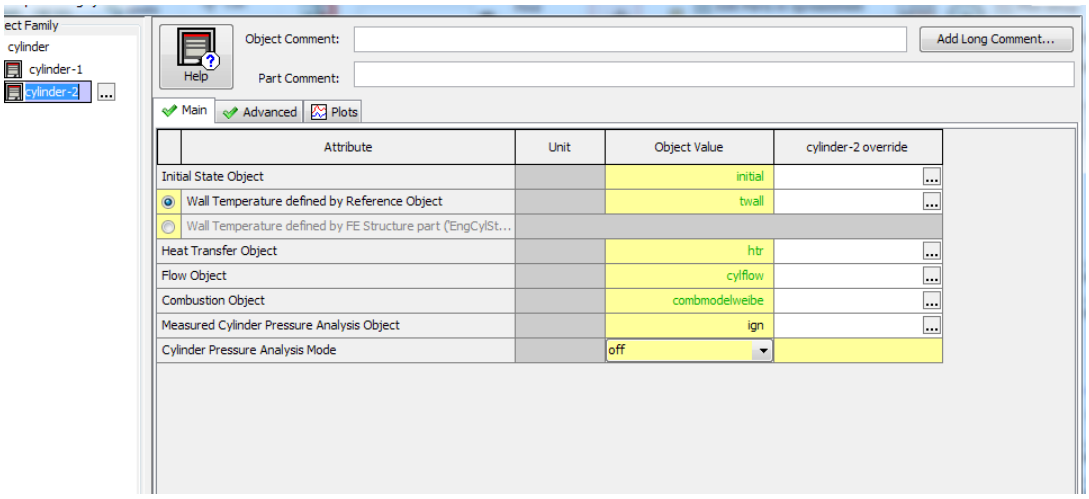

Figure 93: Ambient Temperature setup.

Setting up ambient conditions of 1 bar and 300 deg K

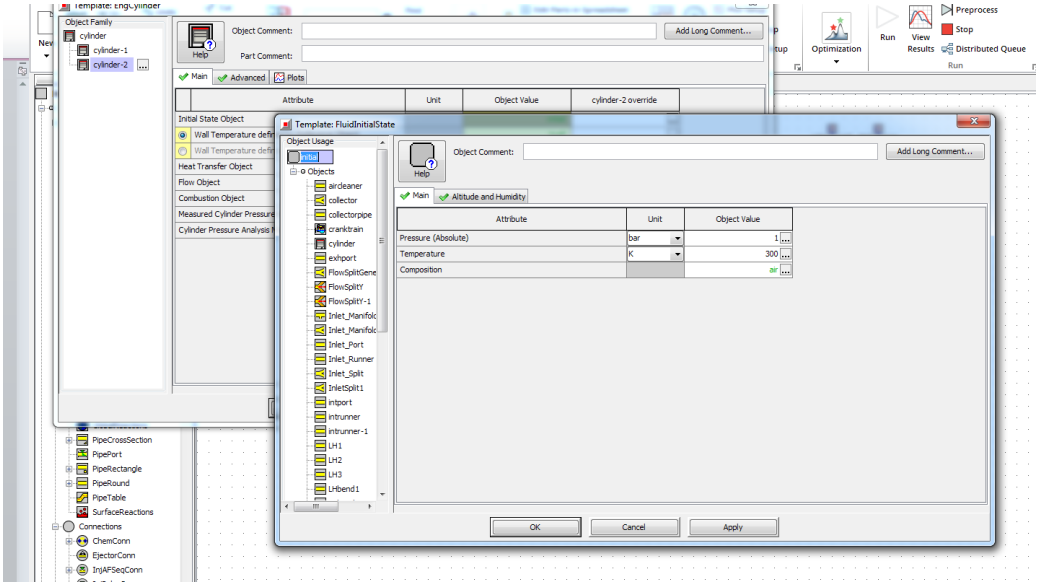

Figure 94: Initial fluid state.

Wiebe model with numbers 5 25 and 2 got from the combustion model

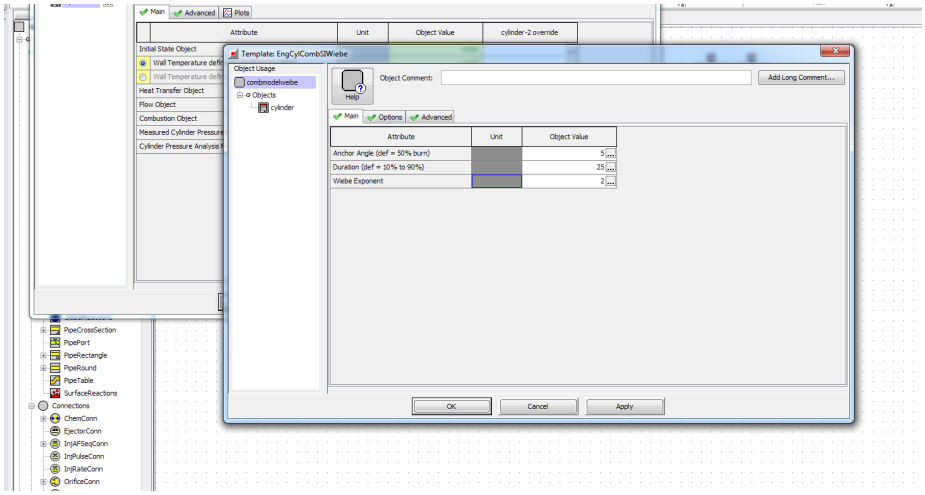

Figure 95: Wiebe model parameters for the GT-Power model

A turbulent flame propagation model, or chemical Kinetic model, can be set up within GT-Power but it is a highly complicated as a spark ignition map needs to be created and then optimised for each case run, for example if a sweep is performed for the runner length then an optimal spark map for each case needs to be created. Also the in-cylinder geometry has to be implemented accurately within the model to allow the flame propagation model to model the combustion phasing and flame propagation accurately.

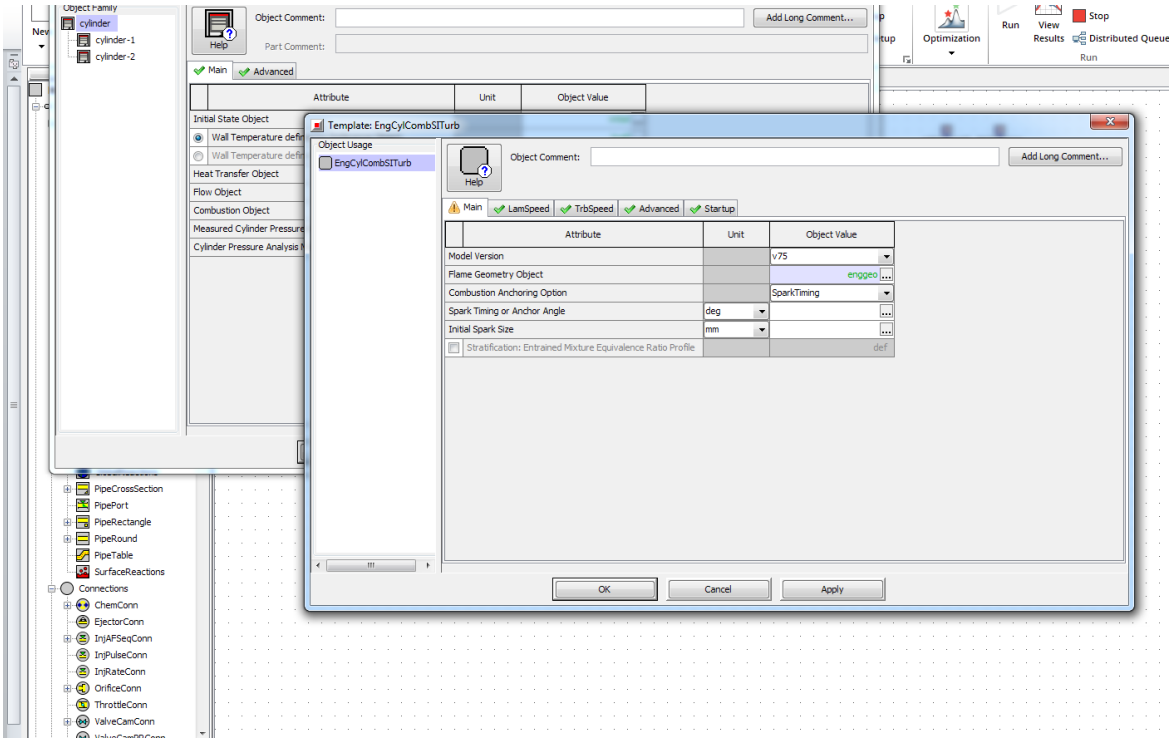

Figure 96: Combustion model settings.

.stl files used to implement piston and cylinder head geometry into GT-Power model to set up an accurate representation.

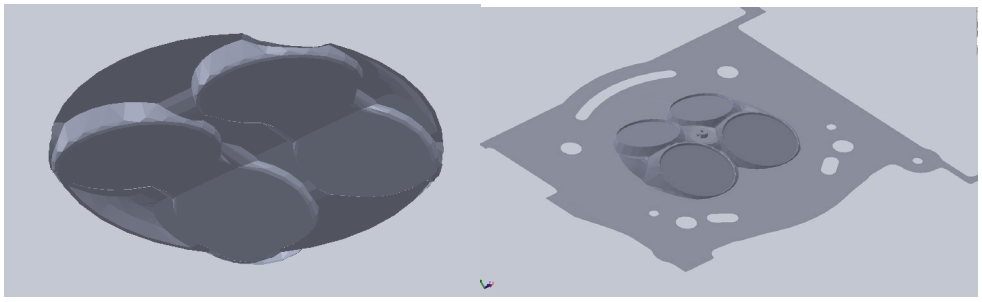

Figure 97: Combustion chamber geometry .stl files.

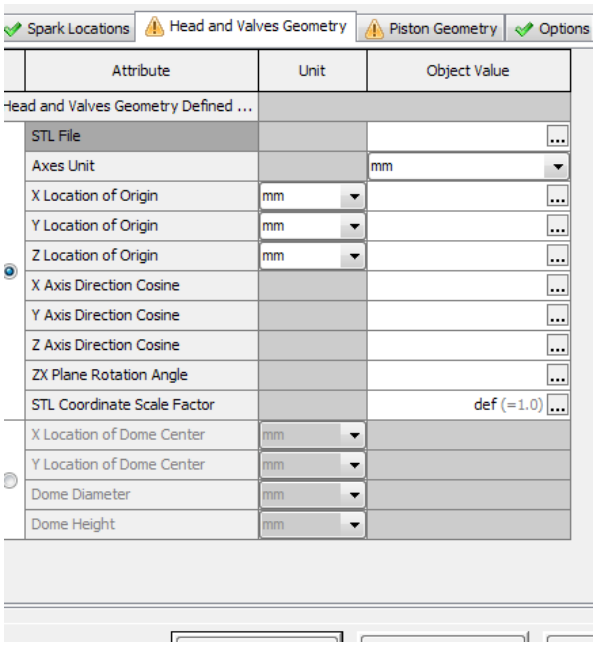

Figure 98: Combustion chamber geometry input graph

The friction model

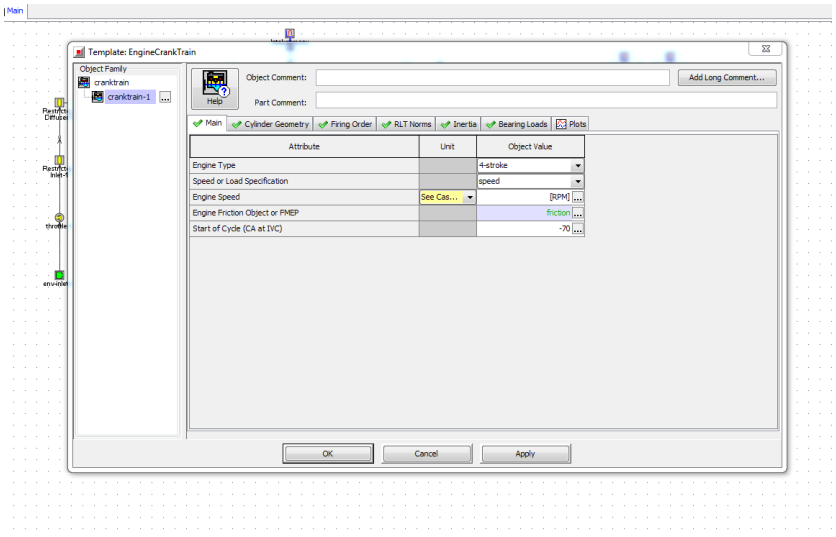

Figure 99: Engine Crank Train model.

And implementation of the friction model

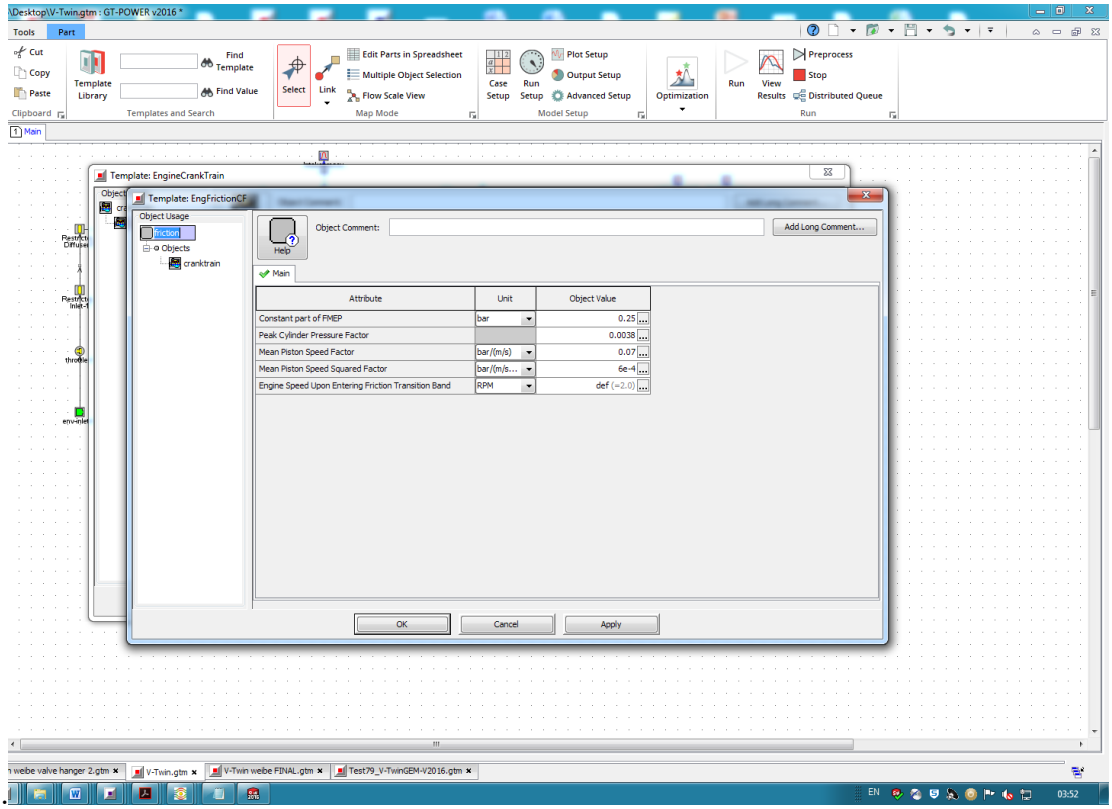

Figure 100: Engine Friction model.

Engine specs and parameters/ geometry

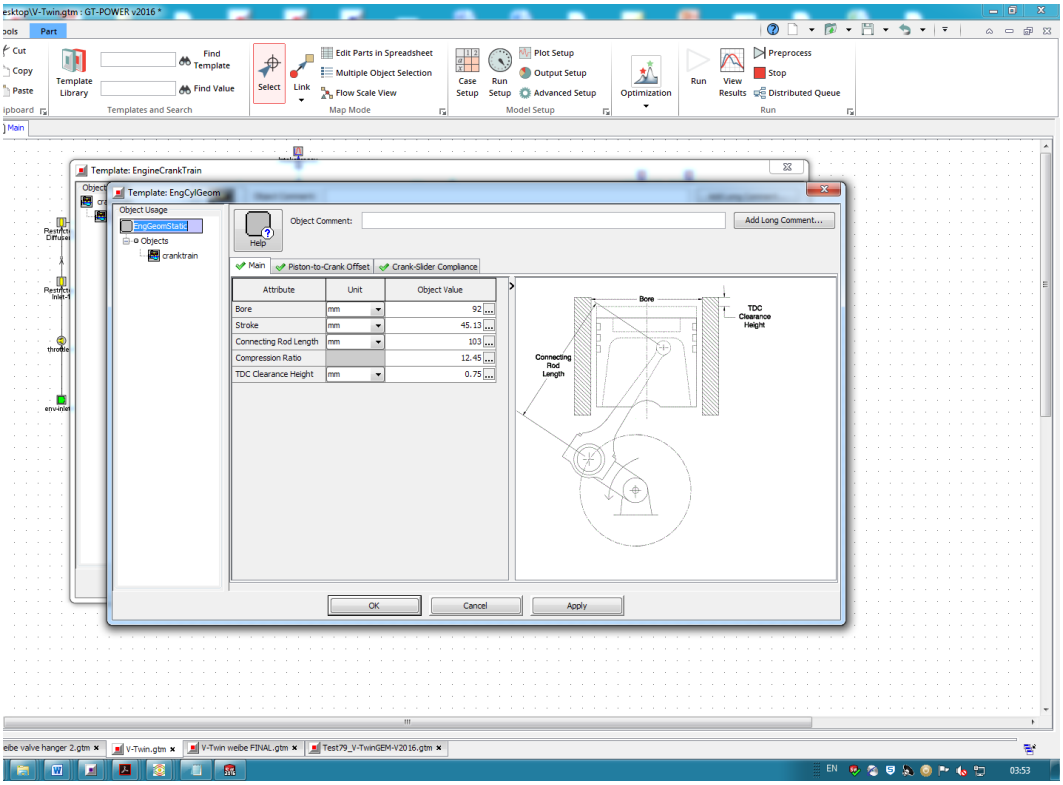

Figure 101: Engine internals' parameters.

Inertia model Engine Effective Rotating Inertia

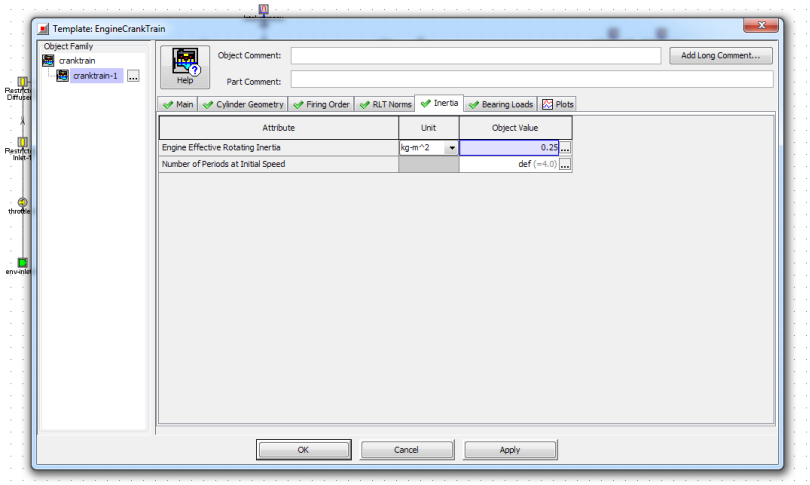

Figure 102: Rotating inertia of the internals.

Optimiser

GT-Power optimizer sweep iteration final results

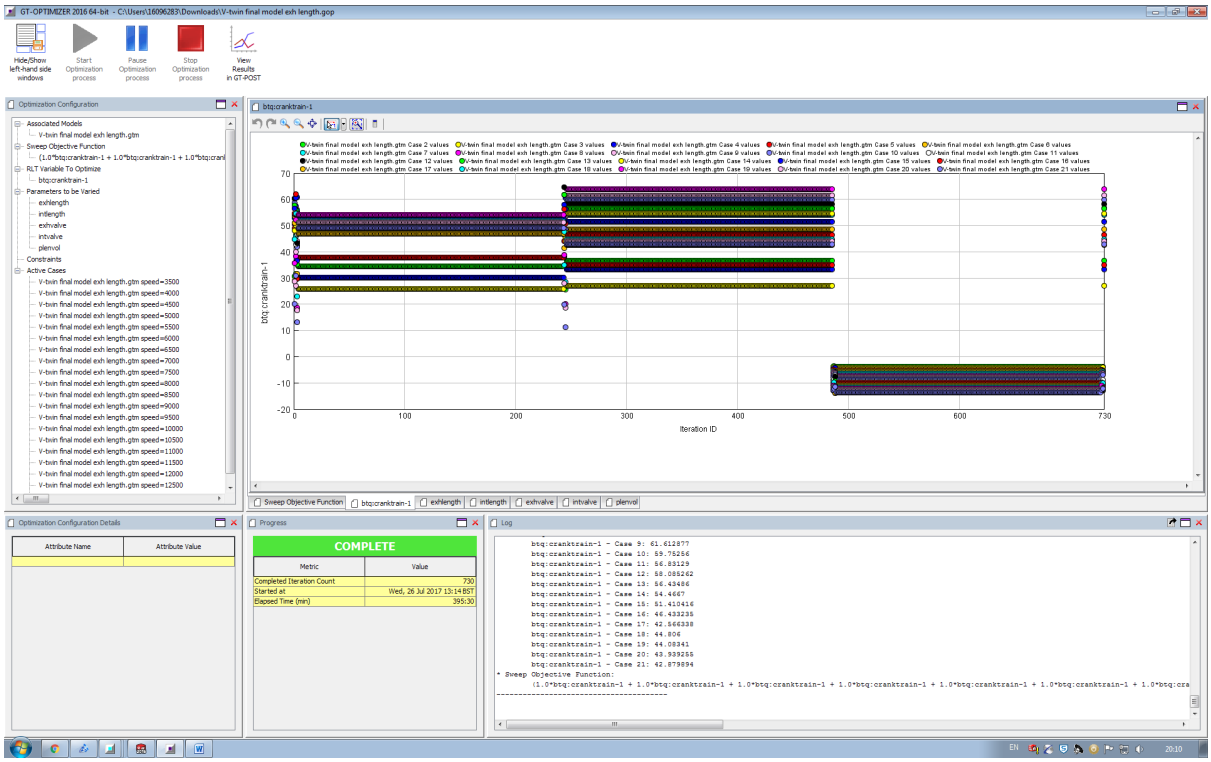

Figure 103: Max Torque optimiser sweep.

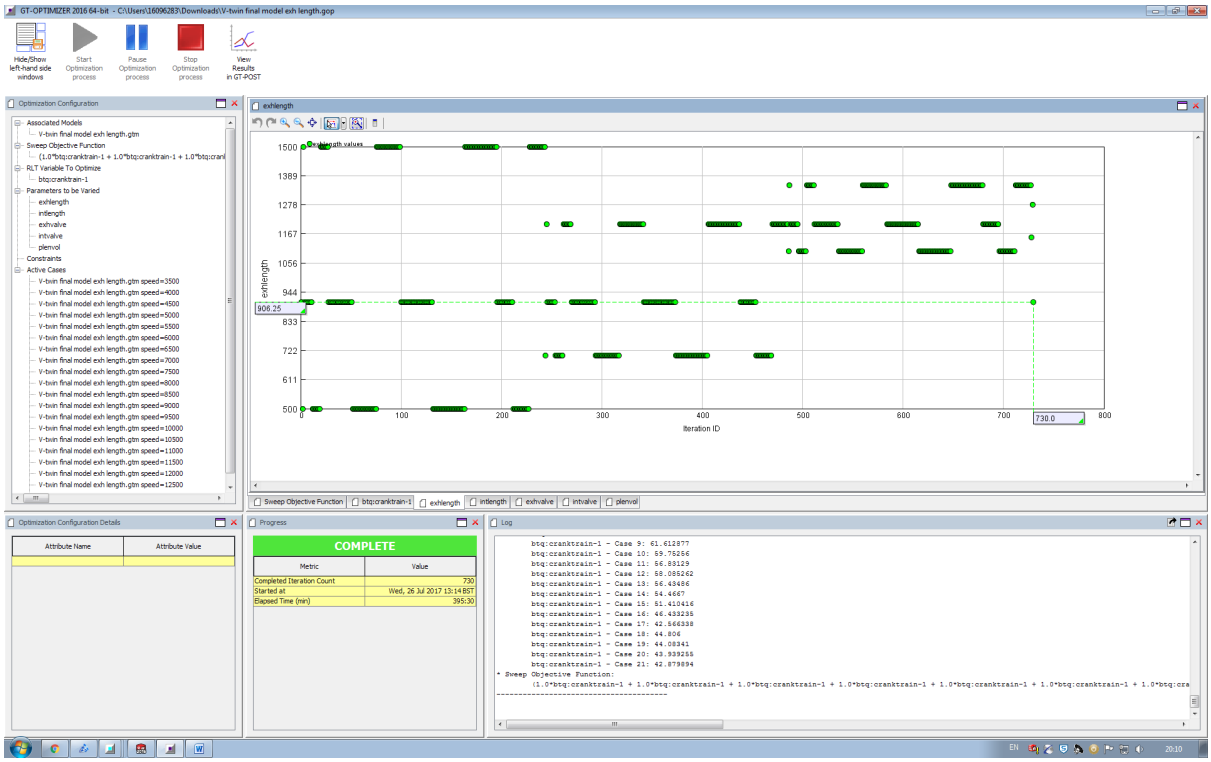

Figure 104: Exhaust length optimiser sweep

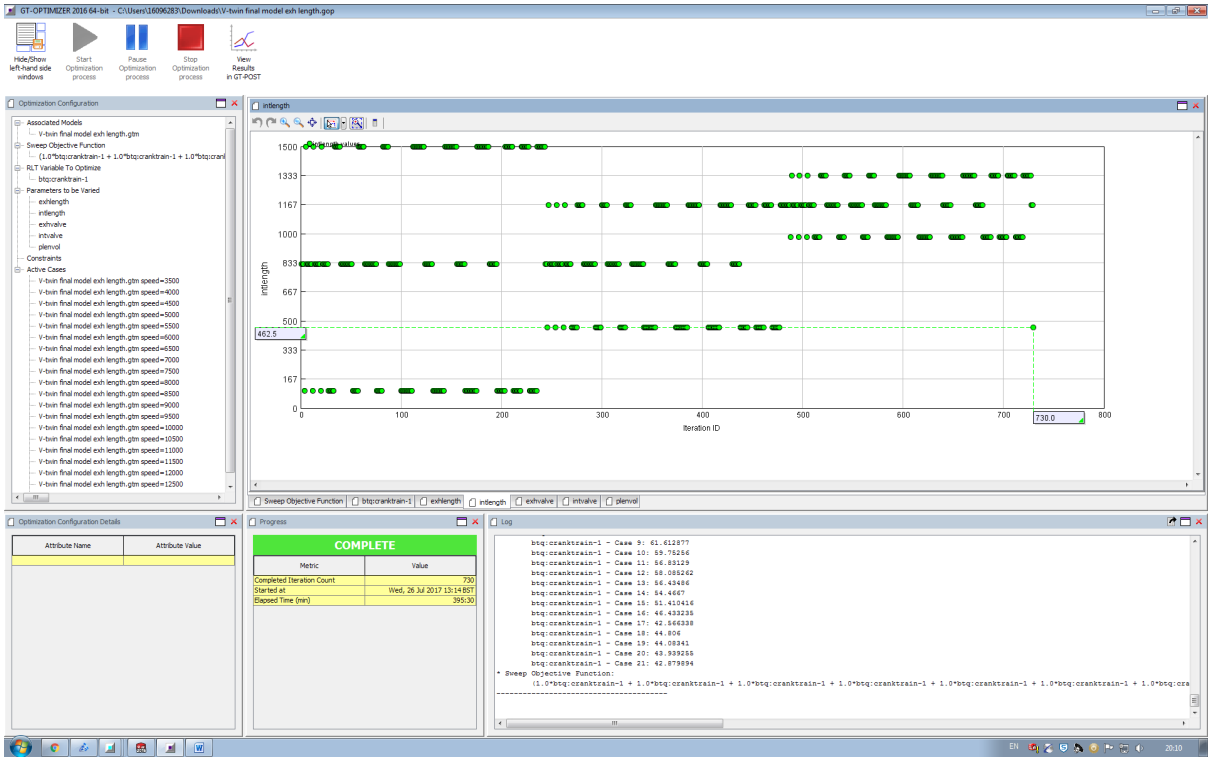

Figure 105: intake runner length optimiser sweep.

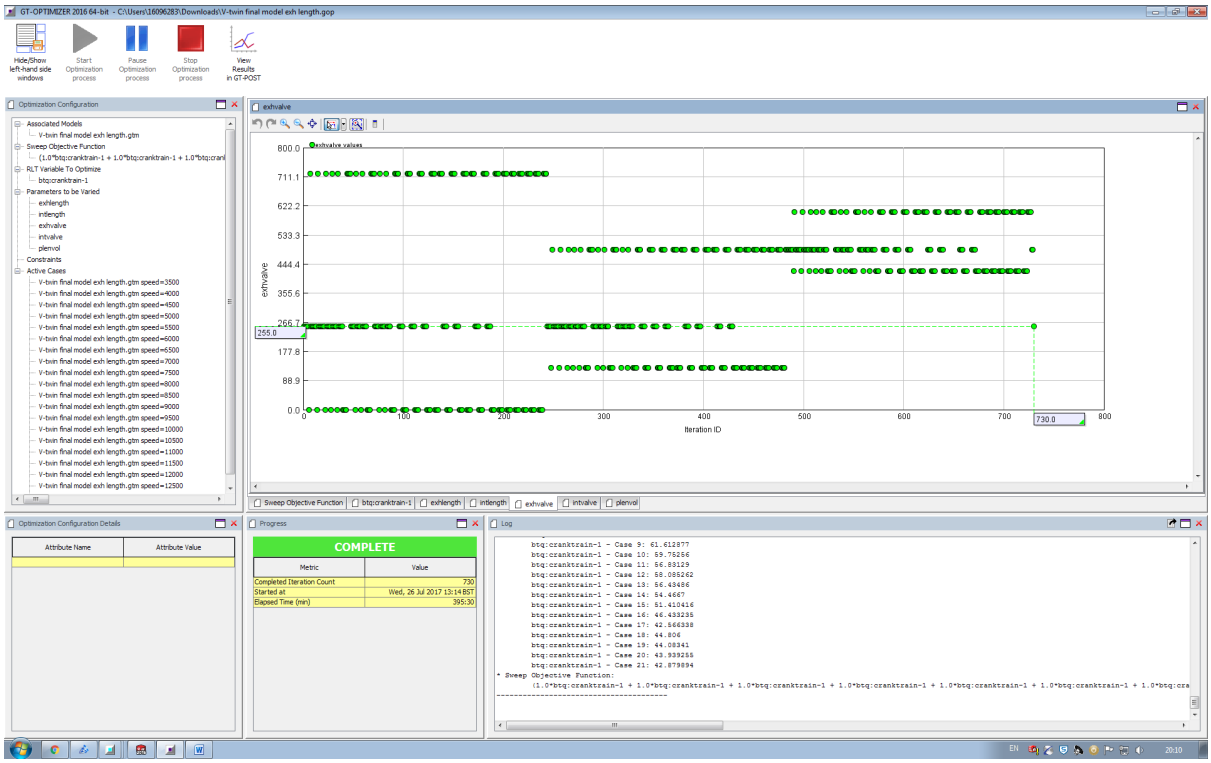

Figure 106: Exhaust valve timing optimiser sweep.

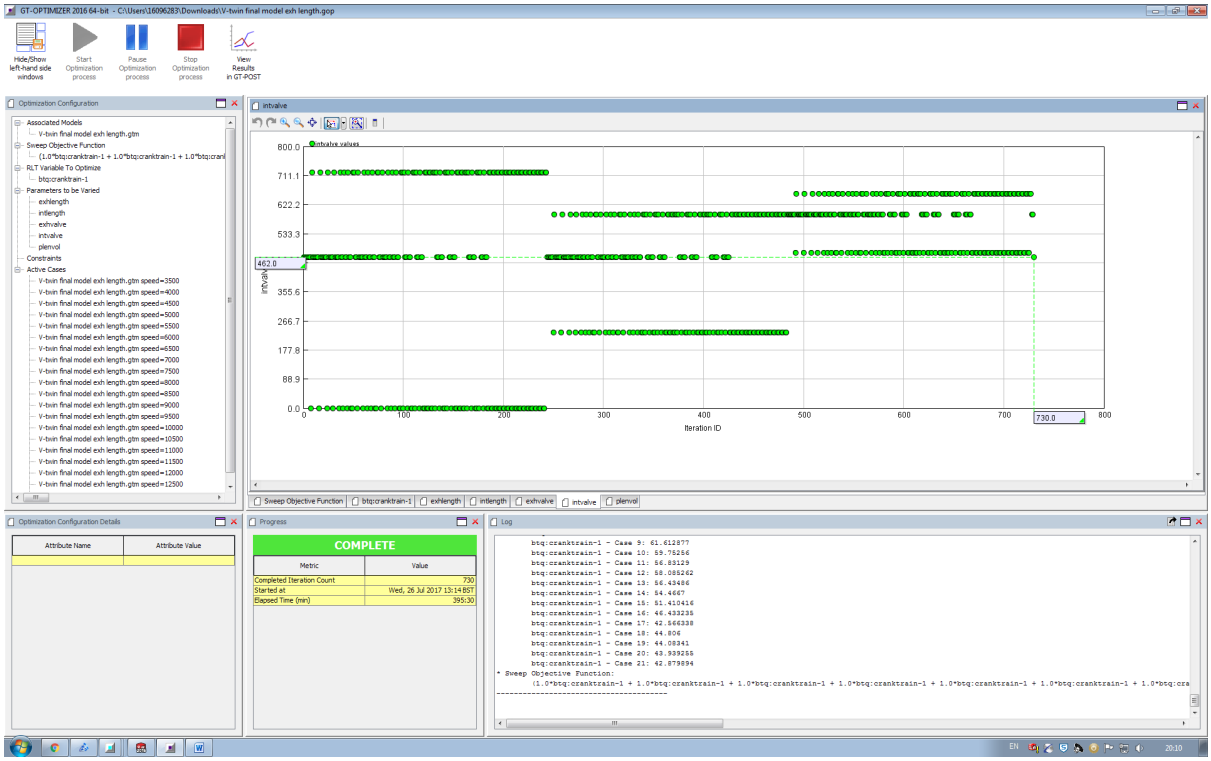

Figure 107: Intake Valve timing optimiser sweep

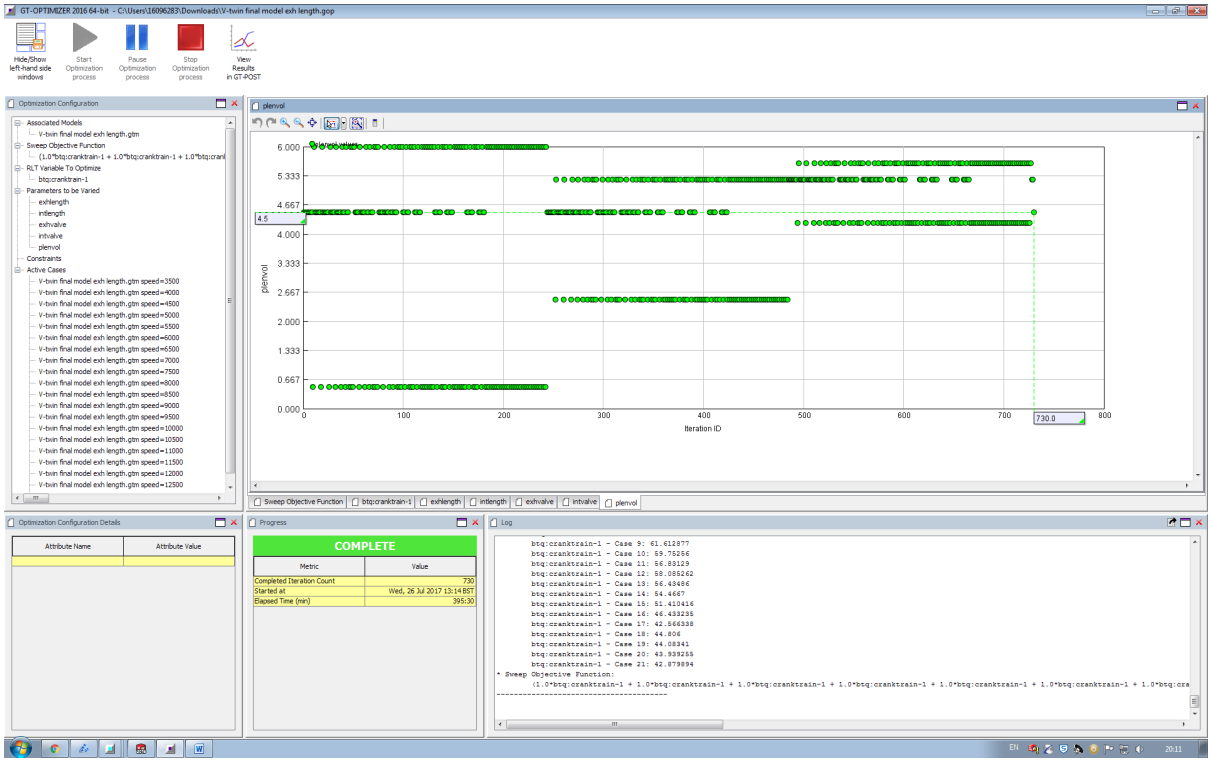

Figure 108: Plenum volume optimiser sweep

Flame Propagation

It was deemed that for this project it would be more appropriate to carry out combustion analysis, using combustion phasing, rather than flame propagation analysis. However, the principals of flame propagation were researched and understood, and this knowledge was applied to combustion model as well as the combustion phasing.

Flame speed assessment

Flame velocity is one of the main ways of assessing flame propagation within a SI engine. When the charge inside the cylinder is ignited, with the spark, a flame kernel is formed, from there a kernel grows into a laminar flame, the expanding laminar flame forms a turbulent flame boundary as the remaining charge burns, this turbulent flame boundary transitions the laminar flame into a turbulent flame. Towards the end of combustion the flame can be considered turbulent, [18].

A flame speed model for both turbulent and laminar flame speeds needs to incorporate all the fundamentals of the SI engines combustion variables. Although the assumption, the flame structure model doesn't employ the flame development angle, must be made. The flame development angle is the total crank angle between the spark ignition and the development of the flame. [18].

The equation to explain the relationship between both laminar and turbulent flames is [18,19]–

$$\frac{S_T}{S_L} = 1 + \left(\frac{R_c}{8}\right)^a \times \left(\frac{\rho_u}{\rho_b}\right)^{\phi_1} \times \left(\frac{p}{p_{ig}}\right)^{\phi_2} \times \left(0.5 \times \frac{\bar{S}_p}{S_L}\right)^b \times \left(1 - exp\left(-\frac{R_f}{c \times B}\right)\right)$$

Where S_T and S_L are Turbulent and laminar flame speed respectively. R_c is the compression ratio, ρ_u and ρ_b are the density of the burnet and unburnt charge. p and p_{ig} are the pressure and he pressure at ignition. $\bar{S}_p$ is the MPS, R_f is the flame radius, B is the cylinder Bore in meters. With a, b and c are constant while Φ_1 and Φ_2 are found using the equations, [18, 19] –

$$\phi_1 = d + e \times (\phi - 1)$$

$$\phi_2 = f + g \times (\phi - 1)$$

With d, e, f and g are adjusted using the fuel experiments procedure, [18, 19]. Ghanaati, Darus, Said and Andwari give the values of a = 1.1, b = 0.7, c = 1.7, d = 0.611, e = 1.4, f = 1.152 and g = -1.5, these figures where determined to allow for the calculated and measured peak pressure had the same value and occurred at the same crank angle, [18]

The engine running and cylinder geometry parameters can be simplified from the equation for $\frac{S_T}{S_L}$ above into the coefficient C, [18, 19].

$$\frac{S_T}{S_L} = 1 + C \times \left(\frac{\rho_u}{\rho_b}\right)^{\frac{1}{2}} \times \left(\frac{u'}{S_L}\right)^b \times \left(1 - exp\left(-\frac{R_f}{r_c}\right)\right)$$

Laminar modelling

A fundamental property of the fuel/air mixture in a combustion engine is the burning velocity normal or relative to the flame front during combustion, better known as laminar burning velocity. [20, 21]

$$S_L = S_{L,o} \left(\frac{T_u}{T_o}\right)^{\alpha} \times \left(\frac{p}{p_o}\right)^{\beta}$$

Where T_0 and p_0 are reference temperature, 298 Kelvin, and pressures, 1 atm, respectively. T_u is the temperature of the unburned mixture. [18, 21, 22, 27]

$$\alpha = 2.18 - 0.8 \times (\phi - 1)$$

$$\beta = -0.16 + 0.22 \times (\phi - 1)$$

$$S_{L,o} = B_m - B_\phi \times (\phi - \phi_m)^2$$

Where Φ_m is the equivalence ratio at which $S_{L,o}$ is a maximum with a value B_m. The values of Φ_m, B_m and B_Φ are given in the table below. $S_{L,0}$ is the reference laminar speed and used as a flame speed correction for the variations in equivalence ratio, [18, 21, 22, 27].

Fuel	Φ_m	B_m m/s	B_Φ m/s
Methanol	1.11	0.369	-1.405
Propane	1.08	0.342	-1.387
IsoOctane	1.13	0.263	-0.847
Gasoline	1.21	0.305	-0.549

Figure 109: fuel parameters [22, 23]

The equation for the laminar flame speed does not take into account the effects of the residual mass fraction [18, 21, 22, 27] –

$$S_L = S_{L,o} \left(\frac{T_u}{T_o}\right)^{\alpha} \times \left(\frac{p}{p_o}\right)^{\beta} \times \left(1 - 2.06 \times {F_R}^{0.77}\right)$$

Turbulence modelling

Damkohler numbers (higher the number the faster the reaction) along kolmogorov length scale [18, 21, 22, 27] –

$$Da = \frac{l}{u \times \tau_c} = \frac{\tau_m}{\tau_c} = \frac{lengthscale}{u'} \times \frac{S_L}{\delta_L}$$

Where $\frac{l}{u'}$ is the mixing time, τ_c is the chemical reaction time, α is the thermal diffusivity, D is the mass diffusivity, K is the thermal conductivity, C_p is the specific heat capacity, ρ is the density, v is the kinematic viscosity, μ is the viscosity.

When the turbulence is homogeneous and isentropic then the Taylor microscale can be represented as [18, 21, 22, 27] –

$$l_m = \overline{U} \times t_m$$

The relationship between the most energetic length scale and the Kolmogorov length scale can be represented as [18, 21, 22, 27] –

$$\frac{l_k}{l} = \left(\frac{v^3}{\varepsilon \times l^4}\right)^{\frac{1}{4}} = \left(\frac{v^3}{u'^3 \times l^4}\right)^{\frac{1}{4}} = Re_t^{\frac{-3}{4}}$$

Where $L = \sqrt{\frac{2}{3} \times u' \times l \times t}$, Re_t is the Reynolds number when turbulent (over 4000), u'l = υ_t is the viscosity of the eddy's, u' is the root mean square of the fluctuating velocity.

Flame front modelling

To model the turbulent flame propagation/front the controls-oriented model is used, it is based on the quasi-dimensional turbulent flame entrainment concept developed by [26, 27, 28, 29]. The model is based on a few assumptions. The assumption can be made that the flame front propagates through the unburned charge entraining turbulent eddies along Kolmogorov-scale vortices. The sum of a convective component, a diffusive component, the laminar flame speed and turbulence intensity defines the entrainment velocity. Only the leading edge and not the whole flame area, which includes the unburned eddies, is used to define the flame front. The turbulence intensity is an order of magnitude larger than the laminar flame speed and is defined as the root mean square velocity of the fluctuation within the cylinder, [22, 26, 27, 28, 29].

$$\frac{dm_e}{dt} = \rho_u \times A_f \times (u' + S_L)$$

Where m_e is the mass entrained by the flame, ρ_u is the unburned charge density in front of the flame, A_f is the flame front area, u' is the turbulence intensity and S_L is the laminar flame speed.

The flame propagation research allowed for a better understanding of the process of combustion while also allowing a comparison of combustion phasing and flame propagation in terms of combustion analysis. A full analysis of combustion via aflame propagation model would have been preferable in terms of the accuracy of the analysis but it was deemed too time consuming and therefor combustion phasing will be sued to describe the combustion events.

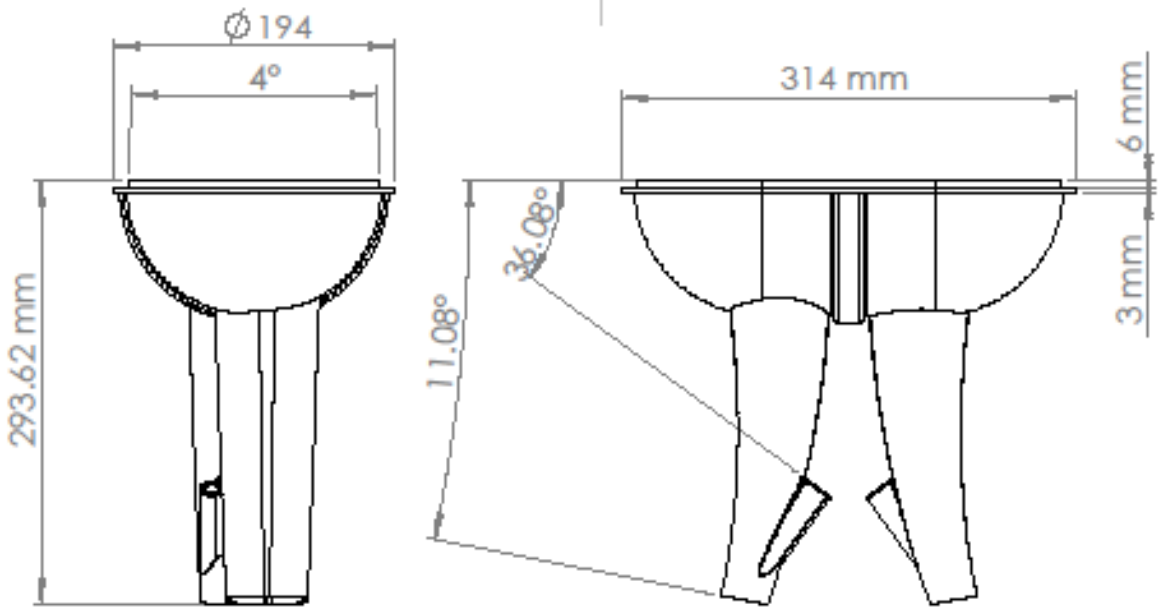

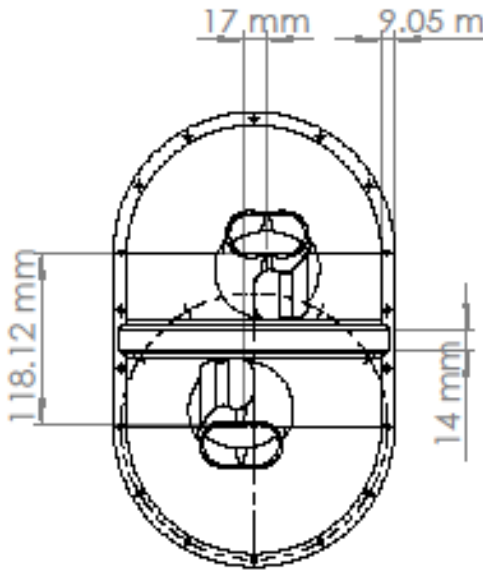

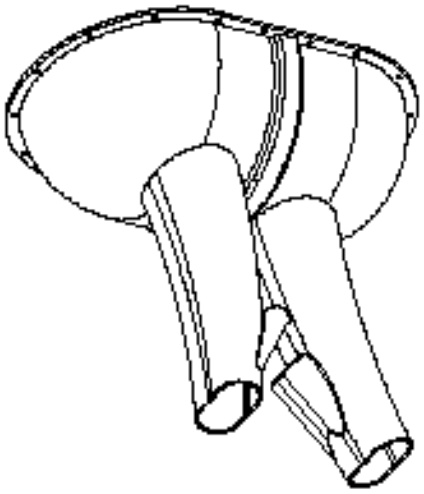

UNLESS OTHERWISE SPECIFIED: DIMENSIONS ARE IN MILLIMETERS SURFACE FINISH: TOLERANCES: LINEAR: ANGULAR:		FINISH:		DEBURR AND BREAK SHARP EDGES		DO NOT SCALE DRAWING	REVISION
	NAME	SIGNATURE	DATE			TITLE:	
DRAWN							
CHK'D							
APPV'D							
MFG							
Q.A				MATERIAL:		DWG NO. finished runner	A4
				WEIGHT:		SCALE:1:5	SHEET 1 OF 1

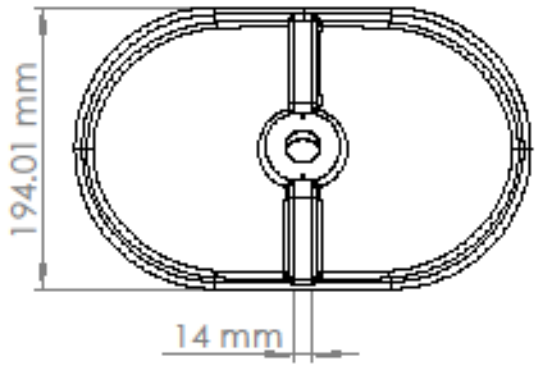

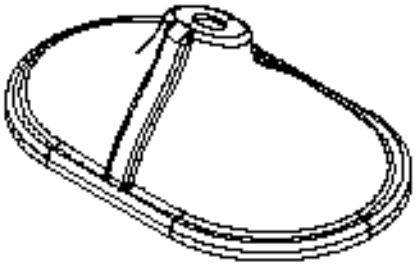

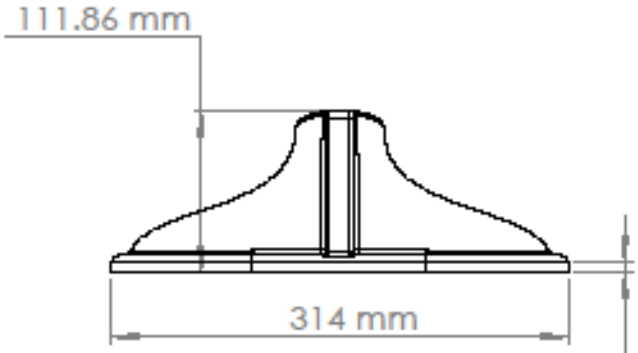

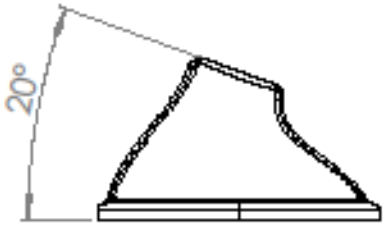

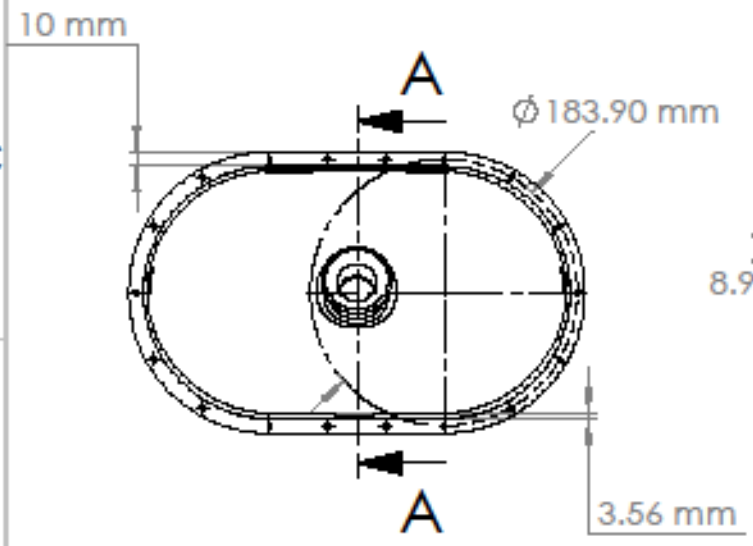

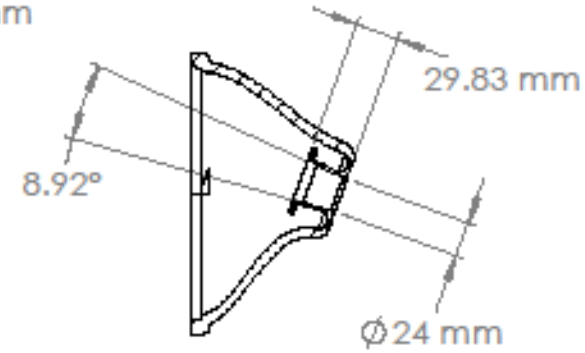

SECTION A-A

UNLESS OTHERWISE SPECIFIED: DIMENSIONS ARE IN MILLIMETERS SURFACE FINISH: TOLERANCES: LINEAR: ANGULAR:		FINISH:		DEBURR AND BREAK SHARP EDGES		DO NOT SCALE DRAWING		REVISION
	NAME	SIGNATURE	DATE				TITLE:	
DRAWN								
CHK'D								
APPV'D								
MFG								
Q.A				MATERIAL:			DWG NO.	A4
				WEIGHT:			SCALE:1:5	SHEET 1 OF 1

plenum top cover angle

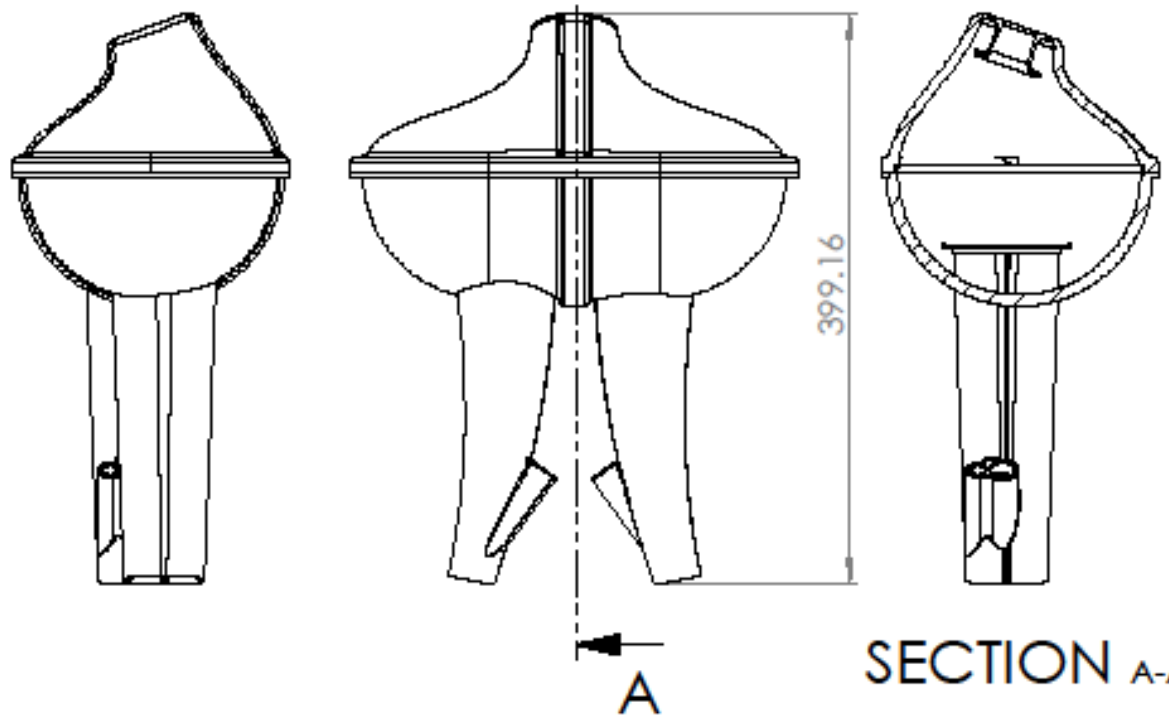

SECTION A-A

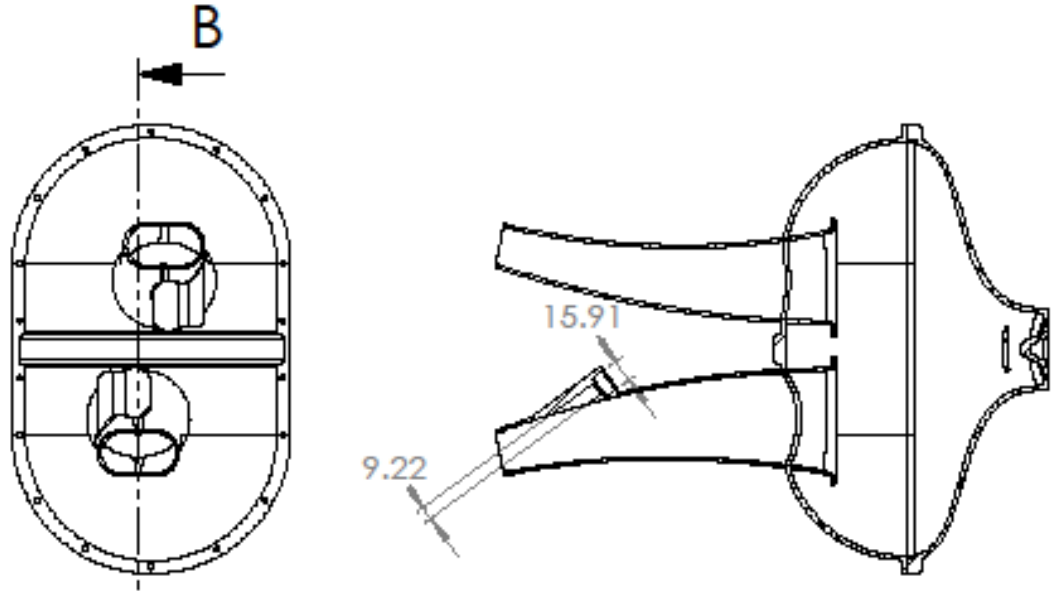

SECTION B-B

UNLESS OTHERWISE SPECIFIED: DIMENSIONS ARE IN MILLIMETERS SURFACE FINISH: TOLERANCES: LINEAR: ANGULAR:		FINISH:		DEBURR AND BREAK SHARP EDGES	DO NOT SCALE DRAWING	REVISION	
	NAME	SIGNATURE	DATE		TITLE:		
DRAWN							
CHK'D							
APPV'D							
MFG							
Q.A				MATERIAL:	DWG NO. final assembly		A4
				WEIGHT:	SCALE:1:5	SHEET 1 OF 1	